Universidad Autónoma de Madrid
Facultad de Ciencias Físicas
Departamento de Física Teórica

Protoplanetary disk evolution in nearby star-forming regions

Álvaro Ribas Gómez

June 2015

Universidad Autónoma de Madrid
Facultad de Ciencias Físicas
Departamento de Física Teórica

Evolución de discos protoplanetarios en regiones de formación estelar cercanas

Tesis dirigida por

Dr. Bruno Merín Martín y **Dr. Hervé Bouy**

Memoria presentada por

Álvaro Ribas Gómez

para optar al título de Doctor en Ciencias Físicas

Madrid, Junio 2015

A mis padres, por enseñarme el camino.

A Raquel, por recorrerlo conmigo.

if you're going to try, go all the
way.
otherwise, don't even start.

if you're going to try, go all the
way.
this could mean losing girlfriends,
wives, relatives, jobs and
maybe your mind.

go all the way.
it could mean not eating for 3 or 4
days.
it could mean freezing on a
park bench.
it could mean jail,
it could mean derision,
mockery,
isolation.
isolation is the gift,
all the others are a test of your
endurance, of
how much you really want to
do it.
and you'll do it
despite rejection and the worst odds
and it will be better than
anything else
you can imagine.

if you're going to try,
go all the way.
there is no other feeling like
that.
you will be alone with the gods
and the nights will flame with
fire.

do it, do it, do it.
do it.

all the way
all the way.

you will ride life straight to
perfect laughter, it's
the only good fight
there is.

Charles Bukowski - *Roll the dice*

Agradecimientos

Aprovecho la ocasión para sincerarme y os diré que esta tesis no es mía. Por casualidades del destino lleva mi nombre, pero es el resultado de la ayuda de un montón de personas que, a sabiendas o sin saberlo, son sus verdaderos artífices. Sin ellos, jamás habría podido terminar este trabajo. *Al César lo que es del César.*

En primer lugar tengo que agradecerles a mis directores, Bruno y Hervé, todo el esfuerzo y dedicación que han puesto en mí. Me disteis una oportunidad única que de otro modo nunca habría tenido. A Bruno, por su entusiasmo contagioso y su pasión por la ciencia, por saber cómo levantar el ánimo en cualquier situación. Por rescatarme cuando me alejaba de la astrofísica, lograr lo imposible para que pudiese hacer el doctorado en ESAC, y demostrarme lo equivocado que estaba. A Hervé por su punto de vista crítico, por enseñarme a ser íntegro (no solo en ciencia) sin perder el humor por el camino. Por sus millones de datos y tener siempre alguna idea alucinante entre manos. Por fiarse de mí y mandarme a Canarias poniendo en peligro sus datos y el telescopio entero. Por descubrirme el vicio del buceo. A ambos por confiar en mí desde el principio y aceptar dirigir mi tesis, por ser siempre cercanos y tener una paciencia infinita conmigo. Por aguantar los problemas siempre con risas y buen rollo. Ha sido una suerte y un honor aprender de vosotros, ojalá pueda seguir haciéndolo en el futuro. ¡Sois un combo brutal!

Un poco más alejado en el tiempo, no puedo olvidarme de David, quien me involucró en su investigación desde el principio cuando yo estaba empezando el máster. Es curioso cómo ese proyecto que parecía secundario acabó determinando mi camino los años siguientes y me trajo hasta aquí. Gracias por abrirme las puertas a la investigación.

Agradezco muchísimo a la División de Operaciones Científicas y la Science Faculty de ESAC que financiasen este proyecto que de otro modo no habría podido realizar, y a ISDEFE que me acogiesen para poder llevarlo a cabo.

Una de las mejores cosas de la tesis ha sido desarrollarla en el LAEFF, y tengo que agradecerle a Miguel que me hiciese un hueco. A toda la gente que trabaja allí, por hacerme sentir como en casa. A Sergio y Antonio por aguantar y frustrar mis repetidos intentos de destruir la informática hasta los cimientos. A Benja por ser tan humilde siendo tan grande, por echar una mano en todo lo que puede e incluso en lo que no. A Mauro por su paciencia con la base de datos y sus conversaciones entre frikazos. A Jose y Nuria por ayudarme cuando lo necesité. A Albert por enseñarme a observar y arriesgarse a dejarnos el telescopio. A Bea, por las charlas mañaneras y los cigarros que te debo. A Margie, por soportar mis desastres burocráticos con una sonrisa. A Jorge por arriesgarse a colaborar conmigo en el proyecto con más altibajos de la historia de la ciencia, por el buen trabajo, la lucha por el cluster, las derrotas compartidas en las becas, y el buen rollo. A Alba por su particular forma de ver el agua y ser una digna

contrincante. A Bea por llevar la risa encendida todo el día y su inigualable tarta. A Paco por las batallas nocturnas, el Monopoly, el pelaíto, fotocasa, las caras de Bélmez y la maldita estadística. A Nacho por haber sido compañero de fatigas, por las carreras en una isla recóndita, por los viajes, sus selfies, por compartir el calvario de HIPE y ser el tipo más auténtico del mundo. Por supuesto, a mis compañeros de despacho (el mejor despacho del mundo), RES-PE-TO y Aristogatos hasta el final. A Jesús por las largas charla sobre la vida, el inicio de una agencia espacial entre los dos, sus habilidades escapistas nocturnas (a las dos serán las tres), los fantásticos intercambios musicales y nuestros planes para hacernos ricos (yo tengo fe). A Irene por las noches de observación intempestivas, las carreras, las conversaciones a cualquier hora, por ostentar estoicamente el honor de ser la persona más saludada de la historia, por tu risa contagiosa y por cambiar tu definición de amigo. A Mario, por haber sido mi hermano indiscutible en el LAEFF hasta el punto de no necesitar decir nada para mantener una conversación entera. Por las cadenas de palabras quasi-infinitas, aquella ola loca y la señora Concha, porque no se me ocurre absolutamente nada que no pueda hablar contigo. Cuando me ría sin motivo sabré por qué es. A los dos por los Valencia y Munich, la tarta de Colacao y las aventuras farmacéuticas. Que nos quede mucho más. Gracias de verdad a todos vosotros. No quiero echaros de menos, así que ya podéis ir pensando en un plan.

Durante el tiempo que he estado en ESAC he tenido la suerte de conocer y colaborar con mucha más gente ajena al LAEFF, y les debo mucho. A Isa, trabajar contigo ha sido una verdadera pasada. Al final me has ayudado más tú a mí que yo a ti. A Pablo, por echarme una mano cuando lo he necesitado, siempre con humor y escepticismo. Nos ha faltado más tiempo para trabajar juntos, pero espero que esto tenga fácil solución. Por supuesto a Miguel, que además de arreglar todas mis meteduras de pata con la burocracia siempre ha estado ahí para hablar de lo que fuese y ayudar en cualquier cosa. A Catarina, por involucrarme en su trabajo desde el principio y tratarme como a un igual sin importar mi experiencia. A Elena, por sus sesiones antiestrés cuando las necesitaba. A ESAC en general, por ser tan único.

A Eric y Gaspard por el tiempo que me dedicaron durante las estancias, lo muchísimo que aprendí de ellos y la paciencia que aún hoy siguen teniendo conmigo.

Por supuesto, gran parte de lo necesario para terminar un trabajo así no tiene nada que ver con la ciencia sino con el alma. A Raúl, Griet (mi hermana de otros padres), a Paloma y a Bea. A los cuatro por estar ahí siempre. Porque las cosas siguen igual aunque no nos hayamos visto en dos semanas o dos años. Y a Mario, Paula y Celes, porque nunca nos perdamos.

A mi segunda familia, José, Concha y Pablo, por acogerme en una casa de locos donde me sentí uno más desde el principio y haberme ayudado siempre e incondicionalmente. Por las discusiones y las risas, las que han sido y las que nos quedan. A los tres, ¡pica

no juego! Y por supuesto a Jazz y Blues, porque las palabras rara vez son necesarias para lo verdaderamente importante.

A mi familia le debo gran parte de lo que soy, y gran parte de esta tesis. A mis tíos y primos por estar siempre ahí, por su apoyo incondicional y haberme querido desde que tengo memoria. En especial a Víctor y Edu, porque compartamos muchos más viajes, fotos, risas e historias. Pero sobre todo y sin lugar a dudas a mis abuelos, a Remedios y especialmente a Antonio, porque sé que en otras circunstancias estarías muy orgulloso de mí. A Ángel, por dejarnos claro a todos que la edad es cuestión de espíritu, su infinito bueno humor y sus incansables ganas de aprender (¡poco más y te doctoras tú!). A Bibi, por ser la persona más dulce y buena del mundo, por las conversaciones y los secretos, por sus canciones de cuna, su cuentos, y por guardar mi "luna rota" todos estos años. Os debo un montón.

A Jorge y Alba, que también son familia. Gracias a los dos por el buen rollo, por ayudarme en tantas cosas y tantas veces. Ojalá nos veamos más, que nos queda mucho por reírnos.

Aquí empieza la parte más complicada, porque ciertas cosas son simplemente imposibles de escribir. A Elena, por ser el mayor ejemplo de bondad, fuerza, superación y nobleza que conozco. Por tus ataques de risa mortales, por tu sencillez, por estar siempre pendiente de todo el mundo y no rendirte nunca. A Diego, porque hay poca gente con la que tenga una conexión igual. Por nuestras charlas nocturnas, las coñas continuas, por las luchas en la habitación, por ser mi amigo además de mi hermano. Porque cada día que paso con vosotros me doy más cuenta de lo especiales que sois. Que pase lo que pase sigamos siendo tres.

La mayor suerte que he tenido en la vida y la verdadera razón de que hoy pueda dedicarme a mi pasión son, por supuesto, mis padres. A mi padre, que desde que era un crío despertó en mí la curiosidad y el pensamiento crítico, por llenarme la cabeza de preguntas que llevaban a más preguntas, por inculcarme el amor por la naturaleza y la ciencia, por la Montaña de las Pirámides, la Machota y el Mirador. Por tus cuentos, por los ánimos continuos, el ajedrez, los chistes malos. Por ser único en tu especie. A mi madre, por enseñarme a ser bueno y justo, por quererme incluso cuando no lo merezco, por ser mi confesora y apoyo tantas veces. Por tu sabiduría infinita en todo aquello que no aparece en las enciclopedias, por tu fuerza y por hacerme creer en mí mismo. Por mostrarme que los libros son algo vital y sagrado. Por las tardes hablando en el sofá, por saber guiarme cuando no veía ninguna solución. A los dos, por haber sacrificado tantísimo para hacernos felices y que nunca nos falte de nada, por vuestro amor incondicional y haber aguantado todas mis locuras y manías. Por las noches mirando el cielo de las Navas. Por estar ahí siempre, en los buenos y malos momentos, estemos cerca o lejos. Por anteponernos a todo lo demás. Sé que nunca encontraré la forma de agradeceros lo suficiente todo lo que habéis hecho por mí. Espero que al menos

algún día lleguéis a estar tan orgullosos de mí como yo lo estoy de ser vuestro hijo. Os quiero muchísimo.

Por último, gracias a Raquel. Gracias por quererme, gracias por no dudar nunca de mí, gracias por seguir a mi lado. Por limitarte a llamarme loco cuando sigo trabajando a las tantas de la madrugada, en vez de pegarme con el ordenador en la cabeza. Por haberme aguantado durante la tesis incluso cuando no me aguantaba yo mismo, jamás habría podido terminarla sin ti. Por querer estar conmigo a pesar de mis manías y mis taras, que son muchas. Por dejarme compartir el día a día contigo y escucharme siempre que necesito hablar con alguien. Por crear un lugar donde depositar mi confianza ciegamente y sin reparos. Por todas tus locuras. Por seguirme a cualquier parte, ya sea a un observatorio perdido en la montaña o debajo del agua. Por no haber dudado ni un momento en hacer las maletas y cruzar el charco conmigo. Por agüiguo y por ut. Por ser mi compañera en el camino, y porque lo seas mucho más tiempo.

Álvaro Ribas Gómez
Junio, 2015

Resumen de la tesis

Los discos protoplanetarios son una pieza clave para entender la existencia de planetas alrededor de otras estrellas: es en ellos donde se forma la enorme cantidad de planetas que hoy en día se sabe que pueblan la Galaxia. Compuestos de gas y polvo, los discos protoplanetarios son producto de la conservación de momento angular durante la formación estelar, y evolucionan en escalas de millones de años hasta convertirse en discos de deshecho o *debris* (similares al cinturón de Kuiper en el Sistema Solar), en muchos casos generando además uno o varios planetas en ese proceso. El estudio de dicha evolución, así como de sus características físicas y composición, permite comprender la enorme diversidad de arquitecturas en sistemas planetarios alrededor de otros soles y poner el Sistema Solar en un contexto galáctico.

Debido a su interés, los discos protoplanetarios se han estudiado activamente durante las últimas décadas. Misiones infrarrojas como IRAS, ISO, el Telescopio Espacial Spitzer (de ahora en adelante *Spitzer*) o el Observatorio Espacial Herschel (de aquí en adelante *Herschel*) han permitido analizar la composición y distribución del polvo para una gran cantidad de objetos. Observaciones de alta resolución de diferentes tipos (óptica adaptativa, interferometría, ...) han podido resolver estructuras en estos discos tales como cavidades o brazos espirales, así como estudiar la dinámica del gas en ellos. Más recientemente, la increíble resolución y sensibilidad de ALMA están produciendo datos con un detalle nunca antes visto que promete revolucionar el campo de la formación planetaria. Junto con importantes avances en el campo teórico, este conjunto de datos han conducido a un conocimiento global de los discos protoplanetarios y su papel en la formación de planetas de forma general. No obstante, en la actualidad existe todavía un gran número de cuestiones abiertas concernientes a estos objetos, entre otros el mecanismo (o mecanismos) responsable de la evolución de los discos, la influencia de determinados factores (tales como la masa de la estrella, su multiplicidad, o su entorno) en dicha evolución, las interacciones entre el disco y los recién formados planetas (causante en muchos casos de migraciones planetarias de varias AUs de distancia), o la posibilidad de que existan diferentes caminos evolutivos para estos objetos.

A grandes rasgos, a día de hoy se sabe que los discos protoplanetarios sobreviven unos diez millones de años a lo sumo, con un tiempo característico de alrededor de tres

millones de años. En esta fase, la estrella incorpora material de las zonas internas del disco, que es remplazado por material de las zonas externas. En algún momento de su vida el disco empieza a evolucionar: ya sea debido a la fotoevaporación producida por la radiación de la estrella, al efecto de una compañera estelar o subestelar, o al propio proceso de formación planetaria (entre otras opciones), el disco comienza a dispersarse. A estos objetos en aparente proceso de transformación se les denomina *discos de transición*, y son el foco de gran cantidad de estudios por razones obvias: si la formación planetaria es la causante de la evolución de (algunos) discos, entonces los discos de transición son el lugar idóneo para encontrar embriones planetarios o planetas recién formados. Este proceso de transición es relativamente rápido (alrededor de un millón de años), y da paso a un disco mucho menos masivo y pobre en gas, compuesto principalmente de planetesimales y asteroides: un disco de *debris*.

En este marco, la presente tesis busca estudiar en más detalle las diferentes escalas de tiempo en la evolución de los discos protoplanetarios. Se prestará especial atención al tratamiento de los datos para garantizar que la muestra utilizada es lo más homogénea posible, teniéndose en cuenta también el efecto de diferentes sesgos. Adicionalmente, se estudiarán datos de *Herschel* de la región de formación estelar Camaleón I, centrándonos sobre todo en lo que este telescopio puede añadir a nuestro conocimiento sobre los discos de transición.

0.1 Objetivos principales de la tesis

Los objetivos principales de este tesis son:

- Estudiar de forma homogénea la evolución de discos protoplanetarios en regiones de formación estelar cercanas. Analizando la fracción de discos en cada región en función de su edad es posible estimar el tiempo de vida de estas estructuras. A pesar de que este tipo de estudios ya existen en la literatura, la gran mayoría de ellos ha utilizado datos provenientes de catálogos y artículos con diferentes límites de completitud y criterios de selección, lo que puede afectar a los resultados. Con una muestra suficientemente grande y limpia, es posible también estudiar la influencia de la masa de la estrella en la evolución de los discos, que puede generar importantes diferencias en las poblaciones de exoplanetas alrededor de estrellas de baja y alta masa (estrellas T Tauri y Herbig Ae/Be respectivamente, con la separación en masa a $\sim 2\,M_{\odot}$). Posteriormente a dicho estudio, utilizaremos el conocimiento adquirido para tratar de entender el posible impacto de los resultados en la formación de sistemas planetarios.
- Además, se analizarán los datos de *Herschel* de la región de formación estelar Camaleón I, en particular enfocándonos en los discos de transición de la región. Utilizando una lista de objetos de este tipo previamente conocidos, podemos estudiar los datos del infrarrojo lejano en comparación con los de discos protoplanetarios y buscar posibles indicadores de evolución en objetos transicionales. El modelado de los discos de transición incluyendo observaciones de *Herschel* y utilizando métodos de análisis Bayesiano y Cadenas de Markov Monte Carlo permitirá también cuantificar la información que dichos datos aportan al proceso, y en particular estudiar su impacto en las incertidumbres de los parámetros modelado.

Estos dos objetivos son complementarios, proporcionando a la vez una visión global de la evolución de los discos protoplanetarios que permite extraer resultados extrapolables a otros ámbitos de la astrofísica, y un análisis más detallado de los discos de transición en una región concreta que permite obtener detalles de la física de los discos inasequibles a los estudios más generales.

0.2 Planteamiento y metodología

Para evitar problemas de completitud y sesgos en el estudio de evolución de discos protoplanetarios, se reunirá una base de datos de objetos estelares pertenecientes a 22 regiones de formación estelar jóvenes (< 100 millones de años) y cercanas ($< 500\,\mathrm{pc}$). Dicha base de datos contendrá objetos de diferentes estudios de poblaciones estelares en las regiones consideradas. Para incluir un objeto en el estudio será necesario que

exista en la literatura una medida espectroscópica de su tipo espectral, evitando así la contaminación por estrellas gigantes rojas y fuentes extragalácticas que suponen un problema para muestras seleccionadas fotométricamente. Posteriormente se cruzará la base de datos con varios catálogos fotométricos cubriendo desde el ultravioleta cercano al infrarrojo medio. Una vez ajustada la extinción interestelar al tipo espectral correspondiente, este proceso producirá distribuciones espectrales de energía para cada objeto, que pueden ser utilizadas para detectar la presencia de material circumestelar mediante la identificación de excesos infrarrojos. A continuación se tendrán en cuenta los posibles sesgos en la muestra para corregir sus efectos. Hecho esto, se calcularán las fracciones de discos protoplanetarios en cada región y se ordenarán en función de su edad, de forma que podamos estudiar su evolución temporal. Posteriormente, se utilizarán isocronas para determinar la masa de las estrellas en la muestra y poder así analizar la presencia o ausencia de tendencias con dicho parámetro.

En el caso de los discos de transición de Camaleón I, se compilará una lista de objetos jóvenes conocidos en la región. Será necesario procesar los datos de *Herschel* para obtener después la fotometría correspondiente de estos objetos. A continuación se complementarán estos datos con fotometría de otros catálogos. De esta forma podrá hacerse una comparación directa entre las distribuciones de energía de los discos protoplanetarios y de transición, identificando posibles diferencias. Un siguiente paso será combinar el código de modelado de discos MCFOST junto con métodos de análisis Bayesiano para estimar el impacto de los datos de *Herschel* en el proceso. Para que esta metodología sea computacionalmente eficiente, se emplearán Cadenas de Markov Monte Carlo en el modelado.

0.3 Resultados de la tesis

Los resultados de esta tesis han sido presentados en forma de tres artículos publicados (Ribas et al. 2013, 2014, 2015), y un artículo adicional en preparación. A continuación se presenta un resumen de los puntos más significativos.

0.3.1 Evolución de discos

– La base de datos de objetos estelares jóvenes producida contiene más de 2 300 objetos con estimación espectroscópica de su tipo espectral, así como un valor de su extinción y fotometría en hasta 35 bandas diferentes en algunos casos, cubriendo desde el ultravioleta cercano hasta el infrarrojo medio. Cada distribución espectral de energía ha sido inspeccionada visualmente para descartar aquellos datos con problemas obvios (saturación, contaminación por objetos cercanos,...), generando la que seguramente es la muestra más completa de objetos jóvenes en regiones de formación estelar hasta la fecha. Independientemente de los resultados científicos

de la tesis, dicha base de datos tiene un inmenso valor para futuros estudios estadísticos, y será puesta a disposición de la comunidad en un futuro.

- Las fracciones de discos protoplanetarios obtenidas revelan un tiempo de vida característico de entre 2.4 y 4 millones de años (dependiendo de la longitud de onda utilizada para detectar discos), y un límite de unos ~ 10 millones de años en el tiempo total de vida de los discos. Este resultado está en acuerdo con estudios anteriores, pero es significativamente más robusto gracias al gran tamaño de la muestra utilizada, el tratamiento homogéneo y la consideración de posibles sesgos en el análisis.

- Encontramos indicios de que los excesos en el infrarrojo cercano desaparecen ligeramente antes y/o más rápido que en longitudes de onda más largas (con diferencias en sus tiempo de vida característico de entre 0.5 y 1 millones de años). A pesar de que los resultados no son estadísticamente concluyentes, esto coincide con un proceso de dispersión de discos de dentro a fuera, tal y como se espera si el mecanismo de evolución es la fotoevaporación (en la actualidad, la comparación de observaciones con modelos parece indicar que este es el proceso dominante). Además, la pequeña diferencia entre los tiempos característicos sugieren que la dispersión del disco, independientemente de su origen, ocurre de forma rápida ($\sim$ 1 millón de años).

- Encontramos un nivel aproximadamente constante de discos evolucionados (de transición y debris) de un $\sim 10\,\%$, independientemente de la edad de las regiones. Para regiones jóvenes (< 10 millones de años), la gran mayoría de estos discos son discos de transición. Este resultado, coincidente también con estudios previos, puede combinarse con el tiempo máximo de vida de los discos (~ 10 millones de años) para estimar el tiempo que pasan los discos en la fase transicional, obteniéndose un valor de un millón de años en acuerdo con el punto anterior. Este valor debe ser tratado con cautela ya que asume que todos los discos protoplanetarios pasan por una fase de transición, algo que puede no ser cierto.

- Quizás el resultado más innovador de la tesis sea la evidencia más robusta hasta la fecha de una dependencia de la evolución de los discos con la masa de su estrella huésped. Encontramos que las estrellas T Tauri entre 1-3 millones de años tienen un 60-65 % de discos protoplanetarios, frente a un 40 % en estrellas Herbig Ae/Be. Para edades más avanzadas (entre 3 y 11 millones de años), un 20 % de estrellas T Tauri mantienen sus discos protoplanetarios, pero no es posible encontrar ninguno alrededor de estrellas Herbig Ae/Be. El análisis de estos resultados demuestra que la diferencia es estadísticamente significativa. Combinado con resultados en regiones más jóvenes ($<$1 millón de años), los resultados sugieren que los discos protoplanetarios evolucionan independientemente de la masa estelar durante el primer millón de años de su vida, y de ahí en adelante se ven afectados por este parámetro.

– Al dividir la base de datos en función de la masa estelar, también encontramos un valor constante de discos evolucionados independientemente de la edad: un 5-15 % de estrellas T Tauri y un 20-30 % de estrellas Herbig Ae/Be están rodeadas de discos de transición o debris. Aunque varios estudios indican que la incidencia de discos de debris es mayor alrededor de estrellas masivas, en el caso de nuestro análisis esto puede deberse a que existan dependencias importantes entre la región del disco que emite a una cierta longitud de onda y la masa de la estrella.

– La dependencia del tiempo de vida de los discos protoplanetarios con la masa de la estrella puede jugar un papel fundamental en la formación y evolución de sistemas planetarios, reduciendo el tiempo disponible para formar planetas alrededor de estrellas Herbig Ae/Be en comparación con objetos T Tauri. Además, la migración de planetas causada por su interacción con el disco también actuará durante períodos más cortos en estrellas masivas, pudiendo así producir diferentes poblaciones de exoplanetas en estrellas de diferentes masas e incluso explicar, al menos en parte, la aparente falta de planetas tipo *hot Jupiter* alrededor de estrellas con masas $M > 1.5\,M_{\odot}$.

0.3.2 Discos de transición en Camaleón I con *Herschel*

– Utilizando fotometría de los instrumentos PACS y SPIRE de *Herschel*, se exploraron las poblaciones de objetos jóvenes en las regiones de formación estelar Camaleón I y II. Se analizó en particular la población de discos de transición en la región. Todos los discos de transición detectados se encuentran en la región de Camaleón I. Se demostró que combinando datos en infrarrojo medio ($\sim 10\,\mu$m) con los flujos a $70\,\mu$m de *Herschel* se pueden identificar eficientemente discos con una pendiente pronunciada en su distribución espectral de energía, una característica típica de los discos de transición. Debido a la gran cantidad de observaciones realizadas por este telescopio, este método es especialmente útil cuando no existen datos a longitudes de onda más allá de $10\,\mu$m (por ejemplo de los instrumentos IRS o MIPS de *Spitzer*). Dicho proceso ha sido aplicado con éxito posteriormente en Lupus (Bustamante et al. 2015) y Ophiuchus (Rebollido et al., submitted), e incluso ha permitido encontrar un nuevo candidato en esta última región.

– Los flujos obtenidos para los seis discos de transición detectados y que cumplen el criterio de identificación propuesto se compararon con los flujos de discos protoplanetarios en la región, encontrándose que todos los objetos transicionales mostraban pendientes más pronunciadas en el infrarrojo lejano, además de excesos a $70\,\mu$m por encima del tercer cuartil de los discos protoplanetarios. Este hecho puede indicar un cierto confinamiento de la masa en regiones intermedias de los discos de transición. Aunque se han encontrado resultados similares en otras

regiones, hasta el momento la evidencia de este fenómeno es marginal y debe ser estudiado en más profundidad.

– El análisis Bayesiano combinando Cadenas de Markov Monte Carlo con MCFOST para tres discos de transición demuestra que los datos de *Herschel* pueden utilizarse para estimar la masa de los discos con incertidumbres de aproximadamente un orden de magnitud si disponemos de datos hasta 500 μm. Además, el radio interno de los discos queda determinado con mayor precisión utilizando dichos datos. Los valores obtenidos en los modelos están en concordancia con resultados previos existentes en la literatura. Estimamos que el procedimiento utilizado es al menos 100 veces más rápido que el método habitual de generar una red de modelos fija, y tiene un gran potencial para futuros análisis de grandes muestras. Debido a la gran cantidad de datos de *Herschel* existentes, supone también un ahorro sustancial en la cantidad de tiempo observacional necesario para estimar la masa de objetos en regiones de formación estelar, ya que en muchos casos podrá medirse la masa realizándose un estudio similar al aquí presentado sin necesidad de observaciones submilimétricas adicionales desde tierra.

– Los valores de masas de polvo obtenidos para los tres discos de transición modelados son similares a los encontrado en otros estudios para discos protoplanetarios. Aunque debido a la gran dispersión e incertidumbres en estas medidas no es posible hacer una afirmación robusta, si esta tendencia ya encontrada por otros autores es real (que los discos de transición son tanto o más masivos que los protoplanetarios) esto podría dar indicaciones del origen de la fase de transición: dado que estos objetos han perdido parte de su masa para alcanzar su estado actual, sus discos primigenios han de ser incluso más masivos. Es posible entonces que los discos de transición sean el resultado de discos protoplanetarios con una gran cantidad de masa que han formado varios planetas gigantes, explicando así las cavidades observadas en ellos.

– El modelado indica también que los discos de transición tienen o bien menos acampanamiento en su estructura, o perfiles de densidad más extremos, dando cuenta así de la pronunciada pendiente en la zona del infrarrojo lejano de sus distribuciones espectrales de energía. El primer caso podría señalar que estos discos han sufrido sedimentación del polvo hacia su plano medio, mientras que el segundo sugiere un apilamiento de masa en regiones intermedias del disco. Ambos resultados están en línea también con otros trabajos previos, aunque la evidencia obtenida únicamente con el modelado de fotometría de *Herschel* es aún estadísticamente poco significativa.

0.4 Trabajo y líneas de investigación futuras

La muestra compilada de objetos estelares jóvenes es una herramienta única que puede utilizarse para una gran variedad de análisis estadísticos, proporcionando una base sólida para futuros estudios de poblaciones estelares y evolución de discos protoplanetarios. Por ejemplo, estudios sobre la supervivencia de discos en presencia de fuertes campos de radiación externos (cerca de asociaciones OB) o en entornos muy/poco poblados podrían revelar otros factores importantes en la evolución de estos objetos. Complementar dicha base de datos con espectros infrarrojos como los tomados por el instrumento IRS de *Spitzer* permitiría un estudio estadístico de la composición del polvo en discos, directamente relacionada con la composición de los planetas que se formen en ellos.

Mediante la aplicación de criterios de selección simples y combinando la base de datos con objetos en la literatura, hemos reunido una muestra de unos 100 discos de transición con distribuciones espectrales de energía que sugieren la presencia de un agujero en su disco, además de otros ~ 50 objetos con posible evolución por sedimentación de polvo hacia su plano medio. En la actualidad, estamos incluyendo los espectros IRS de dichas fuentes para realizar un estudio sistemático de las propiedades de los discos, analizando por ejemplo los diferentes tamaños de sus agujeros para compararlos con las órbitas de exoplanetas conocidos.

El modelado Bayesiano de discos de transición con datos de *Herschel* ha revelado que la fotometría en longitudes de onda submilimétricas del instrumento SPIRE permite estimar la masa de polvo de los discos con una incertidumbre de un orden de magnitud. A pesar de que estas medidas pueden mejorarse con información a longitudes de onda mayores (milimétricas), en muchos casos dichas medidas no existen en la literatura. La combinación de la base de datos con observaciones del telescopio *Herschel* no solo producirá una gran cantidad de distribuciones espectrales de energía completas desde el ultravioleta cercano hasta el infrarrojo lejano, sino que abre la posibilidad de estudiar la distribución de masas de discos con un tamaño de muestra sin precedentes hasta el momento.

Los resultados de esta tesis demuestran que un tratamiento homogéneo de una gran cantidad de datos públicos junto con procedimientos de modelado optimizados para grandes muestras (p.e., Cadenas de Markov Monte Carlo) tienen un potencial enorme para extender nuestro conocimiento de los discos protoplanetarios y su relación con la población de exoplanetas. Dado el creciente número de catálogos públicos y el gran tamaño de archivos científicos como el de *Herschel*, la utilización de estos métodos puede revelar nuevas tendencias en diferentes parámetros de los discos protoplanetarios.

En el futuro cercano, el camino más prometedor para explotar la presente base de datos son las observaciones del telescopio ALMA. Dadas su resolución y sensibilidad, un seguimiento de los objetos más interesantes revelará la estructura y evolución de los

discos en muchísimo más detalle que cualquier trabajo previo. ALMA puede resolver estructuras en los discos que no son identificables en distribuciones espectrales de energía, así como trazar la dinámica del gas e incluso mostrar la posición de la línea de hielo (la distancia a la cual el gas puede formar hielo alrededor de los granos de polvo, facilitando enormemente la formación de planetas). Junto con la información en la base de datos y el estudio mineralógico a partir de espectros de IRS, los datos de ALMA completarán una visión pancromática de los discos protoplanetarios, ayudando así a entender mejor la génesis planetaria.

Universidad Autónoma de Madrid
Facultad de Ciencias Físicas
Department of Theoretical Physics

Protoplanetary disk evolution in nearby star-forming regions

Thesis supervised by

PhD. Bruno Merín Martín and **PhD. Hervé Bouy**

A dissertation submitted by

Álvaro Ribas Gómez

for the degree of Doctor in Physics

Madrid, June 2015

Abstract

The main aim of this work is to better understand the evolution of protoplanetary disks around young stars in the solar neighborhood. It comprises three first authored published papers, a fourth paper about to be submitted, and additional research as participation in six other refereed papers, which I coauthored during the period of this thesis.

To asses disk evolution homogeneously, we compile a large sample of more than 2 300 members of 22 young (< 100 Myr) nearby (< 500 pc) star-forming regions and associations. All these objects have spectroscopic confirmation of membership to their host young association and measurements of their spectral types, which is complemented with photometry from up to 35 different filters covering from near ultraviolet to mid-infrared wavelengths. After considering possible biases, we consistently estimate the fraction of disks as a function of age. We obtain a characteristic disk lifetime of $\sim$3 Myr, in agreement with previous studies. We also find that disk dispersal occurs in ~ 1 Myr and tentative evidence of this process acting from inside out, suggesting that photoevaporation plays an important role in disk evolution. The unprecedented size of this sample provides the most robust confirmation up to date of a dependence of disk evolution with stellar mass, with T Tauri stars maintaining their disks for longer periods than Herbig Ae/Be stars. This result may have an important influence on planet formation and exoplanetary populations. It may also represent the first direct link achieved between a statistical property of protoplanetary disks and a statistical property of the exoplanetary systems at later phases, and constitutes one of the big new results from this thesis.

We also explore the population of young disks in the Chamaeleon star-forming complex with *Herschel* data, in particular focusing on transitional disks in Chamaeleon I. We find that the six transitional targets in the sample detected with *Herschel* have 70 μm excesses higher than 75 % of the Class II objects in the region. Further modeling of these disks reveals that *Herschel* SPIRE photometry can be used to efficiently constrain the mass of dust in these sources, one of the most relevant parameters for planet formation. The modeling also shows evidence for anomalous outer regions of transitional objects when compared to full protoplanetary disks.

Contents

List of Figures

List of Tables

Abbreviations

ADI	**A**ngular **D**ifferential **I**maging
ALMA	**A**tacama **L**arge **M**illimeter **A**rray
AU	**A**stronomical **U**nit
CA	**C**ore **A**ccretion
CTTS	**C**lassical **T** **T**auri **S**tar
DI	**D**isk **I**nstability
FIR	**F**ar-**I**nfra**R**ed
FWHM	**F**ull **W**idth at **H**alf **M**aximum
HST	**H**ubble **S**pace **T**elescope
IR	**I**nfra**R**ed
IMF	**I**nitial**M**ass **F**unction
IRAS	**I**nfra**R**ed **A**stronomical **S**atellite
IRS	**I**nfra**R**ed **S**pectrograph
ISO	**I**nfrared **S**pace **O**bservatory
MCMC	**M**arkov **C**hain **M**onte **C**arlo
MIR	**M**id-**I**nfra**R**ed
MMSN	**M**inimum **M**ass **S**olar **N**ebula
NIR	**N**ear-**I**nfra**R**ed
PACS	**P**hotoconductor **A**rray **C**amera and **S**pectrometer
PSF	**P**oint **S**pread **F**unction
PDF	**P**robability **D**ensity **F**unction
SAM	**S**parse **A**perture **M**asking
SDI	**S**imultaneous **D**ifferential **I**maging
SED	**S**pectral **E**nergy **D**istribution

SPIRE **S**pectral and **P**hotometric **I**maging **RE**ceiver

WTTS **W**eak-lined **T** **T**auri **S**tar

YSO **Y**oung **S**tellar **O**bject

1

Introduction

Understanding our origins has been one of the biggest human quests since the dawn of mankind. In particular, the possibility of other habitable (or even inhabited) worlds is a fascinating thought that has captured human imagination for thousands of years. During the last two decades, we have gone from no known planet outside our Solar System to more than 1 800 worlds around other suns as of this writing, with a diversity greatly beyond our most optimistic expectations. Not only do these distant and exciting planets bring the promise of unprecedented, revolutionary discoveries, but they also hold clues to our own existence allowing to put the Solar System in a a galactic context. For these reasons, understanding the conditions and processes involved in the formation of planetary systems is extremely important, both from the scientific and philosophical perspectives.

In this work, we study different aspects of the evolution of protoplanetary disks (the place of planet formation) in the solar neighborhood. We have compiled a large sample of spectroscopically confirmed young stellar objects in well known nearby star-forming regions and complemented it with multi-wavelength photometry from several catalogs, covering from the near ultraviolet to the mid-infrared. We then applied a homogeneous treatment to all the sources. This sample, together with statistical analyses, allows to consistently study protoplanetary disk lifetimes and their dependence with stellar mass, which may have important consequences for planetary populations. We also use data from the Herschel Space Observatory (*Herschel*) to analyze in greater detail the population of the transitional disks (disks with hints of on-going planet formation) in the Chamaeleon I molecular cloud, and determine the conditions of their outer regions with *Herschel*'s far-infrared (FIR) data

This chapter provides a general introduction to the characteristics and evolution of protoplanetary disks. It contains a general perspective of the history of the field, a

description of the most important parameters of their architecture, and a global view of the current understanding of disk evolution.

1.1 Historical and observational perspectives

Observationally, the fact that T Tauri stars (young, low-mass stars with strong emission lines in their spectra, Joy 1945; Herbig 1962) display excess above photospheric levels both at the ultraviolet and near-infrared (NIR) regimes was first noted in the fifties in color-magnitude diagrams of young clusters (e.g., Walker 1956, 1957, 1959), and later confirmed in dedicated NIR observations (e.g., Mendoza V. 1966, 1968). In a beautiful theoretical study, Lynden-Bell & Pringle (1974) studied several aspects of viscous disks and found them to be a promising explanation for the observed properties of several young stellar objects (YSOs). However, several other explanations could also be given to this phenomenon. Due to the instrumental restrictions to perform infrared (IR) observations for wavelengths $> 10\,\mu$m from ground-based observatories at the time, little data were available and it took one whole decade to get this theory confronted with new data. Using the Kuiper Airbone observatory, Cohen (1983) managed to measure 50 and $100\,\mu$m fluxes for the HL Tau protoplanetary disk, finding strong IR excess with respect to the photosphere and proposing that it could arise from an edge-on disk surrounding this source. That same year, the *IRAS* mission (Neugebauer et al. 1984) was launched, providing the first mid-infrared (MIR) and FIR survey of the whole sky (at 12, 25, 60 and $100\,\mu$m) and opening a completely new wavelength range for new discoveries. Among its large number of findings, IRAS provided evidence of the presence of a debris disk around Vega (Aumann et al. 1984), which was first interpreted as emission from a surrounding shell rather than a disk. Beall (1987) and Adams et al. (1987) found that IRAS observations of YSOs could be easily explained by the disk model in Lynden-Bell & Pringle (1974), and afterwards Adams et al. (1988) noted that a flat-disk model was not completely accurate, since its outer regions had to be slightly warmer to properly reproduce the observed FIR fluxes (the first indication of flaring in disks). Using data from the *IRAS* catalog together with ground-based observatories, Cohen et al. (1989) and Strom et al. (1989) performed the first statistical study of the circumstellar disk population in the Taurus-Auriga region, finding them to be common around YSOs. Beckwith et al. (1990) later found a similar trend using 1.3 millimeter (mm) observations. At the same time, other data were also pointing in the same direction: polarization observations around YSOs by Elsasser & Staude (1978) found a high level of polarized light around these objects, suggesting the presence of dust grains symmetrically arranged around stars. MIR spectroscopy of YSOs revealed silicate emission and absorption features around these objects, giving an indication of the composition of the dust and suggesting that these materials are confined in flattened, disk-like structures, rather than distributed in envelopes. Also, collimated jets

discovered in YSOs pointed to preferential axes in these systems (e.g., Mundt & Fried 1983). Although indirect, evidences of the existence of circumstellar disks were starting to accumulate.

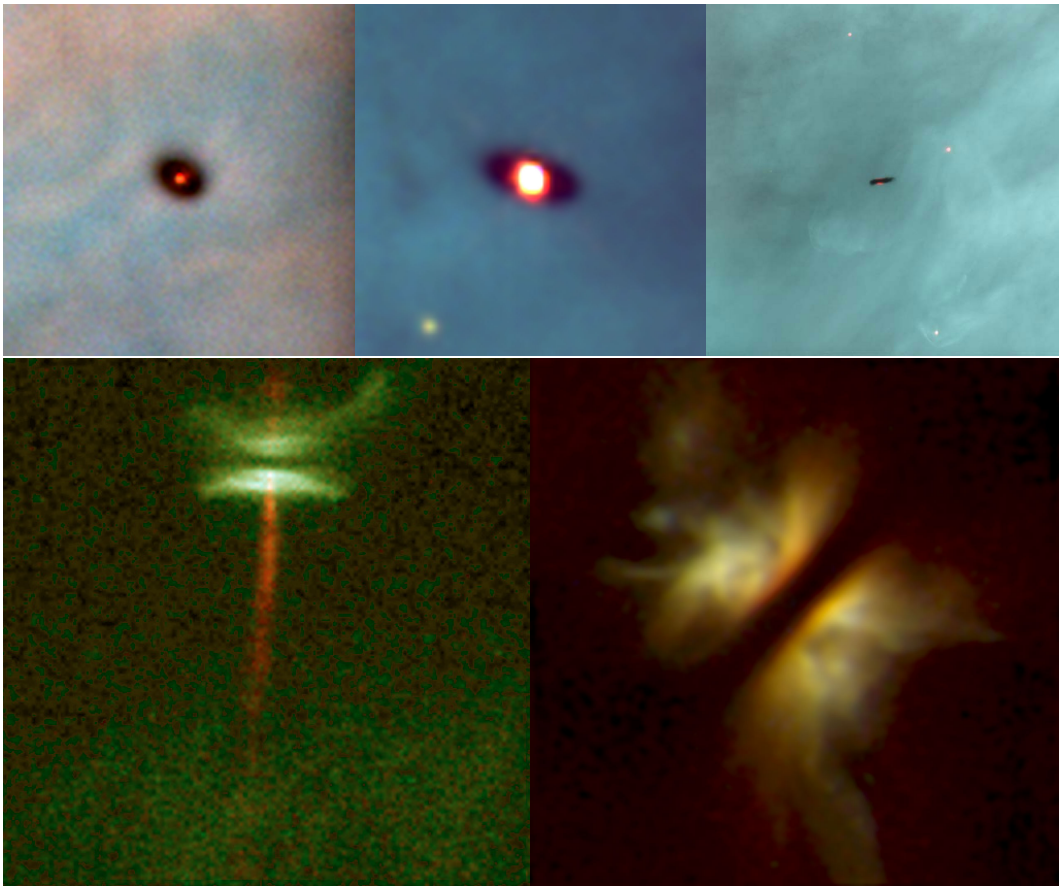

FIGURE 1.1: Top: protoplanetary disk silhouettes in Orion, as observed by *HST* (O'dell & Wen 1994). Bottom: *HST* observations of the HH 30 (left, Burrows et al. 1996) and IRAS04302+2247 (right, Padgett et al. 1999) edge-on disks. These images reveal their flared structures and the presence of jets in these objects. Wavelengths for all these images are optical and/or NIR.

It was through images from the *Hubble Space Telescope* (*HST*) that the predicted disk structure was confirmed. Because of their high opacities, disk silhouettes could be clearly seen in front of the reflection nebula in Orion (O'dell & Wen 1994; McCaughrean & O'dell 1996, see Fig. 1.1). Additional observations of edge-on disks such as HH 30 (Burrows et al. 1996) or IRAS 04302+2247 (Padgett et al. 1999) also confirmed that disks have a certain degree of flaring.

The field of protoplanetary disks experienced a significant expansion with the advent of new observing facilities and surveys with better sensitivity, spatial and spectral resolution, and coverage. The Infrared Space Observatory (*ISO*, Kessler et al. 1996) and specially the Spitzer Space Telescope (*Spitzer*, Werner et al. 2004) yielded MIR observations for thousands of objects, increasing the amount of available data and producing a full, general picture of protoplanetary disks in several star-forming regions (*c2d Spitzer Legacy*

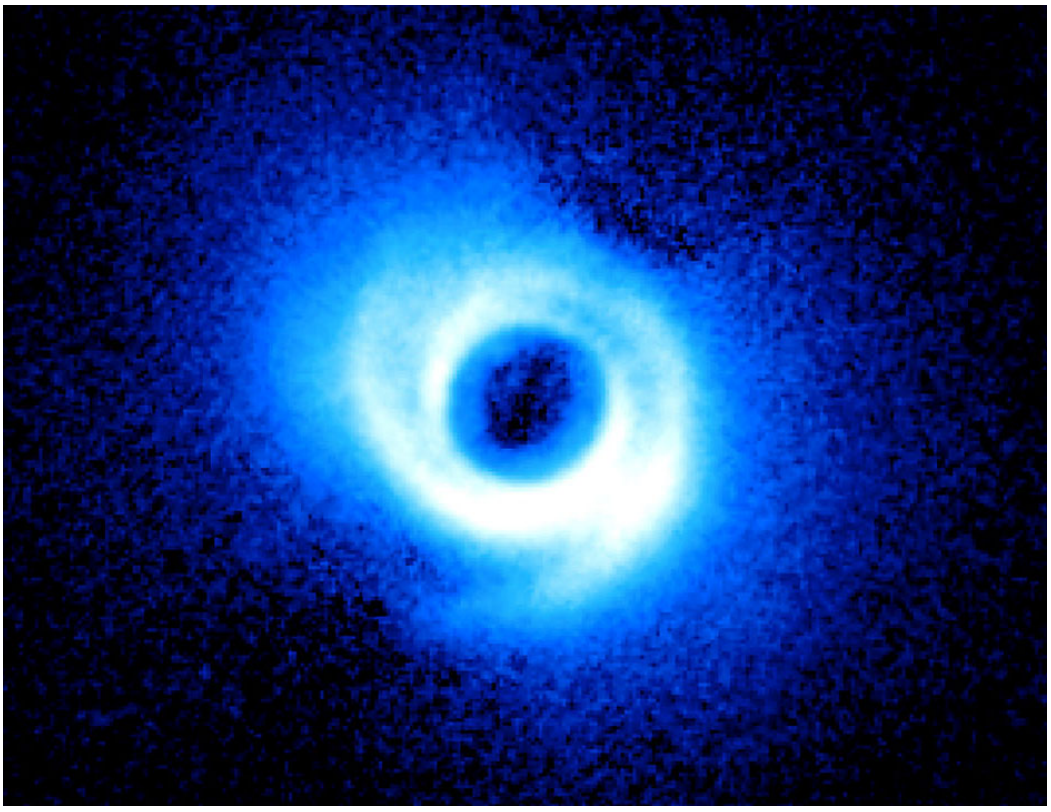

FIGURE 1.2: The SAO 206462 disk as seen in the H band by the HiCIAO instrument at the Subaru Telescope, revealing spiral arms in its structure. These features may be produced by the influence of young planets inside protoplanetary disks. (Muto et al. 2012)

Program, Evans et al. 2009). Interferometric observations in the (sub)mm regime also improved, resolving fainter, smaller structures in disks (e.g., Andrews et al. 2011). Advanced observing techniques such as Sparse Aperture Masking (SAM), spectro-astrometry, and Angular and Simultaneous Differential Imaging (ADI, SDI) are revealing the morphology of these disks with unprecedented detail (e.g., Huélamo et al. 2011; Muto et al. 2012; Cieza et al. 2013; Close et al. 2014, see Fig. 1.2). The AKARI satellite (Murakami et al. 2007) covered the sky from 9 to 180 μm, completing the spectral energy distributions (SEDs) of a large number of sources into the FIR regime. Later, FIR *Herschel* observations covered large areas of the sky and probed the emission from dust and gas in the outer regions of these disks (e.g., Dent et al. 2013). Finally, the incredible resolving power and sensitivity of ALMA will completely revolutionize the whole field in the following years, and has already traced dust traps (van der Marel et al. 2013) and flows of gas in the inner regions of circumstellar disks (Casassus et al. 2013).

For interested readers, the history of this field can be studied in much more detail following publications in the *Protostars and Planets* series, which is held periodically and reviews the current understanding of protoplanetary disks within the star and planet formation context (e.g., Dutrey et al. 2014; Alexander et al. 2014; Espaillat et al. 2014).

1.2 Protoplanetary disks

Protoplanetary disks are rotating, optically thick disks of gas and dust that can be found around young stars (< 10 Myr, e.g., Hernández et al. 2007a, 2008; Mamajek 2009; Ribas et al. 2014). As described in the previous section, they have been widely studied in the past and a global understanding of these objects already exists. Here we describe some of their general properties and evolutionary mechanisms relevant for this work.

1.2.1 Protoplanetary disk formation

Circumstellar disks appear during star formation as a natural consequence of angular momentum conservation. Star formation occurs during the fragmentation of molecular clouds when they become gravitationally unstable, possibly by an external perturbation (e.g., a supernova explosion). As this contraction takes place, sub-regions of the cloud satisfy the Jeans criterion themselves and fragment into smaller, collapsing regions known as pre-stellar cores. These objects have masses between a fraction and some solar masses (e.g., Enoch et al. 2008), and are the precursors of stellar systems (see Li et al. 2014, for a recent review on this topic).

Any initial rotation of the core is tremendously magnified during the contraction to preserve angular momentum, creating a rotating disk around the forming star early in this process (~ 0.5 Myr, Evans et al. 2009). At this point, the star-disk system is still surrounded by a massive, infalling envelope of material (see Fig. 1.3). The initial disk grows rapidly in radius as material from the envelope is accreted onto the disk (Terebey et al. 1984). However, observations reveal that the disk mass remains almost constant once the disk has formed, pointing to a fast transport of material from the disk to the star (Looney et al. 2003; Jørgensen et al. 2009). After ~ 1 Myr, the envelope has been completely dispersed by the mentioned accretion process and possible outflows in the system, leaving a young star with an optically thick disk of gas and dust: a protoplanetary disk.

A complete characterization of this evolutionary stage remains elusive. The envelope reprocesses the emission from the disk at short wavelengths and completely dominates the flux at longer ones, making it extremely challenging to directly observe the disk at this point. Moreover, the formation of a rotationally supported disk from core collapse is not trivial: cores are known to have significant magnetic fields (e.g., Troland & Crutcher 2008; Crutcher 2012; Stephens et al. 2013), usually with strengths of tenths of the local gravitational field. Although not enough to drive the collapse itself, these fields may play an important role during disk formation, but their real contribution and effects are still not well known (Li et al. 2014).

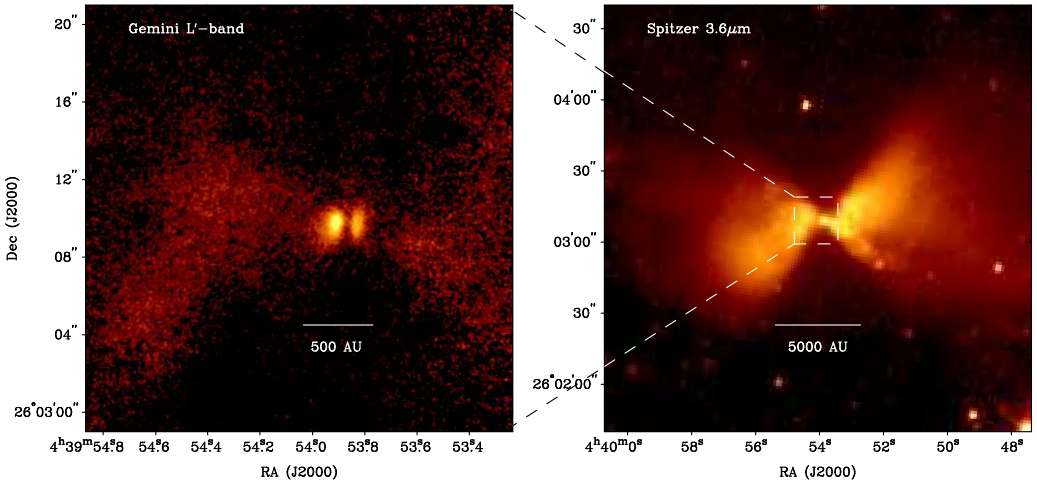

FIGURE 1.3: L' band (left) and IRAC 3.6 μm (right) images of the L1527 protostar in the Taurus star-forming region (Tobin et al. 2010). *Spitzer* images show a bipolar cavity and envelope, thousands of AU wide. Higher resolution L' band observations from the Gemini North telescope resolve the inner source and reveal a smaller disk-like structure seen close to edge-on as two main lobes, probably one of the youngest disks imaged so far.

1.2.2 Physical characteristics of protoplanetary disks

This section describes some of the most important characteristics of protoplanetary disks. A much more detailed review on this topic can be found in Dullemond et al. (2007) from the Protostars and Planets V volume.

1.2.2.1 Mass

The mass of protoplanetary disks is one of the most relevant parameters of these objects, since it represents the available mass reservoir to form planets. However, it is also one of the most difficult and complex quantities to measure given the large uncertainties in several related parameters that come into play.

Most protoplanetary disks are optically thick in a large range of wavelengths, meaning that the observed fluxes are not representative of the total amount of mass in them. However, the disk becomes optically thin at (sub)mm fluxes, and the continuum emission from cold grains provides a direct estimate of the total dust mass in the disk (Beckwith et al. 1990):

$$M_d = \frac{d^2 F_\nu}{\kappa_\nu B(T_c)}$$

where d is the distance, F_ν is the observed flux at frequency ν, κ_ν is the corresponding opacity, and $B(T_c)$ is the characteristic temperature of the dust (Hildebrand 1983). A

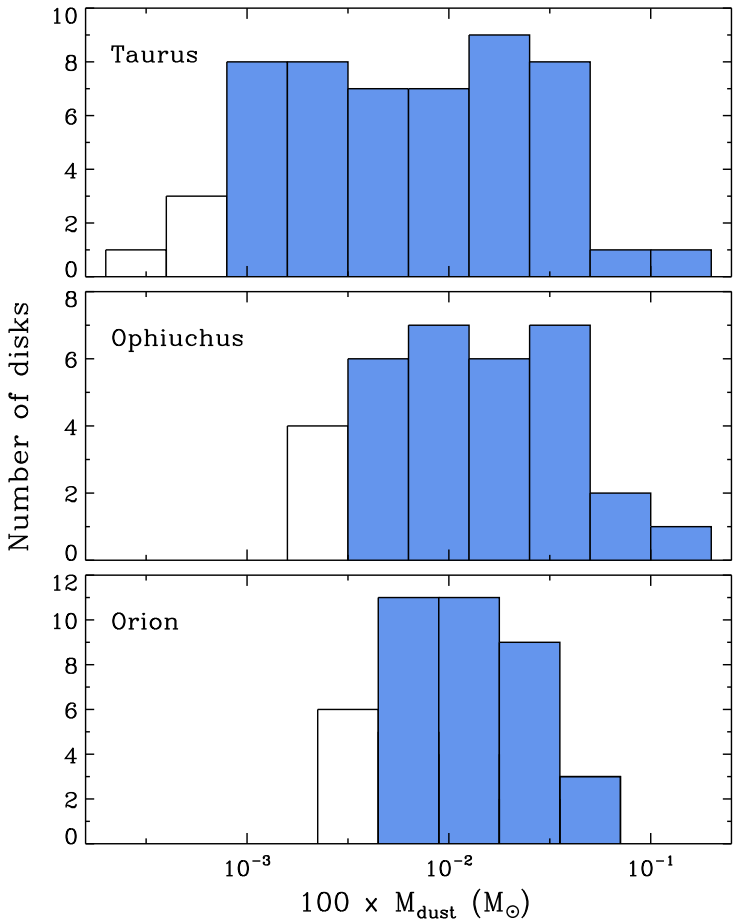

FIGURE 1.4: Observed distribution of protoplanetary disk masses (log-scale) for three star-forming regions: Taurus, Ophiuchus and σ Orionis. Filled bars show ranges where observations are complete. Disk masses were computed assuming a maximum grain size of 1 mm and a gas-to-dust ratio of 100, as shown in the x-axis. For comparison, the estimated value of the Minimum Mass Solar Nebula (the minimum mass required to form the Solar System) is $\sim 0.02\,M_{\odot}$. Figure adapted from Williams & Cieza (2011).

different approach is to develop physical disk models and compare them with observations (e.g., Calvet et al. 2002; Dullemond & Dominik 2004a; D'Alessio et al. 2006; Pinte et al. 2006). This procedure suffers from the same issue than mass estimates via monochromatic fluxes, since (sub)mm fluxes are required to put some constrains on the mass - otherwise, models are insensitive to this parameter. However, these results depend on several other (and mostly poorly constrained) parameters such as the dust composition and opacity, the surface density profile, the amount of mass hidden in large particles (which are inefficient emitters and untraceable by most observations, e.g., D'Alessio et al. 2001; Draine 2006), or the gas-to-dust ratio (usually set to 100:1 as in the interestellar medium, which is probably a naive assumption and may change significantly from one source to another, e.g., Thi et al. 2010, 2014). The combination of all these make disk mass estimates significantly uncertain.

Despite these limitations, several studies have probed dust masses, mainly using (sub)mm data. Beckwith et al. (1990) performed the first large survey of 1.3 mm observations of the Taurus-Auriga region, later extended by Andrews & Williams (2005) in the same region, and in the Ophiuchus molecular cloud by Andrews & Williams (2007). Their results found a median disk mass around $5 \times 10^{-3} M_{\odot} - 1 \times 10^{-2} M_{\odot}$ in these regions, but with a large dispersion (see Fig. 1.4). Additional studies have also revealed that the disk mass typically scales with that of the stellar host, following $M_d/M_* \sim 0.001 - 0.01$ (Andrews et al. 2013; Mohanty et al. 2013). These values are consistent with gravitationally stable disks, i.e., disks with masses not enough to produce important gravitational self-perturbations of themselves (gravitational instabilities require disk masses $\sim 10\,\% \, M_*$ or higher, Lodato et al. 2005).

Finally, it is also interesting to compare these values with the minimum mass solar nebula (MMSN): the disk from which the Solar System formed (Weidenschilling 1977; Hayashi 1981). Rough estimates for the total disk mass required to form a planetary system like our own yield values of $M \sim 0.02\, M_{\odot}$. When confronted with the formerly mentioned measurements protoplanetary disks masses, this suggests that approximately half of the observed YSOs have the potential to develop complete planetary systems like the Solar System. Those with lower masses, however, may also be capable of forming smaller and/or less planets, producing a large variety of planetary architectures around other stars.

1.2.2.2 Inner radius and size

Protoplanetary disks do not reach the surface of their stellar hosts. Instead, they are truncated at a given distance, usually of the order of tenths of an AU. There are two main reasons which are thought to produce this effect:

- Dust sublimates above a given temperature value. The temperature at which this occurs depends on the dust composition, but canonical values for astronomical silicates are in the range of 1400-1500 K. The star-disk distance at which this occurs is known as the *sublimation radius*, and marks the limit at which dust can survive. Because such high temperatures are only reached in the very inner regions of disks, the sublimation radius can only be measured with high resolution interferometry (e.g., Eisner et al. 2005) or modeling of the observed fluxes (e.g., Muzerolle et al. 2003a). These techniques have revealed a good agreement between the observed location of the sublimation radius and theoretical predictions.

- For radii below the sublimation radius, matter can only exist in gaseous form. However, the resulting gaseous inner disk is also truncated at shorter distances due to the magnetic field of the star: at the point where the force of infalling material is overcome by the stellar dipole field, material is accreted onto the star

following the magnetic field lines (e.g., Koenigl 1991). The radius at which this force balance is reached is the *magnetospheric truncation radius*, and its value is usually of a few stellar radii. As in the previous case, gas velocity observations of protoplanetary disks (e.g., CO, Carr 2007) agree with the expected values.

As formerly mentioned, AU-scale structures can only be observed with very high spatial resolution (milliarseconds) even for the closest star-forming regions such as Taurus or Ophiuchus, and direct imaging these structures is beyond the resolution limit in most cases. For this reason, our current knowledge of the real shape and structure of the inner regions of disk comes mainly from models rather than direct detections. Also, the inner radius appears to be much larger than the sublimation radius in some cases. These disks are known as transitional disks, and are particularly interesting for reasons that will be described later in this thesis.

Because the outer regions of disks are very tenuous (see Sect. 1.2.2.3), disk sizes (or outer radius) are also hard to measure. This parameter is usually explored in the mm regime, probing the coldest material in the disk. Either via interferometric imaging or gas observations (e.g., Hughes et al. 2008; Isella et al. 2009; Schaefer et al. 2009; Pineda et al. 2014), a large variety of outer radii are found, typically of some hundreds of AUs (Williams & Cieza 2011). A special mention is required for protoplanetary disk silhouettes in Orion, visible due to the H II emission nebula behind the objects. Using data from *HST*, Vicente & Alves (2005) were able to measure outer radii for 22 YSOs, ranging from 50 AU to 620 AU (see Fig. 1.1).

1.2.2.3 Scale height, disk flaring, surface density, and temperature profiles

Protoplanetary disks are quasi-stable structures, which persist in time for some Myr (e.g., Haisch et al. 2001b; Hernández et al. 2007b; Mamajek 2009; Ribas et al. 2014). This implies that they are in hydrostatic equilibrium, and the disk temperature, density and flaring are interconnected quantities in them.

After the first FIR observations of protoplanetary disks, their FIR fluxes were found to be higher than those predicted for flat disks (Rucinski 1985; Kenyon & Hartmann 1987), indicating that their outer regions were hotter than expected from the flat disk model. Disk flaring is a natural consequence of the hydrostatic equilibrium: stellar gravity confines the material in the disk, whereas thermal energy in the disk tends to expand it. With a flared geometry, the outer disk intercepts more stellar radiation, increasing its temperature and accounting for the larger FIR fluxes observed (Calvet et al. 1992). Because of this flaring, the scale height of the disk (h) increases radially, usually following a power-law dependence of the form $H(r) \propto r^h$, where the flaring index h has values between 1.1 - 1.3 (e.g., Chiang & Goldreich 1997). This value can decrease during the evolution of the disk if the dust in the system settles toward the

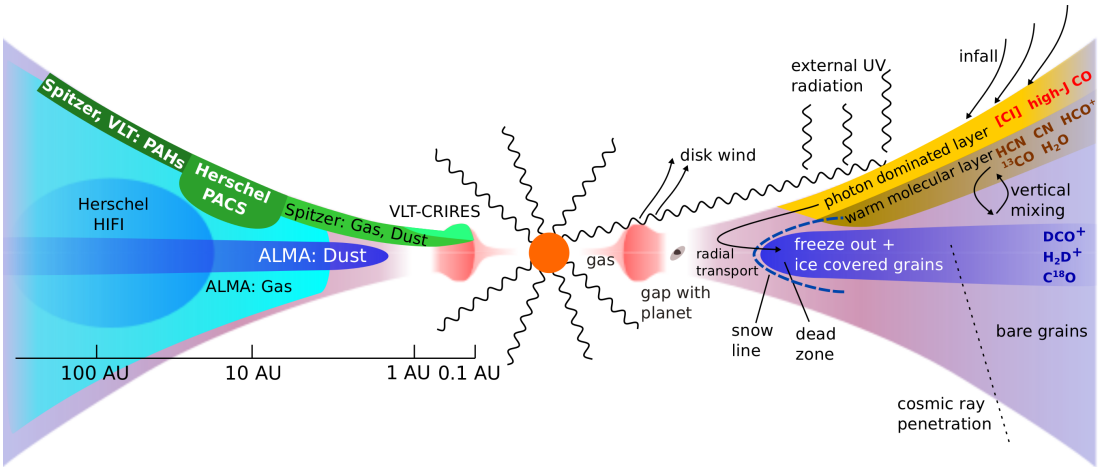

FIGURE 1.5: Schematic view of the structure of a protoplanetary disk. Some of the physical and chemical processes occurring in these objects are shown in the right side of the cartoon. The left side displays the different regions traced by several observatories/telescopes. Figure by S. Bruderer, taken from van Dishoeck (2014).

mid-plane (see Sect. 1.3). A schematic representation of the typical disk geometry is shown in Fig. 1.5.

The temperature of protoplanetary disks decreases with radius. The inner regions are closer to the star and hence hotter, reaching values above 1000 K, while the outer disk is much colder, with temperatures of tens of K. The functional form of the temperature shape with radius depends strongly on the overall characteristics and composition of these structures, and is usually assumed to follow a power-law as in the case of the flaring, $T(r) \propto r^{-q}$ (e.g., Beckwith et al. 1990).

A similar dependence is assumed for the surface density Σ (i.e., the average disk density at a given radius), $\Sigma(r) \propto r^{-p}$, with p having values between 0.5-1 (Andrews et al. 2009). This parameter has a strong impact on planet formation since it determines the amount of mass at different distances from the star (e.g., matter only exists in gaseous form in the very inner regions of the disk, and planets cannot form, whereas the decrease of density at larger distances make it extremely difficult to form large planets). When resolved (usually via high-resolution mm interferometry), the surface density of protoplanetary disks can be compared with a rough estimate of that of the MMSN by studying the masses of planets in the Solar System. These comparisons show that, in several cases, the observed surface densities are similar to that of the predicted progenitor disk of our own planetary system (see Fig. 1.6).

It should be mentioned that protoplanetary disks are significantly more complex, and other effects such as vertical temperature gradients, dust settling, or puffed-up inner rims may play an important role in the described characteristics of these objects. Much more detailed discussion on this is available in the literature, for example in the Protostars and Planets V reviews by Najita et al. (2007) and Dullemond et al. (2007), and in the

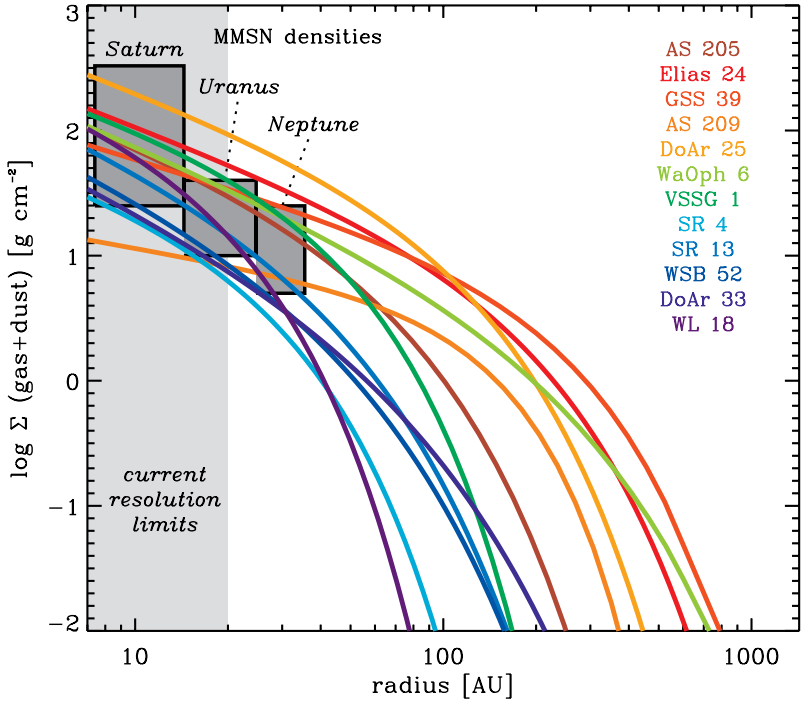

FIGURE 1.6: Comparison of the observed surface density values (colored solid lines) for several objects with the estimated MMSN values for the giant planets in the outer Solar System (gray boxes). The values are compatible in several cases, revealing that the formation of full planetary systems in these disks is a feasible possibility. Figure from Williams & Cieza (2011).

theoretical works in Calvet et al. (1992), the series of papers by Paloa D'Alessio (e.g., D'Alessio et al. 1998, 1999, 2006), Kama et al. (2009), or Armitage (2011) to cite a few.

1.2.3 Spectral energy distributions and classes of protoplanetary disks

One of the most common ways to study protoplanetary disks (and the one mostly used in this work) is via their SEDs, which are a representation of the observed fluxes as a function of wavelength. SEDs contain information about different aspects of the star+disk system, and can be used to derive estimates for several disk parameters.

Following this idea, Lada (1987) proposed a classification of YSOs based on the slope of their SEDs in the IR , defined as:

$$\alpha = \frac{d\log(\nu F_\nu)}{d\log(\nu)} = \frac{d\log(\lambda F_\lambda)}{d\log(\lambda)}$$

This classification used the slope between 2 and 20 μm to separate YSOs in three groups (Class I, II, and III), following different stages of YSO evolution. Later on, André et al. (1993) added an earlier stage (Class 0), and Greene et al. (1994) included a sub-division between Class I and Class II sources. The classification based on α is generally adopted to be as follows:

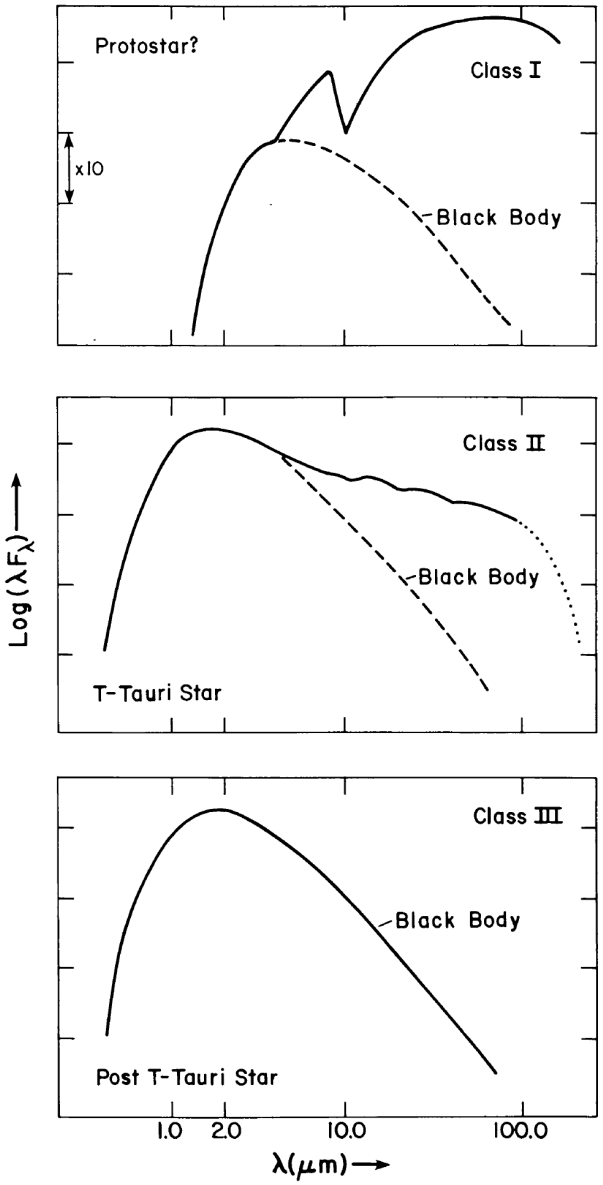

FIGURE 1.7: Schematic SEDs of Class I (top), Class II (middle) and Class III (bottom) YSOs. Solid lines depict the total observed SEDs, dashed lines the corresponding stellar emission, approximated here by blackbodies. Figure from Lada (1987).

– Class 0: $\alpha > 3$ and very faint fluxes (usually undetectable) for wavelengths shorter than 20 μm. This stage corresponds to protostars, and the emission is dominated by the thermal radiation from the surrounding cold dust.

– Class I: objects with $0.3 \leq \alpha \leq 3$. These sources emit the bulk of their radiation in the MIR/FIR regimes, suggesting that a large amount of material is surrounding the central star and reprocessing the stellar radiation. This class corresponds to the initial stages of star and disk formation, when a massive envelope can be found around the star.

– Flat spectrum: objects with $-0.3 \leq \alpha \leq 0.3$. Sources with a dispersing envelope.

– Class II: meeting $-1.6 \leq \alpha \leq -0.3$. These objects, with less IR emission than the previous case, would be typical protoplanetary disks, where most of the IR emission comes from material confined in the disk and no or a very diluted envelope is left around the system.

– Class III: with $\alpha \leq -1.6$. In this case, the emission from the disk is weaker or even negligible, suggesting that most of the material has already been either accreted onto the star or dispersed. This class represent more evolved disks, probably in the last stages of dissipation.

The "Class" system has been extensively used through the literature (see Fig. 1.7 for a graphical representation). Despite its limitations (e.g., Dunham et al. 2014), it has been a key tool to develop a general understanding of the evolution of YSOs across different star-forming regions (e.g., *c2d Spitzer* Legacy program, Evans et al. 2009).

Although not so relevant for this work, YSOs can also be classified with different criteria by their emission features in their optical/NIR spectra (e.g., Edwards et al. 1994; Barrado y Navascués & Martín 2003). Emission lines in young stars are mostly due to mass accretion, and those objects with strong emission features (such as H_α) are typically referred to as "classical T Tauri stars" (CTTSs). Objects with weaker accretion signatures are known as "weak-lined T Tauri stars" (WTTSs). As expected, most CTTSs have Class II SEDs, whereas WTTSs correspond to Class III sources.

1.3 Protoplanetary disk evolution

As described in Sect. 1.2.1, protoplanetary disks are a natural consequence of star formation, but most main sequence stars in the Galaxy are diskless. Also, most disks are found to be accreting gas onto their host stars. This all tells us that protoplanetary disks evolve and disperse after a given time. Understanding the mechanism (or mechanisms) causing this evolution and their timescales provides crucial information to better comprehend planetary systems: as an example, gas giant planets can only form when a considerable amount of mass is still available in the disk, imposing a strict time limit for this process to take place.

If one combines the observed disk masses (0.001 - 0.1 $M_\odot$, Andrews & Williams 2005) with typical accretion rates 10^{-7}-10^{-10} $M_\odot$/yr, protoplanetary disks should run out of mass in some Myr time. Further evidence for this timescale comes from disk fractions in clusters, which have shown that both IR excess and accretion signatures decrease with characteristic times $\tau \sim 3$ Myr (Haisch et al. 2001b; Hernández et al. 2007b; Mamajek 2009; Fedele et al. 2010; Ribas et al. 2014). Moreover, the number of objects with signs of disk clearing (known as "transitional disks", see Sect. 1.4 and Espaillat et al. 2014) is usually 10 % of the total fraction of disks, suggesting that this process occurs rapidly

(Andrews & Williams 2005; Merín et al. 2010; Luhman et al. 2010; Koepferl et al. 2013; Ribas et al. 2014).

The bulk of the mass of protoplanetary disks is in gaseous state (although uncertain, the gas-to-dust mass ratio is usually assumed to be 100:1). Therefore, gas strongly dominates the disk dynamics, and its viscosity plays a crucial role in its evolution. Viscous accretion and evolution are the most important processes at early disk stages (when the disk is gas rich), and the observed disk lifetimes are consistent with theoretical predictions (Shakura & Sunyaev 1973; Lynden-Bell & Pringle 1974; Hartmann et al. 1998; Dullemond et al. 2007). Naively, this process can be understood by considering the angular momentum transport between adjacent gaseous rings in a disk with Keplerian rotation. In reality, this is a much more complex problem involving turbulence, magnetic fields, and several additional processes. Due to the large uncertainties in this, Shakura & Sunyaev (1973) developed the "α-prescription" model of viscous disks, which allows a simple parametrization of viscosity and has been widely used since then. This method estimates a characteristic viscous dissipation timescale of a few million years (Alexander et al. 2014), and is not capable of producing the fast ($10^5 - 10^6$ yr) transition from protoplanetary disks to naked stars revealed by observations. Other processes must be invoked to explain this fast disk dispersal.

Dust settling and growth from micron size grains to planetesimals or planets can trap dust (and some gas) in a few large bodies. Under certain conditions (relative velocities, porosity, size,...), dust grains stick together after collisions, producing larger grains. These larger grains become decoupled from the gas, settling towards the disk mid-plane and increasing the dust density in that region (e.g., Tanaka et al. 2005). This step can help building even larger bodies, eventually forming planets (dust growth is an extremely complex process, see e.g., Testi et al. 2014). In any case, even if most of the dust ends up either in planetesimals/planets or is accreted onto the star, the bulk of the disk mass is in gaseous state and would remain unperturbed by this process: dust growth alone cannot explain the gaps and cavities found in protoplanetary disks (Birnstiel et al. 2012), nor the totality of disk evolution.

The total number of stars in multiple systems in the Galaxy is not negligible: the binarity frequency in Upper Sco is 30-40 % (Kraus et al. 2008), and 50-75 % of the stars in Taurus region are in multiple systems (Kraus et al. 2012). The gravitational influence of a companion can have a significant impact in the disk dynamics: there are evidences of binarity being responsible for diskless stars at early ages (Kraus et al. 2012), specially for close binaries (Harris et al. 2012). Even if the disk is not dispersed by the effect of the binary system, its gravitational influence can result in disk truncation (e.g., GG Tau, CoKu Tau 4, Guilloteau et al. 1999; Ireland & Kraus 2008), which can reduce its lifetime by one order of magnitude (see e.g. the discussion in Williams & Cieza 2011). All these facts imply that multiplicity may play a major role in several disks, and given the inherent difficulties to identify close binaries (usually below the resolution limit of

the observations), they add an important source of uncertainty to our observational knowledge of disk evolution. But in any case, it is obvious that the evolution of single stars must be driven by a different mechanism.

A large number of jets, outflows and winds associated to YSOs have been found across the whole stellar mass spectrum. They provides a mechanism to effectively remove both mass and angular momentum from the system. Whether they are a mere product of star and disk formation or they are important for disk evolution is not clear yet (Frank et al. 2014). Their origin is still a matter of debate, but magnetic fields are likely to play a key role in them (e.g., Hayashi et al. 1996; Li et al. 2014). Actually, certain magnetic field configurations can even prevent disk formation (Li et al. 2011) and in the case of formed, stable disks, may cause outflows and winds via magnetohydrodynamical processes, leading to disk dissipation. Given the large uncertainties in the strength of magnetic fields in YSOs, the real impact of these effects in disk evolution is still unknown (Alexander et al. 2014; Li et al. 2014).

Photoevaporation is likely the dominant process in disk evolution once the accretion rate goes below a certain threshold. The upper layers of disks are heated to large temperatures when illuminated by the high-energy radiation from the star, and at intermediate disk radii and under certain conditions, the resulting thermal energy is larger than the gravitational attraction of the host star, producing gas loss via photoevaporative winds. The location at which this occurs is parametrized by the *gravitational radius* r_g, defined as the place where the local sound speed overcomes the escape velocity. The global consequence of photoevaporation is to remove material from the disk at r_g, opening a gap and decoupling the inner and outer disks. With this configuration, material in the inner region is accreted onto the star, and the inner disk disappears since it no longer can incorporate material from the outer regions (Fig. 1.8). At the same time, the remaining outer disk continues to photoevaporate, leading to disk dissipation in timescales comparable to the observed ones. The theoretical predictions of this process are broadly consistent with the observed properties of protoplanetary disks (e.g., Alexander et al. 2014). Nevertheless, for a subset of objects with large inner holes (transitional disks, see Sect. 1.4) and important accretion rates, other mechanisms must be at play to reproduce their characteristics (Owen et al. 2011).

1.3.1 Disk fractions in star-forming regions and associations

Given the estimated lifetimes of protoplanetary disks of some Myr, it is not feasible to study disk evolution by monitoring individual objects. Instead, one can analyze the population of disks in star-forming regions and associations with different ages to develop an understanding of the process. Because it will have an important weight in this study, this section provides a short review of previous works which have used this method.

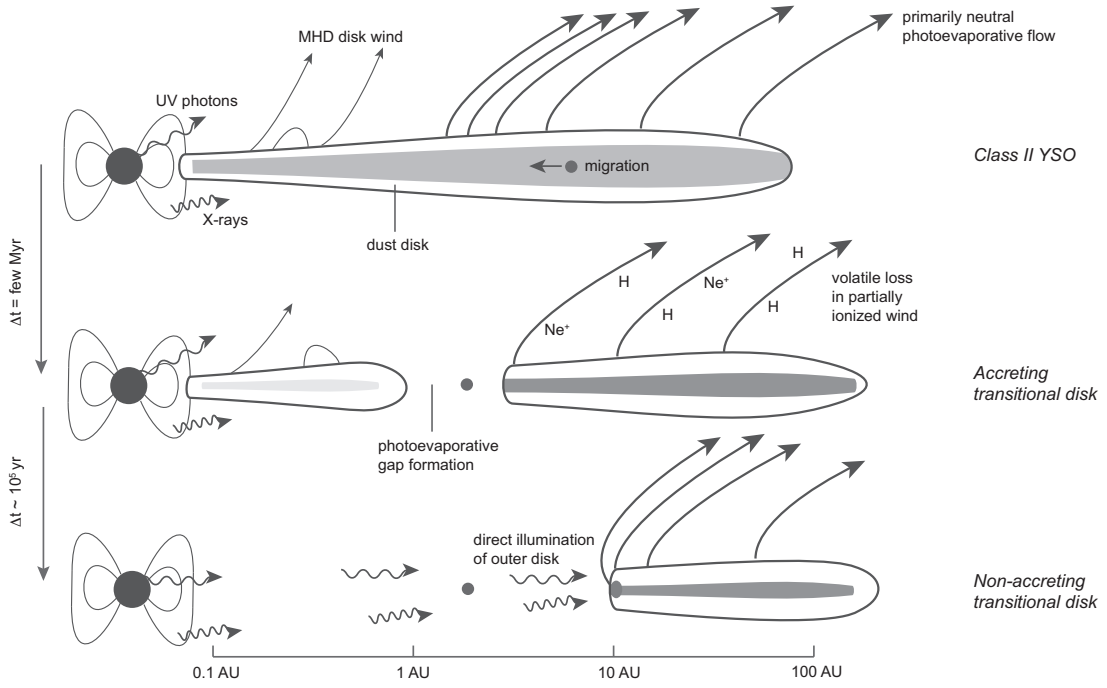

FIGURE 1.8: Scheme of the photoevaporative evolution of protoplanetary disks. At a certain time, photoevaporation carves a hole in the disk at a given radius preventing the replenishment of the inner regions, which are quickly accreted onto the star. Figure from Alexander et al. (2014).

Haisch et al. (2001b) obtained L band photometry for four clusters with age range spanning from 2.5 to 30 Myr, and combined their results with previous measurements of other younger clusters (Lada et al. 2000; Haisch et al. 2001a,c), composing a list of seven clusters covering from 0.3 to 30 Myr. This was the first study of disk fractions as a function of age for a relatively large number of clusters. They found that half of the disks disperse during the first 3 Myr, and estimated that by 6 Myr, all protoplanetary disks have already dispersed. This final result was derived by fitting a straight line to disk fractions. After this study, the advent of *Spitzer* provided MIR photometry for several star-forming regions. Using data from this telescope, Hernández et al. (2007b, 2008) presented an updated version of the "disk fraction vs age" picture, including up to 20 associations. Their results were consistent with those of Haisch et al. (2001b), but also identified some regions of > 5 Myr with disk fractions above 0 %. Later, Mamajek (2009) used 22 associations to propose an exponential decay of protoplanetary disks, finding a characteristic timescale of $\tau \sim 2.5$ Myr. An additional perspective was provided in Fedele et al. (2010) by probing accretion in seven regions down to $10^{-11} M_{\odot}$/yr. Their results show that the timescale of sources with detectable excess with IRAC is $\tau_{\rm IRAC} \sim 3$ Myr from dust continuum emission, but the accretion timescale is $\tau_{\rm acc} \sim 2.3$, suggesting that gas accretion stops slightly earlier than the disk dissipates. Fig. 1.9 presents a compilation of these results. Overall (and although a direct comparison is not trivial given different methodologies completeness limits used), these studies show that half of the disks disperse within the first ~ 3 Myr of the life of the stars, but some can survive

up to 10 Myr. All these works have provided great insights into disk evolution, but they rely partly on inhomogeneous datasets which are often not large enough to obtain statistically conclusive results. It should also be kept in mind that potential differences inherent to the considered regions and associations may also impact the results. Further studies with larger, unbiased, and clean samples are required to achieve an even better understanding of disk evolution.

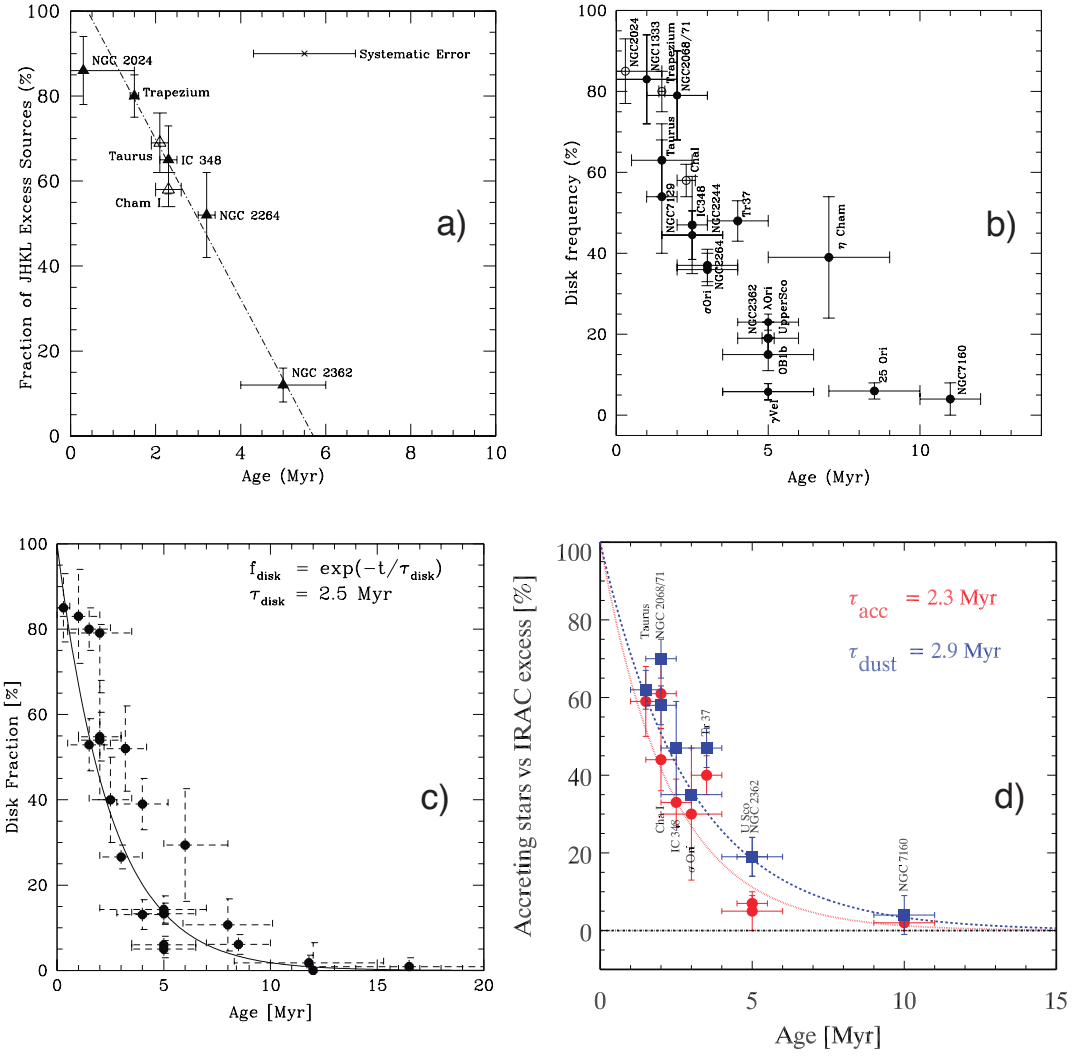

FIGURE 1.9: Disk fractions as a function of cluster age as derived in several studies: a) Haisch et al. (2001b); b) Hernández et al. (2008); c) Mamajek (2009); d) Fedele et al. (2010). These results show that disk dispersal occurs between 1 and 10 Myr, with half of the YSOs losing their disk during the initial 3 Myr of their lives.

1.4 Transitional disks

Transitional disks are protoplanetary disks with signatures of low opacity regions in their structure, which is usually attributed to the presence of gaps and/or cavities in them.

Since they likely represent an intermediate stage in the way from protoplanetary disks to naked stars and could even be directly related with the presence of (proto)planets, they have gained a lot of attention and relevance for star and planet formation theories.

Transitional disks were first identified by Strom et al. (1989), using NIR (2.2 μm) ground based photometry in combination with MIR data from the Infrared Space Telescope (*IRAS,* Neugebauer et al. 1984). While performing a survey of circumstellar material around YSOs in the Taurus-Auriga molecular cloud, they identified some objects with small NIR excesses but considerable MIR ones, and suggested this as a possible signature of disk evolution:

> "The presence of IR excesses for $\lambda \geq 10\,\mu$m (which provide evidence of emission from cool dust located in the outer disk regions, $r > 1$ AU), and the absence of excess emission at $\lambda < 10\,\mu$m (which implies absence of warm dust at $r < 1$ AU) may diagnose *disk clearing* in the inner regions of the disk. If so, these observations may represent the first astrophysical evidence of disks *in transition* from massive, optically thick structures that extend inward to the stellar surface, to low-mass, tenuous, perhaps post-planet-building structures." (Strom et al. 1989)

This first hint was rapidly corroborated by additional measurements from the NASA Infrared Telescope Facility by Skrutskie et al. (1990). Although with a moderate sample size, Skrutskie et al. (1990) were also able to determine that this transitional phase occurs on a timescale of $t \sim 0.3$ Myr, already suggesting that disk dispersal is a fast process which last for only a fraction of the total disk lifetime.

By now, much more is known about this special kind of circumstellar disks, thanks to better observing capabilities and theoretical advances. As shown by Strom et al. (1989) and Skrutskie et al. (1990), transitional disks have SEDs lacking NIR excess but with significant ones at longer wavelengths (see Fig. 1.10). Dust depleted regions have been found in them in a broad range of wavelengths with different techniques: optical/NIR scattered light (e.g., Thalmann et al. 2010), polarimetry (e.g., Mayama et al. 2012; Hashimoto et al. 2012; Follette et al. 2013), high-resolution MIR direct observations and interferometry(e.g., Geers et al. 2007; Cieza et al. 2013; Kraus et al. 2013), and mainly via (sub)mm interferometry (e.g., Brown et al. 2008; Hughes et al. 2009; Andrews et al. 2011, see Fig. 1.11). The Infrared Spectrograph (IRS) instrument on board *Spitzer* yielded hundreds of spectra of YSOs from 5.3 to 37 μm, and has been extensively used to model the inner structure of transitional disks (Calvet et al. 2002; Rice et al. 2003; Espaillat et al. 2007b; Kim et al. 2009; Merín et al. 2010; Espaillat et al. 2011). All these studies have identified different classes of these objects: full transitional disks (objects with a large radial gap in the disk), pre-transitional disks (disks with inner and outer disks, separated by a dust-depleted gap, Brown et al. 2007; Espaillat

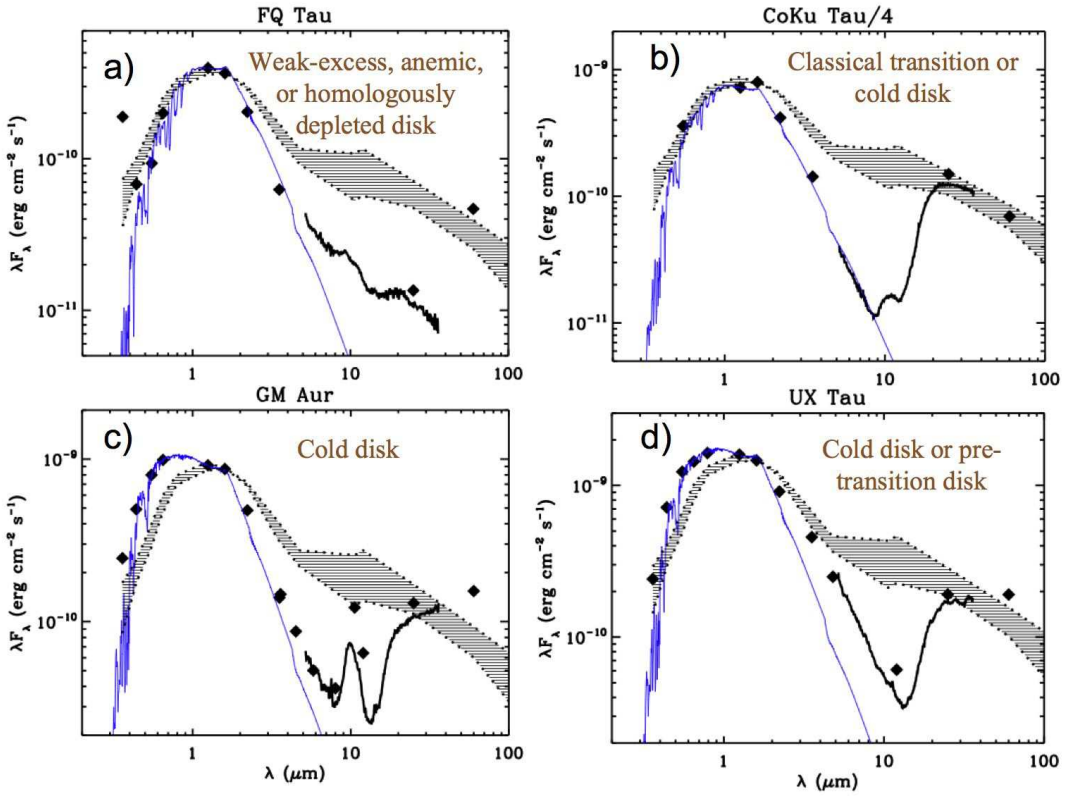

FIGURE 1.10: SEDs of four different transitional disks. Black dots are observed photometric values, black solid lines show IRS spectra. The corresponding photosphere is plotted as a blue solid line, and the dashed region corresponds to the median SED of Taurus. Figure from the review of Williams & Cieza (2011).

et al. 2007b, 2010), or disks with decreasing IR excess at all wavelengths (called anemic, homologously depleted, evolved disks, or weak transition disks, e.g., Lada et al. 2006; Hernández et al. 2007b,a; Muzerolle et al. 2010; Sicilia-Aguilar et al. 2010). Their gap sizes range from a few to some tens of AU (e.g., Kim et al. 2009; Merín et al. 2010; Espaillat et al. 2011), and their population is found to be 5-30 % of the total number of YSOs in star-forming regions (Skrutskie et al. 1990; Kenyon & Hartmann 1995; Andrews & Williams 2005; Cieza et al. 2007; Merín et al. 2010; Ribas et al. 2015). Their accretion rates are still somewhat unclear. Najita et al. (2007) found transitional disks in the Taurus region to accrete at lower rates than Class II disks ($\sim$1 order of magnitude). This could be explained by gap opening in the disk by a Jovian planet(s) (e.g., Skrutskie et al. 1990; Marsh & Mahoney 1992; Calvet et al. 2002; D'Alessio et al. 2005), which would prevent accretion from the outer to the inner regions. Instead, the planet would tunnel material from the outer disk inwards, and theoretical works show that this effect could reduce accretion by a factor of $\sim$ 0.05-0.1 (Lubow & D'Angelo 2006; Varnière et al. 2006). However, more recent works found that transitional disk may instead have accretion rates similar to that of Class II objects (Manara et al. 2014), and more studies on this topic are required to identify the real origin and rates of accretion in these sources. Additionally, the different criteria and definitions of the transitional class may

also account for the observed discrepancies between some authors (e.g., Espaillat et al. 2012).

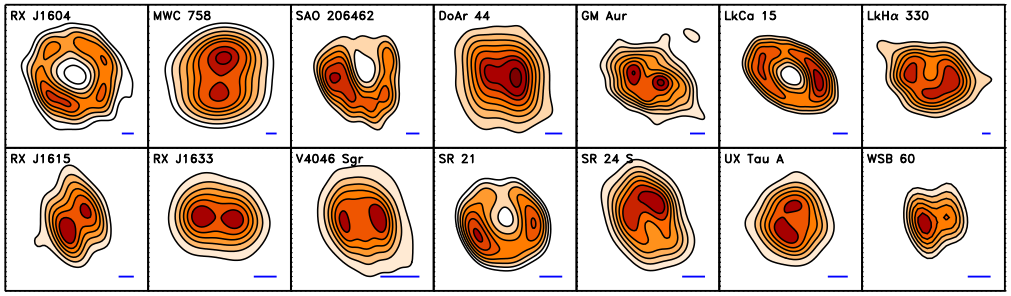

FIGURE 1.11: Submillimetric cavities in (pre)transitional disks as seen at 880 μm by the Submillimeter Array. The blue line at the bottom right of each panel is 30 AU long, roughly the size of Neptune's orbit. These images reveal a rich diversity of cavity shapes and disk morphologies. Figure from the review of Espaillat et al. (2014).

The presence of stellar or planetary companions was soon invoked to explain the SEDs of transitional disks, and was initially found to be plausible solution (Marsh & Mahoney 1992). However, other mechanisms such as dust growth or photoevaporation could also be responsible for the observed gaps.

– Dust growth could produce transitional disk SEDs in two different ways. First, large grains are inefficient emitters, specially in the NIR regime (e.g., D'Alessio et al. 2001; Draine 2006). Therefore, the deficit of NIR flux observed in transitional disks may be explained not by a decrease in their mass, but in the dust NIR emissivity. Additionally, grains decouple from the Keplerian velocity of the gas as they grow, and start suffering a "drag" caused by the gas viscosity. Consequently, dust grains spiral inward and are accreted onto the star (Weidenschilling 1977; Nakagawa et al. 1986). This "radial drift" removes mass from the inner disk, clearing this region and therefore decreasing the NIR emission. Birnstiel et al. (2012) demonstrated that, although dust growth could actually produce SEDs similar to those of transitional disks, it cannot reproduce the observed submm cavities in their density distribution found in several cases(e.g., Andrews et al. 2011).

– Photoevaporation can open gaps in disks, as discussed in Sect. 1.3. It can also account for the large gap sizes observed in transitional disks, and is very likely responsible for at least a fraction of the transition sources. However, photoevaporation alone cannot produce the observed properties of transitional disks with large gaps and high accretion rates (e.g., Alexander & Armitage 2009).

– Finally, the gravitational influence of a companion (stellar or planetary) could carve a hole as the secondary body orbits the central star (Papaloizou et al. 2007; Baruteau et al. 2014). In fact, some transitional disks with large gaps have been found to host stellar companions (e.g., CoKu Tau 4 or CS Cha, Ireland & Kraus

2008; Nagel et al. 2012). However, it is yet not clear that single planets can produce the observed gaps in the disk surface distribution at current sensitivity limits. Some problems also appear to explain the SEDs of transitional disks if gas giant planets are driving accretion: once the material has been transported to the inner regions, the NIR emission would rise again and some excess would be detected. Proposed solutions for this issue involve gap opening by multiple giant planets (Zhu et al. 2011), or dust filtration mechanisms (i.e., dust remains in the gap edge due to the presence of a pressure maximum, whereas gas continues to accrete onto the star, Rice et al. 2006).

Despite all the attention gained by the field, there are still several unknowns regarding transitional disks. Their uncertain accretion properties, the mechanism behind their evolution, or the origin of different SED types are still yet to be understood. Future ALMA observations will provide further insight into this particular class of circumstellar disks and their real link with planet formation.

1.5 Evolution of the field during this thesis

The previous introduction provided a broad overview of the status of the field at the time of writing this thesis. A general understanding of disk evolution and planet formation was already achieved several years ago, both observationally and theoretically. Thus, although several significant contributions have been added during the last three years, the "main ideas" have remained the same.

Despite this, the advent of ALMA has opened a whole new era for circumstellar disk studies. ALMA started its Early Science phase (Cycle 0) in 2011, and it has been improving its capabilities since then. Among several, some examples of its impact are the detection of zones in the disk with a significant accumulation of large dust particles (the so-called dust traps, van der Marel et al. 2013), the finding of gas flows through gaps in transitional disks, (e.g., HD142527, Casassus et al. 2013), or spatially resolved images of the CO snowline (the location in the disk at which a certain molecule freezes) in the TW Hya protoplanetary disk (Qi et al. 2013). However, its most remarkable achievement so far was accomplished in late 2014, when ALMA's highest resolving power (using its longest baseline configuration) provided science verification data of the protoplanetary disk around HL Tau (Fig. 1.12): ALMA reached a spatial resolution of 25 mas, corresponding to 3.5 AU at the distance of the Taurus molecular cloud ($\sim$140 pc, Torres et al. 2007). The resulting image shows an intricate system of gaps and rings in the disk, with several indications pointing to multiple planet formation and resonances as the main cause of these rings (ALMA Partnership et al. 2015), although there are other mechanisms which could also explain these gaps. HL Tau is a young system (1-2 Myr, Briceño et al. 2002), and has a flat SED: surprisingly, gap opening by planet formation is not expected to take place this early in the disk lifetime, challenging the current existing theories of disk evolution. Apart from the obvious and exciting implications of these discoveries, they are also a clear proof of the impact that ALMA will have in this field. With large and complete samples of transitional disks covering broad ranges of stellar masses and initial conditions, ALMA will provide an unprecedented view of stellar and planetary formation.

Additionally, the *Kepler* Spacecraft has produced a whole revolution in the exoplanetary field. It was launched in 2009, and thousands of planet candidates were identified as its time coverage increased (e.g., Batalha et al. 2013), allowing to detect planets with larger periods. Regardless of the failure of two of its reaction wheels in 2012 and 2013 (*Kepler* is now in its "second light" mission) the huge amount of data it yielded is still used to identify and detect new candidates, and by today more than 1 000 planets have been already confirmed with *Kepler*. This dramatic increase in the number of known planets provides the perfect scenario to confront exoplanetary demographics with the properties and theory of protoplanetary disksUltimately, *Kepler* could answer questions

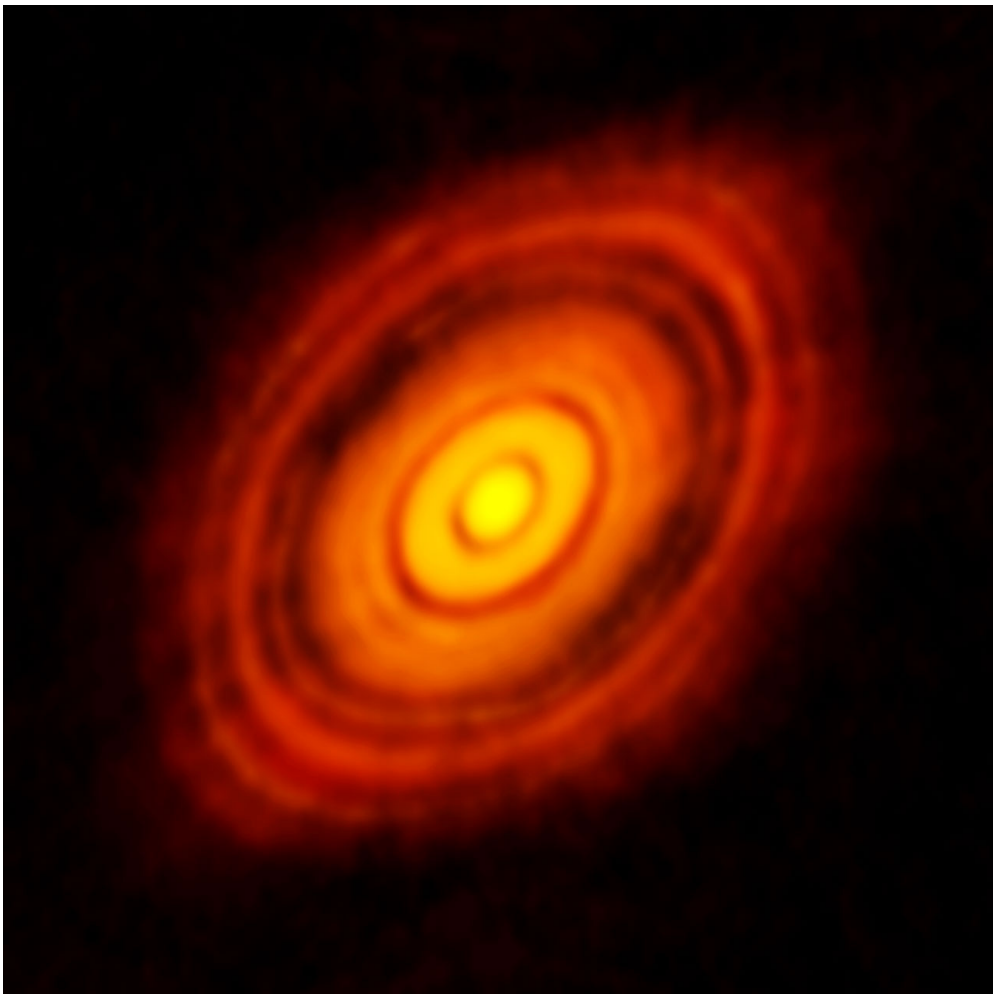

FIGURE 1.12: Long baseline ALMA observations of the protoplanetary disk around HL Tau. The unprecedented ALMA capabilities achieved a resolution of 3.5 AU in the disk, which shows several gaps and rings in its dust distribution. ALMA Science verification data (ALMA Partnership et al. 2015).

such as the possible connection of disks properties and the exoplanetary population, or if we could even compare this information with our own Solar System.

1.6 Goals of this thesis

This thesis consists of two main parts, both of them connected to each other but with different goals and approaches. The first study focuses on the statistical properties of protoplanetary disks in young associations, while the second one presents the analysis and modeling of transitional disks in the Chamaeleon I star-forming region using *Herschel* data.

The first part of this work focuses on improving our knowledge of the evolution of protoplanetary disks. Previous studies have already achieved a general view of this process, but compiling data from many different works, usually with different methodologies, criteria, and completeness limits. All these various effects could hide important biases in our understanding of disk evolution. Moreover, several of these studies used samples which are too small to obtain meaningful statistical comparisons and results, or may include a significant fraction of contaminants (as much as $\sim 30\,\%$ when based on purely photometric selection criteria). We intend to overcome these issues by creating a large and homogeneous database of YSOs in young associations, and querying different public catalogs to build their SEDs from the near ultraviolet to the MIR range. Also, special attention is paid to selection effects, biases, and statistical subtleties that should be considered to perform consistent analyses of disk evolution. We will later use this clean sample to identify disks via IR excess, and study their evolution as a function of stellar age and mass.

The second part of the thesis will study the population of YSOs in the Chamaeleon I and II regions, as observed by *Herschel* (Pilbratt et al. 2010). In particular, we will focus on previously known transitional disks in the regions and compare them with Class II sources in the association. Because *Herschel* has observed large areas of the sky in FIR wavelengths, its observations are available for a large number of sources and can provide further insight into the realm of circumstellar disks. For that reason, we will also apply detailed radiative transfer models, in combination with Bayesian analysis and Markov Chain Monte Carlo (MCMC) methods, to quantify the real contribution of *Herschel* data to our current understanding of transitional disks and explore its improvements with respect to *Spitzer* observations.

Combined, these two complementary parts provide both a panchromatic view of disk evolution, and a more detailed look at the critical transitional (maybe planet-forming) phase of disks around young stars.

Part I

Disk evolution

2

Disk evolution in the solar neighborhood

The evolution of protoplanetary disks may set the fate of planet formation around stars, and several works have studied how the fraction of disks changes with time. In this chapter, we perform a homogeneous analysis of the disk population in 22 young (< 100 Myr) nearby (< 500 pc) star-forming regions and associations. We compile a large sample of YSOs in these regions, and follow careful and homogeneous procedures to minimize the impact of biases in our study. We then look at disk fractions as a function of age, and derive characteristic disk lifetimes at different wavelengths.

This work was published as Ribas et al. 2014, A&A, 561, A54.

Disk evolution in the solar neighborhood

I. Disk frequencies from 1 to 100 Myr

Álvaro Ribas[1,2,3], Bruno Merín[4], Hervé Bouy[2], Luke T. Maud[5]

[1] European Space Astronomy Centre (ESA), P.O. Box, 78, 28691 Villanueva de la Cañada, Madrid, Spain

[2] Centro de Astrobiología, INTA-CSIC, P.O. Box, 78, 28691 Villanueva de la Cañada, Madrid, Spain

[3] Ingeniería y Servicios Aeroespaciales-ESAC, P.O. Box, 78, 28691 Villanueva de la Cañada, Madrid, Spain

[4] Herschel Science Centre, ESAC-ESA, P.O. Box, 78, 28691 Villanueva de la Cañada, Madrid, Spain

[5] School of Physics & Astronomy, EC Stoner Building, University of Leeds, Leeds, LS2 9JT, West Yorkshire, England

Received 3 September 2013; Accepted 13 November 2013

Abstract

Aims: We study the evolution of circumstellar disks in 22 young (1 to 100 Myr) nearby (within 500 pc) associations over the entire mass spectrum using photometry covering from the optical to the mid-infrared.

Methods: We compiled a catalog of 2 340 spectroscopically-confirmed members of these nearby associations. We analyzed their spectral energy distributions and searched for excess related to the presence of protoplanetary disks. The dataset has been analyzed in a homogeneous and consistent way, allowing for meaningful inter-comparison of results obtained for individual regions. Special attention was given to the sensitivity limits and spatial completeness of the observations.

Results: We derive disk fractions as probed by mid-infrared excess in the 22 regions. The unprecedented size of our sample allows us to confirm the timescale of disk decay reported in the literature and to find new trends. The fraction of excess sources increases systematically if measured at longer wavelengths. Disk percentages derived using different wavelength ranges should therefore be compared with caution. The dust probed at 22–24 μm evolves slower than that probed at shorter wavelengths (3.4–12 μm). Assuming an exponential decay, we derive a timescale τ =4.2$\sim$5.8 Myr at 22–24 μm for primordial disks, compared to 2$\sim$3 Myr at shorter wavelength (3.4–12 μm). Primordial disks disappear around 10$\sim$20 Myr. Their decline matches in time a brief increase of the number of "evolved" disks (defined here as including transitional and debris disks).

There is more dispersion in the fraction of excess sources with age when measured at 22–24 μm in comparison to shorter wavelengths.
Conclusions: The increase in timescale of excess decay at longer wavelength is compatible with inside-out disk clearing scenarios. The increased timescale of decay and larger dispersion in the distribution of disk fractions at 22–24 μm suggest that the inner (terrestrial-planet forming) and outer (giant-planet forming) zones evolve differently, the latter potentially following a variety of evolutionary paths. The drop of primordial disks and the coincident rise of evolved disks at 10 Myr are compatible with planet formation theories suggesting that the disappearance of the gas is immediately followed by the dynamical stirring of the disk.

Key words: Planetary systems: protoplanetary disks – stars: formation – (stars:) planetary systems – stars: pre-main sequence

2.1 Introduction

The structure and evolution of protoplanetary disks provide crucial information to better understand stellar and planetary formation (see Williams & Cieza 2011, for a complete review on different aspects of protoplanetary disks evolution). The timescale of disk evolution, and its dependence on stellar age, mass, environment and multiplicity, is a fundamental parameter to constrain stellar formation theories and numerical simulations. The inter-phase between protoplanetary and debris disks is also key to understand the first stages of planetary formation. However, details of the processes involved in the dispersal of protoplanetary disks and the transition to debris disks have been elusive mostly because of the long distances to such disks (hence difficulty to resolved them) and the size of the samples studied so far.

Circumstellar disks are often detected via IR excess over the stellar photosphere: dust in the disk is heated by stellar radiation, and re-emits it in the MIR/FIR regime. The advent of IR observatories such as AKARI, the *Spitzer* Space Observatory, and more recently the *Herschel* Space Observatory produced very sensitive surveys over vast areas in several young nearby associations and clusters (Evans et al. 2009; Ishihara et al. 2010). Combined with all-sky or wide field surveys in the optical (e.g CMC 14, and SDSS) and in the NIR/MIR (e.g DENIS, UKIDSS, and WISE), they provide a sensitive and homogeneous photometric coverage of a large number of nearby regions and make a new and unique database for the study of protoplanetary disks.

We present a sample of 2 340 young stars and brown dwarfs members of 22 nearby (<500 pc) associations (13 star-forming regions and 9 young nearby associations) with ages ranging from 1 to 100 Myr. This sample of unprecedented size is a compilation of 37 spectroscopic studies published in the literature over the past two decades. The spectral energy distribution (SED) of each source was obtained by merging various catalogs covering the wavelength range from the optical (∼V-band) to the MIR (22∼24 μm). The quantity and the quality of the photometric measurements allow us to derive and study disk fractions in a consistent way for all the regions.

The present manuscript is the first of a series of articles where disk evolution will be investigated with a large and representative sample of young stars in the solar neighborhood. In Sect. 2, we present the sample and its characteristics. We describe the astrometric and photometric quality assessment and data curation process in Sect. 3. The SED fitting procedure is described in Sect. 4. In Sect. 5, we describe the method and criterion adopted to identify MIR excesses and the method used to derive excess (disk) fractions. The results are given in Sect. 6, and discussed in Sect. 7.

2.2 Sample

We compiled a sample of spectroscopically confirmed members of nearby regions using catalogs from the literature for the 25 Orionis, Chameleon I & II, Corona Australis, IC 348, λ-Orionis, Lupus, NGC 1333, Ophiuchus, σ-Orionis, Serpens, Taurus, and Upper Scorpius associations and clusters. This original sample was then completed by adding the spectroscopically confirmed members of young nearby associations from the SACY survey presented in Torres et al. (2008), which includes the AB Doradus, Argus, β-Pictoris, Carina, Columba, η-Chamaeleon, Octantis, Tuc-Hor (THA), and TW Hya (TWA) associations. Table 2.1 summarizes of the basic properties of these regions, as well as the references used for the spectroscopically confirmed samples.

Young nearby associations offer several advantages for the study of stellar and planetary formation. Their distances and relative ages are in general relatively well known. Additionally, their proximity and youth make the detection of their least massive members easier, ensuring a complete (or at least representative) census of their stellar content from the most massive members to the substellar and planetary mass objects. As a result, they have extensively been studied over the past four decades (see e.g Reipurth 2008a,b, and references therein). Additionally, nearby associations with ages in the range 5 - 80 Myr provide a good opportunity for studying the transition from protoplanetary to debris disks.

From the various catalogs found in the literature (see Table 2.1), we chose to keep only those objects with spectroscopically-obtained spectral type . This choice was motivated by two main reasons:

- Spectroscopic confirmation minimizes contamination by unrelated foreground or background sources. Photometric surveys are known to include as much as 30% of contaminants (see e.g Oliveira et al. 2009).
- Knowing the spectral type breaks the degeneracy between $T_{\rm eff}$ and visual extinction (A_V) in the SED fitting, making the $A_{\rm V}$ estimation more robust.

A total of 2 627 sources fulfill this first requirement.

2.2.1 Ages and distances

Distances can be measured with different techniques, leading to several (sometimes inconsistent) values in the literature for the same region. With the exception of the SACY sample, most regions considered here are further away than 100 pc, and hence beyond HIPPARCOS' sensitivity limit (Perryman et al. 1997). Ages are difficult to determine, and star formation is probably not an abrupt event but extended in time (see

TABLE 2.1: Young nearby regions (top) and associations (bottom) included in this study.

Name	Age (Myr)	Distance (pc)	Membership and SpT	*Spitzer* photometry	Number of sources
25 Orionis	7-10	330	(1)	(1)	46
Cha I	2	160-165	(2) (3) (4)	(3) (4)	212
Cha II	2±2	178±18	(5)	(38)	47
CrA	1-3	138±16	(6) (7) (8) (9)	(39)	35
IC 348	2	285-315	(10) (11)	(38) (40)	298
λ Orionis	4	400±40	(12)	(41)	114
Lupus	1-1.5	140 - 200	(13) (14) (15) (16)	(38)	217
NGC 1333	1	235±18	(17)	(42)	74
Ophiuchus	2-5	120-145	(18) (19) (20) (21)	(38)	258
σ Orionis	2-3	440±30	(22) (23) (24) (25) (26) (27) (28)	(43)	104
Serpens	2	230±20	(17) (29)	(38)	142
Taurus	1-2	140	(30) (31) (32) (33)	(32) (33)	265
Upper Sco	11±2	140	(34) (35) (36)	(35)	405
AB Dor	50-100	34	(37)	...	92
Argus	40	106	(37)	...	51
β Pic	10	31	(37)	...	54
Carina	30	85	(37)	...	37
Columba	30	82	(37)	...	58
η Cha	4-9	108	(37)	...	27
Octantis	20	141	(37)	...	17
Tuc-Hor	30	48	(37)	...	49
TW Hya	8	48	(37)	...	25

Ages and distances are from Reipurth (2008a) and Reipurth (2008b) unless specified. We also tabulate references to the different studies used to compile the sample of objects and to the *Spitzer* photometry, as well as the number of sources for each region.

(1) Hernández et al. (2007a); (2) Luhman (2007); (3) Luhman et al. (2008a); (4) Luhman & Muench (2008); (5) Spezzi et al. (2008); (6) Neuhäuser et al. (2000); (7) Nisini et al. (2005); (8) Sicilia-Aguilar et al. (2008); (9) Sicilia-Aguilar et al. (2011); (10) Luhman et al. (2003); (11) Alves de Oliveira et al. (2013b); (12) Bayo et al. (2011); (13) Krautter et al. (1997); (14) Allen et al. (2007); (15) Comerón (2008); (16) Mortier et al. (2011); (17) Winston et al. (2009); (18) Natta et al. (2002); (19) Wilking et al. (2005); (20) Alves de Oliveira et al. (2010); (21) Erickson et al. (2011); (22) Zapatero Osorio et al. (2002); (23) Muzerolle et al. (2003b); (24) Barrado y Navascués et al. (2003); (25) Franciosini et al. (2006); (26) Caballero (2007); (27) Sacco et al. (2008); (28) Rigliaco et al. (2012); (29) Oliveira et al. (2009); (30) Luhman (2004b); (31) Monin et al. (2010); (32) Rebull et al. (2010); (33) Rebull et al. (2011); (34) Preibisch et al. (2002); (35) Carpenter et al. (2006); (36) Lodieu et al. (2011); (37) Torres et al. (2008); (38) Evans et al. (2009);(39) Peterson et al. (2011); (40) Lada et al. (2006); (41) Barrado y Navascués et al. (2007); (42) Gutermuth et al. (2008); (43) Luhman et al. (2008b)

e.g. Hartmann 2001). Absolute ages are usually uncertain and sometimes controversial (Bell et al. 2013), but the *relative* age sequence is expected to be accurate enough for the aim of our study and to perform a meaningful comparison of disk properties at different evolutionary stages (Soderblom et al. 2013).

For consistency, we chose to use ages and distances provided in Reipurth (2008a) and Reipurth (2008b) except when updated measurements were found in the literature:

- Age of Cha II from Spezzi et al. (2008),
- Distance to NGC 1333 from Hirota et al. (2008),
- Age and distance to Upper Scorpius from Pecaut et al. (2012),
- Age and distance to 25 Orionis come from Hernández et al. (2007a).

In the rest of our analysis, a conservative 50 % uncertainty level was assumed for the ages, unless a different estimate was provided in the literature.

2.2.2 Mass range covered by the sample

The completeness level of the sample (in terms of mass or luminosity) is critical to assess the relevance of any statistical result, as an incomplete sample would yield biased results. This issue becomes even more important when mixing catalogs from different sources, which may have different completeness levels.

All the star-forming regions selected in this study have been extensively studied in the past (see i.e. Reipurth 2008a,b). The catalogs used to compile the sample presented here come from stellar population-oriented studies whose main objective was to define representative samples of members and derive accurate mass functions. On the high mass end, the various studies used in this analysis are expected to be complete since massive stars are bright and have been known for long. On the low mass end, the stellar population studies used in this analysis are in general complete or representative down the mid or late-M dwarfs. We therefore expect that our study is representative over the luminosity range between the most massive members (typically O, B or A stars depending on the association) and the mid/late-M dwarfs.

2.3 Astrometric and photometric quality assurance

2.3.1 Astrometry

In the past, astrometric calibration was more complicated because of the lack of accurate reference astrometric catalogs. As a result, some of the oldest surveys used in this

study have a poor astrometric accuracy. We undertook a data healing procedure to ensure consistent astrometric accuracy for all objects across the different regions and associations.

For the entire sample, we chose to use the 2MASS astrometry as reference (Skrutskie et al. 2006). 2MASS offers the advantage of homogeneously coverage of the entire sky, with an average astrometric accuracy of $\sim 0\farcs1$. In this process, each target is associated to the closest 2MASS counterpart within $3''$. We a posteriori verify that the mean separation between the original and the 2MASS coordinates is smaller than $0\farcs4$, except in the case of Ophiuchus (from Erickson et al. 2011) and Upper Sco (from Preibisch et al. 2002) where systematic offsets larger than $1''$ with respect to the 2MASS catalog were found and corrected.

Only 89 of the 2 627 objects had no counterpart in 2MASS within $3''$ due to luminosities beyond the sensitivity limit of the survey. They were removed from the sample and ignored for the rest of the study.

2.3.2 Photometry

To include as much photometric information as possible for each source, we searched the literature and different public surveys for photometric measurements from the optical to the MIR.

2.3.2.1 Surveys

We retrieved information from WISE (Wright et al. 2010), Tycho-2 (Høg et al. 2000), the Sloan Digital Sky Survey Data Release 8 (SDSS DR8), UKIRT Infrared Deep Sky Survey (UKIDSS), DENIS (DENIS Consortium 2005), AKARI (Murakami et al. 2007), and the Carlsberg Meridian Catalog 14 (CMC 14). To take the different Point Spread Function sizes of each survey into account, we established an optimized search radius for each of them by fitting a Gaussian to the kernel density distribution of separations between the original (2MASS) and catalog coordinates. The search radius was then set to the average of the Gaussian + $3\,\sigma$. As a sanity check, we verified that the search radius was consistent with the internal accuracy of the different surveys. When the number of sources was too small to derive a meaningful density distribution of separations, the search radius was set to $1''$. This value is a conservative compromise between the astrometric accuracy of the different surveys and the observed separation distribution. During this procedure, upper limits were treated with caution to include them as such. We chose to conservatively redefine as upper limits all fluxes with a signal-to-noise ratio (S/N) < 5 in any 2MASS or WISE bands. We also quadratically added WISE absolute calibration errors of 2.4, 2.8, 4.5 and 5.7 % (respectively to its bands) as recommended in the WISE All Sky Catalog Explanatory Supplement.

2.3.2.2 Optical to MIR photometry from the literature

We complemented the all-sky optical surveys mentioned above with our own optical (r and/or i) photometry from the Canada France Hawaii telescope, when available (Bouy et al., in prep.).

A number of associations presented in Table 2.1 have been observed with the *Spitzer* Space Observatory in the course of various legacy and other programs, and we included the corresponding IRAC and MIPS photometry. The *Spitzer* photometry proved to be extremely important for our study, since protoplanetary disks emit most of their light at MIR wavelengths. According to the *Spitzer* User Manual, absolute calibration of *IRAC* and *MIPS* fluxes is accurate to ∼5%, and we add the corresponding error quadratically when not already included.

In both cases (optical and MIR photometry), a cross-match radius of 1″was used.

2.3.3 Resolved binaries and ultra-cool objects

Multiple systems are frequent among stars (Lada 2006), and most of them are not resolved with the ground based or space (*Spitzer* and WISE) observations used in this work. The spectral type and photometry of such unresolved sources result in biased measurements. To minimize this problem, we performed an internal match for every region with a search radius of 2″. A total of 68 objects (34 pairs, ∼2 % of the whole sample) were found and removed from the sample. Closer systems cannot be identified in the current dataset. We nevertheless note that the properties of multiple systems, and in particular their frequency and distribution of separation, are expected to remain largely unchanged after 1 Myr. Multiplicity frequency is also found to vary little between associations and clusters (Duchêne & Kraus 2013) and should equally affect the various groups studied in this work. The statistics (and in particular the disk fractions) derived and discussed in the present study should therefore be regarded as statistics for the systems, rather than for individual sources.

Finally, we also removed objects with spectral types ≤ L0. These objects, although very interesting for brown dwarf formation studies, are in most cases beyond the completeness limit of the various surveys used in our analysis. After this process, the sample is comprised of 2 452 sources.

2.4 Data processing

2.4.1 SED cleaning and A_V fitting

First, the spectral types were converted to T_{eff} using:

- Schmidt-Kaler (1982) scale for spectral types K8 and earlier.
- Luhman et al. (2003) scale for spectral types later than M0.

In spite of all the precautions described in Sect. 2.3, a blind cross-match of large datasets inevitably contains errors and problems. We therefore visually inspected all the SEDs and rejected problematic sources and photometric measurements.

Extinction toward each source was then estimated by comparing the observed SEDs with a grid of reddened photospheric BT-Settl models from Allard et al. (2012) of the corresponding T_{eff}, and the extinction law of Indebetouw et al. (2005). Normalization of the observed and synthetic spectra was done at the 2MASS J or H band (in this order or priority) when present, and at the closest band otherwise. The photometric bands used for the A_V fitting were:

- All the optical bands, except those displaying obvious excesses. Some optical bands can indeed be strongly affected by emission lines related to accretion and outflows (Shu et al. 1994; Hartmann et al. 1994; Gullbring et al. 2000). This is specially the case for the u band, which was systematically ignored in all fits.
- All the NIR bands up to K_S, included. Excess in these bands is rarer and usually moderate. We therefore chose to use all of them to maximize the number of measurements used for the fit. Small excesses at these bands result in slightly higher A_V values, but are in general tempered by the optical measurements and result mostly in a larger uncertainty.

Following Bayes theory, the best A_V is obtained from the distribution of likelihood among all values computed over the grid. The explored A_V range was 0 to 20 mag in steps of 0.1 mag. At least two photometric measurements in the mentioned wavelength range were required for the A_V to be fitted. For 10 sources, only one measurements was available and the A_V could not be properly fitted. After this cleaning process, the final sample is comprised of 2 340 objects.

Figure 2.1 compares the results of the A_V fitting process with the values from the literature when available. In general, our measurements are in agreement with previous estimates within the large uncertainties. Note that these estimates and uncertainties

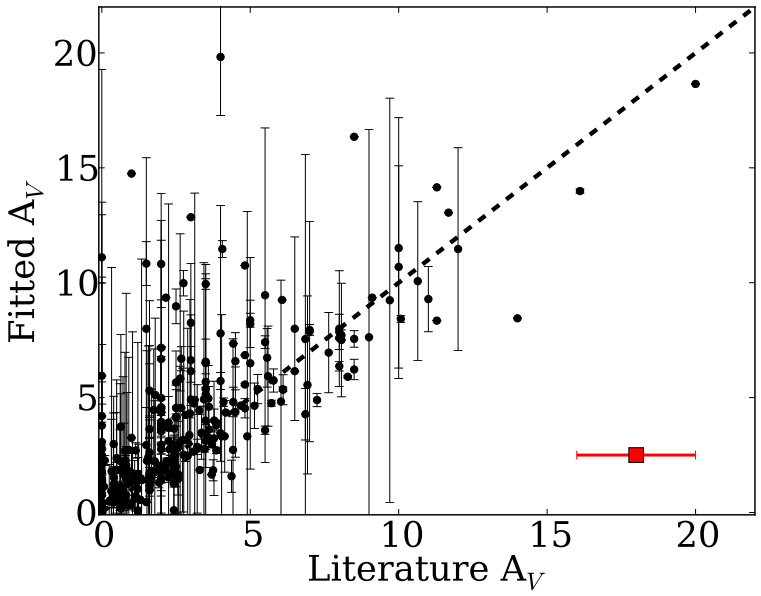

FIGURE 2.1: Comparison between the obtained A_V and the values in the literature. The red square shows the typical uncertainty of spectroscopic A_V estimates from the literature. The identity relation is represented as a dashed line to guide the eye.

are only tentative. Both our measurements and the measurements from the literature are affected by a number of physical and observational biases (variability, accretion, excesses, photometric errors, rotation,etc) which cannot be accounted for. The dispersion in Fig. 2.1 gives a more realistic estimate of the real uncertainties on the A_V.

2.4.2 Discrepancy between *Spitzer* and *WISE* data

A discrepancy between *Spitzer* and WISE data was identified during the visual inspection process. We interpret it as the result of contamination from extended background emission and/or source confusion. A more detailed discussion on this issue is given in Appendix A. Data from the AKARI mission (with PSF sizes larger than those of *Spitzer* and WISE) were also discarded for the same reason.

We therefore discarded all the WISE measurements except for nearby associations from the SACY survey. Given their proximity (< 100 pc), the WISE photometry should not be affected by either extended emission (which is rare in these evolved associations) or confusion (also unlikely, since these associations are extremely lose and extended). Visual inspection of the corresponding SEDs and comparison with *Spitzer* photometry when available confirms that the WISE measurements of SACY sources are indeed not affected by any of these issues, but objects flagged as extended in the WISE catalog were conservatively discarded anyway.

TABLE 2.2: Sensitivity completeness limits for the *Spitzer* photometric data.

Regions	IRAC1 (mJy)	IRAC2 (mJy)	IRAC3 (mJy)	IRAC4 (mJy)	MIPS1 (mJy)
All regions (except Taurus)	0.08	0.05	0.12	0.16	1.03
Taurus (Rebull et al. 2011)	0.18	0.12	0.62	0.62	5.12

2.5 Disk fractions

In this section we study disk fractions as probed by MIR excesses. For the rest of this work, any object with excess at any wavelength longer than 3 μm is considered as a disk-bearing system. Prior to identifying disks and deriving disk percentages, we investigated the sensitivity and spatial completeness of the various MIR surveys.

2.5.1 Sensitivity completeness

Circumstellar disks produce a flux excess at IR wavelengths, and hence disk-bearing stars are easier to detect than pure photospheres. A magnitude limited sample such as the one presented here can thus be biased toward objects with disks, leading to overestimated disk fractions. We corrected from this bias by discarding objects with photospheric flux values (as obtained from models used during the SED fitting, see Sect. 2.4.1) below the detection limits of the different instruments and observations. According to the user manual, the WISE mission (used for the SACY sample) surveyed the whole sky with 5-σ sensitivity limits of 0.08, 0.11, 1 and 6 mJy for the W1, W2, W3, and W4 bands respectively. We estimate that the W1, W2 and W3 sensitivities encompass the entire luminosity range of the SACY sample, while the W4 band is sensitive down to the late-K/late-M dwarfs, depending on the age and distance. *Spitzer* data (used for the rest of the associations, see Table 2.1) come from various surveys with different sensitivities, summarized in Table 2.2. While the optical, NIR and *IRAC* data are sensitive to the entire luminosity range described in Section 2.2.2, the shallower *MIPS* observations define a more limited completeness domain. We estimate that the *MIPS* sensitivity described in Table 2.2 corresponds to early-M/early-K dwarfs depending on the age and distance, respectively.

2.5.2 Spatial coverage

WISE is an all-sky survey, and hence the SACY regions – for which only WISE data was used – were fully covered in the mid-IR. On the other hand, *Spitzer* observations used in this study are covering only fractions of the various associations, resulting in a

number of non detections. These non detections were naturally rejected in the previous step.

2.5.3 Establishing the presence of disks

Circumstellar disks produce MIR/FIR excess in relation to photospheres (Williams & Cieza 2011). Dust around stars is heated by stellar radiation and re-radiates with typical T_{eff} of a few tens or hundreds of kelvin. The amount of excess as a function of wavelength depends on the disk properties, resulting in a wide diversity of SED shapes and making the detection of circumstellar disks sometimes difficult using a single color or luminosity.

To identify excesses, we use the significance index χ_λ, defined as

$$\chi_\lambda = \frac{(F_{\mathrm{observed},\lambda} - F_{\mathrm{model},\lambda})}{\sigma_{\mathrm{Observed},\lambda}}$$

, where $F_{observed,\lambda}$ is the observed flux, $F_{model,\lambda}$ is the corresponding model photospheric flux, and $\sigma_{Observed,\lambda}$ is the error at the corresponding wavelength (λ). We define as "excess" any measurement displaying a $\chi_\lambda \geq 5$, corresponding to a 5-σ detection over the expected photospheric value. We note that flux uncertainties play an important role in the definition of χ and were therefore considered with caution (see Section 2.3.2). Underestimated errors would indeed result in artificially high disk percentages, while over-estimated error would result in artificially low disk fractions.

To investigate the dependence of the presence of excess as a function of wavelength, we defined three wavelength regimes:

- Short wavelength range: sources displaying excess in any band between 3.4–4.6 μm (including IRAC1, IRAC2, WISE1, WISE2),
- Intermediate wavelength range: sources displaying excess in any band between 8.0–12.0 μm (including IRAC4, WISE3),
- Long wavelength range: sources displaying excess in any band between 22–24 μm (including MIPS1 and WISE4).

The MIR emission at different wavelengths probes the disk at different distances from the host star and depth within the disk. Table 2.3 gives an overview of the spatial domains probed by the three wavelength ranges defined above. These values, based on simplifications, should be regarded as indicative only. They nevertheless provide reasonable estimates of the origin of most of the corresponding emission.

TABLE 2.3: Region of the disk probed by the three wavelengths ranges.

Wavelength range (μm)	Disk radius (AU)	Label
3.4-4.6	0.01 - 1	Short
8-12	0.03- 5	Intermediate
22-24	0.3 - 60	Long

MIR excess related to the presence of disks have often been identified using color-color and color-magnitude diagrams. To compare our results with these studies, we also computed fractions for objects detected in all IRAC bands and displaying excess in at least one of them (all regions but SACY) or objects detected in all W1, W2, and W3 bands and excess in any of these three bands (SACY associations).

The "excess" definition based on a conservative 5-σ level of significance might not be optimized for the detection of debris disks. These evolved disks typically display significantly weaker excesses compared to protoplanetary disks (Wyatt 2008). The corresponding debris disk fractions should therefore be regarded as estimates within the boundaries set by the definition of "excess" used here, rather than absolute values. The same applies for NIR excesses, these being intrinsically weaker than MIR ones. Our choice of a more conservative threshold (5 instead of the"usual" $3\,\sigma$) is motivated by the problems encountered with the WISE photometry (see Sect. 2.4.2 and Appendix), which is used mainly for the older regions and therefore for the objects with the weaker MIR excesses. We also note that the usage of two photometric bands in each of the considered wavelength ranges (short, intermediate, long) should mitigate this possible bias.

2.5.4 Disk fraction's values and errors

Disk fractions were calculated as the ratio of objects displaying an excess (as defined before) over the total number of sources after completeness corrections. The large size of our sample allowed us to perform this analysis for the three wavelength ranges defined previously.

Estimating uncertainties on disk fractions using standard error propagation is impractical, as uncertainties on the photometry (errors related to measurement, but also variability, rotation, activity, etc), the fit (A_V) and various models (adopted extinction law, Spectral Type vs T_{eff} relation) are difficult to assess. We chose to estimate errors in an empirical way by using bootstrapping (1000 iterations for each region) and randomly varying the T_{eff} and observed fluxes within normal distributions (with σ of 100 K and σ_{flux}, respectively). For regions with a high number of sources (> 30), disk fraction errors are set as the standard deviation obtained with the boostrapping process. For smaller

TABLE 2.4: Fraction of sources with excess for each region in the three wavelength regimes. The number of sources used is indicated within brackets. Subindexes reference fractions at different wavelength ranges, as defined in Sect. 2.5.3

Name	Fraction $_{\rm IRAC}$(%)	Fraction $_{\rm short}$(%)	Fraction $_{\rm intermediate}$(%)	Fraction $_{\rm long}$(%)
25 Orionis	9 ± 5 [33]	6 ± 4 [34]	9 ± 5 [33]	... [0]
Cha I	52 ± 6 [86]	43 ± 5 [109]	51 ± 5 [102]	66 ± 9 [29]
Cha II	84 ± 9 [19]	61 ± 9 [28]	84 ± 9 [19]	87 ± 9 [15]
CrA	50 ± 13 [16]	31 ± 11 [19]	50 ± 13 [16]	... [4]
IC 348	36 ± 3 [240]	29 ± 3 [262]	30 ± 3 [240]	50 ± 17 [10]
λ-Orionis	26 ± 7 [43]	20 ± 6 [51]	26 ± 6 [43]	... [0]
Lupus	52 ± 5 [85]	38 ± 5 [89]	52 ± 5 [87]	43 ± 7 [49]
NGC 1333	66 ± 6 [67]	47 ± 6 [73]	66 ± 6 [67]	... [2]
Ophiuchus	25 ± 3 [214]	17 ± 3 [253]	25 ± 3 [228]	51 ± 8 [41]
σ-Orionis	39 ± 6 [70]	18 ± 5 [74]	39 ± 6 [70]	... [0]
Serpens	62 ± 4 [125]	44 ± 4 [131]	60 ± 5 [125]	32 ± 11 [29]
Taurus	63 ± 4 [180]	48 ± 3 [212]	63 ± 4 [183]	58 ± 14 [12]
Upper Sco	16 ± 6 [32]	7 ± 2 [250]	11 ± 2 [232]	22 ± 3 [165]
AB Dor	5 ± 3 [78]	4 ± 3 [78]	3 ± 2 [77]	4 ± 3 [51]
Argus	4 ± 5 [44]	0 ± 3 [44]	5 ± 5 [44]	... [3]
β Pic	18 ± 6 [50]	16 ± 5 [50]	8 ± 4 [59]	22 ± 6 [46]
Carina	4 ± 6 [27]	0 ± 3 [27]	4 ± 5 [28]	... [6]
Columba	5 ± 4 [57]	2 ± 2 [57]	5 ± 4 [57]	28 ± 10 [18]
η Cha	21 ± 9 [24]	17 ± 8 [24]	21 ± 9 [24]	30 ± 15 [10]
Octantis	6 ± 7 [17]	0 ± 4 [17]	6 ± 7 [17]	... [1]
Tuc-Hor	8 ± 4 [48]	8 ± 4 [48]	0 ± 3 [48]	12 ± 5 [41]
TW Hya	20 ± 9 [19]	5 ± 6 [19]	16 ± 8 [19]	29 ± 12 [14]

samples, the errors were corrected using the corresponding Student's t distribution with a confidence interval of 68 % (comparable to the $1\,\sigma$ value for larger samples). The derived disk fraction values are given in Table 2.4 and Figs. 2.2 and 2.3. Because of the different sensitivity and spatial completeness levels of the sample, the number of sources varies in each bands. To avoid problems related to small number statistics, we discarded datasets with less than ten objects per region and wavelength range.

2.6 Disk fractions as a function of age

In this section, we investigate disk dissipation timescales as a function of age and wavelength. As a sanity check, we first compare our results with previous studies from Hernández et al. (2007b) and Hernández et al. (2008) for the nine star-forming regions in common: 25 Orionis, Cha I, η-Cha, IC 348, λ-Orionis, NGC 1333, σ-Orionis, Taurus and Upper Sco. Figure 2.2 shows that the results are in good agreement within the estimated uncertainties. We also compare our results for part of the SACY sample from those in Zuckerman et al. (2011): all but one (AB Dor) associations are within a $2\,\sigma$ range. We note that our values are almost systematically lower than the ones given in the literature, as expected given the more conservative disk detection criterion used in this work (see Sect. 2.5.3).

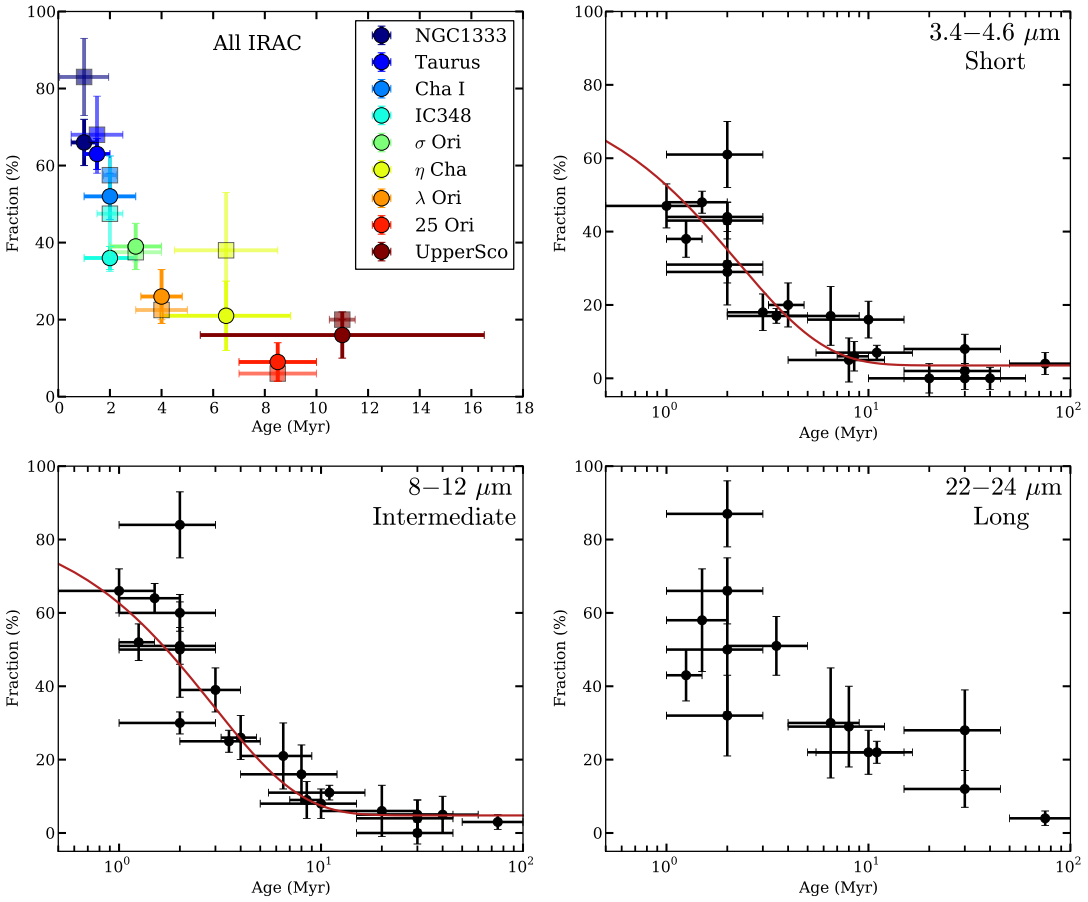

FIGURE 2.2: Upper left panel: comparison of the disk fractions obtained in this study (circles) with those from (Hernández et al. 2007b, 2008) (squares) for regions in common. Upper right and lower panels: disk fractions for all regions in the short, intermediate and long wavelength ranges. The best fit exponential law is over-plotted (red line).

We then study the excess fraction for each of the three wavelength ranges as a function of age (Fig. 2.2, top right and lower panels). Our results show a decay of disk fractions with age at all wavelength ranges The values obtained for Cha II are considerably higher than those of other associations of similar age, but consistent with the value reported by Alcalá et al. (2008). The current dataset does not allow us to explain this difference, and the cause is outside the scope of this study. Figure 2.2 shows that disk fractions for the intermediate (8–12 μm) wavelength range are higher than for the short (3.4-4.6 μm) wavelength range. Although of low statistical significance (within 1-σ), the systematic offset for the entire sample suggests that this relative difference is a real trend.

In this study, we follow Mamajek (2009) and model these distributions with an exponential law of the form:

$$Ae^{-t/\tau} + C \tag{2.1}$$

where t is the age of the region (in Myr), and A, τ and C are left as free parameters. In this simple parametric model, τ can be interpreted as the characteristic timescale of IR

excess decay, and has been previously found to have values between 2∼3 Myr (Mamajek 2009; Williams & Cieza 2011). The best fits obtained for τ in the short (3.4–4.6 μm) and intermediate (8-12 μm) wavelength ranges are 2.3±0.5 Myr and 2.8±0.8 Myr respectively, indistinguishable within the uncertainties and in good agreement with the results from Mamajek (2009). The exponential fit has the advantage of modeling the entire time domain with a single function, and was therefore preferred over the linear fit model used in Haisch et al. (2001b). Further investigation of the possible analytic laws to model this behavior and their corresponding physical interpretation are outside the scope of our work.

Whereas IR excesses in the short and intermediate wavelength ranges are thought to come from primordial optically-thick disks (Williams & Cieza 2011), excesses in the long wavelength range (22-24 μm) can be produced by either primordial, transitional or debris disks (Wyatt 2008). These different types of disk do not necessarily have the same evolutionary mechanisms and timescales (Wyatt 2008). Fitting a simple exponential law to the long wavelength dataset would therefore have no physical meaning and was not attempted here.

To disentangle disks populations in the long wavelength dataset, we split the sample in two groups:

- "Primordial" disks: sources with excess at 22-24 μm *and* at least one shorter wavelength.
- "Evolved" disks: sources with excess at 22-24 μm *only*, including mostly transitional and debris disks. In some cases, edge-on disks can mimic the SED of transitional disks and contaminate the group. Their frequency is nevertheless expected to be very low.

Fig. 2.3 shows the fractions of primordial and evolved disks as a function of time. The distribution is more dispersed than those found at shorter wavelengths (Fig. 2.2), specially at very young ages (<2 Myr). After 2∼3 Myr, it shows a clear and smooth decay and reaches a ∼ zero level around 10∼30 Myr, as observed at shorter wavelengths. To estimate the timescale of excess decay, we fit an exponential law to:

1. The whole primordial disks dataset: τ=5.5 ± 1.4 Myr.
2. The highest values at every given age: τ=4.2 ± 0.6 Myr.
3. The lowest value at every given age: τ=5.8 ± 1.5 Myr.

In all three cases – including the extremes – τ is significantly higher than in the short and intermediate wavelength ranges. Fitted values with their estimated errors for the short, intermediate, and "primordial" long wavelength regimes are given in Table 2.5.

TABLE 2.5: Values and errors obtained from fitting and exponential decay to disk fractions with time. In the case of long wavelength range, only "primordial" disks were fitted, and hence no value is provided for "evolved" disks (see Sect. 2.6).

Wavelength range	A (%/Myr)	τ (Myr)	C (%)
Short	80 ± 10	2.3 ± 0.5	4 ± 2
Intermediate	80 ± 10	2.8 ± 0.8	5 ± 2
Long ("primordial")	$40 - 100$	$4.2 - 5.8$	$0 - 2$

2.7 Discussion

2.7.1 Wavelength-dependent disk fractions

The unprecedented size of our sample and the consistency of our analysis allows for the first time to perform statistically robust measurements of disk fractions as a function of both time and wavelength. Figure 2.2 shows that below 10 Myr, disk fractions derived from MIR excess systematically increase with wavelength (as shown in Table 2.4). We note that this difference could be affected by the stringent "excess" criterion applied here, which could favor the detection of strong excesses typical of MIR bands. We verify that the trend of increasing disk fractions with wavelength up to 10 Myr is still present when a χ >3 cut is used. This result suggests that great care should be taken when comparing studies of disk fractions derived using different wavelength ranges.

2.7.2 Disk decay and dust evolution

The timescale of MIR excess decay obtained in the short and intermediate wavelength ranges are found to be similar, suggesting that the corresponding dust populations evolve on a similar timescale. One the other hand, Fig. 2.2 shows that there is more excess at intermediate wavelengths at a given age than at short wavelengths. The two results combined suggest that the dust emitting at shorter wavelengths – which is in average closer to the star – starts evolving sooner.

The higher MIR excess fractions at all ages and the longer decay times scale in the long wavelength range (22-24 μm) both suggest that the dust at larger radii evolves slower. Although marginal, the higher dispersion of the excesses distribution at long wavelengths points toward a less coherent evolution of the dust in that regime than at shorter wavelengths. The dust populations at larger radii are indeed believed to experience both vertical (settling) and radial (mixing, migration, etc) transfers during the disk evolution. Grain growth, leading eventually to planetary embryos, is also affecting the disk properties and could participate to the observed scatter in time.

2.7.3 Transition from protoplanetary to debris disks

Figure 2.4 shows flux ratios (observed over expected photospheric values) in the long wavelength range (22-24 μm) for all objects as a function of age. Primordial disks display stronger excesses over the photosphere than their evolved counterparts. A sharp decline in flux excess is observed around 10 Myr, indicating a significant change in the disk properties at that stage. On the other hand, Figs. 2.2 and 2.3 show that disk fractions reach a $\sim$ zero level at about the same time. These two results confirm the disk lifetime of $\approx$10 Myr reported previously in the literature (Haisch et al. 2001b; Hernández et al. 2007b, 2008; Mamajek 2009; Williams & Cieza 2011). Unfortunately, current data do not provide information on whether the material found in young debris disks are remnants of the protoplanetary stage, or it is a different dust population produced by planetesimal collisions (Wyatt 2008). Dissecting this transition from the gas rich to gas poor phases is one of the overall long-term goals of this project.

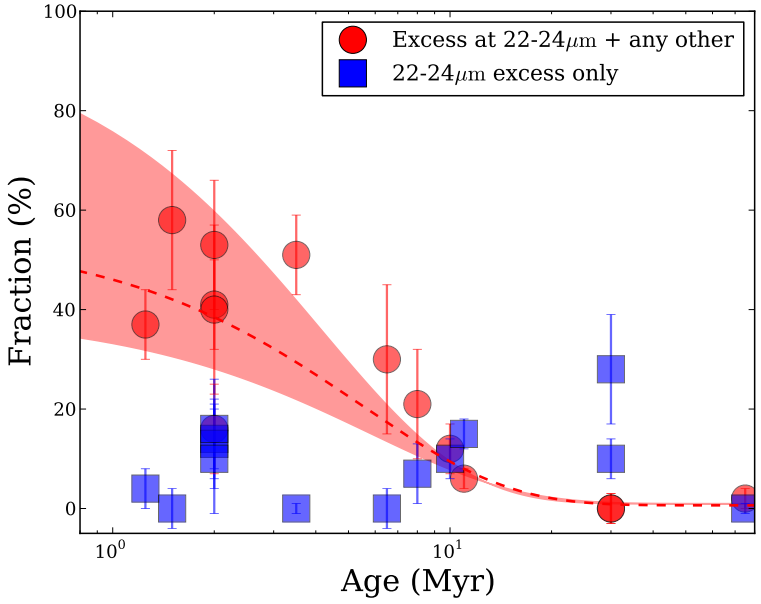

FIGURE 2.3: Fraction of primordial (red circles) and evolved (blue squares) disk as a function of age. The best fit exponential law for the primordial disk percentages is overplotted as a red line. The red shaded area represents the fit obtained for two extreme cases: the highest and lowest values at every age.

Tendencies for "evolved" disks are much harder to determine given their low number at all ages. However, two interesting features can be identified in Fig. 2.3. First, "evolved" disks are not present (or extremely uncommon) at young ages ($\lesssim$ 5 Myr). Second, the fraction of "evolved" disk seems to show a bump starting at $\sim$8 Myr, matching the disappearance of the "primordial" disks. The latter feature, which needs to be confirmed with a larger sample, reproduces the results by Currie et al. (2008) who reported an increase of MIR emission from debris disks at 5–10 Myr, followed by a peak at 10–15 Myr, and a decrease from there on in the double cluster h and χ Persei. They argue that this

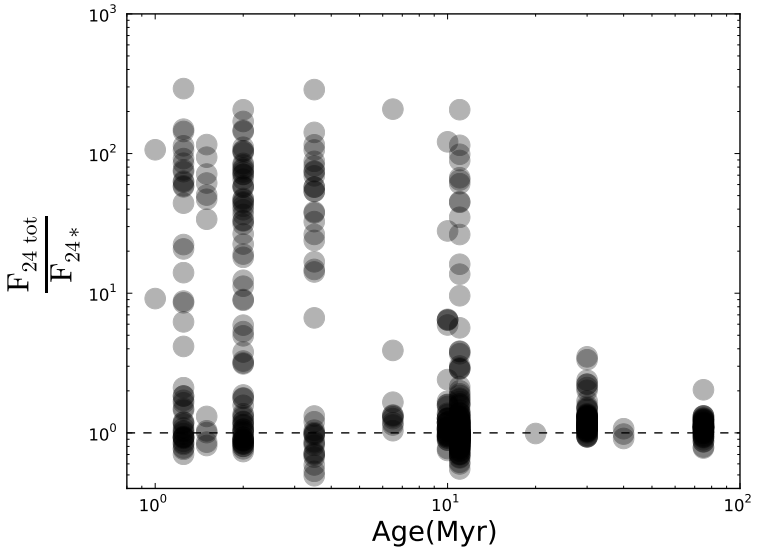

FIGURE 2.4: Ratios of the observed and predicted photospheric values in the long wavelength range (22–24 μm) as a function of age.

qualitatively matches the predictions from the debris disk evolution tracks by Kenyon & Bromley (2004) for disk masses between 3 and 1/3 of the Minimum Mass Solar Nebula, and that kilometer-sized planetesimals already formed between 0 and 2 Myr. This suggest a disk self-stirring process (Wyatt 2008), which would fill the system with dust produced by collisions of planetesimals and increase the MIR flux for some Myr at 22-24 μm. As a result, a higher debris disk detection rate will be obtained, and hence higher disk numbers. The combination of these two features (no "evolved" disks at young ages, plus their fractions tentatively increasing when "primordial" disks start disappearing) reinforces the idea of "evolved" disks being the outcome of "primordial" disk evolution. Interestingly, the disappearance of "primordial" disks, and hence gas (Sicilia-Aguilar et al. 2005, 2006), seems to match in time the period of dust stirring, which indeed require negligible gas to be effective (Wyatt 2008).

2.8 Conclusions

We have compiled a large sample of 2 340 spectroscopically confirmed young stellar objects from 22 nearby (< 500 pc) associations. Spectral energy distributions covering from visible to MIR (22-24 μm) wavelengths have been built and visually inspected for all the sources. We studied the disk fraction as probed by excess over the photosphere in three wavelength ranges: 3.4–4.6 μm (short) , 8–12 μm (intermediate) and 22–22 μm (long), and find:

– The excess fraction is dependent on the wavelength range considered. Transforming excess percentages to disk percentages is therefore not straightforward, and

special care must be taken when comparing disk fractions derived using differing wavelengths.

- Significant discrepancies between the *Spitzer* and WISE photometry are found, mostly due to confusion and extended background emission, and calling for a revision of previous studies based on blind analysis of the WISE luminosities.

- MIR excesses are systematically more frequent at longer wavelength, compatible with inside-out disk clearing scenarios.

- For primordial disks, the dust probed between 22–24 μm seems to evolve more slowly. Assuming an exponential decay, we derive a timescale τ of 4$\sim$6 Myr at 22–24 μm, compared to 2$\sim$3 Myr at shorter wavelengths. This result is also compatible with inside-out disk clearing.

- There is more dispersion in the fraction of excess sources with age when measured at 22–24 μm in comparison to shorter wavelengths, suggesting that other mechanisms are involved in the evolution of the dust at larger radii.

- The fraction of "evolved" disks seems to rise around 8-10 Myr, and decrease again afterward.

- The disappearance of "primordial" (potentially gas-rich) disks at 10$\sim$20 Myr matches in time the brief rise of the number of "evolved" disks. This result is compatible with planet formation theories suggesting that the disappearance of the gas is immediately followed by the dynamical stirring of the debris disk produced by planetesimal collisions that will ultimately lead to planet formation.

- These last two conclusions reinforce the idea of "evolved" disks being the outcome of "primordial" disk evolution.

Future studies based on the present sample will extend these results, obtained for the integrated stellar mass spectrum, by investigating disk fractions and properties as a function of stellar mass, age, and environment. The inclusion of FIR data from *Herschel* will ultimately provide crucial information about outer disk regions and disk masses, contributing to a much more complete picture of disk evolution.

Acknowledgments

This work has been possible thanks to the ESAC Science Operations Division research funds with code SC 1300016149, support from the ESAC Space Science Faculty and of the Herschel Science Centre. We thank the referee for valuable comments that helped to improve the paper, as well as Eric Mamajek for additional suggestions. We also want to thank Neal J. Evans II, Ewine F. van Dishoeck, Paul Harvey, Geoffrey A. Blake, Fernando Comerón, Lucas Cieza, Isa Oliveira, Luisa Rebull, Juan Alcalá, Joanna Brown, Jean-Charles Augereau, Vincent Geers and other members of the c2d team for comments to a previous c2d works on the same topic that had to be abandoned due to inappropriate data for the

intended study. H. Bouy is funded by the Spanish Ramón y Cajal fellowship program number RYC-2009-04497. This work has made an extensive use of Topcat (http://www.star.bristol.ac.uk/~mbt/topcat/, Taylor 2005). This work is based in part on data obtained as part of the UKIRT Infrared Deep Sky Survey. This research made use of the SDSS-III catalog. Funding for SDSS-III has been provided by the Alfred P. Sloan Foundation, the Participating Institutions, the National Science Foundation, and the U.S. Department of Energy Office of Science. The SDSS-III web site is http://www.sdss3.org/. SDSS-III is managed by the Astrophysical Research Consortium for the Participating Institutions of the SDSS-III Collaboration including the University of Arizona, the Brazilian Participation Group, Brookhaven National Laboratory, University of Cambridge, University of Florida, the French Participation Group, the German Participation Group, the Instituto de Astrofisica de Canarias, the Michigan State/Notre Dame/JINA Participation Group, Johns Hopkins University, Lawrence Berkeley National Laboratory, Max Planck Institute for Astrophysics, New Mexico State University, New York University, Ohio State University, Pennsylvania State University, University of Portsmouth, Princeton University, the Spanish Participation Group, University of Tokyo, University of Utah, Vanderbilt University, University of Virginia, University of Washington, and Yale University. This work makes use of data from the DENIS Survey. DENIS is the result of a joint effort involving human and financial contributions of several Institutes mostly located in Europe. It has been supported financially mainly by the French Institut National des Sciences de l'Univers, CNRS, and French Education Ministry, the European Southern Observatory, the State of Baden-Wuerttemberg, and the European Commission under networks of the SCIENCE and Human Capital and Mobility programs, the Landessternwarte, Heidelberg and Institut d'Astrophysique de Paris. This publication makes use of data products from the Wide-field Infrared Survey Explorer, which is a joint project of the University of California, Los Angeles, and the Jet Propulsion Laboratory/California Institute of Technology, funded by the National Aeronautics and Space Administration.

This research used the facilities of the Canadian Astronomy Data Centre operated by the National Research Council of Canada with the support of the Canadian Space Agency.

This publication makes use of data products from the Two Micron All Sky Survey, which is a joint project of the University of Massachusetts and the Infrared Processing and Analysis Center/California Institute of Technology, funded by the National Aeronautics and Space Administration and the National Science Foundation.

This work is based in part on observations made with the Spitzer Space Telescope, which is operated by the Jet Propulsion Laboratory, California Institute of Technology under a contract with NASA.

2.9 Appendix: on the discrepancy between *Spitzer* and WISE data

The WISE mission used four IR bands (3.4, 4.6, 12, and 22 μm, W1, W2, W3 and W4 respectively) to survey the whole sky. On the other hand, the *Spitzer* Space Telescope observed several star-forming regions with its instruments IRAC (3.6, 4.5, 5.8, and 8 μm) and MIPS (24, 70 and 160 μm, the last two not used in this study). IRAC1, IRAC2 and MIPS1 bands are therefore comparable to W1, W2 and W4, respectively. We computed the ratio of measured fluxes (as $\mathrm{WISE_{band}/IRAC_{band}}$) as a function of $\mathrm{IRAC_{band}}$ flux, where *band* corresponds to each of the comparisons mentioned earlier. The results are shown in Fig. 2.5: W1 and W2 are compatible with the corresponding IRAC photometry, whereas W4 deviates significantly from MIPS1 measurements. We found this effect to be more important for weaker fluxes, which could indicate two different issues: (1) a problem with WISE flux estimates for unresolved sources, specially important for confused regions, or (2) an important influence of extended background emission. Figure 2.5 and 2.6 illustrate these two problems in the case of the IC 348 young stellar cluster. IC 348 is a rather dense young cluster with a high and variable background level. WISE fluxes in the W3 and W4 bands were found to be incompatible with the *Spitzer* ones. The full width at half-maximum (FWHM) of the W4 PSF is 11″ (WISE All Sky Release Explanatory Supplement), considerably larger than the 6″ FWHM of the MIPS1 PSF (MIPS Instrument Handbooks), resulting in a higher level of confusion and a greater sensitivity to variable extended background. Figure 2.7 shows an example of a problematic source within IC 348. If we trust the WISE photometry blindly, a MIR excess is found at 12 and 22 μm. The corresponding Spitzer photometry demonstrates that no such excess exists, and that the source most likely does not harbor a disk.

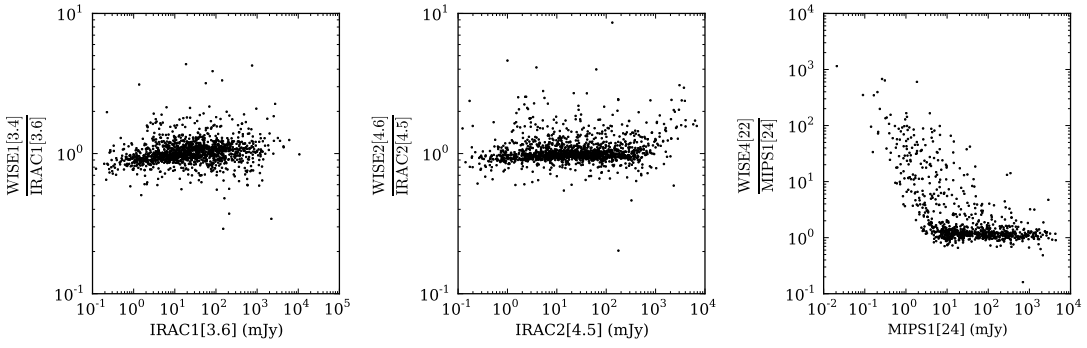

FIGURE 2.5: Differences between WISE and *Spitzer* data as a function of *Spitzer* fluxes for the three comparable bands. Only WISE detections with S/N > 5 are plotted in each band.

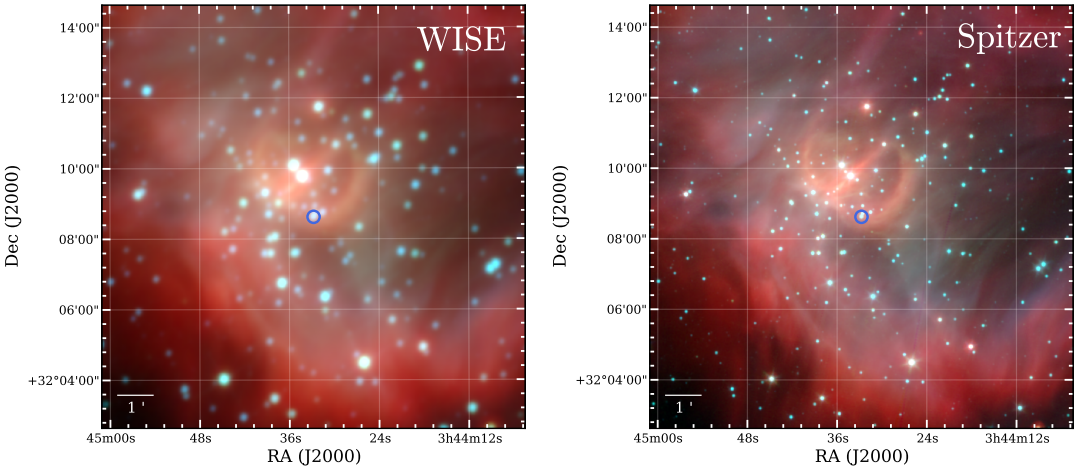

FIGURE 2.6: Three-color composite images of IC 348 as seen by *Spitzer* (left, blue: IRAC1, green: IRAC2, and red: MIPS1) and WISE (right, blue: W1, green: W2, and red: W4). The blue dots marks the position of 2MASSJ03443274+3208374, which SED is shown in Fig. 2.7

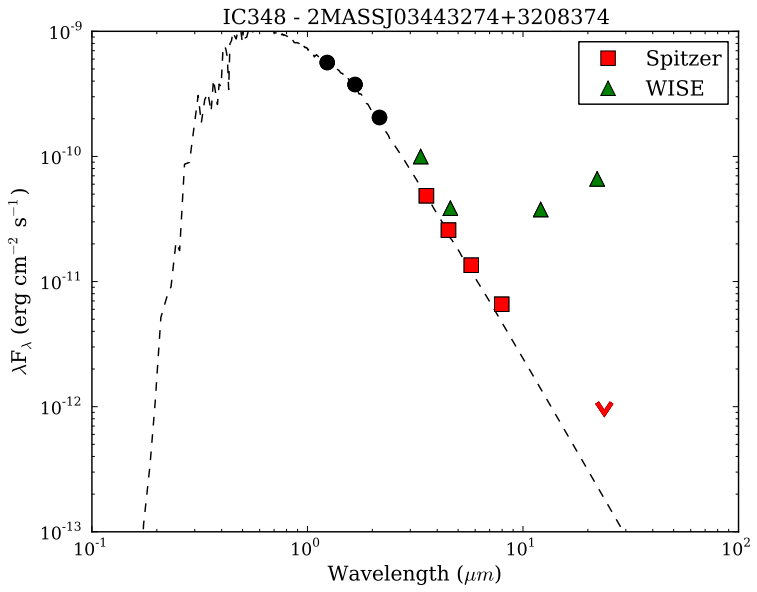

FIGURE 2.7: SED of 2MASSJ03443274+3208374, a source located in a crowded region with variable extended emission (see Fig. 2.6).

3

Disk evolution as a function of stellar mass

Several factors could impact the evolution of protoplanetary disks, both internal to the system (e.g., stellar mass) and external (e.g. radiation fields). If these issues play a role in this evolution, then the outcome of planet formation may be directly linked with stellar and/or environmental properties. In this chapter, we use the database compiled in Chapter 2 to look for dependencies with the mass of the host star. The unprecedented size of this sample allows us to split it in age and mass bins and still obtain statistically robust evidence of different disk evolution timescales around T Tauri and Herbig Ae/Be stars.

This work was published as Ribas et al. 2015, A&A, 576, A52.

Protoplanetary disk lifetimes vs stellar mass and possible implications for giant planet populations

Álvaro Ribas[1,2,3], Hervé Bouy[2], Bruno Merín[4]

[1] European Space Astronomy Centre (ESA), P.O. Box, 78, 28691 Villanueva de la Cañada, Madrid, Spain

[2] Centro de Astrobiología, INTA-CSIC, P.O. Box, 78, 28691 Villanueva de la Cañada, Madrid, Spain

[3] Ingeniería y Servicios Aeroespaciales-ESAC, P.O. Box, 78, 28691 Villanueva de la Cañada, Madrid, Spain

[4] Herschel Science Centre, ESAC-ESA, P.O. Box, 78, 28691 Villanueva de la Cañada, Madrid, Spain

Received 22 August 2014; Accepted 19 January 2015

Abstract

Aims: We study the dependence of protoplanetary disk evolution on stellar mass using a large sample of young stellar objects in nearby young star-forming regions.
Methods: We update the protoplanetary disk fractions presented in our recent work (paper I of this series) derived for 22 nearby (< 500 pc) associations between 1 and 100 Myr. We use a subsample of 1 428 spectroscopically confirmed members to study the impact of stellar mass on protoplanetary disk evolution. We divide this sample into two stellar mass bins ($2\,M_\odot$ boundary) and two age bins (3 Myr boundary), and use infrared excesses over the photospheric emission to classify objects in three groups: protoplanetary disks, evolved disks, and diskless. The homogeneous analysis and bias corrections allow for a statistically significant inter-comparison of the obtained results.
Results: We find robust statistical evidence of disk evolution dependence with stellar mass. Our results, combined with previous studies on disk evolution, confirm that protoplanetary disks evolve faster and/or earlier around high-mass ($> 2\,M_\odot$) stars. We also find a roughly constant level of evolved disks throughout the whole age and stellar mass spectra.
Conclusions: We conclude that protoplanetary disk evolution depends on stellar mass. Such a dependence could have important implications for gas giant planet formation and migration, and could contribute to explaining the apparent paucity of hot Jupiters around high-mass stars.

Key words: Planetary systems: protoplanetary disks, planet-disk interactions – stars: formation – (stars:) planetary systems – stars: pre-main sequence

3.1 Introduction

Studying the evolution of protoplanetary disks around young stellar objects (YSOs) is crucial to better comprehend how planets form. Understanding the effects of fundamental parameters such as age, stellar mass, environment, or binarity provides insight into the planet formation processes, and could shed light onto important relations between planetary systems and their stellar hosts. Several studies on this topic (see e.g. Williams & Cieza 2011; Alexander et al. 2014; Espaillat et al. 2014) have already drawn a comprehensive picture of protoplanetary disk evolution.

In the first paper of this series (Ribas et al. 2014, hereafter R14) we presented a large sample of $\sim 2\,300$ spectroscopically confirmed YSOs in 22 young (< 100 Myr) and nearby (< 500 pc) star-forming regions and associations; R14 used this large sample with very low contamination and high completeness levels to derive accurate disk fractions and protoplanetary disk dissipation timescales. Their results, in good agreement with previous estimates (Haisch et al. 2001b; Hernández et al. 2007b, 2008; Mamajek 2009; Fedele et al. 2010; Murphy et al. 2013) served as a benchmark to test the reliability and robustness of the sample and methods used in R14.

The evolution of protoplanetary disks and planets are closely connected as the disk properties define the initial conditions of planet formation, and the planet evolution subsequently affects the disk properties (e.g. Kley & Nelson 2012; Baruteau et al. 2014). The disk lifetime is a fundamental parameter to understand the interplay between a disk and its planets, since it determines the time available for the planets to form and migrate (e.g. Burkert & Ida 2007; Alexander & Armitage 2009). A dependence of the disk lifetime on the stellar mass could have strong implications for planet formation and migration theories (see e.g. Raymond et al. 2014; Helled et al. 2014; Baruteau et al. 2014, for recent reviews on this topic), and ultimately result in different planetary populations around low-mass and high-mass stars. Previous studies have already found hints of protoplanetary disks evolving faster around massive stars (e.g. Carpenter et al. 2006; Dahm & Hillenbrand 2007; Kennedy & Kenyon 2009; Roccatagliata et al. 2011; Fang et al. 2012; Yasui et al. 2014), but these studies focused on individual regions and/or were potentially affected by different systematics (e.g., low-number statistics, sensitivity biases, contamination from background giant stars, different completeness levels). As a result, a direct comparison of their results is difficult and a statistically robust confirmation of a possible dependence of the disk lifetime with stellar mass has been elusive so far.

In this second paper of the series, we study the influence of stellar mass on disk evolution using the large and homogeneous sample compiled in R14. Section 3.2 updates the study on R14. In Sect. 3.3 we describe the methodology and criteria used to analyze the disk

evolution dependence with stellar mass, and the obtained results are shown in Sect. 3.4. The implications of this study are discussed in Sect. 3.5.

3.2 Updates on paper I

3.2.1 Description of the sample and bias corrections

We first make a short summary of the sample compilation and completeness corrections in R14. The dataset was obtained by combining several stellar population studies of different young regions and associations (see Table 1 in R14 for a complete list of references). These works used a variety of methods to confirm membership depending on stellar masses (e.g. presence of lithium in the spectra, accretion, or X-ray properties). Every object also has a spectroscopic measurement of its spectral type, minimizing the contamination from background giant stars and extragalactic sources. Moreover, these studies were specifically designed to make a complete census of the stellar content over a given mass range and should not be biased towards excess-bearing stars, for example. We therefore expect the compiled sample to be at least representative of (if not complete) the stellar population of each of the considered regions. The covered stellar mass spectrum ranges from O-type to late M-type stars in all regions. We note that R14 did not re-estimate or discuss membership for any target.

Our main aim in R14 was to derive accurate disk fractions for the considered regions via IR excesses. This dependence on the availability of IR data could bias the sample, and two additional steps were considered to prevent this:

- spatial correction, i. e., only sources within the field of view of IR surveys (Spitzer or WISE, see below) were considered. Given that disks are identified via IR measurements, sources lacking these data could be incorrectly classified as "diskless" (since no IR excess is found), even though there is no information to classify them (we do not know whether these sources have IR excess or not). We gathered IR data from the all-sky WISE survey (Wright et al. 2010) to study associations from the SACY sample (Torres et al. 2008), and therefore they were not affected by this problem. For the rest of the regions, however, we used data from different *Spitzer* Space Telescope programs and surveys, which were limited in their spatial coverage. In these cases, we checked the position of each source and did not considered those outside the respective *Spitzer* map;

- sensitivity correction, i. e. only sources with predicted photospheric level above the sensitivity limit of the corresponding observations were considered. Sources with disks have IR excesses, and therefore are easier to detect than naked stars (a process known as the Malmquist bias). We therefore considered only objects with

predicted stellar emission (from photospheric models scaled to match the observed fluxes) above the corresponding sensitivity limit and wavelength. We also took into account the dependence of this limit with the corresponding photometric band and survey. For NIR observations, most of the stars fulfill this requirement, and therefore the sample is expected to be complete down to mid or late M-type stars. In the MIR, the sensitivity of the observations is more restrictive and the completeness level drops down between late K- and mid M-type stars, depending on the distance of the region.

The result of this process is a representative sample of young (1-100 Myr) nearby (< 500 pc) star-forming regions and associations with minimum biases.

3.2.2 Updates of paper I

Ribas et al. (2014) identified IR excesses via excess significance, defined as:

$$\chi_\lambda = \frac{\mathrm{F_{observed,\lambda}} - \mathrm{F_{photosphere,\lambda}}}{\sigma_{\mathrm{Observed,\lambda}}}$$

where $\mathrm{F_{observed,\lambda}}$ is the observed flux, $\mathrm{F_{photosphere,\lambda}}$ is the corresponding model photospheric flux, and $\sigma_{\mathrm{Observed,\lambda}}$ is the error at the corresponding wavelength (λ). In R14, bands with $\chi \geq 5$ were considered to harbor excesses. This procedure allowed us to compute disk fractions for each region at different wavelengths after correcting for sensitivity and spatial completeness (see R14 for a description of the method used).

We updated the study in R14 using new results from the literature as well as improved methods and calculations. In particular:

- the association ϵ Cha was mistakenly named η Cha in R14;
- the distance to Serpens has been updated to 415±15 pc from Very Long Baseline Array observations of one star (Dzib et al. 2010);
- we have improved our estimate of the sensitivity completeness limits for each object by taking into account the extinction. The sensitivity limit should be compared against the reddened photospheric value. Reddened photospheres are flatter (once normalized) than derredened ones, and hence impose looser conditions for the detection limit. As a result, the total number of sources within the completeness limits increased significantly, allowing for better statistics and slightly varying the disk fractions in R14 (see Appendix);
- the disk identification method in R14 is based on excess significances, which depend on the photometric errors (both observational and systematic). Hence, the disk

fractions derived in our study depend strongly on the sensitivity of the *Spitzer* and WISE observations. Smaller errors would result in a higher disk detection rate. The photometric data in R14 were compiled from different programs that used different techniques to estimate the photometric errors. Homogenizing the errors for the whole sample is therefore essential to guarantee a constant and coherent disk detection efficiency in our heterogeneous dataset. Figure 3.1 shows the photometric uncertainties as a function of apparent luminosity in IRAC3 and 4 and MIPS1 bands for the sample of 13 star-forming regions with *Spitzer* data. All regions but two (IC348 and Ophiuchus) have uncertainties at or below 7% in all IRAC 3 and 4 bands, and at or below 12% in MIPS1. We interpret the larger uncertainties for IC348 and Ophiuchus as the result of the conspicuous and highly variable MIR background observed in both regions at these wavelengths. To ensure a homogeneous disk detection rate across the entire sample, we rejected Ophiuchus and IC348 for the rest of our analysis, and set a conservative constant photometric error of 7% for IRAC and WISE1, 2, 3 bands, and 12% for MIPS1 and WISE4 in the χ_λ calculations. The final sample is comprised of 1 809 sources (see Table 3.4).

After these updates, we repeated the analysis in R14 and derived disk fractions in each association. We then fit these disk fractions as a function of time using an exponential law of the form:

$$Ae^{-t/\tau} + C$$

where t is the age of the region (in Myr), and A, τ and C are left as free parameters. In this simple parametric model, A represents the initial fraction of sources with IR excess, τ can be interpreted as the characteristic timescale of IR excess decay, and C is a possible constant level.

The updated values are presented in the Appendix (Tables 3.4 and 3.5, and Figs. 3.7 and 3.8). These results are in agreement with previous studies (e.g. Lada et al. 2000; Hernández et al. 2007b, 2008; Murphy et al. 2013) and supersede our results in R14.

We note that we have combined data for regions at different distances, and therefore the sensitivity limit in spectral type is different for each of them. The overall completeness (all regions combined) for results with NIR data (IRAC-WISE1,2,3) is around 0.1 $M_\odot$. For MIR (MIPS1-WISE4), the sensitivity and the completeness limit increases to 0.4 $M_\odot$.

3.2.3 Impact of new membership estimates and region ages

New membership estimates are available in the literature for some of the regions and associations in this study (e.g. ϵ Cha, TW Hya Murphy et al. 2013; Ducourant et al. 2014), which could have an impact on our results. However, these works have modified

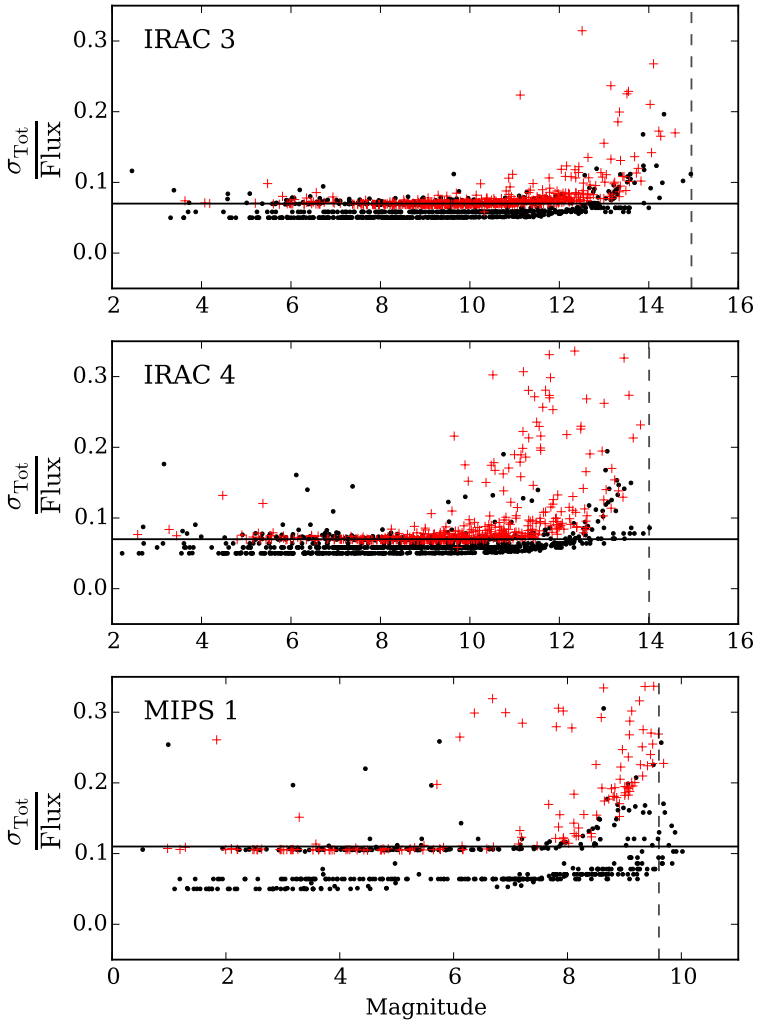

FIGURE 3.1: Ratio of the total uncertainty (observational and systematic) over the observed flux as a function of magnitude. IRAC3, IRAC4, and MIPS1 bands are shown. Sources from discarded regions (IC348 and Ophiuchus) are represented as red crosses, the rest of the sources as black dots. The black solid line corresponds to the homogenized uncertainty levels of 7 % (all IRAC bands) and 12 % (MIPS1). The black dashed line shows the sensitivity limit for each band, as indicated by the observing programs. Objects falling beyond this limit in the MIPS1 plot are caused by noise (e.g., uncertainties in $T_{\rm eff}$, A_V) in the corresponding photosphere fit, and were kept in the sample.

the overall members of these associations by a small factor and moreover, our results will be still valid as long as the considered sample is representative of their stellar population. In addition, the original SACY sample has a homogeneous sensitivity for each region. By including other surveys with completely different selection criteria we might add systematics and biases difficult to detect and account for. Hence, for consistency with R14, we do not update membership or include new objects in this work.

Furthermore, the age estimates for the regions in our study are crucial for our analysis. Absolute ages of young associations are hard to determine, and some recent works have shown that the adopted values may be underestimated by a factor of two (Bell et al. 2013). However, the relative age sequence is easier to derive and is expected to be more

precise (Soderblom et al. 2013). This is actually reinforced by the disk fractions derived for these regions: these measurements are independent of the age of the regions, yet they clearly decrease once sorted by age (see Appendix). We therefore assume the same age values as in R14, and we note that our estimates of disk lifetimes may be subject to modifications by a scaling factor, depending on the real absolute ages.

3.3 Stellar masses and ages

In this section, we study a possible dependence of disk evolution - as probed by disk fractions - as a function of stellar mass. To optimize the disk detection rate, we chose to limit the study to regions observed with the *Spitzer* Space Telescope. Its sensitivity and spatial resolution are significantly better than those of WISE, and allow a search for fainter excesses over the photospheric emission. A total of 1 428 sources from 11 associations were observed with *Spitzer* (see Table 3.1). We note that this value is smaller than the initial sample, since we are not including associations studied with WISE data in R14 (i.e., the SACY sample). The better sensitivity and spatial resolution of the *Spitzer* observations allow us to lower the threshold for excess detection. In the following we consider as excess any photometric measurements displaying $\chi \geq 3$ (instead of $\chi \geq 5$ used in Sect. 3.2).

Stellar luminosities were obtained by scaling the best-fit photospheric model (BT-Settl models, Allard et al. 2012) to the dereddened photometric data (see R14) and integrating it over the entire stellar spectrum. In this way, the calculation does not depend on uncertain bolometric corrections. These luminosities were transformed into masses using the mass-luminosity relationship given by the pre-main sequence isochrones of the corresponding age in Bressan et al. (2012).

To study the influence of stellar mass in the evolution of protoplanetary disks, we divided the sample into two age bins and two mass bins:

- The age cut separating young and old objects was set to 3 Myr. This is similar to the typical timescale of disk decay found in Sect.3.2 (see Appendix) for protoplanetary disks. A total of three regions (25 Ori, λ Ori, and Upper Sco) make up the "old" sample adding up to 489 sources, whereas the rest of the associations (939 sources) make up the "young" sample.
- The mass cut between low- and high-mass objects was set to $2\,M_{\odot}$. Although somewhat arbitrary, this threshold is usually considered as the separation between T Tauri and Herbig stars. Given their different physical properties (e.g. radiation fields, stellar winds or accretion rates, see Calvet et al. 2005; Garcia Lopez et al. 2006; Hillenbrand 2008), it is likely that disks evolve differently around them. In

TABLE 3.1: Young nearby star-forming regions included in the study of protoplanetary disk dependence on stellar mass.

Name	Age (Myr)	Distance (pc)	Membership and SpT	*Spitzer* photometry	Number of sources
25 Orionis	7-10	330	(1)	(1)	46
Cha I	2	160-165	(2) (3) (4)	(3) (4)	212
Cha II	2±2	178±18	(5)	(31)	47
CrA	1-3	138±16	(6) (7) (8) (9)	(32)	35
λ Orionis	4	400±40	(10)	(33)	114
Lupus	1-1.5	140 - 200	(11) (12) (13) (14)	(31)	217
NGC 1333	1	235±18	(15)	(34)	74
σ Orionis	2-3	440±30	(16) (17) (18) (19) (20) (21) (22)	(35)	104
Serpens	2	415±15	(15) (23)	(31)	142
Taurus	1-2	140	(24) (25) (26) (27)	(26) (27)	265
Upper Sco	11±2	140	(28) (29) (30)	(29)	405

(1) Hernández et al. (2007a); (2) Luhman (2007); (3) Luhman et al. (2008a); (4) Luhman & Muench (2008); (5) Spezzi et al. (2008); (6) Neuhäuser et al. (2000); (7) Nisini et al. (2005); (8) Sicilia-Aguilar et al. (2008); (9) Sicilia-Aguilar et al. (2011); (10) Bayo et al. (2011); (11) Krautter et al. (1997); (12) Allen et al. (2007); (13) Comerón (2008); (14) Mortier et al. (2011); (15) Winston et al. (2009); (16) Zapatero Osorio et al. (2002); (17) Muzerolle et al. (2003b); (18) Barrado y Navascués et al. (2003); (19) Franciosini et al. (2006); (20) Caballero (2007); (21) Sacco et al. (2008); (22) Rigliaco et al. (2012); (23) Oliveira et al. (2009); (24) Luhman (2004b); (25) Monin et al. (2010); (26) Rebull et al. (2010); (27) Rebull et al. (2011); (28) Preibisch et al. (2002); (29) Carpenter et al. (2006); (30) Lodieu et al. (2011); (31) Evans et al. (2009);(32) Peterson et al. (2011); (33) Barrado y Navascués et al. (2007); (34) Gutermuth et al. (2008); (35) Luhman et al. (2008b)

addition, such a mass cut has the advantage of separating the sample so that both bins have enough sources for meaningful statistics.

Therefore, for the rest of the study we classified sources as:

- "young" if $1\,\mathrm{Myr} \leq \mathrm{age} \leq 3\,\mathrm{Myr}$, "old" otherwise
- "low-mass" if $\mathrm{M}_* < 2\,\mathrm{M}_\odot$, "high-mass" otherwise

3.4 Disk fractions vs stellar mass and time

The presence of dust around stars is usually detected as IR excess over the photospheric level: the dust is heated by the stellar radiation, and re-radiates with typical temperatures of tens or hundreds of Kelvins. However, the amount and shape of this excess depends strongly on the disk characteristics. Protoplanetary disks display excess at NIR wavelengths ($< 10\,\mu$m, Williams & Cieza 2011): these are disks that extend from the close regions ($< 1\,$AU) of the stellar system to hundreds of AUs. However, the evolution of disks is thought to remove dust from the inner regions (e.g. Koepferl et al. 2013; Alexander et al. 2014, R14), leaving only MIR ($24\,\mu$m) or even FIR ($> 50\,\mu$m) excesses as in the case of transitional and debris disks (Wyatt 2008; Williams & Cieza 2011).

3.4.1 Protoplanetary disks

In this section, we limit the study to NIR excesses observed with IRAC, which offers the best sensitivity to the coolest objects of our sample, and therefore allows us to estimate disk fractions over a larger mass range. Unfortunately, IRAC photometry alone does not allow a fine classification of disks. We therefore define two simple groups:

- protoplanetary disks are defined here as those sources having excesses at wavelengths shorter than $10\,\mu$m (either 5.8 or $8\,\mu$m, i.e., IRAC3 and/or IRAC4 bands). This definition encompasses the classic protoplanetary disks.
- processed disks are defined as sources without excess either at IRAC3 or IRAC4 bands. They could be transitional disks, debris disks, or diskless stars, but are indistinguishable based on IRAC photometry alone. In all cases their disks (if present) have reached a more advanced level of processing than the protoplanetary disks defined above.

We applied the sensitivity completeness correction as defined in Sect. 2 to ensure that the sample is not biased towards disk-bearing sources. A total of 1 033 objects met this criteria for IRAC4 (the strictest sensitivity limit for IRAC bands). However, as pointed

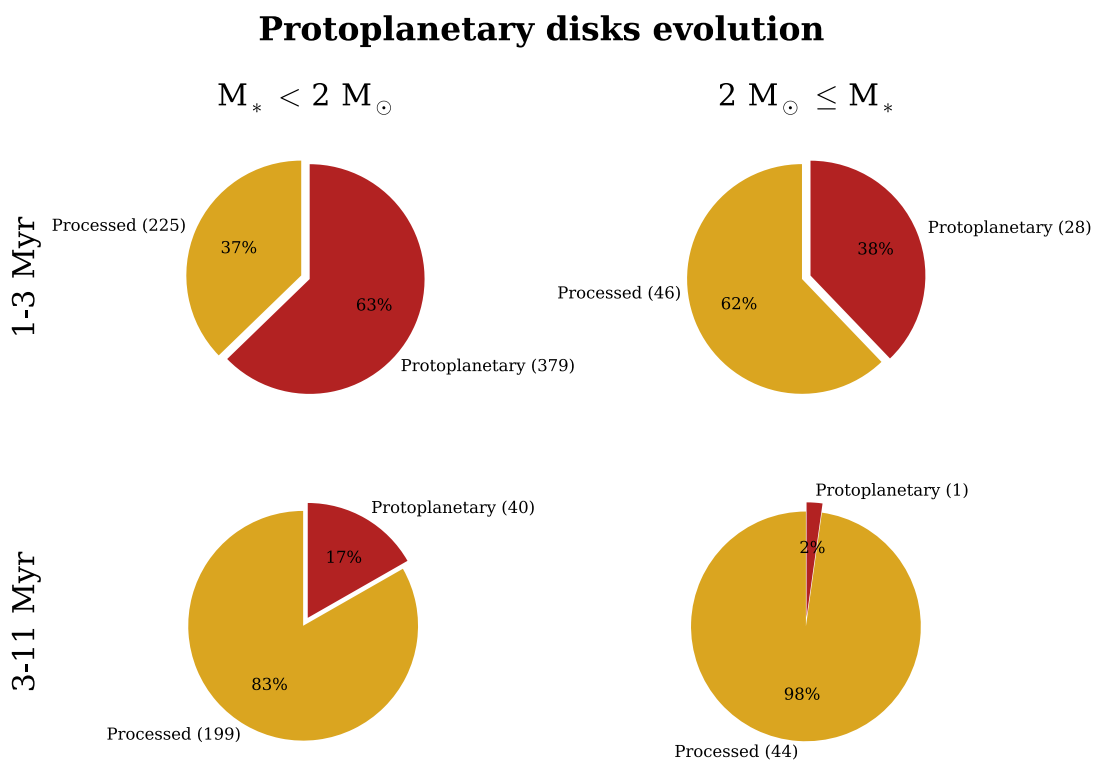

FIGURE 3.2: Evolution of protoplanetary disks (red) and processed (yellow) disks for each mass and age bin. The number of sources in each bin is shown within brackets. Errors are less than 6 % (see Table 3.3).

in Sect. 3.2, the considered regions are at different distances and so the sensitivity limit translates into a different completeness limit in spectral types for each of them. We computed the limiting spectral type for each region, i.e. the latest spectral type detected with the corresponding sensitivity limit (see Table. 3.2). Given its distance and age, 25 Orionis has a significantly earlier limiting spectral type than the rest of the regions, and we do not consider it in the analysis. Therefore, we cut the sample to the most restrictive limiting spectral type (M7, Cha II and λ Orionis). After this procedure, the resulting IRAC sample is comprised of 962 sources.

We then divided this sample using the mass and age cuts described in Sect. 3.3. The result of this process is shown in the form of pie charts in Fig. 3.2 and in Table 3.3. Errors for the disk fractions were estimated using the bootstraping method further described in Sect. 3.4.3, and are typically less than 6 %.

After inspection of Fig. 3.2 some conclusions can be drawn:

- Protoplanetary disks are significantly more frequent around low-mass stars than around high-mass stars, independent of the age.
- As expected, protoplanetary disk fractions decrease significantly at older ages for both low- and high-mass stars.

3.4.2 Evolved disks

As mentioned in Sect. 3.4.1, IRAC photometry alone does not allow a fine classification of processed disks. Photometric measurements at longer wavelengths are required to assess whether a source has a transitional or debris disk or if it is a diskless star. In an attempt to distinguish these categories, we repeated the analysis presented in Sect. 3.4.1 including MIPS1 data. The 24 μm photometry allows he processed disks to be divided into two more precise categories:

- evolved disks, having no excess at IRAC3 or IRAC4, but with an excess at MIPS1. They include transitional and hot debris disks, as well as a small fraction of edge-on disks (e.g Huélamo et al. 2010) and circumbinary disks (e.g Ireland & Kraus 2008).
- diskless stars, displaying no excess at IRAC and MIPS1 bands. They include genuine diskless stars as well as colder (more evolved) debris disks that emit only at FIR wavelengths.

The same special care was taken to avoid any sensitivity bias, and we kept only the sources with predicted photospheric fluxes above the sensitivity limit of the observations. MIPS1 observations are usually less sensitive than IRAC ones. We applied the same procedure as in the previous case and excluded the regions with significantly worse limiting spectral type (σ Orionis). The final sample was limited to spectral types earlier than M4 (the corresponding limiting spectral type of CrA). As a result, the total number of sources meeting this criteria dropped to 389. While smaller and encompassing a narrower mass range, this sample allows a more detailed look at the evolution of the inner disk via the study of transitional (evolved) disks.

The sample was then split into the mass and age bins defined previously. The results are shown in Fig. 3.3 and Table 3.3. We note in particular that

- the results are consistent with those obtained in Section 3.4.1 for protoplanetary disks within the uncertainties (see Sect. 3.4.3);
- evolved disks are more frequent around high-mass stars than around low-mass stars, independently of the age;
- a roughly constant fraction of evolved disks is found at young and old ages. A small difference seems to arise for high-mass stars (23 % to 31 %), but it is not statistically significant.

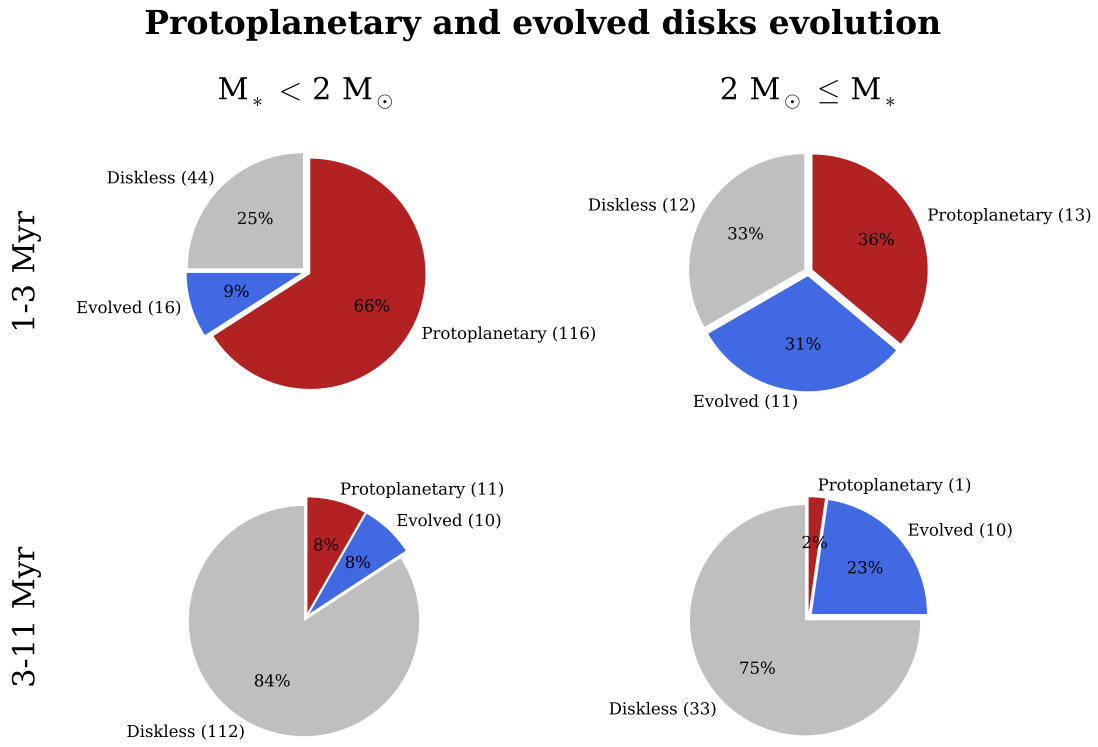

FIGURE 3.3: Frequencies for protoplanetary (red), evolved (blue) and diskless (gray) objects. The number of sources in each bin is shown in brackets. Errors are less than 8 % (see Table 3.3).

TABLE 3.2: Sensitivity limits in spectral type for the IRAC and MIPS1 samples for each association considered in this study. Ellipses indicate that there are no objects in the sample with IRAC/MIPS1 above the corresponding sensitivity limit in that region. The adopted limiting spectral type for each case is marked with an asterisk. Regions not included in the corresponding sample are specified.

Region	IRAC sample	MIPS1 sample
25 Orionis	M5 (excluded)	...
Cha I	M9	M6
ChaII	M7*	M5
CrA	M8	M4*
λ Orionis	M7*	...
Lupus	M9	M9
NGC1333	M8	M5
σ Orionis	M8	M0 (excluded)
Serpens	M9	M8
Taurus	M9	M6
Upper Sco	M9	M5

3.4.3 Significance of the results

The large number of sources included in the various samples in Sects. 3.4.1 and 3.4.2 does not guarantee the significance of the differences observed in Figs. 3.2 and 3.3 and Table 3.3. Calculating uncertainties using standard error propagation or Poisson statistics is neither practical nor trivial in the case of our analysis. The computed fractions depend on several different parameters (e.g., photometric errors, T_{eff} value and A_V fit, photospheric models and adopted isochrones,...) and the age and mass thresholds selected to split the sample could have an impact on the results and their interpretation.

For these reasons, we tentatively estimate uncertainties on the disk fractions by performing bootstrapping (1000 iterations) randomly varying the $T_{\rm eff}$, photometric fluxes, the young/old boundary, the high mass/low mass boundary, and the object distances within normal distributions with σ of 50 K, σ_{flux}, 0.5 Myr, 0.25 $M_\odot$, and error in the region's distance (or 20 pc when no error was available). Uncertainties on the age of the sources were not included in the bootstrapping; although absolute ages are hard to determine, relative ages are expected to be more accurate (Soderblom et al. 2013). Additionally, our analysis considers only two clearly separated age bins.

The bootstrapping yielded probability density functions (PDFs) of disk fraction for each sample, and should account for most uncertainties in the calculations. The standard deviation of the PDFs (which are close to normal) provides a reasonable estimate of the final uncertainties on the disk fractions and are reported in Table 3.3.

Overall, the estimated uncertainties suggest that the differences seen in the disk fractions are statistically significant, and that the distributions for high-mass and low-mass stars are different.

We also checked our results to vary little (a few percentage points) when modifying the mass cut between 1.5 and 2.5 $M_\odot$, and hence our conclusions are robust against the selected mass threshold. Given the lack of regions in the 4-8 Myr regime, it is not possible to test the impact of a different age cut in detail. Our aim is to separate sources which are clearly younger or older, and this value is likely not to have a very strong impact on our study. For this reason, our results are weakly dependent on age uncertainties, as long as relative ages are properly estimated (see discussion in Sect. 3.2.3).

3.4.4 Disk fractions and stellar temperature (mass)

Our definition of protoplanetary, evolved and diskless sources depends on the wavelength at which excess over the photosphere is found. Because the temperature distribution in the circumstellar disk depends directly on the stellar effective temperature and luminosity, the classification probably suffers from a dependence on stellar temperature.

TABLE 3.3: Results from the analysis of disk frequencies as a function of age and mass. See also Figs. 3.2 and 3.3. Errors are one standard deviation from the computed PDFs.

Disk type	Young+Low-mass [%]	Young+High-mass [%]	Old+Low-mass [%]	Old+High-mass [%]
Protoplanetary disks (Section 3.4.1)				
Protoplanetary (IRAC4 detection limit)	63±2	38±6	17±2	2^{+4}_{-2}
Processed (IRAC4 detection limit)	37±2	62±6	83±2	98^{+2}_{-4}
Protoplanetary and evolved disks (Section 3.4.2)				
Protoplanetary (MIPS1 detection limit)	66±4	36±8	8±2	2^{+4}_{-2}
Evolved (MIPS1 detection limit)	9±2	31±7	8±3	23±6
Diskless (MIPS1 detection limit)	25±3	33±8	84±3	75±7

Infrared emission at a certain wavelength likely originates from different regions of the disk for hot (massive) and cool (low-mass) stars, and may even arise from different disk types.

This effect is probably not critical for our analysis of protoplanetary sources (Sect. 3.4.1). These dense and massive disks have complex physical structures, and the IR excess at a certain wavelength is emitted from relatively large areas of the disk. Moreover, the protoplanetary definition is based on the presence of excess over a relatively wide wavelength range, ensuring that the corresponding emission comes from broad areas of the disk regardless of the stellar mass.

On the other hand, our definition of evolved disks relies primarily on IR excess at 24 μm (MIPS1). The area of the disk probed at 24 μm is expected to vary significantly between massive and low-mass stars, and might make the comparison of the excess fractions and their interpretation more difficult.

To test how much this dependence might affect our results, we computed a grid of radiative transfer models of circumstellar disks using the code MCFOST (Pinte et al. 2006). We found that synthetic SEDs classified as evolved according to our criterion always corresponded to higher levels of disk processing regardless of the star's temperature. These simple simulations suggest that our classification scheme is efficient and robust enough to allow a comparison of the results obtained for high and low-mass stars.

Finally, a comparison of the evolution of evolved disks can be performed within the same mass bin, removing most of the previous dependency on stellar temperature. Figure 3.4 shows the PDFs of the "evolved" disk fractions obtained in Sect. 3.4.3 for high-mass stars on the one hand and low-mass stars on the other hand. The PDFs are completely compatible both for low-mass and high-mass stars, pointing to a roughly constant level of evolved disks within the uncertainties at any age regardless of stellar mass.

3.5 Impact of stellar mass on disk evolution

3.5.1 Dependence of protoplanetary disk lifetimes on stellar mass.

Previous observational studies had already found lower protoplanetary disk fractions around high-mass stars and suggested that their protoplanetary disks disperse earlier and/or evolve faster (see e.g Williams & Cieza 2011, for a review). A number of these studies focused on individual regions, making it hard to confirm a global dependence of protoplanetary disk evolution on stellar mass independently of the environment and method used to identify the disks (e.g Lada et al. 2006; Dahm & Hillenbrand 2007; Currie et al. 2009; Carpenter et al. 2006, in IC348, NGC 2362 and Upper Sco). Kennedy & Kenyon (2009) performed an original and coherent study of disk frequencies in nine

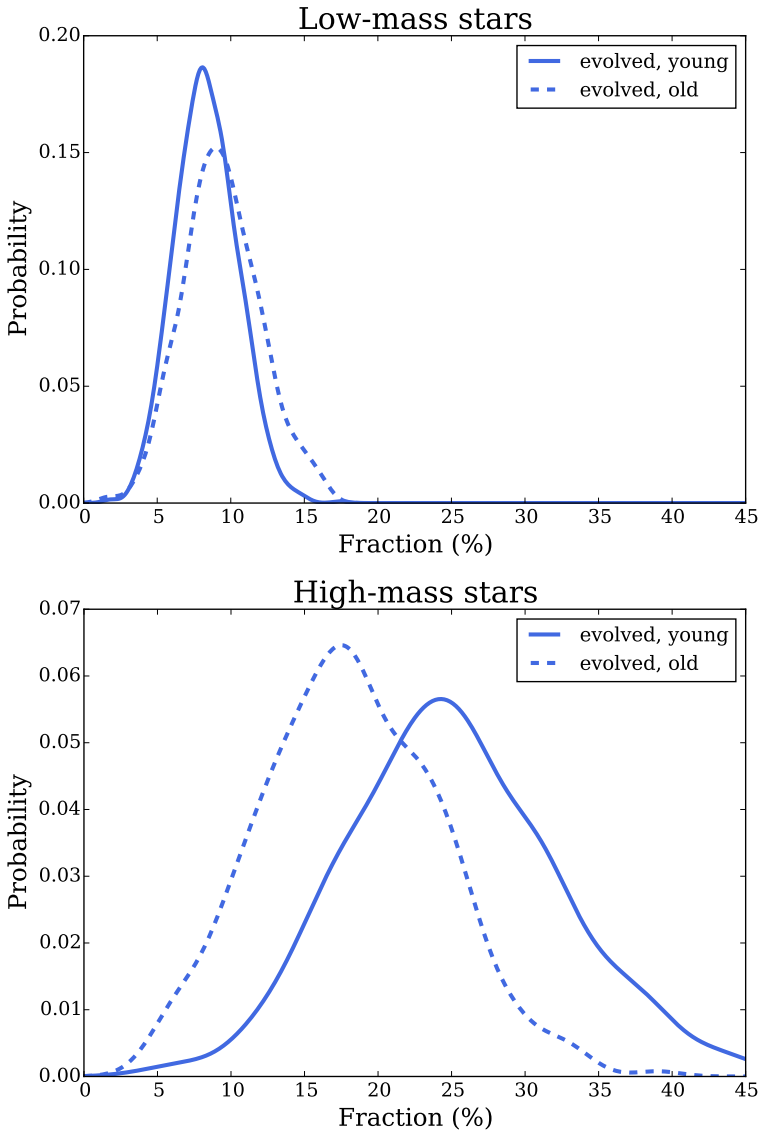

FIGURE 3.4: Comparison of the obtained PDFs for evolved sources as a function of age and for the two stellar mass bins.

young associations by combining optical spectra and IR photometry. In contrast to our study, they found only a weak dependence of disk dispersal on stellar mass. The ages used in their study have been improved and sometimes changed significantly. For example, the age of Upper Sco was recently re-estimated to 11 Myr Pecaut et al. (2012) from an original 5 Myr (Preibisch & Zinnecker 1999), resulting in a noisier distribution of disk fraction as a function of age in their study.

Our results demonstrate quantitatively that protoplanetary disks dissipate significantly faster and/or earlier around high-mass stars, as we find between 10 and 30 % more protoplanetary disks around low-mass stars regardless of the age.

Our data additionally show that the disk fraction for high-mass stars falls to ≈0% anytime between 3 and 11 Myr, and suggest that protoplanetary disks disperse up to

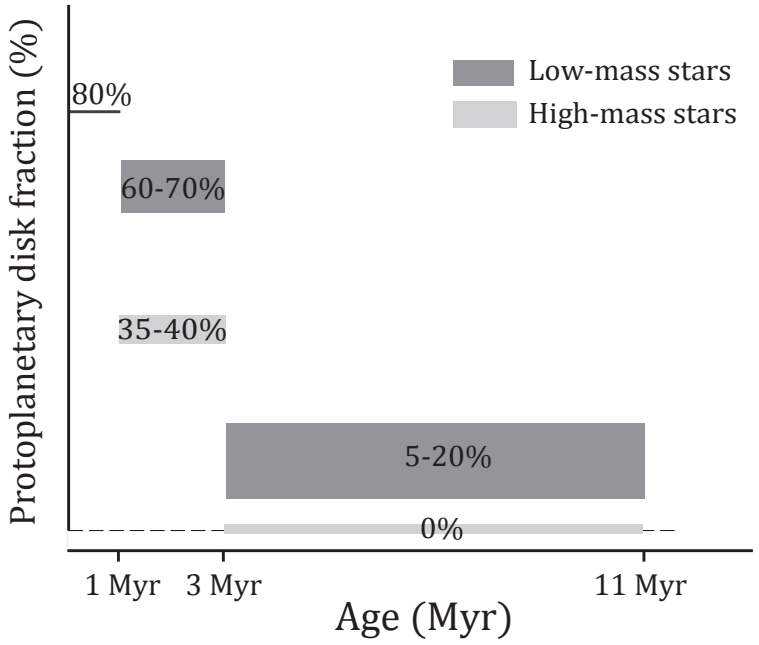

FIGURE 3.5: Evolution of protoplanetary disks as a function of mass, as derived in this study.

two times faster around high-mass stars than around low-mass ones. More data for regions with intermediate ages are needed to better constrain this ratio.

Interestingly, other studies found a higher (80-85 %) protoplanetary disk fraction and no dependence with stellar mass in the younger Trapezium cluster (< 1 Myr, Lada et al. 2000) and NGC 2024 cluster (< 0.4-1.4×10^5 yr, Haisch et al. 2000). Combined with the present study, these results suggest that

- the disk fractions before 1 Myr are in the continuity of the results presented here;
- the dependence of disk fractions on stellar mass appears after the first Myr of the star's lifetime, and persists until no protoplanetary disks are found around ~ 10 Myr

Based on these two suggestions, we propose a scheme of disk evolution as a function of stellar mass (see Fig. 3.5). The timescale of protoplanetary disk formation and evolution is mostly independent of stellar mass until the first Myr. At 3 Myr, significant differences are already observable between the evolution of protoplanetary disks around low- and high-mass stars. By ~ 10 Myr, no protoplanetary disks are found around high-mass stars, but $\approx$10-15 % of low-mass stars still harbor a disk. Stronger radiation fields and higher accretion rates of high-mass stars (Calvet et al. 2005; Garcia Lopez et al. 2006; Hillenbrand 2008) are likely to affect the evolution of protoplanetary disks even during the first Myrs, fastening the processes responsible of disk dispersal (Alexander et al. 2014).

3.5.2 A constant level of evolved disks

We find the fraction of evolved sources to remain constant with age both for low- and high-mass stars: 5-15 % of low-mass stars display this kind of excess, and the fraction increases to 20-30 % for high-mass objects (see Fig. 3.4). Again, the dependence with stellar mass of the disk radii probed at a certain wavelength should be consider and it could, in fact, account for the higher fraction of evolved disks around high-mass stars. Nevertheless, the obtained values at these ages can be established to be within 5-30 %.

The evolved disk definition proposed here includes transitional disks, hot debris disks, edge-on disks and circumbinary disks. Unfortunately, the classification does not allow us to discriminate between these four types of disks. We nevertheless note that simple geometric considerations suggest that edge-on disks must be relatively rare contribute only moderately to the population of evolved disks presented here. Hot debris disks are expected to appear mostly at later stages of disk evolution and must populate mostly the older bin of our analysis. Circumbinary disks are expected to be common given the multiplicity frequency among stars (e.g Bouy 2011), but only the closest systems would mimic the SED of evolved disks defined here (e.g as in Ireland & Kraus 2008; Nguyen et al. 2012). The evolved disks in the young (< 3 Myr) bin are therefore most likely primarily made of transitional and circumbinary disks, and our analysis suggests that these two types of disks can be found even during the very first Myrs of stellar life.

Finally, we also note that the higher fraction of evolved disks – which include circumbinary disks – around high-mass stars is also consistent with their higher multiplicity frequency (Duchêne & Kraus 2013).

3.5.3 Transitional disks

We stress that the current data in our sample cannot be used to isolate transitional disks among evolved disks. With this limitation in mind, it is nevertheless interesting to compare the properties of evolved disks of the present study to the properties of transitional disks as reported in the literature.

Transitional disks are a particularly interesting kind of circumstellar disks that harbor a gap and/or cavity (Andrews et al. 2011). Various mechanisms have been proposed to explain the existence of these gaps and cavities. They can be produced by the formation of planets (Espaillat et al. 2014), grain growth, photoevaporation or the formation of low-mass companions (Birnstiel et al. 2012; Alexander et al. 2014; Papaloizou et al. 2007). The connection between transitional disks and planets – as demonstrated by several resolved images of planetary mass companions within the gap or cavity (e.g Huélamo et al. 2011; Kraus & Ireland 2012; Quanz et al. 2013; Close et al. 2014) – makes them a cornerstone for theories of planet formation and evolution.

First, we note that the fraction of evolved disks derived by our analysis (between 5 and 30%) is consistent with transitional disk fractions reported in the literature (e.g. Skrutskie et al. 1990; Kenyon & Hartmann 1995; Andrews & Williams 2005; Cieza et al. 2007; Merín et al. 2010).

Second, previous studies have established the duration of the transition phase to be ≈ 1 Myr (Alexander et al. 2014), which is in agreement with the combined 5-30 % of evolved sources and the $\approx$10 Myr disk lifetime, if one assumes that all disks go through a transitional phase. Within the planet formation scenario, only Jovian planets are likely to produce a gap in their protoplanetary disk (Lin & Papaloizou 1986; Marsh & Mahoney 1992; Nelson et al. 2000; Calvet et al. 2002; Rice et al. 2003), and so it is also plausible that not all planetary systems go through a transitional phase during their formation. If that is the case, then the estimated ≈ 1 Myr duration of this phase should be regarded as a lower limit.

3.5.4 Implications for planet formation and giant planet migration

To date, there are two main theories explaining the formation of planets: the core accretion model (CA) and the disk instability model (DI) (see Helled et al. 2014; Raymond et al. 2014, for recent reviews on this topic):

- In the CA scenario, a solid planetary embryo is formed by continuum accretion of planetesimals onto this embryo. Terrestrial planets are likely formed in this way. If the solid core becomes massive enough, it will also start accreting gas at an increasing rate until no more gas can be obtained from the disk (either because the disk has dissipated or because the planet has opened a gap in it). The result of this process is a gas giant planet.
- In the DI model, a very massive disk is destabilized by its own gravity, leading to the collapse of a region of the disk and potential formation of a giant planet or brown dwarf.

So far, the CA model seems to better reproduce several observed properties of the known exoplanets. For example, correlations are known to exist, both between the stellar metallicity and giant planet occurrence, and between stellar and planetary metallicities (e.g. Johnson et al. 2010). These correlations can be explained by the CA model, in which higher metallicities result in more efficient planet formation. However, some known exoplanetary systems cannot be explained within the CA frame (e.g. the system around HR 8799, Marois et al. 2008), suggesting that DI may be responsible for the formation of some gas giants at very large radii from their host stars and/or around low-metallicity stars. It could also explain the existence of some brown dwarfs orbiting other stars. The global planet formation process may be a combination of these two scenarios.

If CA is the dominant mechanism, then planets are likely to form below the ice-line (Ida & Lin 2004a): water can freeze into ice around the grains of dust, and increase the efficiency of their aggregation to form the required planetary embryo. On the other hand, formation at very large radii from the host star is also unlikely, since the solid accretion rate of planetary embryos decreases with the distance to the star. As an example, the optimal zone to form planets for a solar-type star is estimated to be between 5-10 AU (Helled et al. 2014). Surprisingly, a significant number of Jovian-like planets are found very close to their stars, and are referred to as hot Jupiters. This particular subgroup of exoplanets suggests that a fraction of these gas giants migrate inwards after their formation: once a gap is opened by the planet, it gets locked to the disk and exchanges angular momentum with it, causing the planet to move closer to its host star (Type-II migration, Papaloizou et al. 2007). Other migration processes such as planet-planet scattering, Kozai resonances, or similar dynamic mechanisms (e.g. Kozai 1962; Wu & Murray 2003; Naoz et al. 2011) are likely responsible for the fraction of hot Jupiters whose spin is found to be misaligned with their planet-star orbits (Triaud et al. 2010; Narita et al. 2010; Morton & Johnson 2011).

Within this theoretical framework, the obtained dependence of stellar mass and disk lifetime would have two main implications:

1. Observational results tentatively suggest that massive stars are more likely to host gas giants than their low-mass counterparts (Johnson et al. 2010). This trend would be the result of two competing factors: high-mass stars have more massive disks (e.g. Andrews et al. 2013), and so are more likely to form gas giants. On the other hand, the present study shows that massive stars disperse their disks earlier. Under some circumstances, the formation of giant planets could even last for some Myr (Helled et al. 2014). Therefore, a fast dispersing disk may not live long enough to form gas giants. If the observed trend (massive stars being more likely to host giant planets) is real, then either a strong correlation between the stellar mass and the ability to form giant planets exists to compensate for the shorter disk lifetime, or giant planet formation is faster than the disk dispersal time regardless of the stellar mass, or most of the planet formation process happens in the first million years.

2. Type-II migration is active while the gaseous disk is present and the planet can exchange angular momentum with it. The distribution of orbital semi-major axes produced by these migration mechanisms is controlled by the ratio of the disk depletion timescale to the viscous diffusion timescale at the distance where Jovian planets form (Armitage et al. 2002; Trilling et al. 2002; Ida & Lin 2004b). A faster dispersal of protoplanetary disks around high-mass stars would result in a shorter disk depletion timescale, and therefore a shorter migration period (Burkert & Ida 2007; Currie 2009). Our results provide a robust confirmation of a faster disk

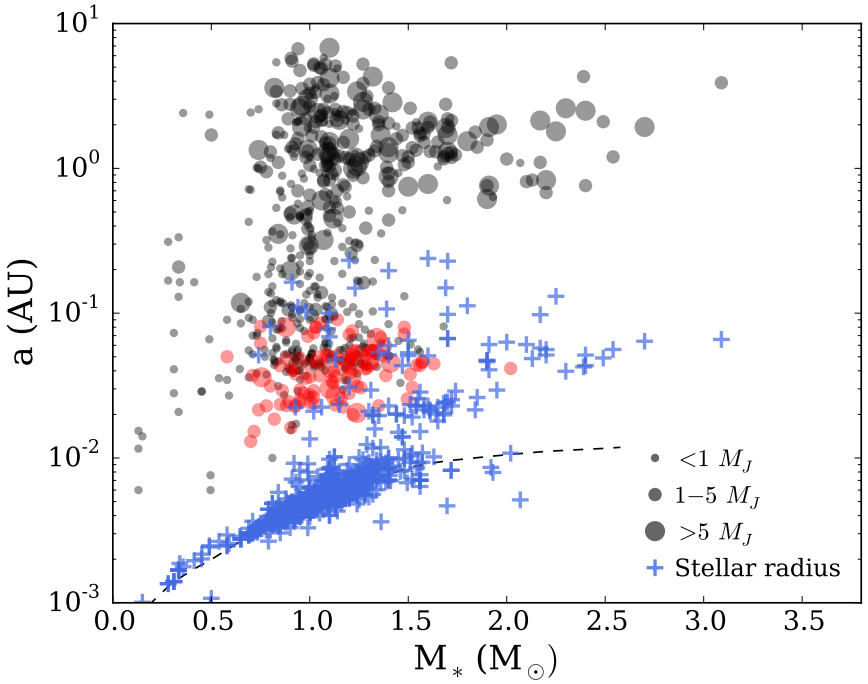

FIGURE 3.6: Orbital semi-major axes as a function of the mass of the host star for the known exoplanet population. Red circles show hot Jupiters ($M > 1\,M_J$, period < 10 days), black circles represent the rest of the sample. The size of the symbols scales with the planet mass. We also show the estimated stellar mass radii of main-sequence stars (Siess et al. 2000) and the stellar radii of the host stars. A clear lack of hot Jupiters is seen for $M_* > 1.5\,M_\odot$.

dispersal around high-mass stars: the disk lifetime could be more than two times shorter for massive stars, reducing significantly the migration period available for Jovian planets and, as a result, a smaller number of hot Jupiters would be present around these stars.

Following Kennedy & Kenyon (2009), point 2 can be linked with the known population of exoplanets. Figure 3.6 shows the orbital semi-major axis distribution as a function of the mass of the host star for the known exoplanets[1] (planets around pulsars are not plotted since they represent a completely different type of object). Considering as hot Jupiters the planets with masses above $1\,M_J$ and periods < 10 days, a clear lack of these objects around massive stars ($> 1.5\ M_\odot$) is easily identified. This paucity of close Jovian planets around massive stars is still a matter of intense debate. Tidal interaction between massive planets and their host stars could lead to planet engulfment (Villaver & Livio 2009; Villaver et al. 2014). Some authors report a real dependence on stellar mass (e.g. Johnson et al. 2011), and have even shown hints of it not being the result of planet engulfing caused by the post-main-sequence evolution of the star (Johnson et al. 2007). On the other hand, other authors suggested that such claims were made on incorrectly assigned stellar masses (Lloyd 2011), and that tidal destruction is responsible for the observed trend (Schlaufman & Winn 2013). By also plotting the radii of the

[1] as in the www.exoplanets.eu database, August 6th 2014

planet host stars in Fig. 3.6, it becomes clear that most low-mass stars ($< 1.5 - 2\,M_{\odot}$) have radii matching those predicted from main-sequence models (Siess et al. 2000). For more massive stars, the stellar radii increase owing to the post-main-sequence phase, overlapping with the loci of the hot Jupiters semi-major axes. It is not possible to tell if the massive stars in Fig. 3.6 have engulfed any close gas giants, but it becomes clear that the post-main-sequence phase of these stars could account for a fraction of the observed paucity of hot Jupiters around them. Assessing the origin of this lack of close gas giants is beyond the scope of this study, but the faster disk dissipation around high-mass stars could contribute to it as well.

This discussion may also apply to some brown dwarfs. Although it is thought that most of these objects form via different mechanisms (Chabrier et al. 2014), the existence of binary systems including a brown dwarf companion suggests that some of them may form in a circumstellar disk around more massive stars. If this is the case, they are very likely formed in similar ways to giant planets, and the same conclusions could be applied to this particular subgroup of brown dwarfs.

Finally, the implications of the faster disk dispersal around high-mass stars for terrestrial planets are harder to determine. As previously mentioned, their formation follows the initial stage of the CA model, accreting planetesimals to form a planetary embryo and eventually a rocky planet, which will not become a gas giant if the planet cannot accrete enough gas for any reason. However, this process is faster than gas giant formation: earth-mass planets can be formed in 1 Myr (Raymond et al. 2014), and so the disk dissipation dependence with stellar mass may not be as relevant as for giant planet formation. Moreover, terrestrial planets do not undergo Type-II migration, and therefore their orbits are less dependent on the disk properties. However, their orbits can be strongly affected by the migration of giant planets in the same system. If the migration history of gas giants has a dependence with stellar mass, it could indirectly produce different orbits for terrestrial planets too. The identification of any possible trend of this effect requires further modeling and study of the known planetary population.

3.6 Conclusions

We have studied the disk lifetime dependence on stellar mass using the sample of YSOs compiled by Ribas et al. (2014). After updating their results, we have divided the sample into low- or high-mass stars (boundary set to $2\,M_{\odot}$) and young or old regions (boundary set to 3 Myr). We then study the fraction of protoplanetary and evolved disks as a function of age and mass. The large number of sources in the sample allows us to confirm the existence of a dependence of disk lifetime on the stellar mass: high-mass stars disperse their disks up to two times faster and/or earlier than low-mass ones. We also find that the fraction of evolved disks (including transitional, circumbinary, and hot

debris disks) remains roughly constant (5-30 %) during the first 10 Myr of the stellar life. The faster dispersal of protoplanetary disks around high-mass stars could have important implications for giant planet formation and migration, and may contribute to the apparent lack of hot Jupiters around these stars.

Acknowledgments

This work has been possible thanks to the ESAC Science Operations Division research funds with code SC 1300016149, support from the ESAC Space Science Faculty and of the Herschel Science Centre. We thank the referee for valuable comments which have helped to improve the paper. We also acknowledge Gaspard Duchêne, Johannes Sahlmann, Jorge Lillo-Box, José Antonio Caballero, and Justin Crepp for helpful discussions on disks, Jovian planet populations, migration and biases in the sample of known exoplanets. H. Bouy is funded by the Spanish Ramón y Cajal fellowship program number RYC-2009-04497. This work has made an extensive use of Topcat (TOPCAT http://www.star.bristol.ac.uk/~mbt/topcat/ and STILTS, Taylor 2005, 2006). This work is based in part on data obtained as part of the UKIRT Infrared Deep Sky Survey. This research made use of the SDSS-III catalog. Funding for SDSS-III has been provided by the Alfred P. Sloan Foundation, the Participating Institutions, the National Science Foundation, and the U.S. Department of Energy Office of Science. The SDSS-III web site is http://www.sdss3.org/. SDSS-III is managed by the Astrophysical Research Consortium for the Participating Institutions of the SDSS-III Collaboration including the University of Arizona, the Brazilian Participation Group, Brookhaven National Laboratory, University of Cambridge, University of Florida, the French Participation Group, the German Participation Group, the Instituto de Astrofisica de Canarias, the Michigan State/Notre Dame/JINA Participation Group, Johns Hopkins University, Lawrence Berkeley National Laboratory, Max Planck Institute for Astrophysics, New Mexico State University, New York University, Ohio State University, Pennsylvania State University, University of Portsmouth, Princeton University, the Spanish Participation Group, University of Tokyo, University of Utah, Vanderbilt University, University of Virginia, University of Washington, and Yale University. This work makes use of data from the DENIS Survey. DENIS is the result of a joint effort involving human and financial contributions of several Institutes mostly located in Europe. It has been supported financially mainly by the French Institut National des Sciences de l'Univers, CNRS, and French Education Ministry, the European Southern Observatory, the State of Baden-Wuerttemberg, and the European Commission under networks of the SCIENCE and Human Capital and Mobility programs, the Landessternwarte, Heidelberg and Institut d'Astrophysique de Paris. This publication makes use of data products from the Wide-field Infrared Survey Explorer, which is a joint project of the University of California, Los Angeles, and the Jet Propulsion Laboratory/California Institute of Technology, funded by the National Aeronautics and Space Administration.

This research used the facilities of the Canadian Astronomy Data Centre operated by the National Research Council of Canada with the support of the Canadian Space Agency.

This publication makes use of data products from the Two Micron All Sky Survey, which is a joint project of the University of Massachusetts and the Infrared Processing and Analysis Center/California Institute of Technology, funded by the National Aeronautics and Space Administration and the National Science Foundation.

This work is based in part on observations made with the Spitzer Space Telescope, which is operated by the Jet Propulsion Laboratory, California Institute of Technology under a contract with NASA.

This research has made use of the Exoplanet Orbit Database and the Exoplanet Data Explorer at exoplanets.org.

3.7 Appendix: updated figures and tables from Ribas et al. 2014

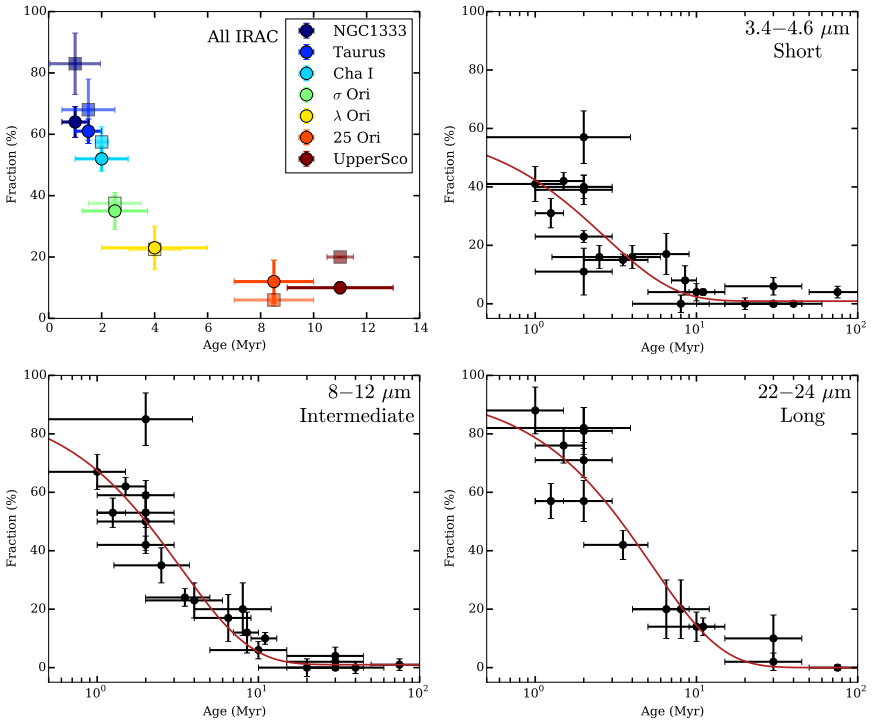

FIGURE 3.7: Upper left panel: comparison of the disk fractions obtained in this study (circles) with those from (Hernández et al. 2007b, 2008) (squares) for regions in common. Upper right and lower panels: disk fractions for all regions in the short, intermediate and long wavelength ranges. The best-fit exponential law is over-plotted (red line).

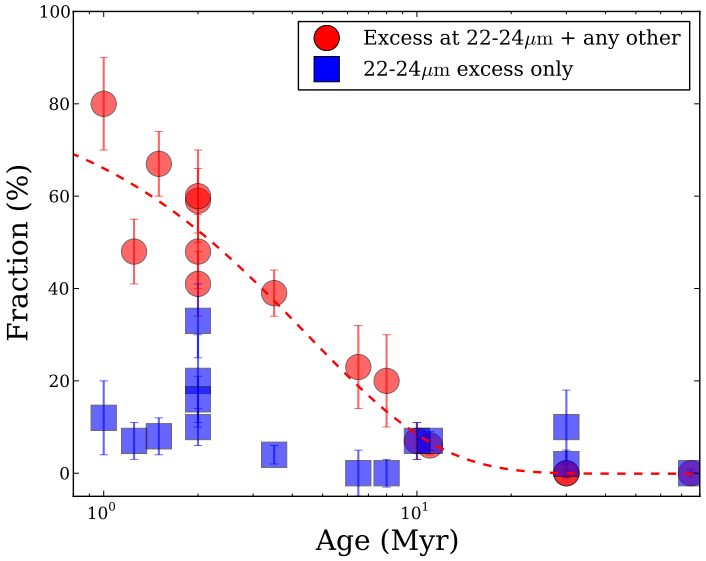

FIGURE 3.8: Fraction of primordial (red circles) and evolved (blue squares) disks as a function of age. The best-fit exponential law for the primordial disk percentages is also shown (red dashed line).

TABLE 3.4: Fraction of sources with excess for each region in the three wavelength regimes (update of Table 4 in R14)

Name	Fraction $_{\rm IRAC}$(%)	Fraction $_{\rm short}$(%)	Fraction $_{\rm intermediate}$(%)	Fraction $_{\rm long}$(%)
25 Orionis	12 ± 7 [26]	8 ± 5 [26]	12 ± 7 [25]	... [0]
Cha I	51 ± 4 [117]	36 ± 5 [109]	52 ± 5 [106]	71 ± 6 [52]
Cha II	75 ± 8 [28]	50 ± 9 [28]	85 ± 9 [20]	82 ± 7 [28]
CrA	40 ± 10 [19]	11 ± 8 [19]	50 ± 10 [16]	... [6]
IC 348	38 ± 3 [253]	17 ± 2 [262]	41 ± 3 [223]	81 ± 8 [27]
λ-Orionis	23 ± 7 [43]	10 ± 4 [51]	23 ± 6 [43]	... [0]
Lupus	53 ± 5 [85]	27 ± 5 [86]	53 ± 5 [85]	57 ± 6 [58]
NGC 1333	64 ± 5 [73]	38 ± 6 [73]	67 ± 6 [70]	88 ± 8 [17]
Ophiuchus	23 ± 3 [248]	13 ± 2 [253]	23 ± 3 [238]	42 ± 5 [113]
σ-Orionis	34 ± 6 [71]	14 ± 4 [74]	34 ± 6 [71]	... [0]
Serpens	57 ± 4 [129]	35 ± 4 [131]	58 ± 5 [128]	57 ± 7 [56]
Taurus	61 ± 4 [202]	39 ± 3 [214]	62 ± 3 [197]	76 ± 6 [49]
Upper Sco	9 ± 2 [250]	4 ± 1 [250]	10 ± 2 [232]	14 ± 3 [186]
AB Dor	4 ± 2 [77]	4 ± 2 [77]	1 ± 2 [77]	0 ± 1 [50]
Argus	0 ± 2 [45]	0 ± 1 [44]	0 ± 2 [44]	... [3]
β Pic	8 ± 4 [50]	4 ± 3 [50]	6 ± 3 [49]	14 ± 5 [43]
Carina	4 ± 3 [28]	0 ± 1 [27]	4 ± 3 [28]	... [6]
Columba	2 ± 2 [57]	0.0 ± 0.9 [57]	2 ± 2 [57]	10 ± 8 [20]
ϵ Cha	21 ± 8 [24]	17 ± 7 [24]	17 ± 8 [24]	20 ± 10 [13]
Octantis	0 ± 3 [17]	0 ± 2 [17]	0 ± 3 [17]	... [1]
Tuc-Hor	6 ± 3 [48]	6 ± 3 [48]	0 ± 1 [48]	2 ± 3 [41]
TW Hya	20 ± 9 [20]	0 ± 3 [20]	20 ± 9 [20]	20 ± 10 [14]

The number of sources used is indicated within brackets. Sub-indexes reference fractions at different wavelength ranges, as defined in R14

TABLE 3.5: Values and errors obtained from fitting and exponential decay to disk fractions with time.

Wavelength range	A (%/Myr)	τ (Myr)	C (%)
Short	60 ± 10	2.7 ± 0.7	1.1 ± 0.9
Intermediate	90 ± 10	3.3 ± 0.6	1 ± 1
Long (primordial)	84 ± 6	4.4 ± 0.5	-0.1 ± 0.4
Long	95 ± 8	5.3 ± 0.9	0 ± 1

The long (primordial) case corresponds to red circles in Fig. 3.8.

Part II

Transitional disks in the Chamaeleon complex with Herschel

4

Transitional disks in Chamaeleon with *Herschel*

Herschel has provided a large amount of FIR data of YSOs, probing the emission from cold dust in disks with unrivaled sensitivity and resolution up to date. Additionally, transitional disks have gained substantial attention during the last decades, given the plausible on-going planet formation in them. In this chapter, we study the population of known transitional disks in the Chamaeleon I and II star-forming regions as seen by *Herschel*. We analyze the FIR fluxes of the detected sources, and compare them with Class II disks in these regions.

This work was published as Ribas et al. 2013, A&A, 552, A115.

Identification of transitional disks in Chamaeleon with *Herschel*

Álvaro Ribas[1,2,3], Bruno Merín[4], Hervé Bouy[2], C. Alves de Oliveira[1], D. R. Ardila[5], E. Puga[4], Á. Kóspál[6], L. Spezzi[7], N. L.J. Cox[8], T. Prusti[6], G. L. Pilbratt[6], Ph. André[9], L. Matrà[10], R. Vavrek[4]

[1] ESAC-ESA, P.O. Box, 78, 28691 Villanueva de la Cañada, Madrid, Spain

[2] Centro de Astrobiología, INTA-CSIC, P.O. Box, 78, 28691 Villanueva de la Cañada, Madrid, Spain

[3] Ingeniería y Servicios Aeroespaciales-ESAC, P.O. Box, 78, 28691 Villanueva de la Cañada, Madrid, Spain

[4] Herschel Science Centre, ESAC-ESA, P.O. Box, 78, 28691 Villanueva de la Cañada, Madrid, Spain

[5] NASA Herschel Science Center, California Institute of Technology, 1200 E. California Blvd., Pasadena, CA 91125, USA

[6] Research and Scientific Support Department, ESTEC-ESA, PO Box 299, 2200 AG, Noordwijk, The Netherlands

[7] European Southern Observatory, Karl-Schwarzschild-Strasse 2, 85748, Garching bei München, Germany

[8] Instituut voor Sterrenkunde, KU Leuven, Celestijnenlaan 200D, B-3001, Leuven, Belgium

[9] Laboratoire AIM Paris – Saclay, CEA/DSM – CNRS – Université Paris Diderot, IRFU, Service d'Astrophysique, Centre d'Etudes de Saclay, Orme des Merisiers, 91191 Gif-sur-Yvette, France

[10] School of Physics, Trinity College Dublin, Dublin 2, Ireland

Received 19 December 2012; Accepted 11 March 2013

Abstract

Context: Transitional disks are circumstellar disks with inner holes that in some cases are produced by planets and/or substellar companions in these systems. For this reason, these disks are extremely important for the study of planetary system formation.

Aims: The *Herschel* Space Observatory provides an unique opportunity for studying the outer regions of protoplanetary disks. In this work we update previous knowledge on the transitional disks in the Chamaeleon I and II regions with data from the *Herschel* Gould Belt Survey.

Methods: We propose a new method for transitional disk classification based on the WISE 12 μm − PACS 70 μm color, together with inspection of the *Herschel* images. We applied this method to the population of Class II sources in the Chamaeleon region

and studied the spectral energy distributions of the transitional disks in the sample. We also built the median spectral energy distribution of Class II objects in these regions for comparison with transitional disks.
Results: The proposed method allows a clear separation of the known transitional disks from the Class II sources. We find six transitional disks, all previously known, and identify five objects previously thought to be transitional as possibly non-transitional. We find higher fluxes at the PACS wavelengths in the sample of transitional disks than those of Class II objects.
Conclusions: We show the *Herschel* 70 μm band to be a robust and efficient tool for transitional disk identification. The sensitivity and spatial resolution of *Herschel* reveals a significant contamination level among the previously identified transitional disk candidates for the two regions, which calls for a revision of previous samples of transitional disks in other regions. The systematic excess found at the PACS bands could be either a result of the mechanism that produces the transitional phase, or an indication of different evolutionary paths for transitional disks and Class II sources.

Key words: stars: formation – stars: pre-main sequence – (stars:) planetary systems: protoplanetary disks – (stars:) planetary systems: formation

4.1 Introduction

Protoplanetary disks surrounding young stars are known to evolve over timescales of a few million years from a more massive and optically thick phase (Class II objects) to optically thin debris disk systems (Class III sources; see Williams & Cieza 2011, for a recent review on the evolution of protoplanetary disks). There are several indications of this evolution with time. Infrared (IR) observations of star-forming regions show a systematic decrease of the IR flux with stellar age (Haisch et al. 2001b; Gutermuth et al. 2004; Sicilia-Aguilar et al. 2006; Currie & Kenyon 2009). In the optical and ultraviolet, observations show that the disk mass accretion rate decreases with time as predicted by disk evolutionary models (Hartmann et al. 1998; Calvet et al. 2005; Fedele et al. 2010; Sicilia-Aguilar et al. 2010; Spezzi et al. 2012). Another important evidence is found in deep MIR spectroscopic observations of young stars with disks that show dust grain growth, crystallization, and settling to the disk mid-plane. These phenomena are found to be correlated with the evolution of the disk structure across two orders of magnitude in stellar mass (Meeus et al. 2001; van Boekel et al. 2005; Kessler-Silacci et al. 2005; Apai et al. 2005; Olofsson et al. 2009).

Most of the evolution of protoplanetary disks is driven by gravitational interaction and viscosity effects in the disk (Pringle 1981). However, some circumstellar disks show evidence of a different evolutionary phase: they are known as transitional disks. Compared to Class II disks, they display a clear dip in their spectral energy distribution (SED) at NIR/MIR (typically around 8-12 μm) and a rising SED with flux excesses similar to that of Class II sources at longer wavelengths (Strom et al. 1989; Calvet et al. 2002; Espaillat et al. 2007a; Andrews et al. 2011). The dips in the SEDs are usually explained in terms of dust-depleted regions and/or cavities in the disks, of typical sizes of some tens of AU (see Merín et al. 2010; Andrews et al. 2011, and references therein).

Several processes have been proposed to explain these gaps and holes: gravitational interaction with a low-mass companion (Bryden et al. 1999; Rice et al. 2003; Papaloizou et al. 2007), photo-evaporation (Clarke et al. 2001; Alexander et al. 2006a,b), or grain growth (Dullemond & Dominik 2005; Tanaka et al. 2005; Birnstiel et al. 2012). Observational evidence of stellar or substellar companions has been obtained in some cases (i.e., CoKu Tau4 or T Cha, see Ireland & Kraus 2008; Huélamo et al. 2011, respectively). If we were able to distinguish between these different explanations would better understand the mechanisms that produce the gaps in transitional disks, and the planetary formation scenario. For this reason, any hint on which process governs the transition phase is relevant.

In this paper, we investigate the contribution of the FIR data from the *Herschel* Space Observatory (Pilbratt et al. 2010) to our understanding of transitional disks. We present a new method for transitional disk identification and apply it to the sample of Class

II objects in the Chamaeleon (Cha) I and II regions. Section 4.2 describes the data reduction process, the sample selection, and the photometry extraction. Section 4.3 explains the proposed method used in the paper to identify and reclassify transitional disks. A more detailed discussion of the sample of transitional disks is given in Sect. 4.4. Section 4.5 summarizes our results.

4.2 Observations and sample

4.2.1 Observations

The Cha I and II regions were observed by the *Herschel* Space Observatory in the context of the Gould Belt Survey (André et al. 2010). These regions are part of the Chamaeleon molecular cloud complex that also includes the Cha III cloud. The complex is located at 150-180 pc (Whittet et al. 1997) and is one of the most often studied low-mass star-forming regions because of its proximity. Cha I has an estimated age of ∼2 Myr and a population of ∼200 young stellar objects (Luhman et al. 2008a; Winston et al. 2012). Cha II harbors a smaller population (∼ 60) of young sources (Young et al. 2005; Spezzi et al. 2008). Because of their age and location, these regions are perfect scenarios for transitional disk search and study.

Two sets of observations were used for each region: a first set taken in parallel mode, using the PACS (70 and 160, μm Poglitsch et al. 2010) and SPIRE (250 350, and 500 μm, Griffin et al. 2010) instruments at a speed of 60″/s, and the 100 μm PACS band at 20″/s from a second set in scan mode. The observing strategy is described in more detail in André et al. (2010). The total observing time in parallel mode for Cha I was ∼8 hours and 6 hours for Cha II, covering a total area of ∼9 deg^2 (∼5.5 and 3.5 deg^2). The PACS 100 μm images covered 2.6 deg^2 in Cha I and 2 deg^2 in Cha II, and add up to a total time of 8 hours and 6 hours, respectively (see Winston et al. 2012; Spezzi et al. 2013, for a detailed description of the datasets). Obsids for Cha I are 1342213178, 1342213179 (parallel mode) and 1342224782,1342224783 (scan mode), and obsids 1342213180,1342213181 (parallel mode), and 1342212708, 1342212709 (scan mode) for Cha II.

The data were pre-processed using the *Herschel* interactive processing environment (HIPE, Ott 2010) version 9. The final maps were created using *Scanamorphos* (Roussel 2012) for PACS, and the *destriper* algorithm included in HIPE for SPIRE. These two algorithms are optimized for regions such as Chamaeleon, which have bright extended emission. Figure 4.1 shows a three-color composite image of Cha I (blue: 70 μm, green: 160 μm, and red: 250 μm).

4.2.2 Sample selection

Luhman et al. (2008a) and Luhman & Muench (2008) presented the largest census of young stellar objects (YSOs) members of Cha I including *Spitzer* photometry, and Alcalá et al. (2008) and Spezzi et al. (2008) did the same for Cha II. We selected from these studies the sources classified as Class II with known extinction values. Since we aim to classify transitional disks, we also included T25, flagged as Class III in Luhman et al. (2008a) but later found to be a transitional source in Kim et al. (2009). We rejected objects with signal-to-noise ratio (S/N) < 5 in any of the 2MASS bands to ensure a good photometry estimation and coordinates measurement. The final sample of Class II objects is comprised of 119 sources.

To our knowledge, 12 sources in the sample are classified as transitional disk candidates in the literature: SZ Cha, CS Cha, T25, T35, T54, T56, and CHXR 22E from Kim et al. (2009), C7-1 from Damjanov et al. (2007), CR Cha, WW Cha, and ISO-ChaI 52 from Espaillat et al. (2011), and ISO-ChaII 29 from Alcalá et al. (2008).

4.2.3 Photometry

We extracted *Herschel* photometry of the Class II sample following these steps:

1. We used the *Sussextractor* algorithm (Savage & Oliver 2007) in HIPE to detect sources with an S/N > 5 in the PACS images. We then visually checked that no obvious source was missing.

2. We cross-matched the initial sample with the detections in the PACS images, using a search radius of $5''$. This radius was chosen based on the size of the point spread functions (PSFs) at these wavelengths ($\sim 5.8'' \times\ 12.1''$, $6.7'' \times\ 7.3''$, and $11.4'' \times\ 13.4''$, for the 70, 100, and 160 μm bands at the corresponding observing speeds). We note that the background emission becomes more significant for longer wavelengths, producing false detections because of bright filaments and ridges. To avoid possible mismatches, we considered as *Herschel*-detected sources only those with counterparts at any PACS band. For SPIRE, we found the *Sussextractor* output to be highly contaminated with false detections. Therefore, we visually inspected the positions of the detected sources individually for these bands.

3. We performed aperture photometry centered on the 2MASS coordinates of each detection. We used the recommended aperture radii and background estimation annulus for each band (see the PACS point-source flux calibration technical note from April 2011, and Sect. 5.7.1.2 of the SPIRE data reduction guide). The values for the apertures, inner and outer annulus radii (in this order) are $12''$, $20''$, $30''$for 70 and 100 μm, $22''$, $30''$, $40''$for 160 μm, $22''$, $60''$, $90''$for 250 μm, $30''$, $60''$, $90''$for 350 μm, and $42''$, $60''$, $90''$for 500 μm.

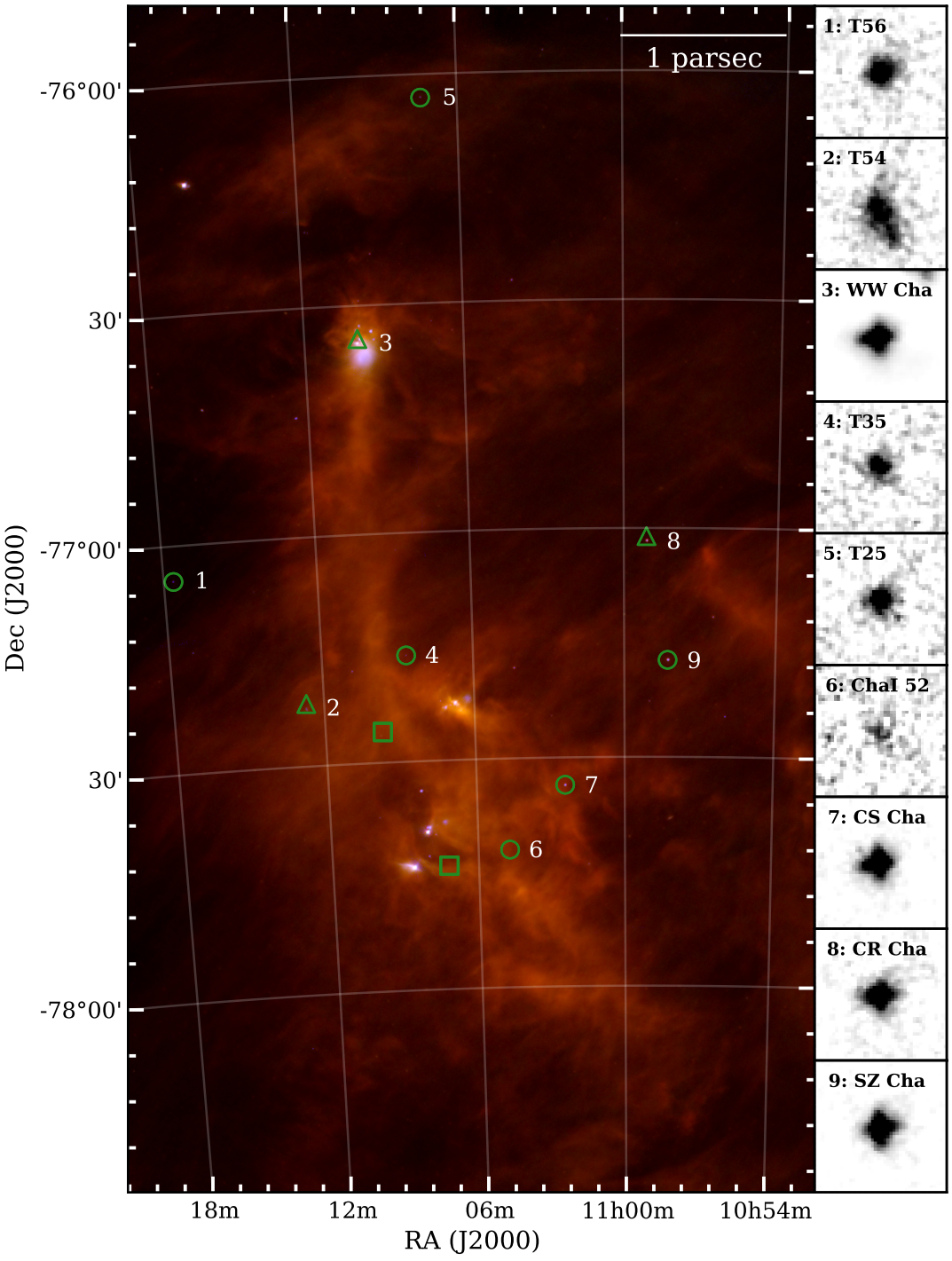

FIGURE 4.1: Left: Three-color composite image of the Cha I region (blue: PACS 70 μm, green: PACS 160 μm, red: SPIRE 250 μm). Circles mark the position of transitional disks detected in the *Herschel* images and classified with the proposed method (see Sect.4.3.3). Triangles show sources not fulfilling our selection criteria, and squares represent non-detected sources. Right: thumbnails of the 70 μm *Herschel* maps ($50'' \times 50''$). The color scale ranges from the median value (background level) to 5 σ over this value (black). In both figures, north is up, and east is left. Note that WW Cha is located on a bright core.

4. Since aperture photometry was used, objects close to bright filaments or cores are likely to suffer from contamination. Also, given the size of the PSF, no photometric measurements can be performed for close objects (separation less than $\sim 10''$). Therefore we rejected ten detections that showed obvious problems in their photometry or enclosed more than one object.

After excluding the transitional disks, the final result of this process is 41 Class II sources detected at any PACS band (26 and 15 in Cha I and Cha II, respectively), nine of them detected also with SPIRE.

We checked that the obtained photometry was consistent with that from other map-making algorithms (such as *photProject* for PACS), and found no significant deviation.

We visually inspected the position of non-detected transitional disks in the original sample and found that C7-1, CHXR 22E, and ISO-ChaII 29 are not detected at any of the *Herschel* bands. Additionally, ISO-ChaI 52 is not detected by *Sussextractor* at 70 μm, but it is at 100 μm. The object is visually found in the 70 μm image with a flux of 150 mJy over a background root mean square (RMS) of 40 mJy. We therefore included the 70 μm flux in our analysis. Source T25 is not in the field of view of the 100 μm map, which is smaller than the parallel mode observations. Coordinates and stellar parameters for the transitional disks in this study can be found in Table 4.1.

4.2.4 Photometric uncertainties and upper limits

The absolute calibration errors for PACS and SPIRE are 5 % and 7 % , respectively (see PACS and SPIRE observer manuals). To ensure a conservative error estimation, we used a 15 % error value for PACS and 20 % for SPIRE, taking into account that the background emission becomes increasingly stronger at longer wavelengths.

When no source was detected, we computed an upper limit calculating the RMS of 100 apertures taken around the source, using the same aperture radii and correction factors as for the detections. The extracted PACS and SPIRE fluxes for the 12 transitional candidates in the considered sample are reported in Table 4.2.

4.3 Identification of transitional disks

4.3.1 Photometric selection

Several selection criteria have been used in the past to separate transitional disks from Class II sources. Fang et al. (2009) used a color-color diagram based on the *Ks* band and on the [5.8], [8.0] and [24] *Spitzer* bands. Muzerolle et al. (2010) proposed a classification

TABLE 4.1: Coordinates and stellar parameters of the 12 transitional disk candidates analyzed in this work.

Name	R.A.$_{J2000}$	Dec.$_{J2000}$	A_V (mag)	SpT Type	T_* (K)	L_* ($L_\odot$)	M_* ($M_\odot$)	R_* ($R_\odot$)	Refs.
CR Cha	10:59:06.97	-77:01:40.3	1.5	K2	4900	3.5	1.9	2.6	1,2,3,4,5,6
CS Cha	11:02:24.91	-77:33:35.7	0.25	K6	4205	1.5	0.9	2.3	1,2,3,5,6,7,8,9
SZ Cha	10:58:16.77	-77:17:17.1	1.90	K0	5250	1.9	1.4	1.7	1,2,3,4,5,6,7,8,9
WW Cha	11:10:00.11	-76:34:57.9	4.8	K5	4350	6.5	1.2	4.5	1,2,3,4,5,6,7,8
T25	11:07:19.15	-76:03:04.9	0.78	M3	3470	0.3	0.3	1.5	1,2,3,4,5,6,7,9
T35	11:08:39.05	-77:16:04.2	3.5	M0	3850	0.4	0.6	0.5	1,2,3,4,5,6,7,9
T54	11:12:42.69	-77:22:23.1	1.78	G8	5520	4.1	2.4	1.5	1,2,3,4,5,6,7,9,10,11
T56	11:17:37.01	-77:04:38.1	0.23	M0.5	3720	0.4	0.5	1.6	1,2,3,4,5,6,7,9
ISO-ChaI 52	11:04:42.58	-77:41:57.1	1.3	M4	3370	0.1	0.3	1.0	2,3,4,5,7
C7-1	11:09:42.60	-77:25:57.9	5.0	M5	3125	...	...	...	3,4,5,7,12
CHXR 22E	11:07:13.30	-77:43:49.9	4.79	M3.5	3400	0.2	...	...	3,5,7,9
ISO-ChaII 29	12:59:10.14	-77:12:13.9	5.57	M0	3850	0.65	...	1.85	13,14

(1) Gauvin & Strom (1992); (2) Espaillat et al. (2011); (3) Luhman (2007); (4) Luhman & Muench (2008); (5) Manoj et al. (2011); (6) Henning et al. (1993); (7) Luhman et al. (2008a); (8) Belloche et al. (2011); (9) Kim et al. (2009); (10) Lafrenière et al. (2008); (11) Preibisch (1997); (12) Damjanov et al. (2007); (13) Spezzi et al. (2008); (14) Alcalá et al. (2008)

TABLE 4.2: *Herschel* photometry of the 12 transitional disks in the sample.

Name	$F_{70\mu m}$ (Jy)	$F_{100\mu m}$ (Jy)	$F_{160\mu m}$ (Jy)	$F_{250\mu m}$ (Jy)	$F_{350\mu m}$ (Jy)	$F_{500\mu m}$ (Jy)
Detected sources						
CR Cha	1.61 ± 0.24	2.19 ± 0.33	2.74 ± 0.41	2.37 ± 0.47	1.69 ± 0.34	1.09 ± 0.22
CS Cha*	3.08 ± 0.46	2.82 ± 0.42	2.32 ± 0.35	0.88 ± 0.18	0.38 ± 0.08	0.13 ± 0.03
SZ Cha	3.88 ± 0.58	3.63 ± 0.54	3.86 ± 0.58	2.85 ± 0.57	1.94 ± 0.39	1.14 ± 0.23
WW Cha	25.91 ± 3.88	32.32 ± 4.85	27.3 ± 4.10	24.92 ± 4.99	12.44 ± 2.49	6.79 ± 1.36
T25	0.52 ± 0.08	...	0.50 ± 0.08	0.20 ± 0.04	0.11 ± 0.02	< 0.10
T35	0.38 ± 0.06	0.36 ± 0.06	0.200 ± 0.03	< 1.69	< 2.10	< 2.06
T54	0.60 ± 0.09	0.77 ± 0.12	0.98 ± 0.15	0.46 ± 0.09	< 1.04	< 1.18
T56	0.68 ± 0.10	0.57 ± 0.09	0.30 ± 0.05	0.30 ± 0.05	0.30 ± 0.06	0.11 ± 0.02
ISO-ChaI 52	0.15 ± 0.02	0.15 ± 0.02	< 1.07	< 1.42	< 2.06	< 2.04
Undetected sources						
C7-1	< 0.04	< 0.08	< 0.94	< 1.24	< 1.69	< 2.10
CHXR 22E	< 0.08	< 0.14	< 1.10	< 1.19	< 1.18	< 0.96
ISO-ChaII 29	< 0.04	< 0.07	< 0.85	< 1.41	< 2.65	< 3.00

* SPIRE photometry is very likely contaminated for this source (see Appendix 4.6).

criterion based on the slope of the SED between 3.6 and 4.8 μm and between 8 to 24 μm. Cieza et al. (2010) also used a color-color diagram, based on the *Spitzer* photometry at 3.6, 4.5 and 24 μm. However, all these methods were found to suffer from different contamination levels, as explained in Merín et al. (2010).

There is a high diversity in the morphology of transitional disks, hence there are various definitions. However, most of them share two common characteristics: (1) they have low or no excess with respect to the photosphere up to the $\lambda_{\rm turn-off}$ or the pivot point, usually found around $\sim$ 8-10 μm, and (2) they have strong excesses for longer wavelengths (see section 7.1 in Williams & Cieza 2011, and references therein). This is translated into a decreasing slope of the SED up to $\lambda_{\rm turn-off}$, and an increasing one for longer wavelengths.

To identify transitional disks using *Herschel* photometry, we computed two spectral indexes (α): one between the *Ks* band and 12 μm (α_{Ks-12}), and the other between 12 μm and 70 μm (α_{12-70}). The spectral index is defined as $\alpha_{\lambda_1-\lambda_2} = \frac{\log(\lambda_1 {\rm F}_{\lambda_1})-\log(\lambda_2 {\rm F}_{\lambda_2})}{\log(\lambda_1)-\log(\lambda_2)}$, where λ is measured in μm and ${\rm F}_\lambda$ in erg s^{-1} cm^{-2} s^{-1}. Therefore, α traces the slope of the SED in the considered range ($\alpha > 0 \rightarrow$ rising SED, $\alpha < 0 \rightarrow$ decreasing SED). This spectral index has been intensively used since its introduction by Lada & Wilking (1984) to classify protostars and young objects.

Figure 4.2 demonstrates that these two slopes together efficiently separate the two populations. The separation is clearer in the 12-70 μm axis, where $\alpha_{12-70} < 0$ corresponds to typical Class II sources, and $\alpha_{12-70} > 0$ is indicative of the transitional nature of the objects. This separation in the slope between 12 μm and 70 μm is an expected feature: for NIR/MIR wavelengths, the slope depends strongly on the presence of weak excess, or on the spectral type of the star if there is no excess. On the other hand, the definition of transitional disks itself guarantees a positive slope for longer wavelengths. This separation also reveals the usefulness of the *Herschel* data for this classification. As a result of the selection method, two disks reported in Espaillat et al. (2011), WW Cha and CR Cha, are not separated from Class II objects and we confirm that they do not deviate significantly from the median SED of the Class II sources in Cha I and II (Fig. 4.5). Based on this evidence, we consider them as non-transitional. The rest of the transitional disks are properly separated from Class II sources. The computed upper limits also allow us to classify C7-1 and ISO-ChaII 29 as non-transitional using this method.

Interestingly, one Class II source shows $\alpha_{12-70} > 0$ in the former diagram. The object, called ESO-Hα 559, has been recently identified as a probable edge-on disk in Robberto et al. (2012) by modeling its SED. Its underluminosity with respect to its spectral type also supports this scenario. We find this type of object to be a source of contamination for this method: edge-on disks can mimic the SED of transitional sources. Their geometry will cause a high circumstellar extinction level, blocking the light from the central star at short wavelengths (Stapelfeldt & Moneti 1999; Wood et al. 2002; Duchêne et al.

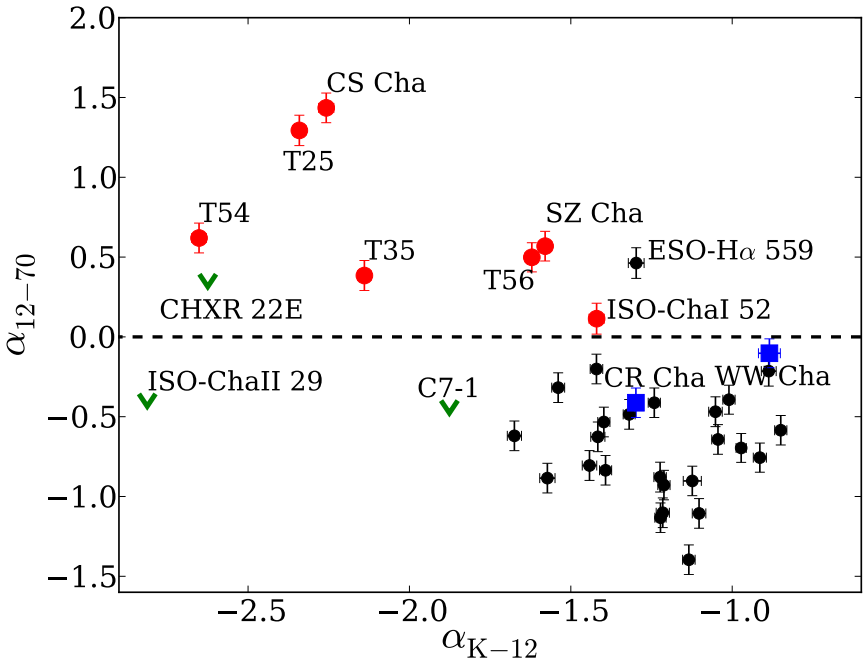

FIGURE 4.2: SED slope between the 12 and 70 μm (α_{12-70}) as a function of the SED slope between the *Ks*-band and 12 μm (α_{Ks-12}). Transitional disks from the literature meeting the selection criterion are marked as red dots, green downward arrows are those for which only upper limits could be estimated. Class II objects are black dots. Blue squares are pre-transitional disks from Espaillat et al. (2011). There is a clear separation between Class II and transitional disks due to the different shape of their SED. The single black dot with $\alpha > 0$ is ESO-Hα 559, an edge-on disk. This diagram shows the potential for transitional disk classification using the 70 μm band.

2010; Huélamo et al. 2010). The disk becomes optically thin for longer wavelengths ($> 24\,\mu$m) and the emission from the star can pass through the disk, resulting in an increase of the flux and hence a positive slope of the SED. When their spectral type is known, edge-on disks can be identified in Hertzsprung–Russell diagrams, as they are often underluminous.

We also note that this method is not suitable for detecting a small subsample of transitional disks called anemic (Lada et al. 2006), homologously depleted (Currie & Kenyon 2009), or weak excess disks (Muzerolle et al. 2010). They are defined as objects with low excess at all infrared wavelengths and show $\alpha_{\rm excess} < 0$. For this reason, they cannot be found with the criterion proposed in this work. On the other hand, the rest of transitional disks should display $\alpha_{12-70} > 0$ and hence can be properly separated.

4.3.2 Morphological classification

We checked whether any of the remaining seven transitional disks were spatially resolved in the *Herschel* images. Extended emission could indeed indicate contamination by a coincident background source, a close by object, or the extended background emission, as shown in Matrà et al. (2012).

Given the estimated distance of 160 pc to the Cha I molecular cloud (Whittet et al. 1997; Luhman & Muench 2008), the full-width at half-maximum of the PSFs for the three PACS bands ($\sim 6''$, $7''$and $12''$, see the official PACS PSF document[1]) would allow us to resolve structures of $\sim$900-2000 AU. It is difficult to define an outer radius for protoplanetary/transitional disks, but typical values range from some tens to $\sim$1000 AU in the most extreme cases (Williams & Cieza 2011). Direct imaging of proplyds and disks in the Trapezium cluster by Vicente & Alves (2005) showed the size distribution to be contained within 50 and 100 AU. On the other hand, the R_c parameter (defined as the radius where the surface density deviates significantly from a power law and the disk density declines rapidly, see Williams & Cieza 2011) has typical values between 15-230 AU (Hughes et al. 2008; Andrews et al. 2009, 2010).

This suggests that none of these sources should be resolved in the *Herschel* images. In each of the PACS band, we compared the radial profile of the transitional disks with an empirical PSF constructed using clean isolated point sources. Of the nine detected sources, only T54 was found to be extended, as shown in Fig. 4.3. Matrà et al. (2012) showed that the excess beyond 100 μm is likely not related to the source, and therefore not originating from a circumstellar disk. This interpretation results in a substantial decrease in the IR excess coming from T54, making its SED not representative of the characteristic inner-hole geometry around transitional disks. The case of T54 shows that one needs to verify the origin of the IR excess in protoplanetary/transitional disks.

We found no other extended sources in the *Herschel* images and conclude that all the detected transitional disks have FIR excesses related to the sources. Therefore all but one (T54) of the transitional disk candidates in the Cha I and II regions are confirmed to be point-sources, up to the resolution of the *Herschel* PACS and SPIRE instruments.

4.3.3 Transitional disk classification

Thanks to the new *Herschel* photometric data, we are able to reclassify the already known transitional disks in the Cha I and II regions based on the shape of their SEDs. CS Cha, SZ Cha, T25, T35, T56, and ISO-ChaI 52 show a typical transitional disk SED.

Two objects from Espaillat et al. (2011) do not fulfill our selection criterion, which is tuned to identify clear signatures of inner holes. These sources were selected by Espaillat et al. (2011) based on their silicate feature strengths, and therefore the different results obtained in this study are not surprising. CR Cha shows weak excess up to 2 μm and a typical Class II SED for longer wavelengths. The SED of WW Cha does not display any decrease in its IR emission, typical for transitional disks. Indeed, the *Herschel* images support one of the scenarios proposed by Espaillat et al. (2011): WW Cha is located on one of the cores in Cha I and presumably accretes at a high rate. Furthermore, it shows

[1] http://herschel.esac.esa.int/twiki/pub/Public/PacsCalibrationWeb/ bolopsf_20.pdf

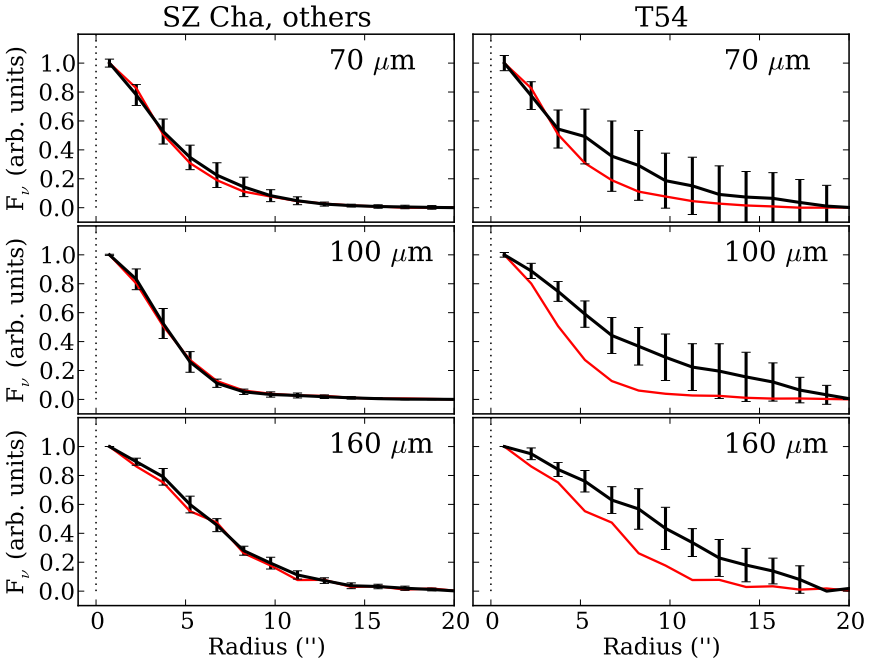

FIGURE 4.3: Average brightness radial profile (black line) for a point source (SZ Cha, left) and an extended source (T54, right) compared to the observational PSF radial profile (red line). The error bars are the RMS of the values. All considered sources present the same behavior as SZ Cha except for T54, whose observed radial profile is clearly above the PSF profile, indicating that this source is extended and all others are point-like in *Herschel* images.

a strong excess along the whole wavelength range and therefore cannot be considered as a transitional disk, but is more likely a Class II source. The dust-rich environment around WW Cha might also contaminate the *Herschel* photometry and account for part of the observed IR excess emission. These sources are then probably non-transitional. Moreover, the morphological analysis of the candidates shows that T54 is extended (Fig. 4.3) and hence a misclassified object.

Conclusions for the non-detected sources are more complicated to draw, and they should be treated with caution, since a non-detection does not directly reject a candidate, but could simply be due to a sensitivity bias. The computed upper limits for C7-1 and ISO-ChaII 29 exclude them as transitional disks according our selection criterion. ISO-ChaII 29 is a special case: the upper limit of 35 mJy in PACS 70 μm is lower than the detection of 56.90±8.63 mJy in the MIPS 70 μm band indicated in Alcalá et al. (2008), and these two measurements are inconsistent. ISO-ChaII 29 shows both strong Li absorption and Hα emission, which confirms it as a YSO (Spezzi et al. 2008). However, it is the only transitional disk in the sample with photospheric fluxes up to 24 μm in our and the Alcalá et al. (2008) sample. These authors also found it to have the steepest α_{excess}. This object is therefore probably misclassified in the *Spitzer* images, as strongly suggested by the non-detection in any of the *Herschel* bands and by the outlier nature of the object if the MIPS detection is considered. We therefore reclassify it as a non-transitional source. We stress that our method is unable to detect transitional disks with weak excesses, and

deeper observations should be made to confirm or reject the presence of disks and holes in these systems. In the case of CHXR 22E it is not possible to extend the analysis further without making strong assumptions about the disk mass and morphology. For this reason, we exclude it for the remainder of the study.

As mentioned in Sect. 4.3.1, it is important to note that the proposed criterion will only select transitional objects with increasing slopes between 12 and 70 μm. This feature is unlikely to be produced by grain growth alone (see Williams & Cieza 2011, for a review on the topic). As a result, the proposed classification criterion may be biased toward detecting only transitional disks with large inner holes produced by photoevaporation, gap opening by unresolved companions, giant planet formation, or a combination of these scenarios. Physical interpretation of this peculiar SED shapes requires detailed modeling, and there is no full consensus yet on which physical phenomena can be safely attributed to each type of SED (see e.g. Birnstiel et al. 2012). A more detailed analysis of this topic will help to determine the real impact of this selection effect.

From the initial sample of 12 transitional disk candidates in the Cha I and II regions we confirm six objects to be transitional disks, reject five sources by photometric or morphological criteria, and leave one object unclassified since it is not detected in the *Herschel* images. These numbers imply a significant ($\sim 45\,\%$) observed contamination level in the transitional disk sample considered in this study. Given the small number statistics, it is premature to extend this result to other samples. However, this result calls for a revision of the known transitional disks: if applicable to the whole sample, this contamination level would imply a shorter transitional-phase lifetime and hence could shed some light on the mechanisms responsible for the evolution of protoplanetary disks.

4.4 Transitional disks in the sample

We searched for additional photometric values in the literature for each of the transitional objects in our sample. Gauvin & Strom (1992) reported optical photometry for all sources in Cha I except for CHXR 22E, ISO-ChaI 52, and C7-1. We have queried the VizieR catalog service and retrieved additional data for these targets from GALEX (Martin et al. 2005), 2MASS (Skrutskie et al. 2006), DENIS (DENIS Consortium 2005), WISE (Wright et al. 2010), and AKARI (Murakami et al. 2007). To avoid possible mismatching, we chose a search radius of 1″around the 2MASS coordinates. We rejected DENIS photometry for T25, T35, and ISO-ChaI 52, since it clearly disagreed with the rest of photometric data. (Sub)millimeter data at 870 μm and 1.3 mm were also included from Belloche et al. (2011) and Henning et al. (1993), respectively. *Spitzer* photometric measurements were included from Damjanov et al. (2007), Luhman et al. (2008a), Luhman & Muench (2008), and Alcalá et al. (2008). We also retrieved the *Spitzer* IRS spectra from the

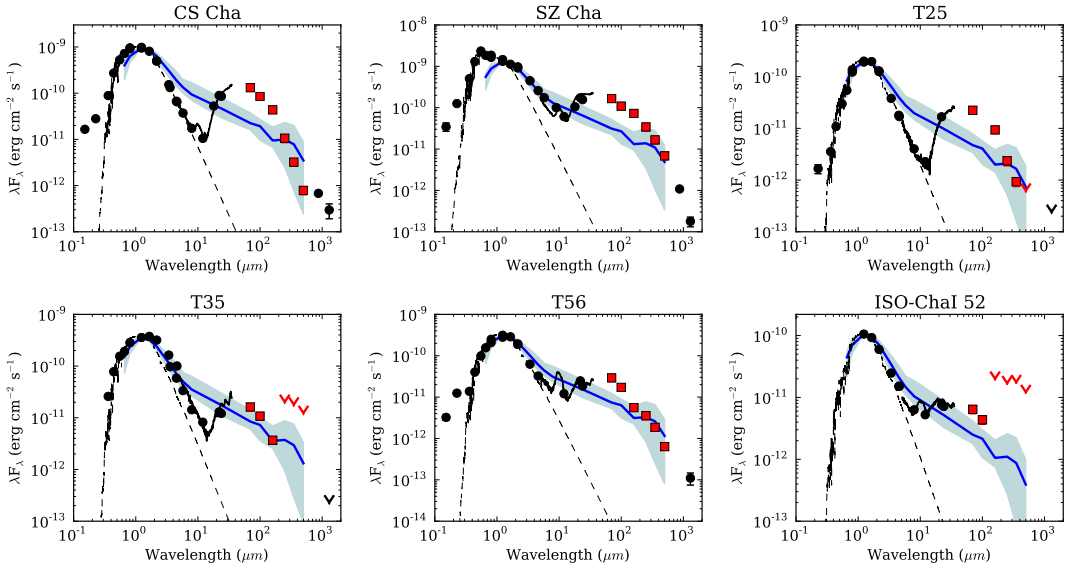

FIGURE 4.4: SEDs of the detected transitional disk candidates, confirmed by our classification criterion and updated with the fluxes from *Herschel*. Black dots are the dereddened observed values from the literature, downward black arrows are flux upper limits from the literature. *Herschel* data are represented in red (squares for detections, downward arrows for upper limits). Uncertainties are within symbol sizes. The IRS spectra from Manoj et al. (2011) (black solid lines) and the photospheres (dashed black lines from the NextGen models from Allard et al. 2012) are also plotted. The median Class II SED (blue solid line) and the first and fourth quartiles (blue area) are shown (see also Sect. 4.4 and Table 4.3).

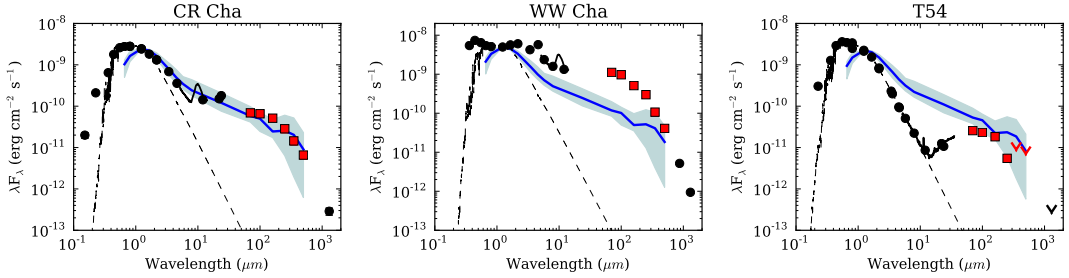

FIGURE 4.5: SEDs of transitional disk that do not fulfill our classification criteria. CR Cha and WW Cha display clear Class II SED. T54 appears extended in the *Herschel* images. Symbols are as in Fig. 4.4.

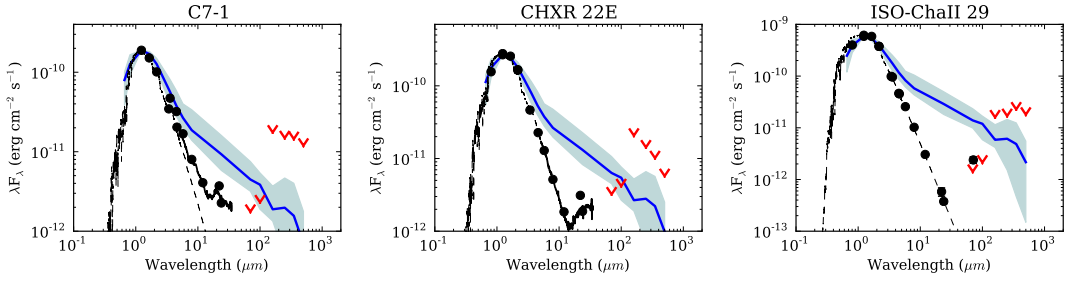

FIGURE 4.6: SED of the transitional disk candidates not detected by *Herschel* for which only flux upper limits could be estimated. Symbols are the same as in Fig. 4.4. The upper limits at 70 μm for C7-1 and ISO-ChaII 29 allow us to classify them as non-transitional with our selection criteria.

TABLE 4.3: Normalized flux densities of the median SED, upper SED (fourth quartile) and lower SED (first quartile) of the Class II objects in Cha I and Cha II, after extinction correction. Transitional disks are not included. The number of stars detected in each band is also indicated. For comparison, we also include the median value for the six transitional disks detected in this study, although we stress its very low number statistics.

$\lambda\,(\mu\mathrm{m})$	Median $_{\mathrm{transitional}}$	Median	Upper	Lower	Detections
	(F_λ arbitrary units)				
R	1.01	0.79	1.00	0.38	32
I	1.22	1.02	1.34	0.74	32
J	1.00	1.00	1.00	1.00	107
H	0.67	0.67	0.72	0.61	107
Ks	0.35	0.38	0.45	0.32	107
IRAC 3.6	7.1e-2	0.10	0.15	7.5e-2	78
IRAC 4.5	3.2e-2	5.5e-2	8.5e-2	4.0e-2	70
IRAC 5.8	2.0e-2	3.0e-2	4.5e-2	2.2e-2	86
IRAC 8.0	4.7e-3	1.5e-2	2.7e-2	1.1e-2	78
MIPS 24	3.5e-3	2.5e-3	4.4e-3	1.6e-3	95
PACS 70	1.8e-3	4.2e-4	7.0e-4	3.0e-4	23
PACS 100	6.8e-4	2.5e-4	3.5e-4	1.2e-4	41
PACS 160	3.5e-4	7.7e-5	1.5e-4	5.5e-5	19
SPIRE 250	5.7e-5	5.1e-5	1.2e-4	1.3e-5	9
SPIRE 350	1.9e-5	2.9e-5	7.5e-5	2.8e-6	9
SPIRE 500	5.2e-6	9.1e-6	2.3e-5	6.3e-7	7

CASSIS database (Lebouteiller et al. 2011). The resulting SEDs for all sources are shown in Figs. 4.4, 4.5, and 4.6. Thumbnails of the transitional disks as seen in the *Herschel* 70 μm images can be found in Fig. 4.1. We note here that the cross-shaped PSF at 70 μm is produced by the parallel mode observations, and does not represent resolved objects.

We compared the *Herschel* fluxes of the sample of transitional disks with the Class II sources in the same region. For this purpose, we first inspected the SEDs of all Class II sources (after removing the transitional disks sample). We identified and removed one object (J11111083-7641574) previously classified as an edge-on disk (Luhman & Muench 2008; Robberto et al. 2012). It could not be identified in the slope-slope diagram since it is only detected at 100 μm. The object is present in the *Herschel* images at 70 μm, but was not detected by *Sussextractor* with the selected threshold. We built the median SED of all Class II objects, extinction corrected and normalized to the *J*-band. We also computed SED of the first ($< 25\,\%$) and fourth ($> 75\,\%$) quartiles. Given the low detection numbers for the SPIRE bands, we used the lowest and highest values instead of the quartiles at those wavelengths. We included photometry from the *R*, *I*, 2MASS, *Spitzer*, and *Herschel* bands. We considered all objects detected in each band (regardless of whether they were undetected in the other bands). The obtained values are given in Table 4.3. We also found the median SED not to vary significantly when only K or M type stars were considered.

The comparison between the SEDs of transitional disks and the median SED of Class II objects in Cha I and II shows a systematic difference in the 70-160 μm range. The six transitional disks found with the selection criterion used in this study display a clear excess over the obtained Class II median SED, and all of them are over the fourth quartile level (uncertainties for T35 are consistent with a flux value below this level).

Even though this median SED was built with a relatively small statistical sample, this result clearly shows that transitional disks are brighter at 70-160 μm than typical Class II sources in these regions.

Similar phenomena were already tentatively described by Winston et al. (2012) in a preliminary study of the YSO population of Cha I and by Cieza et al. (2011) for T Cha, but here we provide consistent results derived from a much larger sample of transitional disks. This excess was not previously found by large programs using the *Spitzer* Space Telescope, such as *cores 2 disks* (Evans et al. 2003, 2009). This can probably be explained by the lower sensitivity of *Spitzer* at 70 μm.

A bias toward the brightest objects could affect these results in two different ways: we might miss the faintest transitional disks and the faintest Class II sources. In the first case, the *Herschel* data are enough to classify eleven out of the twelve previously known transitional objects in the sample (less than 10 % objects missed). This suggests that the proposed method does not suffer from a strong bias effect. The existence of an unknown population of transitional disks not identified with *Spitzer* cannot be ruled out (although this possibility is unlikely, see Merín et al. 2010). However, this would not alter the systematic difference found at the 70-160 μm range between the detected previously known transitional disks and Class II objects in these regions. On the other hand, the second scenario (e.g. missing faint Class II sources) would imply lower values for the Class II median SED in the *Herschel* range, producing an even stronger difference between transitional and Class II disks. As a result, the Class II median SED computed here should be considered as an upper limit.

If the excess at PACS bands is a common feature of transitional objects, two explanations can be proposed to explain it: (1) transitional disks are not the result of the evolution of Class II sources, but a parallel evolutionary path, or (2) the discrepancy between transitional disks and Class II objects is produced during the transitional phase (maybe even by the same mechanism that causes the transitional disk evolution). In this case, the piling-up of mass at some point of the outer disk could produce the steep slope and the excess found at 70 μm (Williams & Cieza 2011). With the available data it is not possible to favor any of these scenarios, so we leave this question open to future studies.

A larger and statistically more significant sample of transitional disks and modeling are required to confirm whether the difference found at the PACS bands applies to the whole transitional disk sample, to identify the real cause (or causes) of the excess, and

to understand whether transitional disks are indeed a later stage of Class II objects or follow a different evolutionary path.

4.5 Conclusions

We presented a new method for identifying transitional disks based on the slope between the WISE 12 μm and PACS 70 μm bands. We have applied this method to the whole sample of known Class II objects in the Cha I and II star-forming regions. We were able to separate known transitional sources from Class II objects, and reclassified five objects as possibly non-transitional. This method could produce false positives due to the presence of edge-on disks, and Hertzsprung–Russell diagrams should be used to reject underluminous sources. As a result, we found an observed contamination level of $\sim 45\%$ among previously identified transitional disks in these regions. The size of our sample is relatively small, and these results cannot be applied to the whole transitional disk sample. However, a revision of the transitional disk population in other star-forming regions is warranted to determine the real contamination level and to account for its effects.

We built the median SED of Class II sources in the regions, and found significantly higher PACS fluxes in the transitional disks compared to it. This excess could be produced during the transitional phase, or be explained in terms of a different evolutionary path for transitional disks and Class II sources.

Future studies of other star-forming regions observed by the *Herschel* Space Observatory will clarify the contamination level of the sample of known transitional objects, and will provide stronger evidence for a systematic excess at PACS wavelengths in transitional disks with respect to Class II sources.

Acknowledgments

We thank the referee for his/her constructive comments. This work has been possible thanks to the ESAC Science Operations Division research funds, support from the ESAC Space Science Faculty and of the Herschel Science Centre. NLJC acknowledges support from the Belgian Federal Science Policy Office via the ESA's PRODEX Program. PACS has been developed by a consortium of institutes led by MPE (Germany) and including UVIE (Austria); KUL, CSL, IMEC (Belgium); CEA, OAMP (France); MPIA (Germany); IFSI, OAP/AOT, OAA/CAISMI, LENS, SISSA (Italy); IAC (Spain). This development has been supported by the funding agencies BMVIT (Austria), ESA-PRODEX (Belgium), CEA/CNES (France), DLR (Germany), ASI (Italy), and CICT/MCT (Spain). SPIRE has been developed by a consortium of institutes led by Cardiff Univ. (UK) and including Univ. Lethbridge (Canada); NAOC (China); CEA, LAM (France); IFSI, Univ. Padua (Italy); IAC (Spain); Stockholm Observatory (Sweden); Imperial College London, RAL, UCL-MSSL, UKATC, Univ. Sussex (UK); and Caltech, JPL, NHSC, Univ. Colorado (USA). This development has been supported by national funding agencies: CSA (Canada); NAOC (China); CEA, CNES, CNRS (France); ASI (Italy); MCINN (Spain); SNSB (Sweden); STFC

(UK); and NASA (USA).This study also makes use of the data products from the Two Micron All Sky Survey (2MASS), a joint project of the University of Massachusetts and IPAC/Caltech, funded by NASA and the National Science Foundation; data products from the Wide-field Infrared Survey Explorer (WISE), a joint project of the University of California, Los Angeles, and the Jet Propulsion Laboratory (JPL)/California Institute of Technology (Caltech); data produts from DENIS, a project partly funded by the SCIENCE and the HCM plans of the European Commission under grants CT920791 and CT940627; the NASA Infrared Processing and Analysis Center (IPAC) Science Archive; the SIMBAD database; and the Vizier service, operated at the Centre de Données astronomiques de Strasbourg, France.

4.6 Appendix: transitional disks detected with *Herschel*

4.6.1 CS Cha

CS Cha was first studied by Gauvin & Strom (1992), who found evidence that it harbors a disk with inner holes. It is known to be a spectroscopic binary system, as confirmed by Guenther et al. (2007) (period ≥ 7 years, minimum mass of the companion $\sim 0.1\,M_{\odot}$), although previously Takami et al. (2003) suggested this option based on the large gap found in its disk. This previously unknown feature is probably the reason for the spectral type inconsistency found in the literature (Henize & Mendoza v 1973; Appenzeller 1977; Rydgren 1980; Appenzeller et al. 1983; Luhman 2004a). In this study we used the K6 spectral type found by Luhman (2007). The binary nature makes the disk around CS Cha into a circumbinary disk. The disk has been modeled intensively, initially excluding the effect of the binary system (Espaillat et al. 2007a, 2011) and evidence of an inner hole of ~ 40 AU was found. Espaillat et al. (2011) also pointed out the need for a different mass distribution in CS Cha compared to that of disks around single stars. A more recent analysis by Nagel et al. (2012) also accounted for the binary effect. To reproduce the variations found at the IR wavelengths, the model includes the emission from the inner disk structure generated by the double system, with a ring and streams of material falling from the ring to the circumstellar disks around the individual stars. Another 2MASS source is found at $5''$away. It is 6 magnitudes weaker than CS Cha in the 2MASS J band and undetected in the rest of the 2MASS bands. Contamination from this object is therefore very unlikely.

CS Cha is located in front of a bright background. Therefore, the SPIRE fluxes are very likely underestimated because the background emission was probably overestimated during the photometry extraction.

4.6.2 SZ Cha

This source was cataloged as a K0 star by Rydgren (1980) and was first identified as a disk with a possible inner gap by Gauvin & Strom (1992). Luhman (2007) reviewed its properties, and it was lately confirmed by Kim et al. (2009) as a transitional disk. It has sometimes been referred to as a pre-transitional disk, given the small excess found at 3-10 μm. The first modeling results by Kim et al. (2009) suggested an inner disk radius of ~ 30 AU. Espaillat et al. (2011) modeled this object in detail, noting flux variations from IRS spectra at different epochs on periods shorter than three years. These variations are attributed to changes in the height of the optically thick disk wall (from 0.006 to 0.08 AU), and they do not modify the 10 μm silicate emission feature. SZ is known to be a wide binary (Vogt et al. 2012). A companion is found at $\sim 5''$(projected distance of 845 AU), which could be causing truncation of the outer disk. The contribution of

this source to the total measured fluxes in this study is likely to be negligible, since it is 4 magnitudes weaker than SZ Cha in the 2MASS J band. However, the possibility of an increase in its FIR measurements cannot be excluded.

4.6.3 T25

T25 was identified as an M3 star by Luhman et al. (2008a) and was found to be a transitional disk by Kim et al. (2009). The lack of IR excess at wavelengths $< 8\,\mu$m indicates that the inner regions of the disk are well depleted of small dust particles. The modeling by Kim et al. (2009) yields an inner radius of 8 AU for the disk. It is the only detected transitional object, together with T35, lacking the silicates feature at $10\,\mu$m, another indication of an efficient depletion of small particles in the inner disk region. T25 has no known stellar companions (Nguyen et al. 2012).

4.6.4 T35

Gauvin & Strom (1992) classified this source as an M0 star, and it was later identified as a possible a pre-transitional disk by Kim et al. (2009) because it displays weak excess at short IR wavelengths. In this case, the inner disk radius is located at 15 AU (Espaillat et al. 2011). As in T25, there is no sign of silicate emission. The excess at $70\,\mu$m is lower than in other cases, but does not resemble the typical Class II SED. It has no confirmed known stellar or substellar companions (Nguyen et al. 2012). However, recent sparse aperture masking observations of this source by Cieza et al. (2013) showed and asymmetry in its K-band flux. On the basis of modeling, these authors found the inner disk radius to be $\sim$8.3 AU. They were also unable to distinguish between the close-companion scenario and the asymmetry being produced by the starlight scattered off the disk itself.

4.6.5 T56

This source was found to be an M0.5 start in Gauvin & Strom (1992). Kim et al. (2009) identified it as a transitional disk with a inner disk radius of 18 AU. As in the other transitional disks in this study, its excess is higher than the expected Class II flux at the PACS bands. It has no known bound companions (Nguyen et al. 2012).

4.6.6 ISO-ChaI 52

ISO-ChaI 52 is an M4 star (Luhman 2004a). Espaillat et al. (2011) proposed it as a transitional disk, finding the source to be an extreme case among their sample: based

on variations of its *Spitzer* spectrum, models require the inner wall height to increase by about 400 % (from 0.0006 to 0.003 AU). We also found it to be an outlier in the sense that it has the flattest SED between 12 and 70 μm. No bound companions are known for ISO-ChaI 52 (Nguyen et al. 2012).

4.6.7 CR Cha

CR Cha is an M0.5 star (Gauvin & Strom 1992). Furlan et al. (2009) found it to be an outlier in their sample when comparing the equivalent width of the silicates emission and the spectral slope between 13 and 31 μm: it was beyond the parameter space considered in their study. The explanation given in Furlan et al. (2009) is that this source could be a pre-transitional disk. For this reason, Espaillat et al. (2011) included it in their sample of transitional disks. In this study, we found this object to be compatible with a Class II object. It is also located among other Class II objects using the proposed classification method (Fig.4.2). Therefore, although we cannot completely rule out the possibility that this object is in a pre-transitional disk phase given its strong silicates emission, it would be in a very early stage of the transitional phase.

4.6.8 WW Cha

This source was first classified as a K5 object by Gauvin & Strom (1992). It was included in the analysis of Espaillat et al. (2011) for the same reason as CR Cha, and modeled as a pre-transitional disk. Comparison with the median SED of the Class II sources shows that WW Cha is well above the median. The SED of WW Cha resembles a typical Class II object, probably still embedded in the core, as suggested by its high extinction ($A_v \sim$ 4.8 mag) and its position in the *Herschel* maps. The dusty environment in which it is located could significantly pollute the photometry and, hence, our conclusions about this object.

4.6.9 T54

T54 is known to be a misclassified transitional disk (Matrà et al. 2012), and therefore we excluded it from our analysis. The *Herschel* images show contamination from close-by extended emission, which affected our photometry and, hence, our conclusions. The non-transitional nature of this object is also supported by the fact that it would be the only transitional disk in our sample with no excess emission at 70 μm with respect to the median SED Class II disks.

5

Modeling transitional disks in Chamaeleon with *Herschel*

With the advent of *Herschel*, FIR photometry is available for large samples of YSOs, making standard radiative transfer modeling techniques based on the computation of large grids of models impractical. Modern techniques using advance statistical methods such as Markov Chain Monte Carlo are the only way to model large samples of YSOs in reasonable computational times. In this chapter, we model three transitional disks in the Chamaeleon I star-forming region, and use Markov Chain Monte Carlo (MCMC) techniques to derive posterior functions for the used free parameters. We also explore the addition of *Herschel* data to our knowledge of these targets and compare our results with previous studies of these targets.

5.1 Introduction

Transitional disks are one of the main research topics within the current paradigm of planet formation: these are protoplanetary disks with signatures of cavities and/or gaps in their dust distribution, which could be directly linked to forming planets (see Espaillat et al. 2014, for an updated review on this field). For this reason, a proper characterization of these systems could set strong constrains on the conditions under which planets come to be. However, these gaps could also be produced by other mechanisms such as photoevaporation, dust growth and settling towards the disk middle plain, dynamic clearing by (sub)stellar companions, or a combination of several of these (e.g. Ireland & Kraus 2008; Birnstiel et al. 2012; Alexander et al. 2014; Espaillat et al. 2014). Despite the large number of studies of transitional disks covering the whole wavelength domain with several observing techniques (e.g., photometry, spectroscopy, polarimetry, or interferometry), there are several open questions about them: what is the connection between transitional disks and planet formation? Do all disk go through a transitional phase? What are the main processes responsible for their formation and evolution?

The spectral energy distributions (SEDs) of full, optically thick circumstellar disks (Class II) have significant infrared (IR) excess with respect to their photospheric level from the near-infrared (NIR, 1-5 μm) to millimeter wavelengths (Williams & Cieza 2011). In contrast, SEDs of transitional disks normally display a very distinctive shape, with small or no NIR excess, but with important excess at mid-infrared (MIR, 5-50 μm) and far-infrared (FIR, 50 μm and longer) wavelengths. This lack of NIR emission is usually attributed to dust depleted inner regions in the disk, and the location and shape of this change in the SED behavior (around $\sim$10 μm) can be used to partially characterize the gap structure (e.g. Calvet et al. 2005; Espaillat et al. 2010, 2011). For this reason, transitional disks have been extensively studied and modeled in the past with MIR spectra from the IRS instrument (Houck et al. 2004) on board the *Spitzer Space Telescope*, which yielded thousands of IR spectra of circumstellar disks between 5-38 μm and provided detailed information about their dust composition and the morphology of the inner regions (e.g. Kim et al. 2009; Merín et al. 2010; Espaillat et al. 2011; Furlan et al. 2011). At these wavelengths, the disk is unfortunately optically thick, and several important parameters such as the disk flaring or mass remain poorly or completely unconstrained with SED modeling and lack of information for larger wavelengths. This later parameter is specially relevant, since it gives an estimate of the amount of mass available for planet formation. A more in-depth knowledge of transitional disks can be achieved in the (sub)mm domain, where the disk becomes mostly optically thin and the flux can be related to the disk mass (e.g., Andrews & Williams 2005; Andrews et al. 2013). The advent of the Herschel Space Observatory *Herschel* produced a large number of FIR observations of protoplanetary and transitional disks between 70 and 500 μm,

providing information at larger wavelengths that can be used to better constrain some parameters of transitional disks.

In this paper, we study the contribution of *Herschel* data to our knowledge of transitional and (pre)transitional disks (objects with small excesses in the NIR and significant excesses at longer wavelengths) in the Chamaeleon I star-forming cloud. This region is located at 160-180 from the Sun (Whittet et al. 1997, and references therein), and is part of the Chamaelon-Musca molecular cloud complex (Luhman 2008). Chamaelon-I is $\sim$2 Myr old (Luhman et al. 2008a) and given its proximity, it has been a common target for star-formation and YSOs population studies in the past (e.g., Luhman 2007; Luhman et al. 2008a; Belloche et al. 2011), which have identified more than 200 YSOs in the region. It was also one of the clouds observed by *Herschel* as part of the of the Gould Belt survey (André et al. 2010), and some studies have already provided a *Herschel* view of YSOs this region (Winston et al. 2009), disks around low-mass stars (Olofsson et al. 2013), and transitional disks in the region (Ribas et al. 2013; Rodgers-Lee et al. 2014). Here, we focus on the improvement of parameter constrains when including *Herschel* data in the modeling of three transitional disks in Chamaeleon I. We combine radiative transfer modeling with Markov Chain Monte Carlo (MCMC) methods to conduct a Bayesian analysis of the properties of these sources. Sect. 5.2 describes the sample and data used. The modeling procedure can be found in Sect. 5.3, and the results of the process are described in Sect. 5.4. Finally, we discuss the implications of our analysis in Sect. 5.5.

5.2 Observations of transitional disks in Chamaeleon I

5.2.1 The sample of transitional disks in Chamaeleon I

A total of 12 sources classified as (pre)transitional disks in the Chamaeleon I region: C7-1, SZ Cha, CS Cha, T21, T25, T35, T56, CHXR 22E, CR Cha, WW Cha, ISO-ChaI 52, and 2MASS J11241186-7630425 (Damjanov et al. 2007; Luhman et al. 2008a; Furlan et al. 2009; Kim et al. 2009; Espaillat et al. 2011; Manoj et al. 2011). We note that the definition of transitional disk is not unique, and therefore other sources may meet this category. In a previous study (Chapter 4, Ribas et al. 2013), we used a selection criterion to identify transitional disks with strong changes in their SED slopes using *Herschel* PACS 70 μm data. In that study, we selected the six transitional disks (SZ Cha, CS Cha, T25, T35, T56, and ISO-ChaI 52) which were both detected in *Herschel* maps and met the criterion in Ribas et al. (2013). Another object, ESO-H$_\alpha$ 559 met the mentioned criterion. Robberto et al. (2012) proposed this source is an edge-on disk based on SED modeling. Rodgers-Lee et al. (2014) noted that this source is not under-luminous, and Olofsson et al. (2013) presented detailed Bayesian modeling of this source. We have queried the NACO archives and found K_S band observations of this target (program

TABLE 5.1: Coordinates and stellar parameters used in this work for the considered sample of (pre)transitional disks.

Name	R.A.$_{J2000}$	Dec.$_{J2000}$	A_V (mag)	SpT Type	T_* (K)	L_* ($L_\odot$)	M_* ($M_\odot$)	R_* ($R_\odot$)
SZ Cha	10:58:16.77	-77:17:17.1	1.9	K0	5250	1.9	1.4	1.7
CS Cha	11:02:24.91	-77:33:35.7	0.8	K6	4205	1.5	0.9	2.3
T25	11:07:19.15	-76:03:04.9	1.6	M3	3470	0.3	0.3	1.5
T35	11:08:39.05	-77:16:04.2	3.5	M0	3850	0.4	0.6	0.5
T56	11:17:37.01	-77:04:38.1	0.6	M0.5	3720	0.4	0.5	1.6
ISO-ChaI 52	11:04:42.58	-77:41:57.1	1.3	M4	3370	0.1	0.3	1.0

075.C-0042(A)). The images show no signatures of an edge-on disk, in agreement with Rodgers-Lee et al. (2014). All these evidences support the idea of ESO-H_α 559 being a transitional disk. However, since it has been already modeled, we chose not to include it in this analysis. For the six aforementioned transitional disks, we used the stellar parameters in Espaillat et al. (2011), and refer the reader to this study for further references. Table 5.1 lists the adopted stellar properties.

5.2.2 Herschel data of the Chamaeleon I region

In Ribas et al. (2013), we presented *Herschel* aperture photometry measurements of the six mentioned transitional disks in Chamaeleon I. In that previous study, we visually inspected the position of the known Class II sources in the region (see Ribas et al. 2013, for a complete description of the sample), and in this paper we maintain the detections/upper limits classification. Later, Rodgers-Lee et al. (2014) identified a systematic discrepancy between those values and the ones in Winston et al. (2012), which used the *getsources* algorithm (Men'shchikov et al. 2012). We attribute such differences to the different map-making algorithms used, but more detailed discussion on this can be found in Appendix 5.7. Here, we describe the adopted map-making algorithms and updated photometry extraction method.

The Chamaelon I region was observed with *Herschel* (Pilbratt et al. 2010) as part of the Gould Belt Key Program (André et al. 2010). Parallel mode observations from this program (OBSDIs: 1342213178, 1342213179) provided PACS (Poglitsch et al. 2010) 70 and 160 μm and SPIRE (Griffin et al. 2010) 250, 350 and 500 μm maps at a scan speed of 60″/s. Additional PACS 100 and 160 scan observations are also available at scan speed of 20″/s (OBSIDs: 1342224782, 1342224783). Although with smaller coverage, this last set of observations is deeper and has a slower scan speed (hence a smaller point spread function, PSF), so we chose to use them for the 160 μm band. We note that T25 is outside the smaller scan maps, and no 100 μm photometric measurement is available for this target. Its 160 μm flux was obtained from the parallel mode data.

TABLE 5.2: *Herschel* fluxes of the modeled (pre)transitional disks disks in this study. Ellipsis indicate non-detected sources

Name	F70 (Jy)	F100 (Jy)	F160 (Jy)	F250 (Jy)	F350 (Jy)	F500 (Jy)
SZ Cha	4.01±0.80	3.74±0.75	3.56±0.71	2.53±0.51	1.85±0.37	1.02±0.20
CS Cha	3.20±0.64	2.88±0.58	2.27±0.45	1.31±0.26	1.04±0.21	...
T25	0.53±0.11	...	0.38±0.08	0.25±0.05	0.17±0.03	0.06±0.01
T35	0.43±0.09	0.32±0.06	0.15±0.03	...	...	...
T56	0.76±0.15	0.60±0.12	0.48±0.10	0.25±0.05	0.17±0.03	0.09±0.02
ISO 52	0.20±0.04	0.22±0.04	0.24±0.05	...	...	...

We used the Herschel Interactive Processing Environment (HIPE Ott 2010) version 12.1 to process the maps of the region. We adopted the standard map-making algorithms used in the *Herschel* Science Archive, i.e., *jscanam* for PACS maps (a HIPE adaptation of the *Scanamorphos* software Roussel 2013), and *destriper* for SPIRE maps. In the case of *jscanam* we chose to remove turnarounds with speeds 50 % or more higher than the nominal value, and we do not use the extended emission gain option for *destriper*, as recommended for point source photometry.

We used the *AnnularSkyAperturePhotometry* task in HIPE to estimate fluxes in the PACS maps. Medium or fast scan speeds and the combination of scan and cross scans can produce elongated PSFs, and we adopted aperture radii of 15″, 15″, and 22″ for PACS 70, 100 and 160 bands, respectively (see Appendix 5.7). The background was estimated within an annulus with inner and outer radii of 25″and 35″. We then applied the corresponding aperture corrections of 1.206, 1.222, and 1.372 (Balog et al. 2014). The thermal emission from the outer disk of transitional disks peaks at these wavelengths, and their SEDs are roughly flat in this regime. For this reason, we chose not to apply color corrections in this case. For SPIRE, we used the recommended procedure and fit the sources in the timeline (Pearson et al. 2014). This method does not require aperture corrections. We also note that this procedure successfully detected T25 at 500 μm. This source was previously marked as an upper limit in this band in Ribas et al. (2013) due to the strong background surrounding it, but we chose to use this detection given the better method used here and its consistency with the overall shape of the SED. Conversely, the timeline fitter does not detect CS Cha at 500 μm probably due to difficulty in disentangling the emission from the object and the cloud with sufficient confidence, and therefore we do not include this wavelength in its SED. SPIRE traces the Rayleigh-Jeans regime of the disk emission, and we applied the color correction factors corresponding to black-body emission (0.945, 0.948, 0.943 for SPIRE 250, 350, and 500 bands, respectively, see SPIRE Handbook Version 2.5). Finally, we adopted conservative uncertainties of 20 % to account for different effects (see Appendix 5.7). The obtained *Herschel* values can be found in Table 5.2.

5.2.3 Near/mid IR photometric data of transitional disks

In Ribas et al. (2013), we compiled photometry from several surveys and catalogs to build well-sampled SEDs of the six transitional disks mentioned in Sect. 5.2.1. However, the aim of this paper is to model these SEDs, and hence we only select non-redundant photometric data. We therefore chose to include the following bands in the near/mid-IR: 2MASS *J*, *H*, and *Ks*, and IRAC1 and IRAC2 bands. This selection provides a nice coverage of the 1-6 μm regime, key to separate (pre)transitional disks from transitional disks (Espaillat et al. 2010). It also avoids redundancy (including several data in a small wavelength domain), which could give excessive weight to certain parts of the SED in the model fitting process. Typical photometric uncertainties of these measurements are below 5 %, but given the main scope of this paper (i.e., modeling transitional disks), possible IR variability of the sources should also be considered to derive proper uncertainties in the physical parameters (Muzerolle et al. 2009). To account for these two effects (photometric uncertainties and variability), we chose to set uncertainties to be a 10 % of the observed fluxes.

Finally, all photometric points were derredened using the corresponding A_V (see Table 5.1 and the extinction law in Indebetouw et al. (2005).

5.2.4 IRS spectra of transitional disks

We retrieved low resolution IRS spectra from the Corner Atlas of Spitzer/IRS Sources (CASSIS) database (Lebouteiller et al. 2011) for the six (pre)transitional disks in our study. CASSIS provides optimally extracted IRS spectra, and is well suited for our purposes. For these spectra, we first separate the clean zones of the IRS spectra (7 to 14 μm and 20.5 to 35 mum for the first order, $< 20.5\,\mu$m for second one), and reject bad pixels (e.g. negative or NaN values). As a compromise between estimating monochromatic fluxes required for model fitting (see Sect.5.3) while reducing the impact of possible artifacts in the spectra, we chose to bin them in ten equally spaced wavelengths throughout the spectra coverage, and estimate the fluxes for each of them as the mean value of ten pixels centered around each corresponding wavelength. We checked this procedure to produce nice sampling of the IRS spectra (see Fig. 5.1 for an example), while being a good compromise for the SED fitting: a whole IRS spectra typically contains 300-400 good pixels, and fitting them all would put most of the weight on the IRS spectra itself. By reducing its contribution to a comparable number to that of photometric data ($\sim$ 10) we ensure that all parts in the SED contribute to the fitting procedure in a similar manner. As in Sect. 5.2.3, we assigned 10 % uncertainties to the binned data, a typical variability value for these disks (Espaillat et al. 2011).

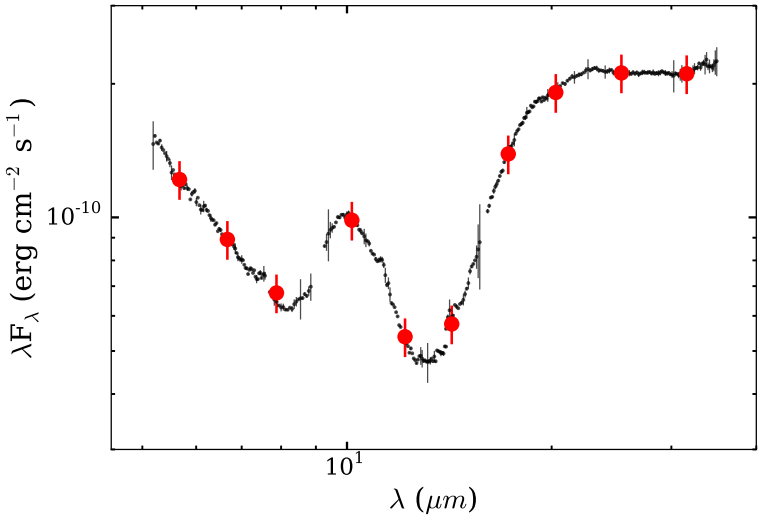

FIGURE 5.1: Derredened IRS spectrum of SZ Cha. Black dots show the CASSIS spectrum of this source (after bad pixels rejection) with the corresponding error bars. The binned spectrum and assumed errors is shown as red, larger dots. It properly traces the shape of original data including the silicate feature at 10 μm.

5.3 Modeling

We aimed at modeling the transitional disks in Chamaeleon I region and quantifying the impact of adding photometric *Herschel* data to this process. For this reason, we used two different datasets for each object. The first dataset comprises the available data from 2MASS, IRAC1/IRAC2, and the binned IRS spectra. The second dataset also includes *Herschel* photometry.

We used the MCFOST software (Pinte et al. 2006) version 2.19 to model these disks. MCFOST uses a Monte Carlo raytracing procedure to generates synthetic SEDs and images of circumstellar disks. First, it produces temperature and density maps of the disk using the provided stellar and disk parameters. In this case, we used 10^7 photons in this step (enough to produce smooth and well-sampled temperature maps of the disks). Second, a list of wavelengths is provided, and MCFOST computes the corresponding synthetic monochromatic fluxes. We required 2 000 photons to be received for each wavelengths, corresponding to noise levels of 2-3 % in the flux estimates and well below the assumed observational uncertainties (10-20 %).

Our models include seven free parameters: disk dust mass (M_{dust}), inner and outer radii (R_{in}, R_{out}), scale height at 100 AU (H_{100}), flaring index (h), surface density exponent (p), and the maximum grain size (a_{max}). M_{dust} and a_{max} can take values within several orders of magnitude, and we chose to explore them in logarithmic scale. Given the complex structures of circumstellar disks, there are several degeneracies and dependencies in these parameters, and some may even be totally unconstrained with the available data. We did not attempt to fit the mineralogy of the disks. Instead, we assumed

typical astronomical silicate compositions, and fixed the minimum grain size to 0.01 μm. Although very interesting, this would add an important source of complexity to modeling and we preferred not to include it in our comparative analysis. Following Espaillat et al. (2011), we also fixed the inclination of all disks to i=60 °. Although somewhat arbitrary, none of these objects show signatures of high-inclination (e.g., silicate features in absorption or underluminous photospheres). Moreover, for wavelengths $> 13\,\mu$m, the mid-IR continuum is almost insensitive to this effect unless the disk is very close to edge-on (Furlan et al. 2006; D'Alessio et al. 2006).

Among the objects in the sample, four of them (SZ Cha, T35, T56 and ISO 52) have NIR excess over the photospheric emission. This feature is characteristic of pre-transitional disks, sources with an optically thick inner disk, separated from the outer disk by a gap in the radial dust distribution (e.g., Espaillat et al. 2007b). Additionally, CS Cha has no NIR excess but a prominent silicate emission feature at 10 μm, indicating the presence of optically thin dust in its inner hole. The inner disks of these objects have already been modeled in detail (e.g., Espaillat et al. 2007a; Kim et al. 2009; Manoj et al. 2011) and we do not attempt to fit them: instead, we included an additional disk structure in these cases, and found a reasonable combination of disk parameters that reproduced the NIR SED shape. The inner disks remained fixed during the fitting process. This may have an impact in our final results, as discussed later in the paper (see Sect. 5.5.1).

5.3.1 Fitting procedure

We used a Bayesian approach to properly derive confidence intervals for the outer disk parameters. Bayesian techniques have been increasingly used in Astrophysics during the past years, and we do not intend to explain them in detail. Instead, we refer the interested reader to introductory works such as Trotta (2008). Here we describe the priors used and the Markov Chain Monte Carlo (MCMC) method using ensemble samplers with affine invariance.

5.3.1.1 Prior selection

The selection of restrictive priors may have a significant effect on the fitting results. However, priors are also important tools to force parameters to remain within certain ranges, avoiding non-physical solutions. We used flat priors for all the parameters, and constrain them to reasonable values for transitional disks. The prior ranges used were as follows:

- $\log M_{dust}$: from -6 to -2 $\log M_{\odot}$,
- R_{in}: from 1 AU to r_{in-out},

- R_{out}: from r_{in-out} to 500 AU,
- H_{100}: from 0.5 to 25 AU,
- h: from 0.8 to 1.3,
- p: from -2.5 to 1,
- $\log a_{max}$: from -1 to $4 \log \mu$m,

where r_{in-out} depends on the target, and is used to avoid the outer disk becoming smaller than the inner one during the evolution of the MCMC. Based on previous results (Kim et al. 2009; Espaillat et al. 2011), we set r_{in-out} to 40 AU for SZ Cha, 50 AU for CS Cha, and to 30 AU for the rest of objects. Since we are using flat priors, r_{in-out} does not modify our results in any way unless it prevents R_{in} or R_{out} from reaching their true vale (i.e., the prior distribution does not include the optimal R_{in} or R_{out} values, if any). Nevertheless, this issue can be easily identified if we find that most of the posterior distribution is accumulated at the limit of the priors range. Also, modeling of ISO 52 by Olofsson et al. (2013) obtained an inner disk radius of $\sim$3 AU, which is at the very edge of the prior for this parameter. For this reason, we extended the R_{in} prior range for this target down to 0.1 AU.

5.3.1.2 MCMC and ensemble samplers with affine invariance

MCMC methods have several advantages for fitting: they sample directly from the posterior distribution, and unlike other methods (e.g., model grids) are not impacted by the "curse of dimensionality" (rapid increase of the number of required models with the number of free parameters). They are also useful to identify degeneracies between different parameters. However, they are very dependent on the initial position of the chain: if this position is far from the best-fit, they usually require a large number of iterations to reach convergence.

A variant of this method known as ensemble samplers with affine invariance (Goodman & Weare 2010) provides an elegant solution to this issue. This method uses several "walkers" or individual chains. At every step, random linear combinations of walker pairs are used to evolve the chain (a full mathematical description of the method can be found in Goodman & Weare 2010). This approach has shorter autocorrelation times, i.e., convergence is reached earlier in the chain evolution. We implemented the "parallel stretch move" following Foreman-Mackey et al. (2013) to ensure detailed balance required for MCMC sampling. In every iteration, the chain comprises 100 walkers. To maintain the acceptance rate of newly proposed positions between 10 and 50 % (a good compromise between a random walk and discarding most of the new positions), we

tuned the stretch parameter of the walk (a) to 1.5. We assumed Gaussian errors for our photometry, and used the typical likelihood function for this case:

$$\mathcal{L} = \prod_{i=0}^{N} \frac{1}{\sqrt{2\pi}\sigma_i} \exp - \frac{(F_{obs,i} - F_{model,i})^2}{2\sigma_i^2} = \exp - \frac{\chi^2}{2} \prod_{i=0}^{N} \frac{1}{\sqrt{2\pi}\sigma_i} \tag{5.1}$$

where N is the number of photometric points, $F_{obs,i}$ is the derredened observed flux at a given wavelength, σ_i is the corresponding uncertainty, F_{model} is the model flux at that wavelength, and χ is the chi square. To avoid dependencies with the distance to the objects, we normalize every model to the J band prior to estimating the likelihood. This should have no impact in our results, since the J band traces photospheric emission in transitional disks and does not depend on disk parameters, hence all models obtained for a given object have always the same J flux.

When available, we set the initial position of the chains around previous results in the literature (Kim et al. 2009; Espaillat et al. 2011). In any case, the posterior from MCMCs are only valid once the system has lost memory of their initial values. This can be quantified using the autocorrelation time of the chains, which gives and estimate of the required number of iterations to draw independent samples. For every case in this study, we computed the autocorrelation time for each walker in each parameter, and took the maximum value for conservative purposes. We then left the system evolve for five autocorrelation times (typically $\sim$500 iterations). At this point, the results are independent of the initial position, and the chain is now sampling the posterior distribution. We then estimated the posterior function with other five autocorrelation times (i.e., 50 000 models, the result of the 500 iterations per 100 walkers used). A typical chain evolution is shown in Fig. 5.2.

Despite this method represents an important improvement with respect to full model grids (see discussion in Sect. 6.2), MCMC analysis with raytracing methods is still computationally demanding and by the time of writing this thesis, only the modeling of SZ Cha, CS Cha, and T25 has been completed. The following results describe these three objects.

5.4 Results

5.4.1 Fitting results without *Herschel* data

We first use the dataset without *Herschel* data to explore which parameters can be constrained with NIR/MIR information. The resulting posterior distributions for the sources are shown in Fig. 5.3, and the yielded values in Table 5.3. The adopted procedure also allows to study degeneracies between different parameters by plotting positions of

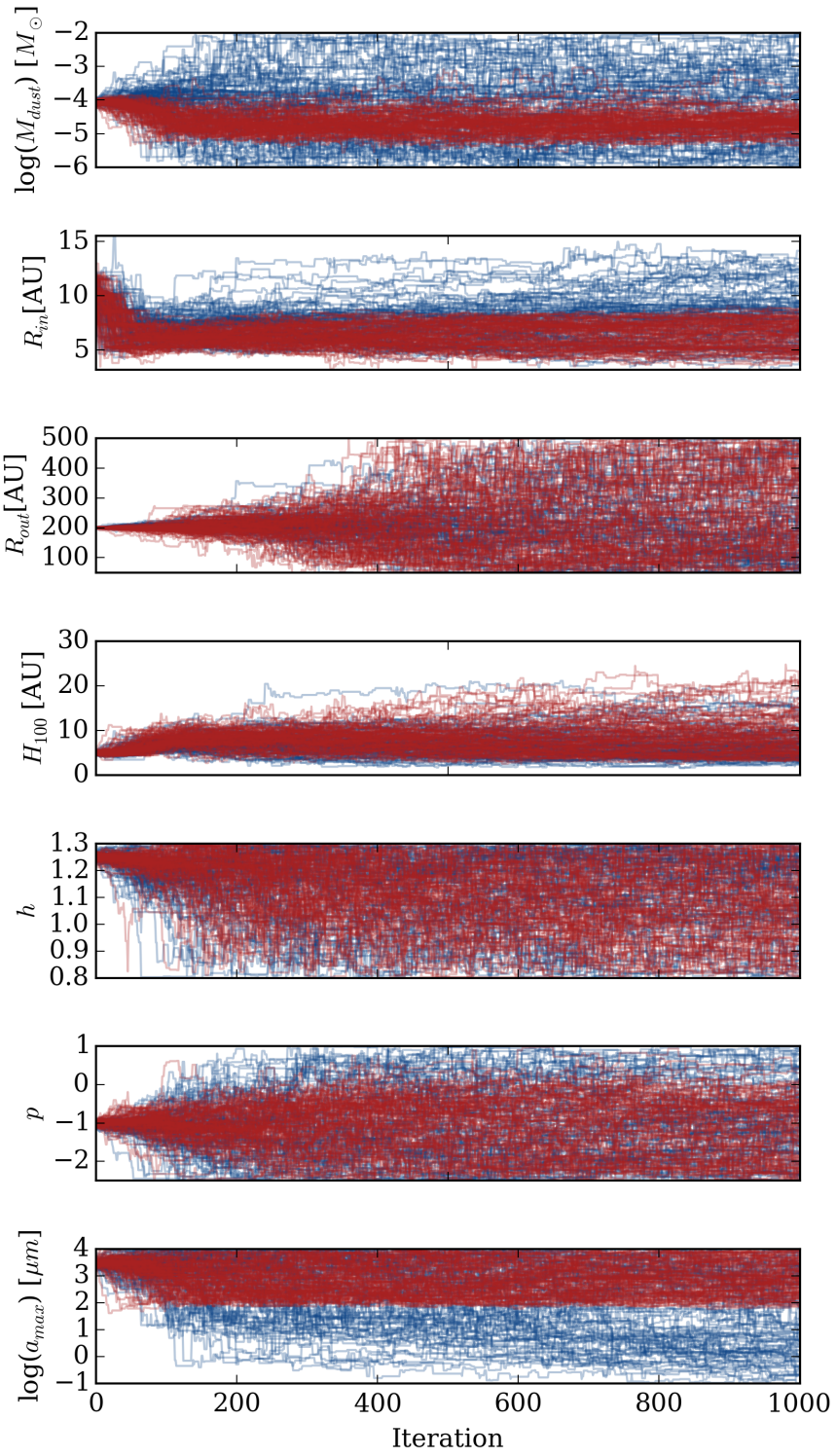

FIGURE 5.2: MCMC chain evolution for T25. Each line represents the evolution of one of the 100 walkers used in the process. The results for modeling without *Herschel* data (blue) and with *Herschel* photometry (red) are shown. Specially for M_{dust}, the impact of FIR data is clearly visible.

the chains in different 2-D projections. The degeneracies are very similar in all cases (Figs. 5.5 to 5.7) show the cornerplots for the considered objects.

Several conclusions can be drawn from the resulting posterior functions for the considered parameters by analyzing 5-95 % confidence intervals (Fig. 5.3):

- M_{dust}: as expected, it is not possible to constrain the mass of dust at all using data up to MIR wavelengths.
- R_{in}: in all cases, IRS data are enough to constrain the location of the inner wall within 5-20 AU.
- R_{out}: MIR data do not provide any information about the outer disks.
- H_{100}: the scale height, on the other hand, should be at least partially constrained with these data. Different scale heights modify the amount of stellar flux intercepted by the disk, changing the emission from the inner disk. Our results agree with these expectations, and we find that IRS spectra can constrain H_{100} within 10 AU.
- h: the flaring index has small influence in MIR data, and therefore is poorly traced in this dataset. Despite this, large values of h are preferred.
- p: because MIR data trace mostly the emission from the disk inner wall, it is unlikely that they can constrain the surface density distribution. This is consistent with our results, which place no constrain on this parameter.
- a_{max}: any observation at a wavelength λ is only sensible to emission from grains of the size $a \sim \lambda$ (Draine 2006), hence MIR data should pose no constrain at all in this parameter, which may even be degenerate: if a_{max} is small enough ($< 10\,\mu$m), it could produce substantial changes in the SED and therefore play a role in the modeling, which is in fact clearly visible in the form of double peaked posterior distributions. Although much larger grains are generally expected in disks, our data are not enough to solve this effect.
- As expected, several degeneracies appear in all cases, the most obvious being inner radius with scale height, and scale height with flaring index. In some cases, the inner radius also shows a dependence with the maximum grain size.

5.4.2 Fitting results with *Herschel* data

We repeated the modeling procedure including *Herschel* data for the three transitional disks remaining in the sample. As in the previous case, the resulting posterior distributions are shown in Fig. 5.3, and full corner plots in Figs. 5.5 to 5.7. Fig. 5.4 show the

observed SEDs and modeling results, and Table 5.3 provides the numeric values of this process.

- M_{dust}: we find that *Herschel* can narrow down the amount of mass in the disks. For SZ Cha and T25, the posterior distributions show it to be constrained within one order of magnitude, whereas for CS Cha the distribution is broader ($\sim$2 dex). This is also expected, since CS Cha lacks a detection at 500 μm, in contrast with the other two sources.
- R_{in}: *Herschel* data also help to improve the estimate of the inner disk, decreasing its uncertainty down to 5-10 AU.
- R_{out}: as with the *Spitzer*-only dataset, there is no information about the outer radius in photometric data.
- H_{100}: the scale height is better constrained with *Herschel* for SZ Cha and CS Cha, reducing the uncertainties by a factor of ~ 2. For T25, there is no improvement in the estimate of this parameter.
- h: as in the previous case, the 5-95 % confidence intervals for this parameter cover basically the full extent of the prior, but interestingly the distributions show a weak preference for values around 1-1.1.
- p: surface density shows a similar behavior than h with *Herschel* data, yielding distributions suggesting small values specially for SZ Cha and CS Cha. Combined, the results of h and p may indicate anomalous outer disks for these objects, which will be discussed in the following section.
- a_{max}: *Herschel* data break the two-peak degeneracy in the maximum grain size estimation. Although they are not enough to provide a real estimate of this value, they inform us that this value is very likely larger than 100 μm in all cases.
- most of the formerly mentioned degeneracies are still present when *Herschel* photometry is included in the analysis. However, as discussed in the previous point, they are sufficient to rule out small values of a_{max}.

5.5 Discussion

5.5.1 Limitations and future prospects

We have used a radiative transfer software (MCFOST) to produce synthetic SEDs of transitional disks. This offers several advantages (e.g., SEDs of very complex disks without an analytic solution can be computed), but it does not guarantee that the disk

TABLE 5.3: Results of the MCMC fitting for the seven free parameters considered. We tabulate the obtained median value and the 5 % and 95 % confidence intervals. For each column, results obtained without *Herschel* data (left) and with them (right) are provided.

Object	$\log M_{dust}$ ($\log M_\odot$)	R_{in} (AU)	R_{out} (AU)	H_{100} (AU)
SZ Cha	$-3.6^{+1.5}_{-2.0}$ | $-3.4^{+1.0}_{-0.5}$	17^{+7}_{-7} | 13^{+2}_{-4}	220^{+240}_{-170} | 200^{+240}_{-120}	$8.8^{+5.0}_{-3.1}$ | $7.6^{+2.9}_{-1.7}$
CS Cha	$-3.8^{+1.6}_{-2.0}$ | $-3.8^{+1.4}_{-0.8}$	19^{+16}_{-7} | 18^{+6}_{-5}	200^{+250}_{-130} | 210^{+250}_{-140}	$5.8^{+10.4}_{-2.7}$ | $4.6^{+4.2}_{-1.3}$
T25	$-4.2^{+2.0}_{-1.6}$ | $-4.7^{+0.6}_{-0.5}$	$8.0^{+4.4}_{-3.4}$ | $6.6^{+1.6}_{-2.1}$	190^{+260}_{-150} | 220^{+250}_{-160}	$6.0^{+8.1}_{-3.0}$ | $7.6^{+9.0}_{-3.8}$

Object	h -	p -	$\log a_{max}$ ($\log \mu m$)
SZ Cha	$1.1^{+0.2}_{-0.3}$ | $1.0^{+0.2}_{-0.2}$	$-1.0^{+1.7}_{-1.3}$ | $-1.6^{+1.9}_{-0.8}$	$0.2^{+3.5}_{-0.6}$ | $2.9^{+1.0}_{-1.1}$
CS Cha	$1.1^{+0.2}_{-0.3}$ | $1.0^{+0.3}_{-0.2}$	$-1.1^{+1.8}_{-1.3}$ | $-1.6^{+1.9}_{-0.9}$	$2.4^{+1.5}_{-2.8}$ | $2.7^{+1.1}_{-2.1}$
T25	$1.1^{+0.1}_{-0.3}$ | $1.1^{+0.2}_{-0.2}$	$-1.0^{+1.8}_{-1.3}$ | $-1.1^{+1.1}_{-1.2}$	$1.8^{+2.0}_{-2.3}$ | $2.9^{+1.0}_{-0.9}$

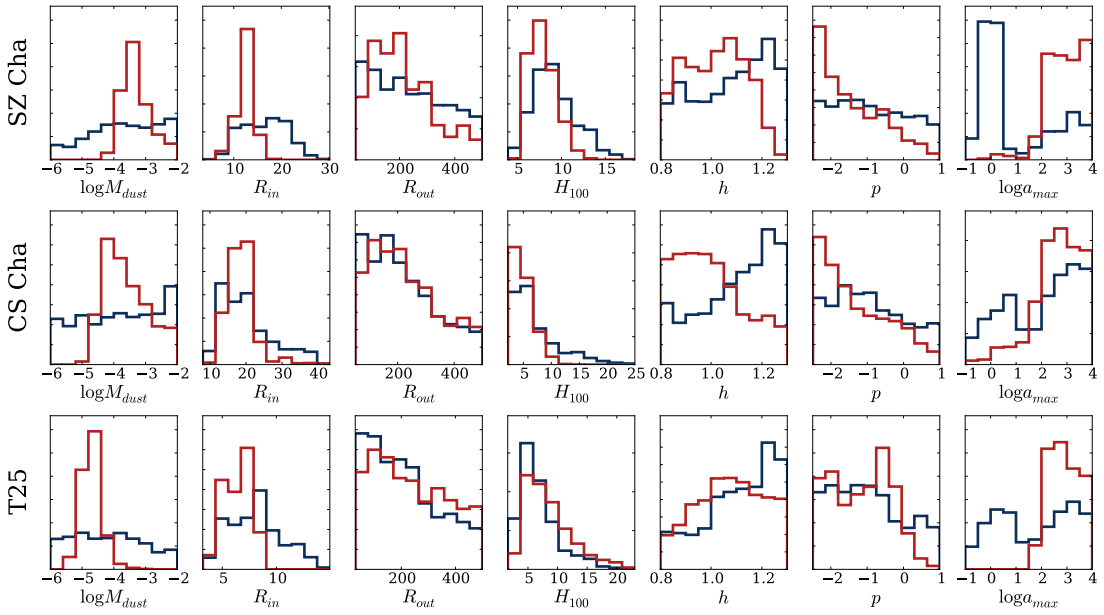

FIGURE 5.3: Posterior distributions of the free parameters for the considered transitional disks in this study. Results without *Herschel* data are shown in blue, those including *Herschel* in red.

structure is physically consistent. We have set physically meaningful priors to try to overcome this issue, but the final combination of parameters is driven by the MCMC process and there is no physical constrain in them. In the future, physically consistent models like those by D'Alessio et al. (2006) can be used to complement these results, although this different set of models relies on significantly uncertain parameters such as the disk viscosity and accretion rates, and should also be considered with caution.

We have not fit the inner disk of pre-transitional objects, but fixed it to reproduce the NIR emission when present, specially the silicate emission. Although we are focusing on the outer disks, this may have some impact in our results: there are several degeneracies in SED fitting, and different inner disks could produce very similar near-IR excess. If this is the case, the shadow cast by the inner disk on the outer wall (e.g., Espaillat et al. 2010, 2011) could be different, altering the temperature distribution and changing the obtained inner radii. We have not explored the effect of different mineralogies in our results, which could also modify the results (see e.g. the case of LkCa 15, Espaillat et al. 2010, 2011). Further extension of this analysis will also include additional free parameters of an inner disk in the case of pre-transitional sources, as well as a more in-depth treatment of the dust composition.

Finally, we have assumed simple disk models, with axial symmetry and one single gap in all cases. Holes in (pre)transitional disks have been found to harbor significant inhomogeneities such as spiral arms or dust traps (e.g., Andrews et al. 2011; van der Marel et al. 2013). An striking example of this was provided by ALMA long-baseline observations of the protoplanetary disk around HL Tau (ALMA Partnership et al. 2015), which revealed an incredibly complex system of radial gaps in its dust distribution.

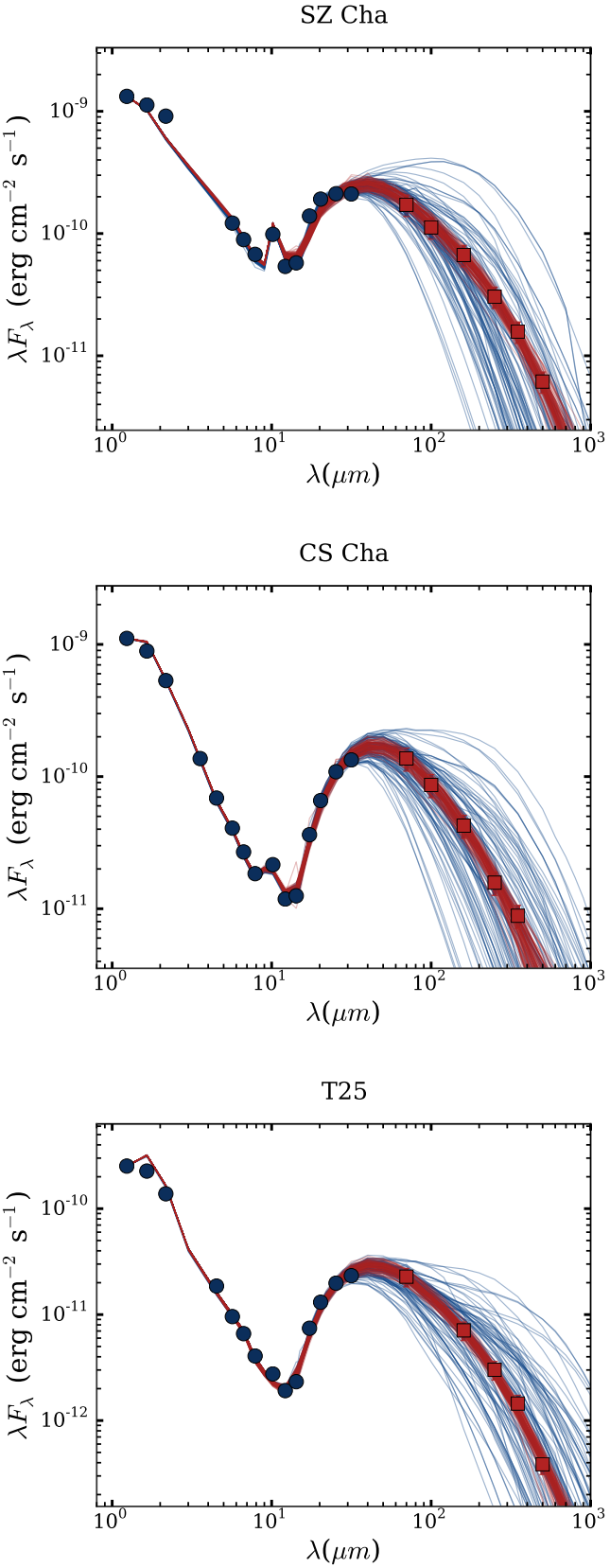

FIGURE 5.4: Observed SEDs for the transitional disks in this study. Photometric data from previous studies are shown as blue solid circles, *Herschel* measurements as red squares. Uncertainties are plotted, although in several cases are smaller than symbol sizes. We also show 100 randomly selected models from the obtained posterior distributions for each case: blue lines correspond to fitting without *Herschel* data, red lines the resulting models when including *Herschel* photometry. This gives an idea on the total uncertainties in the SEDs of the modeled disks.

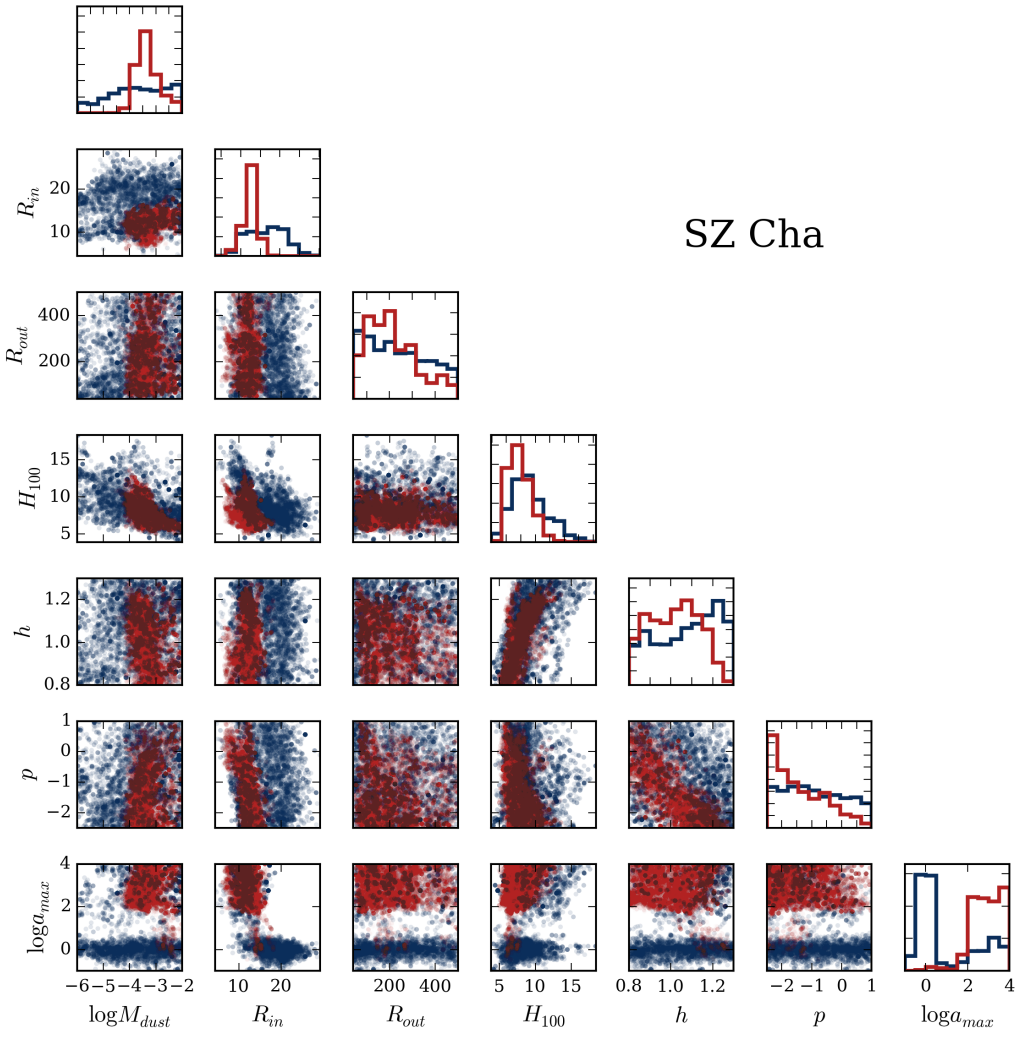

FIGURE 5.5: Cornerplot for SZ Cha. Histograms show the posterior distribution for each free parameter, scatter plots display the position of each chain in two parameter spaces to trace degeneracies. The results without *Herschel* data are shown in blue, those including *Herschel* in red.

Although not obvious in the SEDs, transitional disks may display much more complicated architectures, and hence our models are only a naive approach to their study.

5.5.2 Masses and inner radii

Two of the considered parameters in our models have been found to improve significantly when including *Herschel* data: the disk dust mass and its inner radius.

The mass of the disk is arguably one of the most important parameters for planet formation. It determines the available reservoir to build up planets in the system, is related to disk viscosity and accretion, and can even modify the planet formation mechanism (the disk instability scenario require high M_{disk}/M_* values, e.g., Lodato et al.

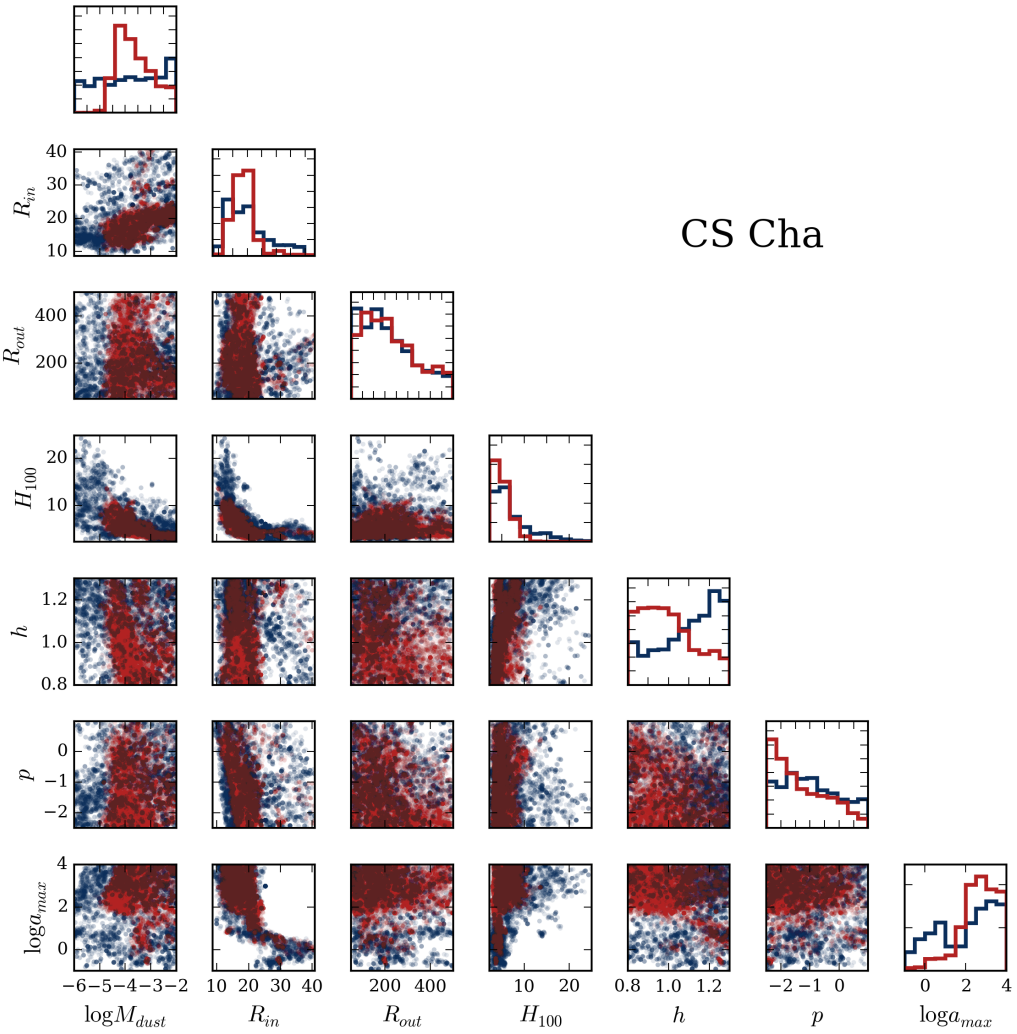

FIGURE 5.6: Cornerplot for CS Cha. Scheme and colors as in Fig. 5.5.

2005). Although the bulk of mass in protoplanetary disks is in gaseous form, photometric IR data are only sensitive to emission from dust particles, which are efficient radiation absorbers and emitters. Hence, only the dust mass is constrained with the presented data. A total disk mass estimate requires either direct gas mass measurements (e.g., ^{13}CO, C^{18}O, Panić et al. 2008) or assumptions on the gas-to-dust ratio. Since the former is only available for a few disks, most authors assume a typical gas-to-dust ratio of 100. We adopt this value for meaningful comparisons with previous studies, but are aware that such an assumption may not be true in many cases, as the gas-to-dust ratio is likely to change with time and from one source to another (Thi et al. 2010, 2014) . Regardless of this, our results show that *Herschel* data can be used to constrain the mass of dust in transitional disks within $\sim$one order of magnitude, which is a tremendous improvement with respect to MIR photometry only and opens the exciting possibility of studying this parameter for the large number of sources observed with *Herschel*. As expected and illustrated by the case of CS Cha, the longest wavelengths (SPIRE 500) are the most

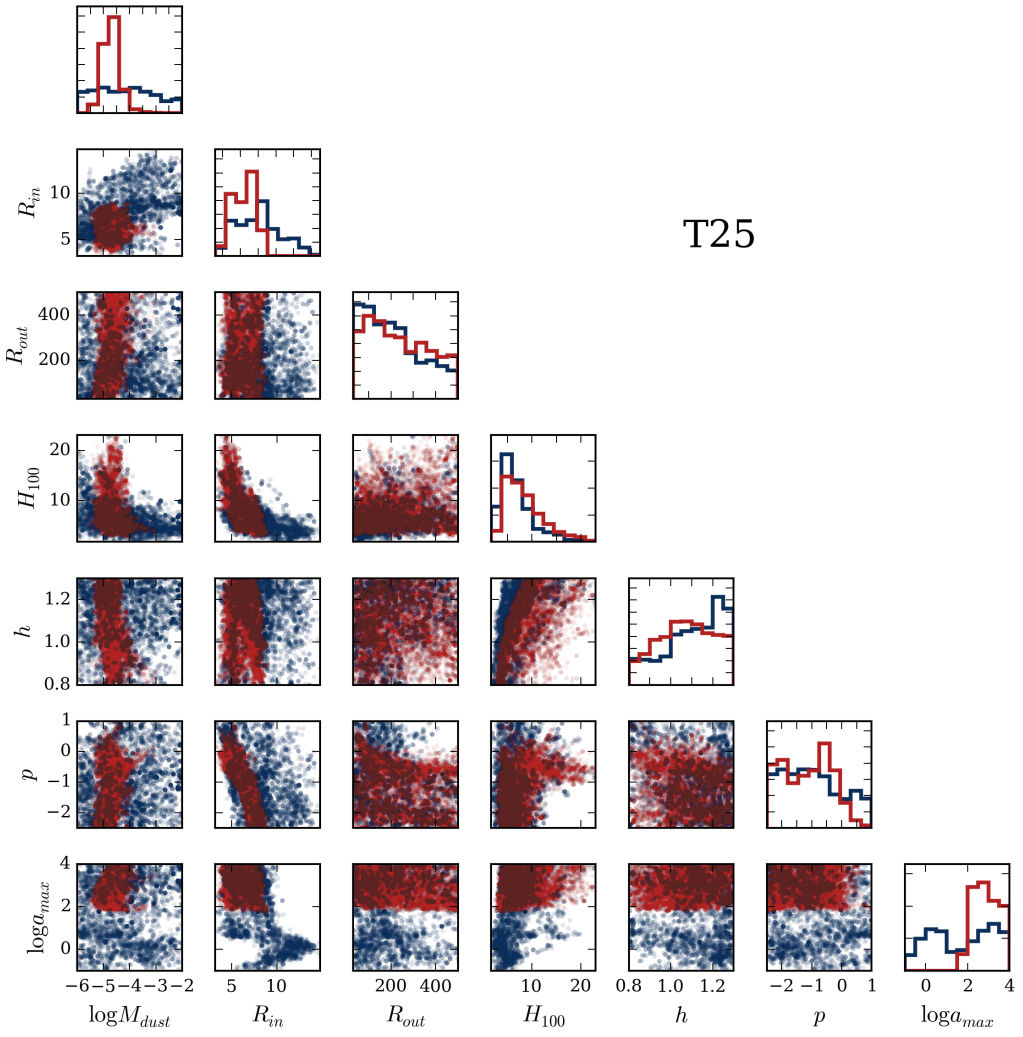

FIGURE 5.7: Cornerplot for T25. Scheme and colors as in Fig. 5.5.

important ones to constrain the mass. As such, SPIRE photometry will play a key role in future statistical studies of disk masses, and whenever a disk mass is needed for our analysis we shall concentrate our efforts on objects detected at these wavelengths.

The inner radii of the disks are also significantly better constrained with *Herschel* data, decreasing previous uncertainties by a factor of two. This improvement likely arises from PACS data, which probes the material in the mid-plane of the inner disk. It should be mentioned that using unbinned IRS spectra could also provide even better estimates for these values.Nevertheless, it is clear that at least some information about this structure is contained in *Herschel* data.

To test the validity of our results, we compare the obtained values with previous estimates in the literature. There are three main studies which can be used for this purpose, Kim et al. (2009), Espaillat et al. (2011), and Rodgers-Lee et al. (2014). Kim et al. (2009) presented detailed modeling of the IRS spectra of transitional disks in Chamaeleon I with

an analytic model including emission from the optically thin disk and wall, plus emission from the outer disk treated as a blackbody. In Espaillat et al. (2011), the authors used a more complex irradiated disk model (D'Alessio et al. 2006) including shadowing of the outer disk by the inner disk (Espaillat et al. 2010) to analyze variability in the IRS spectra of several transitional disks. Finally, Rodgers-Lee et al. (2014) performed a multiwavelength study of Chamaeleon I including *Herschel* data from Winston et al. (2012), and analyzed transitional disks in the region with a physical disk model (Beckwith et al. 1990).

– Regarding disk masses, values from two different methods are available for all the targets: via mm data (Kim et al. 2009; Rodgers-Lee et al. 2014) and via the accretion-to-viscosity ratio (Espaillat et al. 2011) following D'Alessio et al. (1998). Our results are generally in very good agreement with all these previous values, and match within a factor of two for all cases except for the mass value of CS Cha in Espaillat et al. (2011), and T25 from Kim et al. (2009). In the former case, a value of $0.3\,M_{\odot}$ is quoted, more than one order of magnitude larger than our estimated median value ($0.015\,M_{\odot}$) but within the 95 % confidence interval range. Therefore, the two results are consistent within uncertainties. Additionally, the value in Espaillat et al. (2011) depends on the disk viscosity, which is usually largely uncertain and could account for this difference. In the case of T25, Kim et al. (2009) estimate a $0.007\,M_{\odot}$ disk mass via 1.3 mm fluxes from Henning et al. (1993), but used a characteristic disk temperature of 50 K. Our study yields a disk mass for T25 of $0.002\,M_{\odot}$, with their value lying just at the border of the corresponding confidence interval. As discussed in Rodgers-Lee et al. (2014), the 50 K value assumed in Kim et al. (2009) may be unrealistically high, explaining the discrepancy. Interestingly, Rodgers-Lee et al. (2014) found that *Herschel* data within the 160-500 μm range can be used to estimate disk masses within a factor of 3 without the need of detailed modeling. Our results do not support this statement: despite the complete agreement of their mass values with our own, the obtained posterior distributions show mass uncertainties of 1 order of magnitude, even when using full SEDs and detailed disk modeling. This different result possibly arises when considering the additional uncertainties produced by several other parameters such as the disk structure and composition, an effect that MCMC calculations include naturally.

– Disk inner radii estimates are available both in Kim et al. (2009) and Espaillat et al. (2011). Our results using MIR data only are in general good agreement with their values, with the discrepancy of CS Cha. These two works estimated its inner disk radii to be 41 and 38 AU, respectively, while we obtain 19^{+16}_{-7} AUs with similar data (i.e., excluding *Herschel*). Their results fall outside the 95 % confidence intervals derived in this study. Two different effects can explain this apparent discrepancy. First, there is no uncertainty estimation in the quoted studies: if we assume their

results to have similar uncertainties to ours, the resulting distributions would overlap significantly and yield consistent values. Additionally, these two works included more complex dust compositions, which can modify the grain emissivity and therefore change the location of the inner radius. We also note that Kim et al. (2009) estimated a 29 AU gap for T25, although the improved measurement of 18 AU in Espaillat et al. (2011) is completely consistent with ours.

The mass ranges of these transitional disks are similar to those of Class II disks in other star-forming regions (e.g., Ophiuchus, Taurus, Andrews et al. 2010, 2013), a result already found by Andrews et al. (2011) for 12 transitional disks observed with sub-mm interferometry. This is somehow intriguing: if transitional disks are an evolved stage of protoplanetary disks, then we would expect them to have significantly lower masses. In fact, other works found transitional disks to have masses even higher than those of Class II sources (Najita et al. 2007, 2015). If that is the case, transitional disks (at least classical ones, those with large holes in their dust distribution) could be the evolution of high-mass disks which have formed multiple giant planets (explaining their gaps, Zhu et al. 2011), and not a general evolutionary stage for all protoplanetary disks. Finally, SZ Cha and CS Cha have disk mass estimates of the same order of magnitude ($0.04\,M_{\odot}$ and $0.015\,M_{\odot}$, respectively), whereas T25 has a lower value ($0.002\,M_{\odot}$). An interesting exercise is to compare these values with that of the Minimum Mass Solar Nebula (MMSN), the minimum mass required to form the Solar System. A typical value of this quantity is $\sim 0.02\,M_{\odot}$ (Davis 2005; Desch 2007). Both SZ Cha and CS Cha are above or close to this value, meaning that despite being in a transitional stage, they still have enough mass to form a significant number of planets (although this does not guarantee that planet formation will take place in the future). The derived gap sizes are larger than the typical location of disk snowlines (the distance from the star at which molecules in gaseous state can form ice around dust particles, making it easier to grow large bodies), and therefore could already harbor planets in them. Our data are not enough to identify the origin of these observed trends, but they can host clues to better understand planet formation and deserve further attention.

5.5.3 Anomalous outer disks

Our results show a general trend for flaring indexes (h) close to ~ 1, slightly smaller than those usually found in protoplanetary disks ($\sim$ 1.1-1.3, e.g., Chiang & Goldreich 1997; Olofsson et al. 2013). Additionally, *Herschel* data suggest strongly negative surface density profiles, with no peak at -1, as typically assumed and found in protoplanetary disks (e.g., Andrews et al. 2009). Surprisingly, the obtained values are closer to that of the estimated for the MMSN (Desch 2007). These two facts point in the same direction: these targets have a significant amount of excess in the MIR range up to 70-100 μm (already hinted in Cieza et al. 2011; Ribas et al. 2013), but their 250-500 μm fluxes are

lower than those of typical Class II disks. This is obvious when comparing the obtained SEDs with the median SED of the Chamaeleon I and II regions (see Chapter 4 and Fig. 4.4): the considered sources have bluer FIR slopes than full disks. The two formerly mentioned results (steep surface density indexes and flaring indexes values close to one) have the effect of reducing the flux at longer wavelengths (SPIRE), and increasing it for shorter wavelengths (20-150 μm, IRS, MIPS, and PACS). Low flaring indexes could arise if significant dust settling towards the mid-plane has already occurred in these disks, which translates into a smaller disk surface exposed to the stellar radiation specially in the outer regions of the disk. On the other hand, smaller (more negative) surface densities imply that more mass is distributed close to the star, leaving a fainter outer disk which will emit poorly in the FIR regime. Combined, these results suggest that the modeled transitional disks have anomalous outer disks compared to Class II objects. The same fact is found for the T Cha transitional disk using *Herschel* data (Cieza et al. 2011) and in the Lupus region (Bustamante et al. 2015), reinforcing this idea. With the available data, however, we cannot identify the true origin of this trend: transitional disks may either have steeper surface density profiles, decreased flaring as a result of dust settling, or a combination of these two results.

We note that this interpretation is based on weak evidences, and should be considered with caution. First, the posterior functions of these parameters are broad and do not discard typical values, but simply make them less probable. Therefore, the indication of this phenomenon does not arise from individual sources, but from the fact that all sources show this same marginal behavior. Also, we have not used a tapered-disk profile (e.g., Lynden-Bell & Pringle 1974; Hartmann et al. 1998): this modified surface density profile includes less material in the outer regions of the disk, and may partially explain the steep SED slope. However, several Class II sources have been usually been modeled with this profile finding canonical values, and therefore this is unlikely to completely solve the discrepancy. On the other hand, the exposed wall of the disk can be significantly heated, resulting in puffed-up structures (e.g., Dullemond et al. 2001). If this is the case, these structures can cast shadows in the disk behind, altering their SED. Given that MCFOST does not perform hydrodynamic calculations, this effect is not included in our modeling and its influence is left for future studies. In turn, these inferences of the disk structure from SEDs including *Herschel* data are promising since they hint at interesting physical differences between transitional and protoplanetary disks, but the results are yet inconclusive. Further evidence for flattened disks can be gained by combining accretion and [OI] measurements. Keane et al. (2014) studied *Herschel* [OI] data for 26 transitional disks, finding that either they have smaller gas-to-dust ratios compared to Class II disks, or smaller flaring indexes. If accretion is ongoing in these systems, it would imply that a significant amount of gas is still present in these disks, favoring the explanation of flatter disks. We will perform this study in the future to better understand the origin of the apparently anomalous outer regions in transitional

disks. ALMA observations of these targets can reveal their real gas content and probe their structure, shedding light on this open issue.

5.6 Conclusions

In this work, we have used *Herschel* photometry of transitional disks in the Chamaeleon I star-forming region to perform detailed MCMC modeling of their SEDs and study the impact of *Herschel* data in the obtained results. We find that *Herschel* photometry, specially from the SPIRE instrument, can be used to constrain the dust mass in disks within one order of magnitude, as shown by the obtained posterior distributions. *Herschel* data can also help narrowing down the location of the inner radius of the disk. Our results are in good agreement with previous studies.

For the subset of objects for which modeling is already available (SZ Cha, CS Cha, T25), we find disk masses comparable to those of Class II sources in other star-forming regions. Because transitional disks are likely to represent a more evolved stage of disk evolution, the fact that they do not have significantly lower masses could suggest that the typical transitional disk class (i.e., disks with large gaps in their dust distributions) are the evolutionary outcome of massive Class II sources, with enough mass to form several giant planets which may have cleaned their inner regions. Additionally, we find evidence for bluer FIR slopes in transitional disks than those of Class II sources, hinting that they may have undergone some dust settling or have stepper surface density profiles than protoplanetary disks. However, this result is tentative and requires further analysis. A larger sample of transitional disks, combined with [OI] and accretion measurements as well as resolved images of these targets could help solving this issue and shed light on the origin of transitional disks and their real connection with planets.

5.7 Appendix: on the discrepancies in photometry of *Herschel* maps

As formerly mentioned, Rodgers-Lee et al. (2014) found the fluxes of the six transitional disks studied in Ribas et al. (2013) to be $\sim 20\,\%$ higher than those in Winston et al. (2012). In that latter study, photometry was obtained using the *getsources* algorithm (Men'shchikov et al. 2012). This software is specially designed to deal with source extraction in highly structured background or crowded fields. In contrast, in Ribas et al. (2013) we used a simpler approach by performing aperture photometry. Here, we extend the discussion on the adopted methodology to extract *Herschel* fluxes and on the possible origin of the observed discrepancies.

5.7.1 PACS photometry

We used aperture photometry to obtain photometry in the PACS maps. Although this procedure is unreliable with strong, structured background emission, it should produce reliable results for isolated sources. There is almost no background emission at the PACS wavelengths in the case of the Chamaeleon I region (see thumbnails in Fig. 4.1), and all the transitional disks in the sample display clean isolated PSFs. Therefore aperture photometry should be suitable for these objects.

The Chamaeleon I maps were obtained with medium or fast scan speeds, and are a combination scan and cross-scan observations. The PSF resulting from this process is elongated in the two scan directions, and displays a cross-like shape. To properly estimate optimal aperture radii, we build growth curves of our targets by performing aperture photometry with increasing radii. We then applied the corresponding aperture corrections (Balog et al. 2014)[1]. The resulting curves for SZ Cha are shown in Fig. 5.8. After this process, we decided to use aperture radii to 15″, 15″, 22″, for PACS 70, 100, and 160 bands, respectively, as we found aperture photometry to stabilize at these values. The background was estimated in an annulus with inner and outer radii of 25″and 35″. We note that the aperture corrections used were computed for optimum PSF observations, and hence may underestimate in a few percent the true correction values for distorted PSFs as in this case. More precise corrections could be achieved by re-processing calibration observations in a similar manner to the Chamaeleon I maps and deriving empirical aperture corrections, but this requires a significant amount of work and is beyond the scope of this paper. Because the emission of transitional disks peaks at PACS wavelengths, their SEDs are mainly flat in this wavelength regime and we prefer not to apply color corrections, which in any case are only of a few percent. To account for uncertainties in the aperture and color corrections, calibration and background estimation, we assigned a 20 % uncertainty to the measured PACS values.

5.7.2 SPIRE photometry

SPIRE maps are significantly more complex than PACS observations, due to the conspicuous background emission arising from the molecular cloud (see Fig. 4.1). In this case, we prefer to use the *destriper* algorithm within HIPE, combined with timeline fitting, which is currently the recommended procedure for SPIRE point source photometry (Pearson et al. 2014). This procedure fits sources in the timeline directly, and does not suffer from uncertainties in the map projection process. It also does not require any aperture correction. SPIRE bands trace the Rayleight-Jeans part of the disk emission, and we applied the color correction factors corresponding to blackbody emission (0.945,

[1]A full description of PACS PSFs can be found at
http://herschel.esac.esa.int/twiki/pub/Public/PacsCalibrationWeb/bolopsf_20.pdf

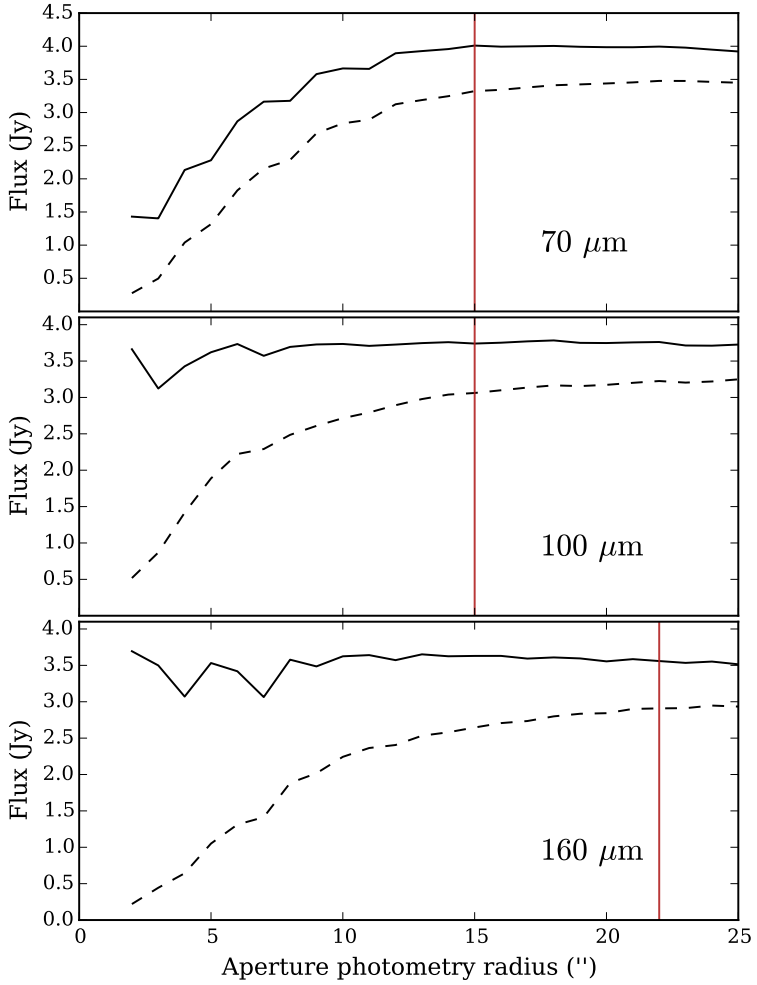

FIGURE 5.8: Growth curves for SZ Cha obtained with aperture photometry at the three PACS bands. Raw curves are shown as black dashed lines, aperture corrected curves as solid black lines. We decided to use aperture radii of 15″, 15″, and 22″for the 3 bands, respectively (vertical red solid lines).

0.948, 0.943 for SPIRE 250, 350, and 500 bands, respectively, as quoted in the SPIRE Handbook Version 2.5). We chose the standard values for the timeline fit, and note here that different background parameters may yield different results depending on the real background emission. However, this issue is beyond the scope of this paper and we do not investigate it in more detail. Nevertheless, the obtained fluxes show a very good match with PACS photometric values. Given the mentioned dependency with the background estimate, we use a conservative 20 % uncertainty at SPIRE bands.

5.7.3 Possible origin of the flux discrepancies between Winston et al. (2012) and Ribas et al. (2013)

We find that our results are 15-25,% higher than those in Winston et al. (2012), but in general agreement with those in Ribas et al. (2013) despite the different map-making algorithm used in this latter case (*jscanam*, instead of *Scanamorphos* used in Ribas

et al. 2013). That is also found for SPIRE values, which were obtained using also a different procedure (timeline fitting in this work versus previous aperture photometry). The systematic higher fluxes in Ribas et al. (2013) with respect to Winston et al. (2012), suggest that the different map-making algorithms and photometry methods may be the key to explain this differences. Given the overall good agreement of the results of this paper with those in Ribas et al. (2013), we prefer to maintain them instead of using the values in Winston et al. (2012).

Part III

Discussion and conclusions

6

General discussion

Although the works in this thesis have been discussed individually already, here we provide a more general view of our findings and their connection with the current state of the field.

6.1 Disk evolution

Previous works have already found a characteristic disk lifetime of ∼3 Myr (Haisch et al. 2001b; Hernández et al. 2007b, 2008; Mamajek 2009, see also Chapter 1 and the discussion in Chapters 2 and 3) by analyzing disk fractions as probed by near-infrared (NIR) and/or mid-infrared (MIR) excesses in associations with different ages. These results have a great value for constraining the planet formation phase (especially for giant planets), but in many cases their samples came from heterogeneous catalogs which could suffer from different biases. The work presented in Chapter 2 and revisited in Chapter 3 mitigated these effects by using a large, homogeneous database and taking into account all possible biases. The extremely reduced contamination of this sample, its size, and the homogeneous treatment of all the objects is new to the literature, confirms these previous findings, and provides the most recent and complete study of disk evolution so far (Ribas et al. 2014).

We also find hints of NIR excesses disappearing slightly faster than MIR ones (with characteristic dissipation times of 2.7±0.7 against 3.3±0.6 or 4.4±0.5 depending on the wavelength, as updated in Table. 3.5 and in Ribas et al. 2015). We speculate that this is an indication that the disk dispersal mechanism acts from inside out: by removing the hot dust in the inner regions first, the NIR fluxes will decrease earlier/faster than MIR ones. When placed in the current paradigm of disk evolution, these results are consistent

with photoevaporation being the main mechanism driving disk dispersal, which up to date is the preferred explanation for this process (Alexander et al. 2014). Although with a different sample, a similar result was also found in Koepferl et al. (2013) by studying color-color diagrams of young stellar objects (YSOs). In the case of this effect being a real signature of disk evolution, it also contains information about the timescales of this process: the difference in the lifetime of NIR and MIR excess is of the order of 0.5-2 Myr, suggesting that once disk clearing has started, the process is relatively fast compared to disk lifetimes. Additional confirmation of this idea comes from the $\sim 10\,\%$ incidence of evolved disks found at all ages, which combined with their ~ 10 Myr overall lifetime suggests a 1 Myr timescale for disk dispersal.

The large size of the compiled database ($\sim$2 300 objects versus typical samples of a few hundred sources) allowed us to obtain the most statistically robust evidence so far of different disk evolution timescales around T Tauri ($M < 2\,M_{\odot}$) and Herbig Ae/Be stars (more massive objects). Previous studies had already found hints of a faster disk dispersal around high-mass stars, both in individual regions (e.g., IC348, Upper Sco, Lada et al. 2006; Carpenter et al. 2006, respectively) and in larger studies (Kennedy & Kenyon 2009). However, in most of these works the evidence for this trend was not statistically conclusive: for individual regions, the number of YSOs is significantly smaller than the size of the database presented in this thesis, and analyzing different stellar mass regimes requires that the initial sample is split in two or more groups. As a result, the statistical uncertainties increase importantly, specially in the high-mass regime given the shape of the initial mass function (IMF). On the other hand, the more complete analysis by Kennedy & Kenyon (2009) compiled data for nine star-forming regions and used both IR excesses and accretion signatures to look for this effect. By combining all these regions, they identified a different evolution of disks around solar and intermediate-mass stars, and a less clear dependence between low-mass and solar-mass stars. The results of our research (Chapter 3 and Ribas et al. 2015) are totally consistent with their findings. Combined, these two works build an important evidence for such a dependence, which should be carefully considered in planet formation models.

One of the most interesting implications of this latter trend may be its possible relation with the paucity of hot Jupiters found around massive stars ($M > 1.5\,M_{\odot}$, see Fig. 3.6). As discussed in Chapter 3, if disks disappear earlier around high-mass stars, the mechanism causing the migration of giant planets may stop acting earlier in these sources and therefore the number of hot Jupiters could be smaller than in low-mass systems. It should be noted that other mechanisms could also explain this trend: it is possible that a population of these hot Jupiters exists around massive stars, but are engulfed during the post-main sequence phase of the star due to strong tidal interactions (Villaver & Livio 2009; Villaver et al. 2014). Even more, the mentioned scarcity of hot Jupiters may simply an observational effect produced by the shorter lifetimes of high-mass stars (i.e., only a few planets around massive stellar hosts are known). Other works have suggested

that this trend is real (e.g., Johnson et al. 2007). It is clear that more data and further investigation is required to better understand the underlying origin of this effect, which could be tightly connected with the properties of the parental protoplanetary disks.

Additional to the statistical study of the global properties of disks, we also performed detailed analysis of the most promising class of disk in the context of planet formation: transitional disks. In the course of our research on the large sample of disks, we had the opportunity to analyze *Herschel* data of transitional disks in Chamaeleon I star-forming region.

6.2 Transitional disks in Chamaeleon with *Herschel*

Herschel has been used in many works to study YSOs in several star-forming regions, and a large number of detailed programs focused on disks around stars (e.g., GASPS, DIGIT). Most of them have taken advantage of the *Herschel* spectroscopic capabilities, although some works have also used photometry to study the outer regions of protoplanetary disks. The far-infrared (FIR) wavelengths of *Herschel* probe the emission from cold material in the outer regions and deeper layers of these disks.

The usage of color-color diagrams or slope measurements to identify and classify different targets is not new to the literature (e.g., Lada 1987; Harvey et al. 2006, to cite a few). In Ribas et al. (2013), we demonstrate how *Herschel* data, in particular PACS 70 μm fluxes, can be used to effectively separate Class II sources and transitional disks with significant changes in their SED slopes. This method has already been successfully applied in the Lupus region (Bustamante et al. 2015), and even identified a new transitional disk candidate in Ophiuchus (Rebollido et al. submitted, see Appendix A.4). The large areas of the sky observed with *Herschel* host a great potential for discoveries of new transitional sources in young regions.

One of the intriguing results of this thesis is related to *Herschel*/PACS fluxes of transitional disks in Chamaeleon I: when compared to SEDs of Class II sources in the region, we found the six detected transitional disks to have higher 70 μm excesses than the 75% percentile of full disks. This feature is also present in other transitional sources, such as GM Tau, UX Tau or T Cha (see for example Fig. 9 in Williams & Cieza 2011; Cieza et al. 2011), and we obtained the same result in Bustamante et al. (2015, see also Appendix A.4) for a sample of transitional disks in Lupus. When studying the transitional disk around T Cha, Cieza et al. (2011) also found a steep SED slope in the *Herschel* regime, as some of the targets in our study (e.g., CS Cha, T25).

Via Bayesian modeling of three transitional disks (SZ Cha, CS Cha, and T25), we found that *Herschel* data, in particular SPIRE observations, can be used to constrain the disk mass within one order of magnitude. The obtained values are in good agreement

with previous estimates and also with the masses of Class II sources in other regions (e.g., Taurus, Ophiuchus, Andrews et al. 2009, 2013). As explained in Chapter 5, this is not completely in line with expectations: transitional disks are supposedly a more evolved stage of protoplanetary disks, and most of the proposed mechanisms to explain their existence require some mass loss in the disk, either by accretion onto the star or by confining the mass in planetesimals and planets. Therefore, one would expect their masses to be significantly lower when compared with Class II objects. This trend gets even more confusing when we consider other works which found transitional disks to have masses even four times larger than Class II disks (e.g. Najita et al. 2007, 2015). Within our modeled sources, SZ Cha and CS Cha have masses close to or higher than that of the minimum mass solar nebula (MMSN), meaning that the amount of mass in them is still enough to form a full Solar System analog. If the observed disk masses are a fraction of that of their primordial disks, then their initial amount of mass must have been even higher. All these evidences suggest that typical transitional disks (i.e., disks with large holes) are the evolutionary path of initially massive disk which could have formed multiple giant planets, responsible for the observed gaps (e.g., Zhu et al. 2011). It should be kept in mind, however, that both protoplanetary and transitional disks display large scatters in their mass distribution, and that detection biases are also at play. Despite not being able to conclude anything on this matter with the present data, this is an extremely interesting topic and should be further investigated.

Our modeling efforts also provided indications that the outer regions of transitional disks may be different from those of Class II sources. Their bluer FIR slope with respect to protoplanetary disks in the region are better fitted with small flaring indexes and steep surface density profiles. Physically, these scenarios mean that transitional disks have most of their mass piled-up at intermediate regions, or they have undergone some dust settling towards their mid-plane, or maybe both. As formerly mentioned, Cieza et al. (2011) found a similar result for the T Cha transitional disk, proposing two interpretations for this case: either its disk is very narrow (ring-shaped), or it has an extremely steep surface density profile. ALMA observations of this target (Huélamo et al. 2015) detected CO(3-2), ^{13}CO(3-2), and CS(7-6) gas molecules, revealed its surface density exponent to lay between -1 and -3, and that most of its mass lays within 50 AU, strongly supporting the scenarios found by our SED modeling. Also of interest for this trend is the comparison of 26 transitional disks with 33 protoplanetary sources using PACS [OI] 63.18 μm spectroscopic measurement, which revealed that transitional sources have [OI] line fluxes ~ 2 times fainter than full disks (Keane et al. 2014). Further modeling of this sample suggested that transitional disks have either lower gas-to-dust ratios or are flatter than protoplanetary objects. We realize that, although with large individual uncertainties, our Bayesian modeling found flaring index values close to 1, smaller than the typical value of 1.1-1.3 for protoplanetary disks (Chiang & Goldreich 1997). Although our results do not allow to go deeper into this matter and it could be explained by other scenarios, Bayesian comparative analyses of large samples of

transitional and protoplanetary disks, combined with ALMA observations probing the disk structures and gas contents, will help revealing the origin of this possible hint of disk evolution.

The presented modeling shows the real value of combining *Herschel* data with Markov Chain Monte Carlo (MCMC) techniques for this type of studies. To show its impact, we can compare it with the typical approach of computing a complete model grid per target. Assuming that we distributed 10 different values for each of the seven free parameters within the proposed prior distributions (which would still yield significantly lower resolutions than those obtained with MCMC methods in many cases), that would mean computing 10^7 MCFOST models per source (since stellar parameters are mostly different for each target, a whole grid is required per target). Our chains require approximately 10^5 models for each source, effectively reducing the total computation time by at least factor of 100. Assuming a typical duration of an MCFOST run of ~ 10 minutes, such a difference becomes a crucial issue. For example, considering the size of the full sample of disks (~ 2000 targets), we could model all these objects with MCMC procedures by the time required to create full grids for only ~ 20 objects. Moreover, certain configurations that are naturally excluded by the MCMC method (such as very massive, narrow disks) would still be required in model grids. Such configurations can take much longer for MCFOST to compute (up to some hours), dramatically increasing the total computational time. Finally, if we were to include additional free parameters (e.g., fitting the inner disk of pre-transitional targets, the minimum grain size, or more complex structures such as spiral arms), the required number of models for a grid would increase exponentially (usually called "curse of dimensionality"), whereas MCMC methods do not suffer from this issue (although it is important to ensure that we are not overfitting the data). With such a decrease in computing time and the significant improvement in the disks mass estimate from *Herschel* data, it now becomes possible to perform statistical studies of this crucial parameter using the compiled sample of YSOs and the currently available data in the *Herschel* Science Archive.

6.3 The big picture and open questions

One of the main objectives of the study of protoplanetary disks is to connect stellar formation with the planetary systems at the end of the whole process, and it is reasonable to expect that the properties of disks may play a major role in the outcome of planet formation. Therefore, in principle one could do some predictions on what the resulting planets could be based on the disk characteristics, and also infer some information of the progenitor disk by analyzing a planetary system.

To explore this possibility, we first review the two mechanisms proposed to explain planet formation: core accretion (CA) and disk instability (DI). They may well be

responsible for (at least some of) the observed trends in the exoplanet populations, and are required to draw connections between disks and planets. A more in-depth analysis of these processes can be found in Helled et al. (2014).

- CA starts by dust growth and aggregation, which end up forming ∼km-sized bodies called *planetesimals*. These planetesimals collide oligarchically, forming a core of mass $\sim M_{\oplus}$ surrounded by a low-mass gas envelope. By the time the core is massive enough, it accretes gas from its surroundings, increasing the mass of its envelope. If the accretion is interrupted in between these two stages, the outcome of this process would be a rocky planet, maybe hosting an atmosphere (i.e., covering from Mercury-like to super-Earth planets). If accretion continues, once the total mass in the protoplanet reaches a crossover point, runaway gas accretion starts, rapidly increasing the mass of the envelope and forming a giant planet. CA can take up to 10^8 yr if it occurs in-situ, much longer than the disk lifetime. However, when planet migration is invoked, the planet accretes material from a more extended area of the disk and the process becomes up to 100 times faster, matching within the $\lesssim 10$ Myr lifetimes of disks. Migration also allows the planet to incorporate more solid material, enhancing its metallicity. Estimates of the best location for CA planet formation is between 5-10 AU: beyond the snowline (where gas can freeze around dust grains, dramatically increasing dust growth) , but sufficiently close for the disk density to be high enough to form planetesimals (although as mentioned, the planet may migrate after forming).

- DI is caused by gravitational instabilities: if the disk's self-gravity is strong enough, it produces a collapse of part of the disk, leading to a very fast ($\sim 10^4$ yr) formation of a gas giant planet or a brown dwarf. For this to occur, the disk has to be significantly massive with respect to the star to meet Toomre's instability criterion (Toomre 1964), but the resulting clumps (with masses between 1-10 M_J) also need to be able to cool efficiently (e.g., Rice et al. 2004). These two conditions are easier satisfied in the outer regions of young massive disks during the embedded phase ($\sim 10^5$yr), when a significant amount of mass is still infalling from the surrounding envelope. The observed trends of exoplanets suggest that DI is not the dominant planet forming mechanism, but it could explain peculiar systems with one or several giant planets with large orbits found via direct imaging (e.g., HR 8799, Marois et al. 2008).

Once the planet is formed, migration caused by planet-disk interactions can substantially change the planet location. Initially, the planet interchanges angular momentum with the surrounding disk but is not massive enough to open a gap in it (Type-I migration). As the mass of the planet increases to $\sim 0.1 - 0.2\, M_J$, so does its gravitational influence, and a gap develops in the density distribution of the disk. When this occurs, the planet gets tidally locked to the gap. If the disk is massive enough, material will keep on

entering the gap and the planet will move inwards (Type-II migration), otherwise it will stay at its current location, preventing the replenishment of the inner disk: it is accreted onto the star and a cavity opens in the disk. Both migration mechanisms act on timescales of $\sim 10^5$ yr. For intermediate mass planets, a particular case of Type-II runaway migration (called Type-III) could also occur, pushing the planet inwards on timescales of 10^4 yr. All these processes could significantly alter the architecture of the planetary system (via scattering events). Recent reviews on planetary migration can be found in Lubow & Ida (2010) and Baruteau et al. (2014).

Regarding disks, their mass is a crucial parameter in planet formation. Apart from the disk lifetime dependence with stellar mass (Kennedy & Kenyon 2009; Ribas et al. 2015, see also Chapter 3), the disk mass is known to scale with that of their host star roughly linearly, following a power-law $M_{disk} \propto M_*^{1-1.5}$ (Andrews et al. 2013). In relative terms, the typical disk-to-star mass ratio is ∼0.2-0.6 %. Also, as described in Chapter 5, there are indications that several transitional disks are at least as massive as Class II objects (Najita et al. 2007; Andrews et al. 2009, 2013; Najita et al. 2015). If that is the case, transitional disks may be the evolutionary path of the most massive disks only.

With all these pieces of information, we can try to create some speculative connections between protoplanetary disks and some of the observed statistical properties of exoplanets (see the review by Howard 2013, for a detailed description of observed properties of exoplanets).

- At least 50 % of stars have one or more planets with periods $P < 100$ days (Howard 2013), corresponding to ~ 0.5 AU orbits for solar-mass stars. The total fraction of stars with planets may be even higher if we consider the difficulties in detecting planets at larger distances. In turn, this shows that planet formation is a very efficient mechanism: at least 50 % of protoplanetary disks meet the conditions to form planets at some point of their lives.

- In contrast, only ∼10 % of FG-type stars harbor one or multiple giant planets (0.3-10 M_J) with periods within 2-2000 days (i.e. 0.03-3 AU) (Udry et al. 2003; Marcy et al. 2005). Statistical extrapolations suggest that 17-20 % stars host giant planets with semi-major axis (a) smaller than 20 AU. Combined with the previous point, at least 30 % of planetary systems host no gas giant. In these cases, it is unlikely that the lack of giant planets is caused by a combination of migration and planet engulfment by the star: the migration of a giant planet into its host star would probably destabilize the whole planetary system via planet-planet interactions (e.g., scattering, unstable orbits). If we combine this premise with the assumption that all transitional disks with large holes are produced by the clearing effect of giant planets (something far from being confirmed yet), then we find that a non-negligible 30 % of protoplanetary disks (those which form telluric planets only) would not undergo a transitional disk phase. This is also in line

with our previous discussion regarding the possible differences in the evolution of protoplanetary disks: massive disks could easily form massive planets and develop large cavities, whereas less massive disks may never enter such a phase and evolve via other mechanisms.

– Regarding hot Jupiters, only 1 % of Solar-type stars harbor one (Wright et al. 2012), and they are even rarer around more massive ($> 1.5 M_{\odot}$) stars (Johnson et al. 2011). These fractions tell us that significant planet migration is either very efficient or extremely uncommon: combined with the previous point, we find that only 5-10 % of giant planets turn into hot Jupiters. Maybe planet migration acts so quickly that most migrating giant planets end up their lives falling into their host star, or simply most of them do not migrate for long distances. The available data so far do not allow us to discriminate between these two scenarios.

– Disks with large masses (hence, around massive stars) can form giant planets easier than lower-mass disks. However, they also evolve faster, leaving less time for this process to take place. Therefore, a competition exists between these two factors if we consider planet formation to occur by CA. Nevertheless, very massive disks could also undergo DI, which requires timescales of $\sim 10^4$ Myr well below the disk lifetimes derived in Ribas et al. (2015) for disks around massive stars. If DI occurs in these cases, a significant population of massive planets and brown dwarfs could be found orbiting massive stars at large distances. More direct imaging surveys may reveal this trend in the future.

– 23 % of the stars identified by *Kepler* as planet host candidates are found to be multiple systems (Burke et al. 2013). As discussed in Sect. 1.3 and Chapter 3, multiplicity can account for the early dispersal of disks in several cases. Even in very young regions (1 Myr), the fraction of protoplanetary disks is not 100 % (Kraus et al. 2012; Ribas et al. 2014), possibly due to this effect. The non-zero fraction of planets in multiple systems implies that, in several cases and despite possible unstable disk configurations in multiple systems, protoplanetary disks around binary stars (such as CS Cha) are capable of forming planets too.

– Finally, stars with high metallicities have higher probabilities of hosting a giant planet at $a < 5$ AU (Santos et al. 2004; Fischer & Valenti 2005), as expected if the dominant planet formation mechanism is core accretion. Smaller planets show no apparent trend with metallicity.

These are just some of the hints that are found with the data available so far. Several of them (maybe all) will be solved in the coming years thanks to new telescopes and instruments (e.g., ALMA, Sphere and GPI, Espresso, JWST), which will reveal all these processes in more detail. But regardless of the arriving of new generation observing facilities, evidence so far suggests that planet formation and the final architecture of

planetary systems are strongly dependent on a large number of factors, from the disk properties to different migration processes. In many cases, there are large dispersions observed in these factors, and their evolution may be disconnected in time by stochastic processes (e.g., the memory of the initial disk properties could be lost after giant planet migration), making it difficult to connect all the pieces of the puzzle. In turn, this could mean that a general and unambiguous connection of all these phenomena, i.e., forecasting planetary systems based on our understanding of protoplanetary disks, may simply not be feasible. Instead, it may require individual studies of the systems at each key evolutionary stage to make correct, meaningful predictions.

Despite these limitations, we note that a possible direct connection between disks and planets has been found in this thesis, i.e., the lack of hot Jupiters around massive stars may be caused by the faster evolution of their disks. This achievement was only possible thanks to the large sample of YSOs used in this study, and reveals that at least in some cases, planetary systems may still maintain information about their primordial disk. It could be that such a connection is only feasible for massive stars, for which evolutionary timescales are short and only a few mechanisms have enough time to come into play. Or maybe a deeper understanding of these processes can be reached by combining large samples with more detailed modeling to reveal more subtle differences in disk masses, inner radii and structures. Complemented with *Herschel* data and spatially resolved information, the sample and methodologies presented here will be used to effectively model a large number of protoplanetary and transitional disks, which could ultimately lead to the finding of additional trends and help building connections between the properties of disks and the population of planets in our Galaxy.

7

Conclusions and future work

7.1 Conclusions

In this section, we summarize the main results and conclusions achieved during the course this thesis.

7.1.1 Disk evolution

– We built a large database of YSOs in nearby (< 500 pc), young (< 100 Myr) star-forming regions and associations, comprising more than 2 300 sources selected from different stellar population studies. All objects in the sample have a spectroscopic estimation of their spectral type, which dramatically reduces the contamination by background red giant stars and extragalactic sources. We then cross-matched the dataset with several photometric catalogs from near-ultraviolet to MIR wavelengths, including up to 35 photometric filters. We estimated extinction values in parallel with visual inspection of the SEDs, discarding problematic measurements (e.g., affected by saturation or contamination by close sources). Stellar luminosities were computed by integrating the corresponding stellar spectra. By using evolutionary tracks and region ages, we also estimated stellar masses for each object in the sample. The resulting database is a very powerful tool that can be exploited for several purposes, and will be made available for the scientific community in the future.

– We performed a carefully study of disk evolution using the compiled sample and paid special attention to different biases, minimizing their effect in our study. We then derived disk fractions as a function of age and wavelength. We found characteristic disk lifetimes of 2.5-4 Myr depending on the IR wavelength used, in complete agreement with previous studies. We estimated a roughly constant value of ~ 10 % of disks with signatures of evolution (transitional and debris disks) at all ages. We also found tentative evidences of protoplanetary disk dissipation occurring from inside out, and of this process being fast ($\sim$0.5-1 Myr) compared to total disk lifetimes ($\sim$10 Myr). These results were presented in Ribas et al. (2014), and improved in Ribas et al. (2015).

– We obtained statistically robust evidence of a dependence of disk evolution with stellar mass. We found that 65 % T Tauri stars ($M < 2\,M_{\odot}$) host protoplanetary disks at ages 1-3 Myr, and this value decreases to 10-20 % for older sources (3-11 Myr). In contrast, only 40 % of Herbig Ae/Be stars have protoplanetary disks between 1-3 Myr, while its number decreases to 0 between 3 and 11 Myr. Combined with previous studies, these results suggest that protoplanetary disks evolve similarly regardless of the mass of their stellar host during the first Myr of their lives, and a significant deviation occurs for low/high-mass stars at older ages (Ribas et al. 2015).

– We found a roughly constant fraction of evolved disks at all ages (1-11 Myr) both for T Tauri (5-15 %) and Herbig Ae/Be (20-30 %) star. The higher fraction of evolved disks around massive stars could be produced by complex dependencies between the disk region probed at a certain wavelength and the stellar mass, and should be considered with caution (Ribas et al. 2015).

– The dependence of disk evolution with stellar mass can play an important role in planetary system architectures. The shorter lifetime of disks around massive stars reduces the available time to form planets, which may be specially relevant for gas giants. Also, the fast disappearance of the disk around massive stars removes the main mechanism causing planet migration. Interestingly, there is an observed scarcity of hot Jupiters around stars with masses $M > 1.5\,M_{\odot}$. Although it is too early to claim any connection of this trend with dependence of the disk lifetime with stellar mass, it may account for at least part of the hot Jupiter desert around high-mass stars (Ribas et al. 2015)

7.1.2 Transitional disks with *Herschel*

– We have explored the population of YSOs in the Chamaeleon I and II regions using *Herschel* data. We obtained photometry of known YSOs and analyzed formerly known transitional disk in these clouds. We showed that 70 μm fluxes combined

with MIR data are a powerful tool to separate transitional targets with clear gaps in their SEDs from Class II disks, specially in the absence of data at wavelengths longer than 10 μm (e.g., from the IRS and MIPS instruments). This procedure has already been applied to the Lupus star-forming region (Bustamante et al. 2015), and identified a new transitional disk candidate in Ophiuchus (Rebollido et a., submitted).

– When compared with the obtained SEDs for Class II objects in the region, all transitional disks have 70 μm excesses above the third quartile. This feature may be the result of mass confinement at intermediate radii in transitional disks, and suggests that their outer disks contribute less to their SED than those of Class II objects (Ribas et al. 2013). These results are also consistent with previous studies, but further data are required to completely understand this finding.

– We used MCMC methods to perform Bayesian modeling of three transitional disks in Chamaeleon I and study the impact of *Herschel* data in parameter estimation. This methodology reduces the computing time required for disk modeling by at least a factor of 100 when compared with usual fitting procedures, and has a great potential for future studies of large samples. The MCMC analysis shows that both the estimates of mass of dust in the disk and the location of the inner radius are significantly improved when including *Herschel* data up to 500 μm.

– We found transitional disk masses to be comparable to those of typical Class II sources, a result which could imply that the progenitor disks of transitional objects are the massive Class II disks, and not all protoplanetary disks evolve into disks with large holes.

– Our modeling results also showed tentative indications of the outer regions of transitional disks being different from those of typical protoplanetary disks, either by being flatter or having steeper surface density profiles. Nevertheless, the obtained posterior distribution functions are broad and spatially resolved observations are required to confirm this possible trend.

7.2 Future work

The compiled database of YSOs is an unique tool for statistical research of protoplanetary disks, providing a firm ground to better comprehend stellar and planetary formation and how different factors may affect these processes. There is a large number of additional studies that could be performed using this database, such as analyzing the influence of strong external radiation fields or disk evolution in loose/compact environments. Complementing this database with IRS spectra will also allow to statistically study dust composition and processing in disks, which can also be connected with the chemical composition of planets.

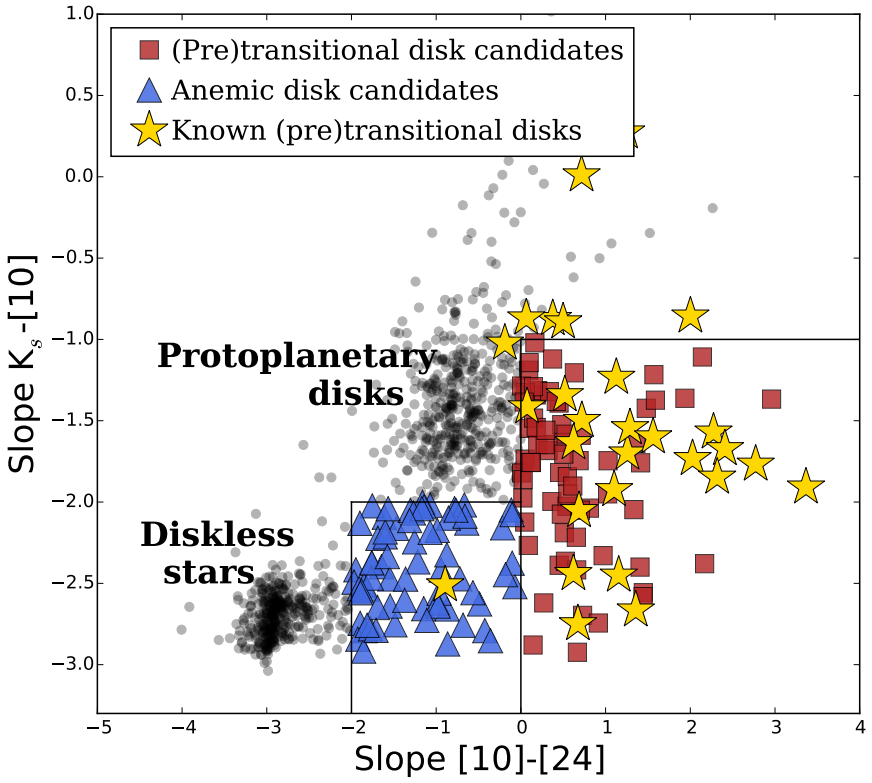

FIGURE 7.1: Slope-slope diagram of the compiled sample of YSOs in this thesis. The two selected slopes aim at separating objects based on their NIR and MIR SEDs. Most sources concentrate around two locations in this diagram: diskless stars and full disks. Red squares and blue triangles show the location of transitional and anemic disks, respectively, based on their typical slope values. Additionally, we have included several formerly known transitional disks (yellow stars) from the samples in Espaillat et al. (2014) and Manara et al. (2014).

A particularly interesting usage of this database would be a statistical study of the properties of transitional disks. By means of a simple slope-slope diagram, we can separate different targets in our sample and identify known and/or unknown transitional disks in it (see Fig. 7.1). By combining our dataset with those in Espaillat et al. (2014) and Manara et al. (2014), we find $\sim$100 transitional disks, and other $\sim$50 anemic disks. We are compiling IRS spectra for all these targets, and working on Bayesian analysis of these sources using a physical disk model. With the available data and proposed approach, we expect to identify possible relations between the location of the inner radius and stellar host properties. This research will also allow to study the distribution of gap sizes, compare it with the semi-major axis of known planets, and test it against predictions from different disk clearing models.

Our Bayesian modeling of transitional disks with *Herschel* has also revealed that, in the presence of SPIRE data, it is possible to derive disk masses within one order of magnitude. *Herschel* has probed large portions of the sky, and a significant number of objects in the sample are included in those areas. Complementing our database with these data and MCMC methods will not only cover the FIR regime of the corresponding

SEDs, but also yield disk mass estimates for hundreds of targets, allowing to statistically study disk masses for an unprecedented number of objects.

Finally, the most promising pathway to exploit this sample is, without any doubt, future ALMA follow-up observations. Several transitional targets shown in Fig. 7.1 may be new to the literature, and ALMA has the exciting potential to resolve gaps and holes in them, confirming their transitional nature. Its data would also complement the obtained SEDs by probing their gas content, dust radial distribution and settling, or azimuthal asymmetries possibly related with the presence of planetary embryos and newborn planets. A large, unbiased sample of protoplanetary disks observed by ALMA will reveal disk evolution and planet formation in never-before-seen detail.

A

Other studies

Apart from the main research topics of this thesis, during my PhD I was able to join and participate in other related studies. In the following sections I provide a summary of some of these works closely connected to the subject of this thesis, and my personal contributions to these studies.

A.1 YSOs in the Chamaeleon II molecular cloud as probed by *Herschel*

The *Herschel* Gould Belt Survey in Chamaeleon II: Properties of cold dust in disks around young stellar objects

L. Spezzi, N.L.J. Cox, T. Prusti, B. Merín, Á. Ribas, C. Alves de Oliveira, E. Winston, Á. Kóspál, P. Royer, R. Vavrek, Ph. André, G.L. Pilbratt, L. Testi, E. Bressert, L. Ricci, A. Men'shchikov, V. Könyves

Published in A&A. Received 11 March 2013; Accepted 17 May 2013

In this work, we analyzed the population of YSOs in the the Chamaeleon II star-forming region using *Herschel* observations of the Gould Belt Survey (André et al. 2010). Chamaeleon II is a young (2-4 Myr Spezzi et al. 2008) low-mass star-forming region located in the Chamaeleon-Musca complex at $\sim$180 pc (Whittet et al. 1997), with a population of 63 YSOs (e.g., Schwartz 1977; Gauvin & Strom 1992; Barrado y Navascués & Jayawardhana 2004; Alcalá et al. 2008; Spezzi et al. 2008).

After processing the data and performing photometry on them using the *getsources* algorithm (Men'shchikov et al. 2012), we detected 29 sources from the known sample of YSOs in Chamaeleon II. The obtained data were used to explore different color-color diagrams with *Herschel*, and propose a locus with these data which can be used to effectively identify and separate YSOs from extragalactic sources (see Fig.A.1). After this process, we complemented *Herschel* photometry with fluxes from other studies and catalogs, producing complete SEDs from 0.5 to 500/1300 μm. Combined with stellar parameters from Alcalá et al. (2008); Spezzi et al. (2008), we then created a grid of models with the RADMC code (Dullemond & Dominik 2004b) and compared the compiled SEDs with it. Our results show that the inner disk radii and masses are comparable to previous estimates in Alcalá et al. (2008), while the characteristic radius of the surface density profile is 50 % larger than those derived in this study, probably due to better SED sampling when including *Herschel* data. The inclination angle is poorly constrained in all cases, as expected for SED modeling alone (e.g., D'Alessio et al. 1999; Alcalá et al. 2008).

I contributed to this work by processing and producing the *Herschel* maps used to derive the photometry of the sample of YSOs.

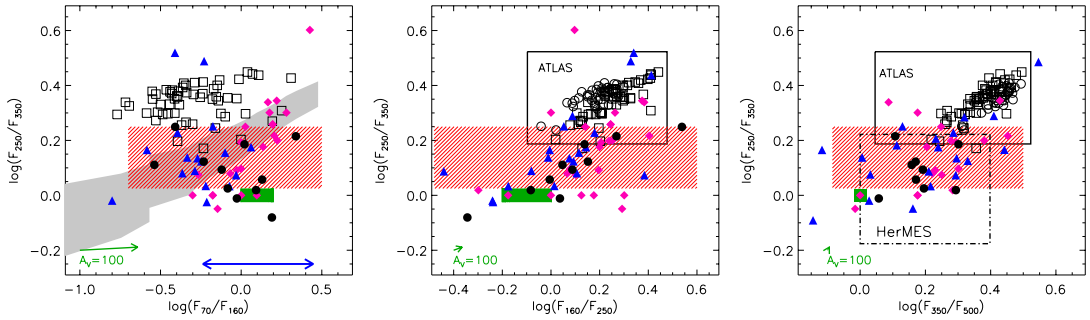

FIGURE A.1: PACS/SPIRE color-color diagrams for the YSOs in the study. Colors are defined as the logarithm of the ratio between *Herschel* fluxes at different wavelengths. Black filled circles show detected YSOs in Chamaeleon II (this study), magenta diamonds for Chamaeleon I sources (Winston et al. 2012), blue triangles for objects in Serpens (Bressert, private communication). Open squares and circles represent extragalactic sources (Corbelli et al. 2012; Dale et al. 2012). Dashed red regions are the proposed locus for YSOs. The green areas correspond to photospheric colors, and the green arrow is the reddening vector for A_V=100. The large, black squares (solid and dashed) are the predicted loci of galaxies and quasars in the *Herschel*-ATLAS and *Herschel*-HerMES surveys, respectively. In the left panel, the blue arrow is the color range of low mass stars in Harvey et al. (2012), and the gray area is the protostar locus predicted in Ali et al. (2010). Figure from Spezzi et al. (2008).

A.2 The filamentary structure of the Chamaeleon dark clouds

Herschel's view of the large-scale structure in the Chamaeleon dark clouds

C. Alves de Oliveira, N. Schneider, B. Merín, T. Prusti, Á. Ribas, N. L. J. Cox, R. Vavrek, V. Könyves, D. Arzoumanian, E. Puga, G. L. Pilbratt, Á. Kóspál, Ph. André, P. Didelon, A. Men'shchikov, P. Royer, C. Waelkens, S. Bontemps, E. Winston, L. Spezzi

Published in A&A. Received 24 January, 2014; Accepted 23 April, 2014

In this paper, we study the characteristics of the filamentary structure of the Chamaeleon complex. This region comprises the Chamaeleon I, II, and III molecular clouds (together with the Musca region, Cox et al. in prep), which show very different scenarios: Chamaeleon I ($\sim$2 Myr) is an active star-forming region with a population of more than 200 YSOs (e.g., Luhman et al. 2008a; Winston et al. 2012), a smaller population of YSOs ($\sim$60, Alcalá et al. 2008; Spezzi et al. 2008) is found Chamaeleon II ($\sim$4 Myr), whereas no YSO has been identified in Chamaeleon III. We used *Herschel* data of the Gould Belt Survey (André et al. 2010) to analyze the dust emission arising from the filaments in these regions, aiming at understanding the origin of the diverse conditions in these clouds.

The *Herschel* observations were used to derive temperature maps by projecting them on a common grid. We then fit each individual pixel with a modified blackbody to estimate its temperature. Assuming the opacity law used in other Gould Belt related studies (e.g., Könyves et al. 2010), we also estimated column density maps of the three regions. We found Chamaeleon I to be clearly dominated by a main ridge, with surrounding faint and cold (11-13 K) striations (small, less dense filaments). Chamaeleon II shows a more fragmented behavior, and comprises several cold (11-14 K) clumps. In contrast, Chamaeleon III displays the most obvious filamentary structure, with several of these across the whole region (Fig. A.2). We also used the DisPerSe algorithm (Sousbie 2011) to trace the filamentary structure of the clouds, and computed filamentary masses per unit length and characteristic filamentary widths. Interestingly, the characteristic width of 0.110-0.125 AU is very similar to the values derived by Arzoumanian et al. (2011)

in IC 5146, which could suggest that filaments may have a natural width (related to hydrostatic equilibrium and thermal turbulence conditions) not very sensitive to the external environment. Additional studies of other star-forming regions are required to confirm this last result.

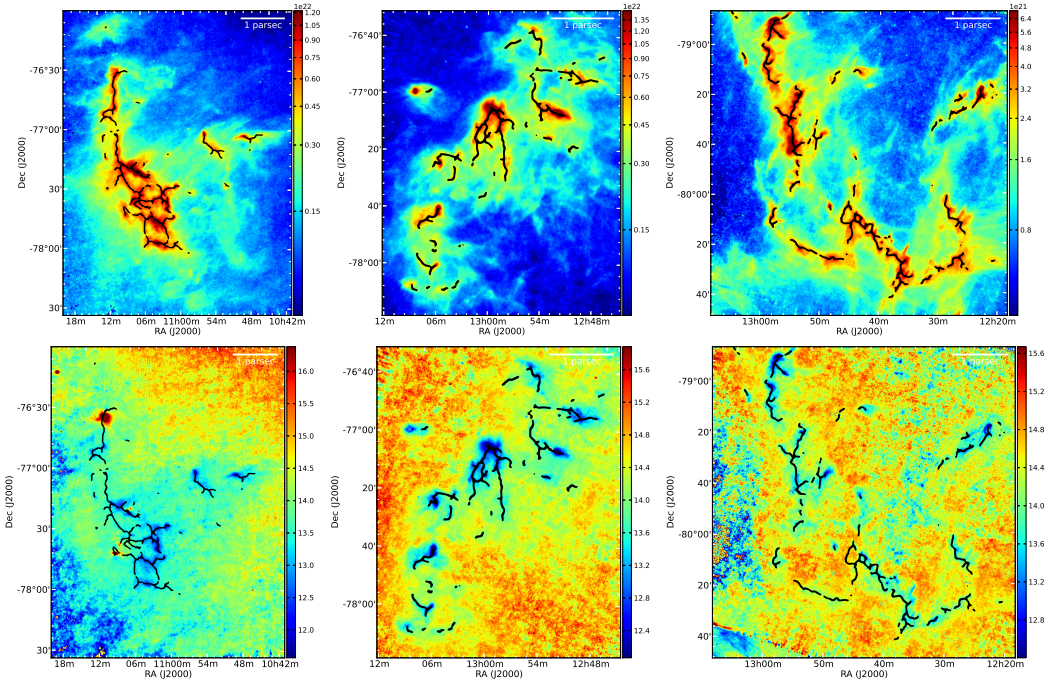

FIGURE A.2: Column density ($N_{H_2}(cm^{-2})$) *(top)* and temperature (K) *(bottom)* maps of Chamaeleon I, II, and III *(from left to right)*. The black lines trace the filaments detected by the DisPerSe algorithm (Sousbie 2011). Figure from Alves de Oliveira et al. (2014)

We also applied different statistical procedures (e.g., probability distribution functions of pixels, Δ-variance methods) to the computed column density maps to quantitatively estimate the physical conditions of the clouds. Our results suggest that Chamaeleon I is reaching the end of its star formation, Chamaeleon II is actively forming star, and Chamaeleon III has not started this process yet. If these three clouds are part of a whole complex (as suggested by ^{12}CO observations, Mizuno et al. 2001), the origin of such differences is extremely intriguing: the possible influence of the nearby Sco-Cen OB associations via stellar winds, or different magnetic fields strengths could affect the global dynamics of the clouds and account for the observed contrast in the star-forming history of these regions.

My main contribution to this work, as in the previous case, was the processing of *Herschel* observations of these three clouds.

A.3 Warm debris disks with *Herschel*

Herschel/PACS photometry of transiting-planet host stars with candidate warm debris disks

B. Merín, D. R. Ardila, Á. Ribas, H. Bouy, G. Bryden, K. Stapelfeldt , D. Padgett

Published in A&A. Received 31 October 2013; Accepted 2 August 2014

Debris disks are the remnant of planet formation, and are cold (50 K) gas poor disks made out of planetesimals and dust particles orbiting their host star at hundreds of AUs, analogously to our Kuiper belt (see Wyatt 2008, for a review). They are common around main sequence stars (16-20 % FGK stars have debris disks, as shown by *Spitzer* and *Herschel*, e.g., Trilling et al. 2008; Eiroa et al. 2013), and survive for Gyr-long periods (much longer than gas rich protoplanetary disks). These objects show FIR excess, but no disk emission in the NIR of MIR regimes: the latter requires dust particles to exist at a few AU from their host stars, but grains at such distances have very short dynamic timescales and neither terrestial planet formation nor debris disk evolutionary models are capable of maintaining such excesses (e.g., Kenyon & Bromley 2005; Wyatt et al. 2007). Their origin is therefore likely transient, and may be caused by planetesimal collisions in the systems (e.g., as in the case of η Corvi, Lisse et al. 2012; Duchêne et al. 2014). In this work, we presented follow-up observations of warm debris disk candidates (confirmed planet hosting stars or Kepler candidates, also having IR excess at 12 and/or 22 μm) identified in Ribas et al. (2012) using MIR photometry from the WISE Preliminary Catalog. Prior to these follow-up observations, Kennedy & Wyatt (2012) used the updated WISE All Sky Survey to statistically analyze these excesses, finding that they are likely caused by background IR emission.

To study the presence or absence of cold dust in these system, we obtained *Herschel* PACS 100 and 160 μm observations of 19 candidates to host MIR excesses as probed by WISE. The observations reached a 1-σ detection level of 1 mJy in the case of the 100 μm band, and 2-5 mJy for 160 μm. None of the targets was clearly detected in the *Herschel* maps, although few of them tentatively show some FIR extended emission, especially at 160 μm (see e.g. Fig. A.3). However, the projected sizes of these extended features are of the order of 10 000 AU, and therefore not arising from debris disks in these systems but likely produced by background emission/sources.

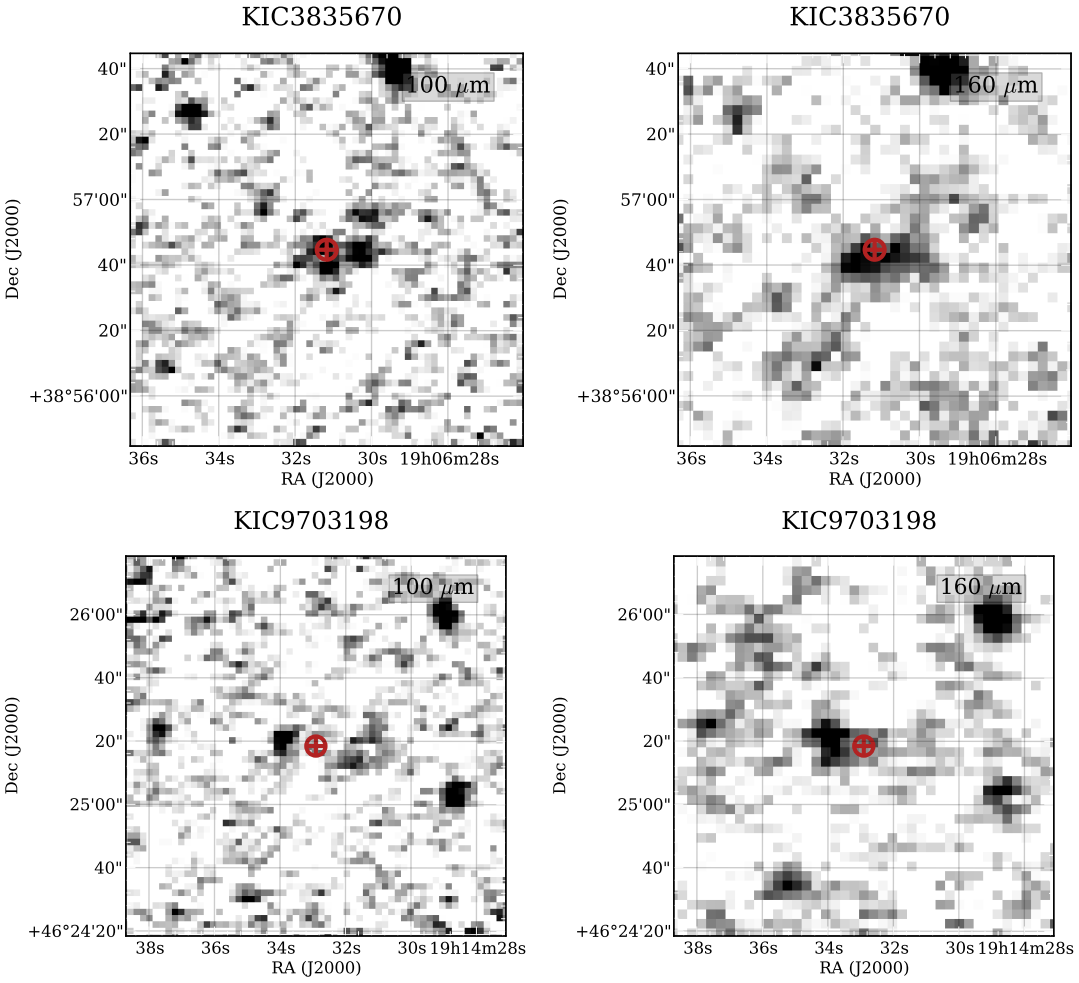

FIGURE A.3: *Herschel*/PACS observations of two targets in the considered sample: KIC3835670 (top) and KIC9703198 (bottom). The 100 μm (left) and 160 μm (right) maps are shown. The images are centered at the nominal positions of the sources, marked with a red cross. Extended emission is seen in both cases, probably arising from background FIR sources. Figure from Merín et al. (2014)

The upper limits computed from the *Herschel* maps allow us to put some constrains to the presence of debris disks in these systems. Because of the low photospheric fluxes at such long wavelengths, these upper limits can only rule out the existence of massive debris disks such as the one aroundβ Pictoris (Vandenbussche et al. 2010). In the case of the planet hosting star WASP-33, the upper limits are low enough to also reject the possibility of it harboring an η Corvi-like debris disk. Combined with the results from Kennedy & Wyatt (2012), the non-detections in the *Herschel*/PACS maps imply that at least most of the warm excesses detected in the sample come from IR background emission and are not associated to the candidates (Merín et al. 2014). MIR observations with higher spatial resolution (e.g. VISIR, Canaricam) should be therefore used to confirm or discard possible warm excesses identified with WISE data.

I contributed to this study by producing the sample of candidates, helping with the *Herschel* proposal for observations, and analyzing excesses of the resulting SEDs.

A.4 Transitional disks with *Herschel*

Identification of new transitional disk candidates in Lupus with *Herschel*

I. Bustamante, B. Merín, Á. Ribas, H. Bouy, T. Prusti, G. L. Pilbratt, Ph. André

Published in A&A. Received 24 April 2014; Accepted 15 January 2015

and

Identification of transitional disk candidates in the center of Ophiuchus with *Herschel*

Isabel Rebollido, Bruno Merín, Álvaro Ribas, Ignacio Bustamante, Hervé Bouy, Pablo Riviere-Marichalar, Timo Prusti, Göran L. Pilbratt, Philippe André, Péter Ábrahám

Submitted to A&A. Received 19 December 2014

These two works have a similar aim to that in Ribas et al. (2013), i.e., studying transitional disks in star-forming clouds using *Herschel* data. In these cases, we analyzed the Lupus and Ophiuchus regions. The Lupus complex is formed by several connected molecular clouds, and is one of the closest star-forming regions(140-200 pc, see Comerón 2008, for a complete review on this region). It has four main star-forming sites, one of them (the Lupus III cloud) being very rich in T Tauri objects. The work presented in Bustamante et al. (2015) focused in the Lupus I, III, and IV clouds. On the other hand, the Ophiuchus region (Wilking et al. 2008) is located at only $\sim$130 pc. It displays a dense core (L1688, A_V = 50-100 mag) surrounded by several filamentary structures and contains more than 300 known YSOs. The central part of this region was analyzed in Rebollido et al. (in prep, see Fig. A.4).

These two works used *Herschel* data from the Gould Belt Survey (André et al. 2010), complemented with data from Rygl et al. (2013) for Lupus, and from Alves de Oliveira et al. (2013a) for Ophiuchus. We obtained photometry of the samples presented in

Ribas et al. (2014), and produced full *Herschel* catalogs of YSOs in the regions. We then complemented them with additional data to build complete SEDs from the optical to the FIR.

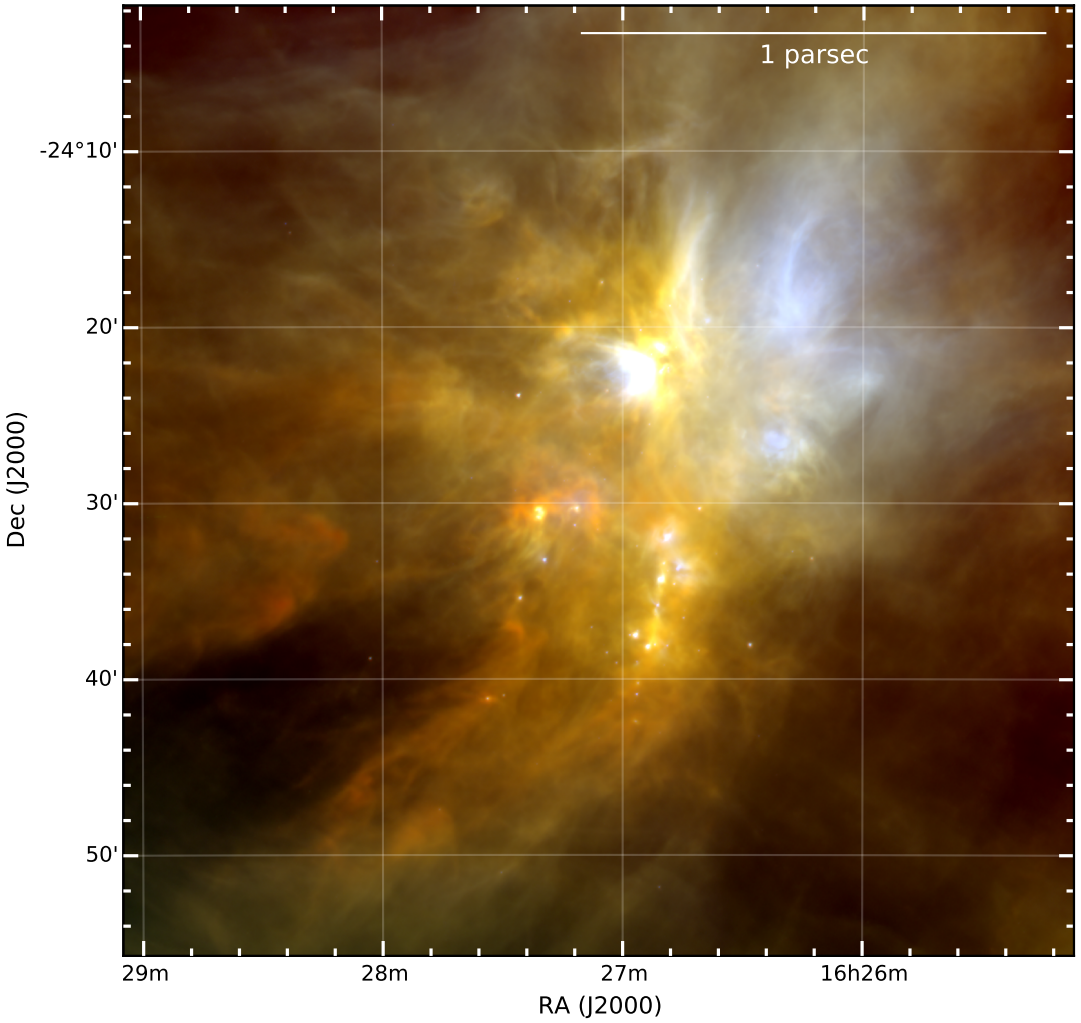

FIGURE A.4: *Herschel* three color composite image of the core of Ophiuchus (blue: PACS 70 μm, green: PACS 160 μm, red: SPIRE 250 μm). This image shows the complex structure of the cloud and its strong background emission. Figure adapted from Rebollido et al. (submitted).

We then used the slope criterion proposed in Ribas et al. (2013) to look for possible new transitional disk candidates in the sample. We successfully separate the previously known transitional disks in Lupus (Sz 91 and Sz 111). In Ophiuchus, we combined this procedure with an additional criterion based on *Spitzer* data to identify up to 18 tentative transitional disks candidates. In particular, one new target clearly meets the slope condition in Ribas et al. (2013) and shows a promising SED (see Fig. A.5), making it a very interesting new source for follow-up studies.

Because these two works follow Ribas et al. (2013) in several aspects, I was able to contribute significantly by helping the authors with the analysis of these data and

providing them with the sample and complementary photometry obtained in Ribas et al. (2014) for the samples of YSOs.

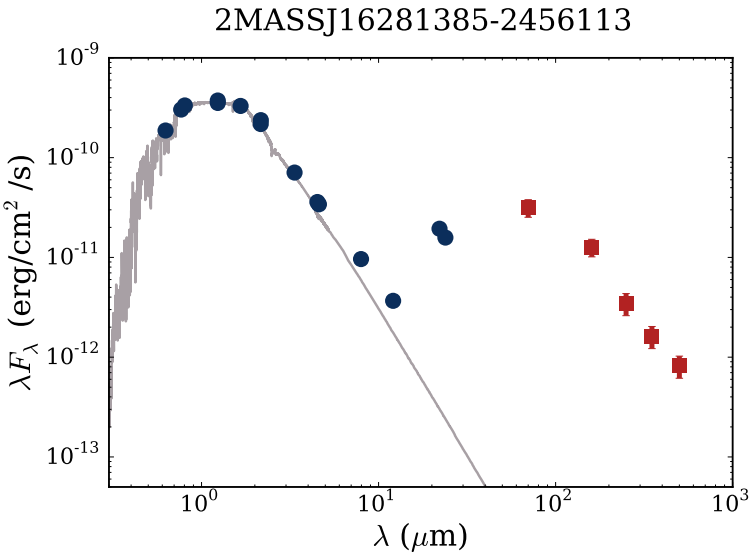

FIGURE A.5: SED of the new transitional disk candidate identified in Ophiuchus with *Herschel*. Blue dots are previous measurements from the literature, red squares show the new *Herschel* photometry. The corresponding photosphere is shown as a gray line. The significant FIR excess, together with lack of NIR excesses, make this new target a strong transitional disk candidate

A.5 Searching for massive planets and brown dwarfs with *Kepler*

Apart from the well known modulation in the radial velocities of stars, planets can have a variety of effects on their stellar hosts. In particular, close massive planets or brown dwarfs can distort the spherical shape of the star, producing a stellar elongation in the direction of the companion. As the system rotates, this will produce a change in the total stellar surface exposed to the observer, hence slightly increasing the measured stellar flux (see Fig A.6). Such variations are known as *ellipsoidal*, and have the additional interest of providing a measurement of the mass of the planet and therefore an alternative confirmation of the planetary/substellar nature of the companion (e.g. Lillo-Box et al. 2014). In this work (Lillo-Box & Ribas et al., in prep) we aim at detecting reflection-ellipsoidal-beaming variations (REBs) in the light-curves of stars observed by the *Kepler* spacecraft (Borucki et al. 2010).

By using the different estimates in the *Kepler* catalog for the systems (e.g., stellar mass and luminosity, orbital and transit parameters), we selected 914 Kepler Objects of Interest (KOIs) with values capable of producing REBs in their light-curve. We then processed the corresponding *Kepler* light-curves in an alternative way to that of the standard *Kepler* pipeline by using splines. This step is required to ensure that the REB signal is not removed by the processing. We then checked that, in the cases of known planets with ellipsoidal variations such as Kepler-13b (Mislis & Hodgkin 2012), we recover the correct shape of the light-curve.

We set a model including the following contributions:

- a transit, using the models by Mandel & Agol (2002) and the limb darkening and gravity coefficients by Claret & Bloemen (2011),
- reflection, i.e., the phase of the planet,
- the ellipsoidal variation produced by the gravitational influence of the planet on the star,
- and beaming, which accounts for the effect of the Doppler shift in the photometry. Given that the photometric *Kepler* band has a fixed wavelength, its convolution with the light from the star will change according to its Doppler shift, modifying the total flux observed.

The models are implemented as in Lillo-Box et al. (2014). We then use a modified MCMC method (using ensemble samplers with affine invariance, e.g. Goodman & Weare 2010; Foreman-Mackey et al. 2013) to model the observed data.

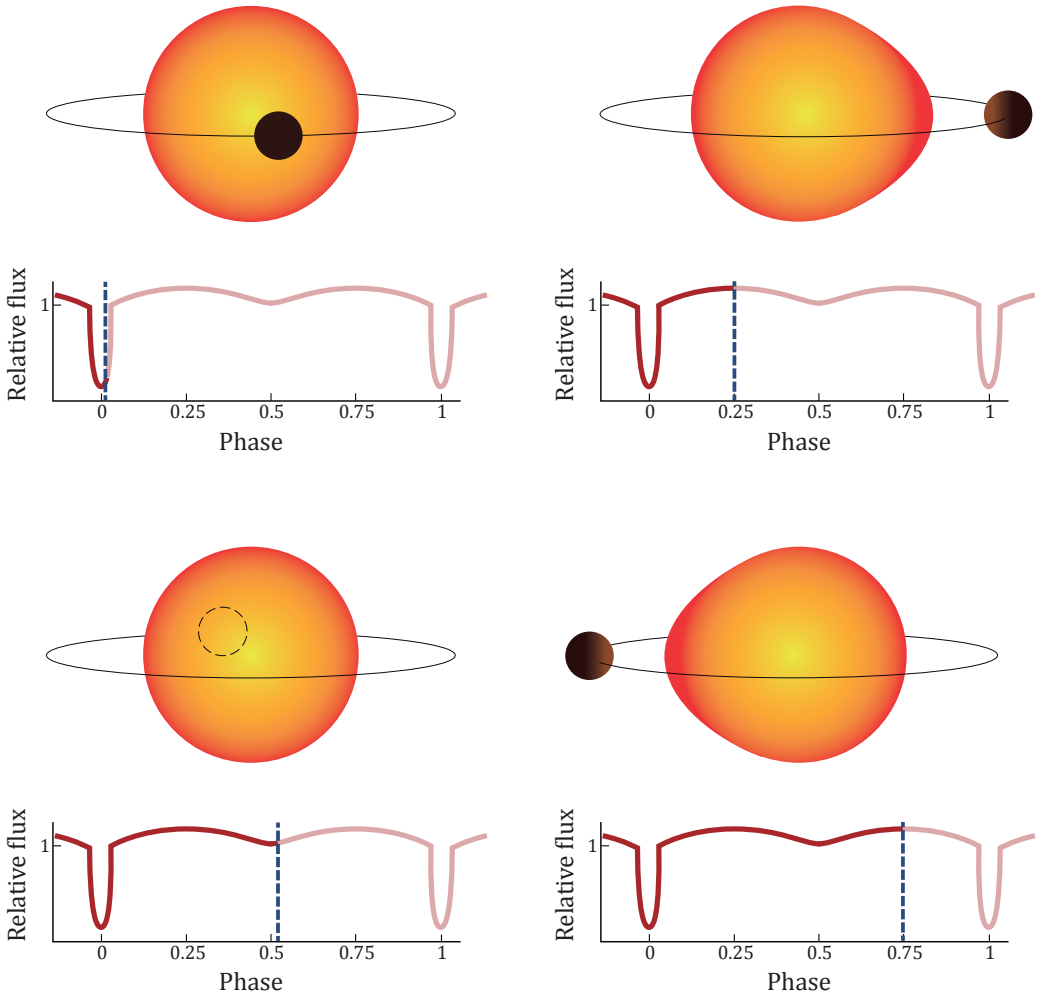

FIGURE A.6: Stellar elongation produced by a close massive companion as a function of orbital phase: during transit (top left), at phase= 0.25 (top right), secondary transit (bottom left), and phase= 0.75 (bottom right). At phases 0.25 and 0.75, the increase of visible stellar surface reaches it maximum, and so does the flux. At the same time, the phase of the planet also changes, reflecting part of the stellar radiation and increasing the total flux.

This project is still in progress, but we have already identified several targets with promising light-curves (see Fig. A.7). The estimated masses of the companions fall into the gas giant-brown dwarf regimes, which will be confirmed later with radial velocity measurements. Regardless of the debate on the similar or different origin of brown dwarfs and planets, all these companions lie very close to their stellar host ($a < 1\,\mathrm{AU}$) and hence are very likely to have undergone a formation process similar to that of planets. Additionally, some of these objects are found around massive, giant stars, which makes them extremely interesting targets: given their mass estimates, these planets are likely hot Jupiters around giant stars. As described in Chapter 3, there is an observed paucity of hot Jupiters around massive stars, and therefore these objects could help to understand whether this scarcity of hot Jupiters is an observational effect or if, instead, it could have any connection with formation and migration mechanisms (e.g., Ribas et al. 2015).

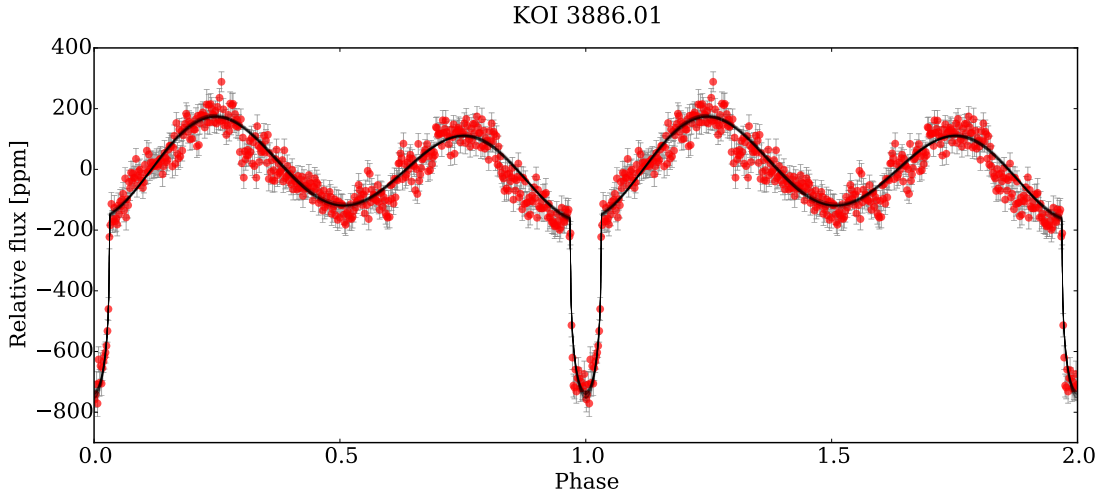

FIGURE A.7: Results of fitting the light-curve of KOI 3886.01. Red dots show the processed light-curve, binned to 500 data points. The black lines show 100 models randomly selected from the posterior distribution. Both the transit and REB effects are clearly visible.

My contributions to this work have been the retrieval and processing of the *Kepler* light-curves, and the implementation of the REB model and MCMC methods.

Bibliography

Adams, F. C., Lada, C. J., & Shu, F. H. 1987, ApJ, 312, 788

Adams, F. C., Lada, C. J., & Shu, F. H. 1988, ApJ, 326, 865

Alcalá, J. M., Spezzi, L., Chapman, N., et al. 2008, ApJ, 676, 427

Alexander, R., Pascucci, I., Andrews, S., Armitage, P., & Cieza, L. 2014, Protostars and Planets VI, 475

Alexander, R. D. & Armitage, P. J. 2009, ApJ, 704, 989

Alexander, R. D., Clarke, C. J., & Pringle, J. E. 2006a, MNRAS, 369, 216

Alexander, R. D., Clarke, C. J., & Pringle, J. E. 2006b, MNRAS, 369, 229

Ali, B., Tobin, J. J., Fischer, W. J., et al. 2010, A&A, 518, L119

Allard, F., Homeier, D., & Freytag, B. 2012, Royal Society of London Philosophical Transactions Series A, 370, 2765

Allen, P. R., Luhman, K. L., Myers, P. C., et al. 2007, ApJ, 655, 1095

ALMA Partnership, Brogan, C. L., Perez, L. M., et al. 2015, ArXiv e-prints

Alves de Oliveira, C., Ábrahám, P., Marton, G., et al. 2013a, A&A, 559, A126

Alves de Oliveira, C., Moraux, E., Bouvier, J., et al. 2010, A&A, 515, A75

Alves de Oliveira, C., Moraux, E., Bouvier, J., et al. 2013b, A&A, 549, A123

Alves de Oliveira, C., Schneider, N., Merín, B., et al. 2014, A&A, 568, A98

André, P., Men'shchikov, A., Bontemps, S., et al. 2010, A&A, 518, L102

André, P., Ward-Thompson, D., & Barsony, M. 1993, ApJ, 406, 122

Andrews, S. M., Rosenfeld, K. A., Kraus, A. L., & Wilner, D. J. 2013, ApJ, 771, 129

Andrews, S. M. & Williams, J. P. 2005, ApJ, 631, 1134

Andrews, S. M. & Williams, J. P. 2007, ApJ, 671, 1800

Andrews, S. M., Wilner, D. J., Espaillat, C., et al. 2011, ApJ, 732, 42

Andrews, S. M., Wilner, D. J., Hughes, A. M., Qi, C., & Dullemond, C. P. 2009, ApJ, 700, 1502

Andrews, S. M., Wilner, D. J., Hughes, A. M., Qi, C., & Dullemond, C. P. 2010, ApJ, 723, 1241

Apai, D., Pascucci, I., Bouwman, J., et al. 2005, Science, 310, 834

Appenzeller, I. 1977, A&A, 61, 21

Appenzeller, I., Krautter, J., & Jankovics, I. 1983, A&AS, 53, 291

Armitage, P. J. 2011, ARA&A, 49, 195

Armitage, P. J., Livio, M., Lubow, S. H., & Pringle, J. E. 2002, MNRAS, 334, 248

Arzoumanian, D., André, P., Didelon, P., et al. 2011, A&A, 529, L6

Aumann, H. H., Beichman, C. A., Gillett, F. C., et al. 1984, ApJ, 278, L23

Balog, Z., Müller, T., Nielbock, M., et al. 2014, Experimental Astronomy, 37, 129

Barrado y Navascués, D., Béjar, V. J. S., Mundt, R., et al. 2003, A&A, 404, 171

Barrado y Navascués, D. & Jayawardhana, R. 2004, ApJ, 615, 840

Barrado y Navascués, D. & Martín, E. L. 2003, AJ, 126, 2997

Barrado y Navascués, D., Stauffer, J. R., Morales-Calderón, M., et al. 2007, ApJ, 664, 481

Baruteau, C., Crida, A., Paardekooper, S.-J., et al. 2014, Protostars and Planets VI, 667

Batalha, N. M., Rowe, J. F., Bryson, S. T., et al. 2013, ApJS, 204, 24

Bayo, A., Barrado, D., Stauffer, J., et al. 2011, A&A, 536, A63

Beall, J. H. 1987, ApJ, 316, 227

Beckwith, S. V. W., Sargent, A. I., Chini, R. S., & Guesten, R. 1990, AJ, 99, 924

Bell, C. P. M., Naylor, T., Mayne, N. J., Jeffries, R. D., & Littlefair, S. P. 2013, MNRAS

Belloche, A., Schuller, F., Parise, B., et al. 2011, A&A, 527, A145

Birnstiel, T., Andrews, S. M., & Ercolano, B. 2012, A&A, 544, A79

Borucki, W. J., Koch, D., Basri, G., et al. 2010, Science, 327, 977

Bouy, H. 2011, in IAU Symposium, Vol. 270, Computational Star Formation, ed. J. Alves, B. G. Elmegreen, J. M. Girart, & V. Trimble, 41–44

Bressan, A., Marigo, P., Girardi, L., et al. 2012, MNRAS, 427, 127

Briceño, C., Luhman, K. L., Hartmann, L., Stauffer, J. R., & Kirkpatrick, J. D. 2002, ApJ, 580, 317

Brown, J. M., Blake, G. A., Dullemond, C. P., et al. 2007, ApJ, 664, L107

Brown, J. M., Blake, G. A., Qi, C., Dullemond, C. P., & Wilner, D. J. 2008, ApJ, 675, L109

Bryden, G., Chen, X., Lin, D. N. C., Nelson, R. P., & Papaloizou, J. C. B. 1999, ApJ, 514, 344

Burke, C. J., Bryson, S., Christiansen, J., et al. 2013, in American Astronomical Society Meeting Abstracts, Vol. 221, American Astronomical Society Meeting Abstracts, 216

Burkert, A. & Ida, S. 2007, ApJ, 660, 845

Burrows, C. J., Stapelfeldt, K. R., Watson, A. M., et al. 1996, ApJ, 473, 437

Bustamante, I., Merín, B., Ribas, Á., et al. 2015, A&A, 578

Caballero, J. A. 2007, A&A, 466, 917

Calvet, N., D'Alessio, P., Hartmann, L., et al. 2002, ApJ, 568, 1008

Calvet, N., D'Alessio, P., Watson, D. M., et al. 2005, ApJ, 630, L185

Calvet, N., Magris, G. C., Patino, A., & D'Alessio, P. 1992, Rev. Mexicana Astron. Astrofis., 24, 27

Carpenter, J. M., Mamajek, E. E., Hillenbrand, L. A., & Meyer, M. R. 2006, ApJ, 651, L49

Carr, J. S. 2007, in IAU Symposium, Vol. 243, IAU Symposium, ed. J. Bouvier & I. Appenzeller, 135–146

Casassus, S., van der Plas, G., M, S. P., et al. 2013, Nature, 493, 191

Chabrier, G., Johansen, A., Janson, M., & Rafikov, R. 2014, ArXiv e-prints

Chiang, E. I. & Goldreich, P. 1997, ApJ, 490, 368

Cieza, L., Padgett, D. L., Stapelfeldt, K. R., et al. 2007, ArXiv e-prints, 706

Cieza, L. A., Lacour, S., Schreiber, M. R., et al. 2013, ApJ, 762, L12

Cieza, L. A., Olofsson, J., Harvey, P. M., et al. 2011, ApJ, 741, L25

Cieza, L. A., Schreiber, M. R., Romero, G. A., et al. 2010, ApJ, 712, 925

Claret, A. & Bloemen, S. 2011, A&A, 529, A75

Clarke, C. J., Gendrin, A., & Sotomayor, M. 2001, MNRAS, 328, 485

Close, L. M., Follette, K. B., Males, J. R., et al. 2014, ApJ, 781, L30

Cohen, M. 1983, ApJ, 270, L69

Cohen, M., Emerson, J. P., & Beichman, C. A. 1989, ApJ, 339, 455

Comerón, F. 2008, The Lupus Clouds, ed. B. Reipurth, 295

Corbelli, E., Bianchi, S., Cortese, L., et al. 2012, A&A, 542, A32

Crutcher, R. M. 2012, ARA&A, 50, 29

Currie, T. 2009, ApJ, 694, L171

Currie, T. & Kenyon, S. J. 2009, AJ, 138, 703

Currie, T., Kenyon, S. J., Balog, Z., et al. 2008, ApJ, 672, 558

Currie, T., Lada, C. J., Plavchan, P., et al. 2009, ApJ, 698, 1

Dahm, S. E. & Hillenbrand, L. A. 2007, AJ, 133, 2072

Dale, D. A., Aniano, G., Engelbracht, C. W., et al. 2012, ApJ, 745, 95

D'Alessio, P., Calvet, N., & Hartmann, L. 2001, ApJ, 553, 321

D'Alessio, P., Calvet, N., Hartmann, L., Franco-Hernández, R., & Servín, H. 2006, ApJ, 638, 314

D'Alessio, P., Calvet, N., Hartmann, L., Lizano, S., & Cantó, J. 1999, ApJ, 527, 893

D'Alessio, P., Cantö, J., Calvet, N., & Lizano, S. 1998, ApJ, 500, 411

D'Alessio, P., Hartmann, L., Calvet, N., et al. 2005, ApJ, 621, 461

Damjanov, I., Jayawardhana, R., Scholz, A., et al. 2007, ApJ, 670, 1337

Davis, S. S. 2005, ApJ, 627, L153

DENIS Consortium. 2005, VizieR Online Data Catalog, 2263, 0

Dent, W. R. F., Thi, W. F., Kamp, I., et al. 2013, PASP, 125, 477

Desch, S. J. 2007, ApJ, 671, 878

Draine, B. T. 2006, ApJ, 636, 1114

Duchêne, G., Arriaga, P., Wyatt, M., et al. 2014, ApJ, 784, 148

Duchêne, G. & Kraus, A. 2013, ARA&A, 51, 269

Duchêne, G., McCabe, C., Pinte, C., et al. 2010, ApJ, 712, 112

Ducourant, C., Teixeira, R., Galli, P. A. B., et al. 2014, A&A, 563, A121

Dullemond, C. P. & Dominik, C. 2004a, A&A, 417, 159

Dullemond, C. P. & Dominik, C. 2004b, A&A, 417, 159

Dullemond, C. P. & Dominik, C. 2005, A&A, 434, 971

Dullemond, C. P., Dominik, C., & Natta, A. 2001, ApJ, 560, 957

Dullemond, C. P., Hollenbach, D., Kamp, I., & D'Alessio, P. 2007, Protostars and Planets V, 555

Dunham, M. M., Stutz, A. M., Allen, L. E., et al. 2014, Protostars and Planets VI, 195

Dutrey, A., Semenov, D., Chapillon, E., et al. 2014, Protostars and Planets VI, 317

Dzib, S., Loinard, L., Mioduszewski, A. J., et al. 2010, ApJ, 718, 610

Edwards, S., Hartigan, P., Ghandour, L., & Andrulis, C. 1994, AJ, 108, 1056

Eiroa, C., Marshall, J. P., Mora, A., et al. 2013, A&A, 555, A11

Eisner, J. A., Hillenbrand, L. A., White, R. J., Akeson, R. L., & Sargent, A. I. 2005, ApJ, 623, 952

Elsasser, H. & Staude, H. J. 1978, A&A, 70, L3

Enoch, M. L., Evans, II, N. J., Sargent, A. I., et al. 2008, ApJ, 684, 1240

Erickson, K. L., Wilking, B. A., Meyer, M. R., Robinson, J. G., & Stephenson, L. N. 2011, AJ, 142, 140

Espaillat, C., Calvet, N., D'Alessio, P., et al. 2007a, ApJ, 664, L111

Espaillat, C., Calvet, N., D'Alessio, P., et al. 2007b, ApJ, 670, L135

Espaillat, C., D'Alessio, P., Hernández, J., et al. 2010, ApJ, 717, 441

Espaillat, C., Furlan, E., D'Alessio, P., et al. 2011, ApJ, 728, 49

Espaillat, C., Ingleby, L., Hernández, J., et al. 2012, ApJ, 747, 103

Espaillat, C., Muzerolle, J., Najita, J., et al. 2014, ArXiv e-prints

Evans, II, N. J., Allen, L. E., Blake, G. A., et al. 2003, PASP, 115, 965

Evans, II, N. J., Dunham, M. M., Jørgensen, J. K., et al. 2009, ApJS, 181, 321

Fang, M., van Boekel, R., King, R. R., et al. 2012, A&A, 539, A119

Fang, M., van Boekel, R., Wang, W., et al. 2009, A&A, 504, 461

Fedele, D., van den Ancker, M. E., Henning, T., Jayawardhana, R., & Oliveira, J. M. 2010, A&A, 510, A72

Fischer, D. A. & Valenti, J. 2005, ApJ, 622, 1102

Follette, K. B., Tamura, M., Hashimoto, J., et al. 2013, ApJ, 767, 10

Foreman-Mackey, D., Hogg, D. W., Lang, D., & Goodman, J. 2013, PASP, 125, 306

Franciosini, E., Pallavicini, R., & Sanz-Forcada, J. 2006, A&A, 446, 501

Frank, A., Ray, T. P., Cabrit, S., et al. 2014, Protostars and Planets VI, 451

Furlan, E., Hartmann, L., Calvet, N., et al. 2006, ApJS, 165, 568

Furlan, E., Luhman, K. L., Espaillat, C., et al. 2011, The Astrophysical Journal Supplement Series, 195, 3

Furlan, E., Watson, D. M., McClure, M. K., et al. 2009, ApJ, 703, 1964

Garcia Lopez, R., Natta, A., Testi, L., & Habart, E. 2006, A&A, 459, 837

Gauvin, L. S. & Strom, K. M. 1992, ApJ, 385, 217

Geers, V. C., Pontoppidan, K. M., van Dishoeck, E. F., et al. 2007, A&A, 469, L35

Goodman, J. & Weare, J. 2010, Comm. App. Math. Comp. Sci., 5, 65

Greene, T. P., Wilking, B. A., Andre, P., Young, E. T., & Lada, C. J. 1994, ApJ, 434, 614

Griffin, M. J., Abergel, A., Abreu, A., et al. 2010, A&A, 518, L3

Guenther, E. W., Esposito, M., Mundt, R., et al. 2007, A&A, 467, 1147

Guilloteau, S., Dutrey, A., & Simon, M. 1999, A&A, 348, 570

Gullbring, E., Calvet, N., Muzerolle, J., & Hartmann, L. 2000, ApJ, 544, 927

Gutermuth, R. A., Megeath, S. T., Muzerolle, J., et al. 2004, ApJS, 154, 374

Gutermuth, R. A., Myers, P. C., Megeath, S. T., et al. 2008, ApJ, 674, 336

Haisch, Jr., K. E., Lada, E. A., & Lada, C. J. 2000, AJ, 120, 1396

Haisch, Jr., K. E., Lada, E. A., & Lada, C. J. 2001a, AJ, 121, 2065

Haisch, Jr., K. E., Lada, E. A., & Lada, C. J. 2001b, ApJ, 553, L153

Haisch, Jr., K. E., Lada, E. A., Piña, R. K., Telesco, C. M., & Lada, C. J. 2001c, AJ, 121, 1512

Harris, R. J., Andrews, S. M., Wilner, D. J., & Kraus, A. L. 2012, ApJ, 751, 115

Hartmann, L. 2001, AJ, 121, 1030

Hartmann, L., Calvet, N., Gullbring, E., & D'Alessio, P. 1998, ApJ, 495, 385

Hartmann, L., Hewett, R., & Calvet, N. 1994, ApJ, 426, 669

Harvey, P. M., Chapman, N., Lai, S.-P., et al. 2006, ApJ, 644, 307

Harvey, P. M., Henning, T., Liu, Y., et al. 2012, ApJ, 755, 67

Hashimoto, J., Dong, R., Kudo, T., et al. 2012, ApJ, 758, L19

Hayashi, C. 1981, Progress of Theoretical Physics Supplement, 70, 35

Hayashi, M. R., Shibata, K., & Matsumoto, R. 1996, ApJ, 468, L37

Helled, R., Bodenheimer, P., Podolak, M., et al. 2014, Protostars and Planets VI, 643

Henize, K. G. & Mendoza v, E. E. 1973, ApJ, 180, 115

Henning, T., Pfau, W., Zinnecker, H., & Prusti, T. 1993, A&A, 276, 129

Herbig, G. H. 1962, Advances in Astronomy and Astrophysics, 1, 47

Hernández, J., Calvet, N., Briceño, C., et al. 2007a, ApJ, 671, 1784

Hernández, J., Hartmann, L., Calvet, N., et al. 2008, ApJ, 686, 1195

Hernández, J., Hartmann, L., Megeath, T., et al. 2007b, ApJ, 662, 1067

Hildebrand, R. H. 1983, QJRAS, 24, 267

Hillenbrand, L. A. 2008, Physica Scripta Volume T, 130, 014024

Hirota, T., Bushimata, T., Choi, Y. K., et al. 2008, PASJ, 60, 37

Høg, E., Fabricius, C., Makarov, V. V., et al. 2000, A&A, 355, L27

Houck, J. R., Roellig, T. L., van Cleve, J., et al. 2004, ApJS, 154, 18

Howard, A. W. 2013, Science, 340, 572

Huélamo, N., Bouy, H., Pinte, C., et al. 2010, A&A, 523, A42

Huélamo, N., de Gregorio-Monsalvo, I., Macias, E., et al. 2015, A&A, 575, L5

Huélamo, N., Lacour, S., Tuthill, P., et al. 2011, A&A, 528, L7

Hughes, A. M., Andrews, S. M., Espaillat, C., et al. 2009, ApJ, 698, 131

Hughes, A. M., Wilner, D. J., Qi, C., & Hogerheijde, M. R. 2008, ApJ, 678, 1119

Ida, S. & Lin, D. N. C. 2004a, ApJ, 604, 388

Ida, S. & Lin, D. N. C. 2004b, ApJ, 616, 567

Indebetouw, R., Mathis, J. S., Babler, B. L., et al. 2005, ApJ, 619, 931

Ireland, M. J. & Kraus, A. L. 2008, ApJ, 678, L59

Isella, A., Carpenter, J. M., & Sargent, A. I. 2009, ApJ, 701, 260

Ishihara, D., Onaka, T., Kataza, H., et al. 2010, A&A, 514, A1+

Johnson, J. A., Aller, K. M., Howard, A. W., & Crepp, J. R. 2010, PASP, 122, 905

Johnson, J. A., Clanton, C., Howard, A. W., et al. 2011, ApJS, 197, 26

Johnson, J. A., Fischer, D. A., Marcy, G. W., et al. 2007, ApJ, 665, 785

Jørgensen, J. K., van Dishoeck, E. F., Visser, R., et al. 2009, A&A, 507, 861

Joy, A. H. 1945, ApJ, 102, 168

Kama, M., Min, M., & Dominik, C. 2009, A&A, 506, 1199

Keane, J. T., Pascucci, I., Espaillat, C., et al. 2014, ApJ, 787, 153

Kennedy, G. M. & Kenyon, S. J. 2009, ApJ, 695, 1210

Kennedy, G. M. & Wyatt, M. C. 2012, MNRAS, 426, 91

Kenyon, S. J. & Bromley, B. C. 2004, AJ, 127, 513

Kenyon, S. J. & Bromley, B. C. 2005, AJ, 130, 269

Kenyon, S. J. & Hartmann, L. 1987, ApJ, 323, 714

Kenyon, S. J. & Hartmann, L. 1995, ApJS, 101, 117

Kessler, M. F., Steinz, J. A., Anderegg, M. E., et al. 1996, A&A, 315, L27

Kessler-Silacci, J. E., Hillenbrand, L. A., Blake, G. A., & Meyer, M. R. 2005, ApJ, 622, 404

Kim, K. H., Watson, D. M., Manoj, P., et al. 2009, ApJ, 700, 1017

Kley, W. & Nelson, R. P. 2012, ARA&A, 50, 211

Koenigl, A. 1991, ApJ, 370, L39

Koepferl, C. M., Ercolano, B., Dale, J., et al. 2013, MNRAS, 428, 3327

Könyves, V., André, P., Men'shchikov, A., et al. 2010, A&A, 518, L106

Kozai, Y. 1962, AJ, 67, 591

Kraus, A. L. & Ireland, M. J. 2012, ApJ, 745, 5

Kraus, A. L., Ireland, M. J., Hillenbrand, L. A., & Martinache, F. 2012, ApJ, 745, 19

Kraus, A. L., Ireland, M. J., Martinache, F., & Lloyd, J. P. 2008, ApJ, 679, 762

Kraus, S., Ireland, M. J., Sitko, M. L., et al. 2013, ApJ, 768, 80

Krautter, J., Wichmann, R., Schmitt, J. H. M. M., et al. 1997, A&AS, 123, 329

Lada, C. J. 1987, in IAU Symposium, Vol. 115, Star Forming Regions, ed. M. Peimbert & J. Jugaku, 1–17

Lada, C. J. 2006, ApJ, 640, L63

Lada, C. J., Muench, A. A., Haisch, Jr., K. E., et al. 2000, AJ, 120, 3162

Lada, C. J., Muench, A. A., Luhman, K. L., et al. 2006, AJ, 131, 1574

Lada, C. J. & Wilking, B. A. 1984, ApJ, 287, 610

Lafrenière, D., Jayawardhana, R., Brandeker, A., Ahmic, M., & van Kerkwijk, M. H. 2008, ApJ, 683, 844

Lebouteiller, V., Barry, D. J., Spoon, H. W. W., et al. 2011, ApJS, 196, 8

Li, Z.-Y., Banerjee, R., Pudritz, R. E., et al. 2014, Protostars and Planets VI, 173

Li, Z.-Y., Krasnopolsky, R., & Shang, H. 2011, ApJ, 738, 180

Lillo-Box, J., Barrado, D., Moya, A., et al. 2014, A&A, 562, A109

Lin, D. N. C. & Papaloizou, J. 1986, ApJ, 307, 395

Lisse, C. M., Wyatt, M. C., Chen, C. H., et al. 2012, ApJ, 747, 93

Lloyd, J. P. 2011, ApJ, 739, L49

Lodato, G., Delgado-Donate, E., & Clarke, C. J. 2005, MNRAS, 364, L91

Lodieu, N., Dobbie, P. D., & Hambly, N. C. 2011, A&A, 527, A24

Looney, L. W., Mundy, L. G., & Welch, W. J. 2003, ApJ, 592, 255

Lubow, S. H. & D'Angelo, G. 2006, ApJ, 641, 526

Lubow, S. H. & Ida, S. 2010, Planet Migration, ed. S. Seager, 347–371

Luhman, K. L. 2004a, ApJ, 602, 816

Luhman, K. L. 2004b, ApJ, 617, 1216

Luhman, K. L. 2007, ApJS, 173, 104

Luhman, K. L. 2008, Chamaeleon, ed. B. Reipurth, 169

Luhman, K. L., Allen, L. E., Allen, P. R., et al. 2008a, ApJ, 675, 1375

Luhman, K. L., Allen, P. R., Espaillat, C., Hartmann, L., & Calvet, N. 2010, ApJS, 186, 111

Luhman, K. L., Hernández, J., Downes, J. J., Hartmann, L., & Briceño, C. 2008b, ApJ, 688, 362

Luhman, K. L. & Muench, A. A. 2008, ApJ, 684, 654

Luhman, K. L., Stauffer, J. R., Muench, A. A., et al. 2003, ApJ, 593, 1093

Lynden-Bell, D. & Pringle, J. E. 1974, MNRAS, 168, 603

Mamajek, E. E. 2009, in American Institute of Physics Conference Series, Vol. 1158, 3–10

Manara, C. F., Testi, L., Natta, A., et al. 2014, A&A, 568, A18

Mandel, K. & Agol, E. 2002, ApJ, 580, L171

Manoj, P., Kim, K. H., Furlan, E., et al. 2011, ApJS, 193, 11

Marcy, G., Butler, R. P., Fischer, D., et al. 2005, Progress of Theoretical Physics Supplement, 158, 24

Marois, C., Macintosh, B., Barman, T., et al. 2008, Science, 322, 1348

Marsh, K. A. & Mahoney, M. J. 1992, ApJ, 395, L115

Martin, D. C., Fanson, J., Schiminovich, D., et al. 2005, ApJ, 619, L1

Matrà, L., Merín, B., Alves de Oliveira, C., et al. 2012, A&A, 548, A111

Mayama, S., Hashimoto, J., Muto, T., et al. 2012, ApJ, 760, L26

McCaughrean, M. J. & O'dell, C. R. 1996, AJ, 111, 1977

Meeus, G., Waters, L. B. F. M., Bouwman, J., et al. 2001, A&A, 365, 476

Mendoza V., E. E. 1966, ApJ, 143, 1010

Mendoza V., E. E. 1968, ApJ, 151, 977

Men'shchikov, A., André, P., Didelon, P., et al. 2012, A&A, 542, A81

Merín, B., Ardila, D. R., Ribas, Á., et al. 2014, A&A, 569, A89

Merín, B., Brown, J. M., Oliveira, I., et al. 2010, ApJ, 718, 1200

Mislis, D. & Hodgkin, S. 2012, MNRAS, 422, 1512

Mizuno, A., Yamaguchi, R., Tachihara, K., et al. 2001, PASJ, 53, 1071

Mohanty, S., Greaves, J., Mortlock, D., et al. 2013, ApJ, 773, 168

Monin, J.-L., Guieu, S., Pinte, C., et al. 2010, A&A, 515, A91

Mortier, A., Oliveira, I., & van Dishoeck, E. F. 2011, MNRAS, 418, 1194

Morton, T. D. & Johnson, J. A. 2011, ApJ, 729, 138

Mundt, R. & Fried, J. W. 1983, ApJ, 274, L83

Murakami, H., Baba, H., Barthel, P., et al. 2007, PASJ, 59, 369

Murphy, S. J., Lawson, W. A., & Bessell, M. S. 2013, MNRAS, 435, 1325

Muto, T., Grady, C. A., Hashimoto, J., et al. 2012, ApJ, 748, L22

Muzerolle, J., Allen, L. E., Megeath, S. T., Hernández, J., & Gutermuth, R. A. 2010, ApJ, 708, 1107

Muzerolle, J., Calvet, N., Hartmann, L., & D'Alessio, P. 2003a, ApJ, 597, L149

Muzerolle, J., Flaherty, K., Balog, Z., et al. 2009, ApJ, 704, L15

Muzerolle, J., Hillenbrand, L., Calvet, N., Briceño, C., & Hartmann, L. 2003b, ApJ, 592, 266

Nagel, E., Espaillat, C., D'Alessio, P., & Calvet, N. 2012, ApJ, 747, 139

Najita, J. R., Andrews, S. M., & Muzerolle, J. 2015, MNRAS, 450, 3559

Najita, J. R., Strom, S. E., & Muzerolle, J. 2007, MNRAS, 378, 369

Nakagawa, Y., Sekiya, M., & Hayashi, C. 1986, Icarus, 67, 375

Naoz, S., Farr, W. M., Lithwick, Y., Rasio, F. A., & Teyssandier, J. 2011, Nature, 473, 187

Narita, N., Hirano, T., Sanchis-Ojeda, R., et al. 2010, PASJ, 62, L61

Natta, A., Testi, L., Comerón, F., et al. 2002, A&A, 393, 597

Nelson, R. P., Papaloizou, J. C. B., Masset, F., & Kley, W. 2000, MNRAS, 318, 18

Neugebauer, G., Habing, H. J., van Duinen, R., et al. 1984, ApJ, 278, L1

Neuhäuser, R., Walter, F. M., Covino, E., et al. 2000, A&AS, 146, 323

Nguyen, D. C., Brandeker, A., van Kerkwijk, M. H., & Jayawardhana, R. 2012, ApJ, 745, 119

Nisini, B., Antoniucci, S., Giannini, T., & Lorenzetti, D. 2005, A&A, 429, 543

O'dell, C. R. & Wen, Z. 1994, ApJ, 436, 194

Oliveira, I., Merín, B., Pontoppidan, K. M., et al. 2009, ApJ, 691, 672

Olofsson, J., Augereau, J., van Dishoeck, E. F., et al. 2009, A&A, 507, 327

Olofsson, J., Szűcs, L., Henning, T., et al. 2013, A&A, 560, A100

Ott, S. 2010, in Astronomical Society of the Pacific Conference Series, Vol. 434, Astronomical Data Analysis Software and Systems XIX, ed. Y. Mizumoto, K.-I. Morita, & M. Ohishi, 139

Owen, J. E., Ercolano, B., & Clarke, C. J. 2011, MNRAS, 412, 13

Padgett, D. L., Brandner, W., Stapelfeldt, K. R., et al. 1999, AJ, 117, 1490

Panić, O., Hogerheijde, M. R., Wilner, D., & Qi, C. 2008, A&A, 491, 219

Papaloizou, J. C. B., Nelson, R. P., Kley, W., Masset, F. S., & Artymowicz, P. 2007, Protostars and Planets V, 655

Pearson, C., Lim, T., North, C., et al. 2014, Experimental Astronomy, 37, 175

Pecaut, M. J., Mamajek, E. E., & Bubar, E. J. 2012, ApJ, 746, 154

Perryman, M. A. C., Lindegren, L., Kovalevsky, J., et al. 1997, A&A, 323, L49

Peterson, D. E., Caratti o Garatti, A., Bourke, T. L., et al. 2011, ApJS, 194, 43

Pilbratt, G. L., Riedinger, J. R., Passvogel, T., et al. 2010, A&A, 518, L1

Pineda, J. E., Quanz, S. P., Meru, F., et al. 2014, ApJ, 788, L34

Pinte, C., Ménard, F., Duchêne, G., & Bastien, P. 2006, A&A, 459, 797

Poglitsch, A., Waelkens, C., Geis, N., et al. 2010, A&A, 518, L2

Preibisch, T. 1997, A&A, 320, 525

Preibisch, T., Brown, A. G. A., Bridges, T., Guenther, E., & Zinnecker, H. 2002, AJ, 124, 404

Preibisch, T. & Zinnecker, H. 1999, AJ, 117, 2381

Pringle, J. E. 1981, ARA&A, 19, 137

Qi, C., Öberg, K. I., Wilner, D. J., et al. 2013, Science, 341, 630

Quanz, S. P., Amara, A., Meyer, M. R., et al. 2013, ApJ, 766, L1

Raymond, S. N., Kokubo, E., Morbidelli, A., Morishima, R., & Walsh, K. J. 2014, Protostars and Planets VI, 595

Rebull, L. M., Koenig, X. P., Padgett, D. L., et al. 2011, ApJS, 196, 4

Rebull, L. M., Padgett, D. L., McCabe, C.-E., et al. 2010, ApJS, 186, 259

Reipurth, B. 2008a, Handbook of Star Forming Regions, Volume I: The Northern Sky, ed. Reipurth, B.

Reipurth, B. 2008b, Handbook of Star Forming Regions, Volume II: The Southern Sky, ed. Reipurth, B.

Ribas, Á., Bouy, H., & Merín, B. 2015, A&A, 576, A52

Ribas, Á., Merín, B., Ardila, D. R., & Bouy, H. 2012, A&A, 541, A38

Ribas, Á., Merín, B., Bouy, H., et al. 2013, A&A, 552, A115

Ribas, Á., Merín, B., Bouy, H., & Maud, L. T. 2014, A&A, 561, A54

Rice, W. K. M., Armitage, P. J., Wood, K., & Lodato, G. 2006, MNRAS, 373, 1619

Rice, W. K. M., Lodato, G., Pringle, J. E., Armitage, P. J., & Bonnell, I. A. 2004, MNRAS, 355, 543

Rice, W. K. M., Wood, K., Armitage, P. J., Whitney, B. A., & Bjorkman, J. E. 2003, MNRAS, 342, 79

Rigliaco, E., Natta, A., Testi, L., et al. 2012, A&A, 548, A56

Robberto, M., Spina, L., Da Rio, N., et al. 2012, AJ, 144, 83

Roccatagliata, V., Bouwman, J., Henning, T., et al. 2011, ApJ, 733, 113

Rodgers-Lee, D., Scholz, A., Natta, A., & Ray, T. 2014, MNRAS, 443, 1587

Roussel, H. 2012, ArXiv e-prints

Roussel, H. 2013, PASP, 125, 1126

Rucinski, S. M. 1985, AJ, 90, 2321

Rydgren, A. E. 1980, AJ, 85, 444

Rygl, K. L. J., Benedettini, M., Schisano, E., et al. 2013, A&A, 549, L1

Sacco, G. G., Franciosini, E., Randich, S., & Pallavicini, R. 2008, A&A, 488, 167

Santos, N. C., Israelian, G., & Mayor, M. 2004, A&A, 415, 1153

Savage, R. S. & Oliver, S. 2007, The Astrophysical Journal, 661, 1339

Schaefer, G. H., Dutrey, A., Guilloteau, S., Simon, M., & White, R. J. 2009, ApJ, 701, 698

Schlaufman, K. C. & Winn, J. N. 2013, ApJ, 772, 143

Schmidt-Kaler, T. 1982, in Landolt-Bornstein, Group VI, Vol. 2, ed. K.-H. Hellwege (Berlin: Springer), 454

Schwartz, R. D. 1977, ApJS, 35, 161

Shakura, N. I. & Sunyaev, R. A. 1973, A&A, 24, 337

Shu, F., Najita, J., Ostriker, E., et al. 1994, ApJ, 429, 781

Sicilia-Aguilar, A., Hartmann, L., Calvet, N., et al. 2006, ApJ, 638, 897

Sicilia-Aguilar, A., Hartmann, L. W., Hernández, J., Briceño, C., & Calvet, N. 2005, AJ, 130, 188

Sicilia-Aguilar, A., Henning, T., & Hartmann, L. W. 2010, ApJ, 710, 597

Sicilia-Aguilar, A., Henning, T., Juhász, A., et al. 2008, ApJ, 687, 1145

Sicilia-Aguilar, A., Henning, T., Kainulainen, J., & Roccatagliata, V. 2011, ApJ, 736, 137

Siess, L., Dufour, E., & Forestini, M. 2000, A&A, 358, 593

Skrutskie, M. F., Cutri, R. M., Stiening, R., et al. 2006, The Astronomical Journal, 131, 1163

Skrutskie, M. F., Dutkevitch, D., Strom, S. E., et al. 1990, AJ, 99, 1187

Soderblom, D. R., Hillenbrand, L. A., Jeffries, R. D., Mamajek, E. E., & Naylor, T. 2013, ArXiv e-prints

Sousbie, T. 2011, MNRAS, 414, 350

Spezzi, L., Alcalá, J. M., Covino, E., et al. 2008, ApJ, 680, 1295

Spezzi, L., Cox, N. L. J., Prusti, T., et al. 2013, A&A, 555, A71

Spezzi, L., de Marchi, G., Panagia, N., Sicilia-Aguilar, A., & Ercolano, B. 2012, MNRAS, 421, 78

Stapelfeldt, K. & Moneti, A. 1999, in ESA Special Publication, Vol. 427, The Universe as Seen by ISO, ed. P. Cox & M. Kessler, 521

Stephens, I. W., Looney, L. W., Kwon, W., et al. 2013, ApJ, 769, L15

Strom, K. M., Strom, S. E., Edwards, S., Cabrit, S., & Skrutskie, M. F. 1989, AJ, 97, 1451

Takami, M., Bailey, J., & Chrysostomou, A. 2003, A&A, 397, 675

Tanaka, H., Himeno, Y., & Ida, S. 2005, ApJ, 625, 414

Taylor, M. B. 2005, in Astronomical Society of the Pacific Conference Series, Vol. 347, Astronomical Data Analysis Software and Systems XIV, ed. P. Shopbell, M. Britton, & R. Ebert, 29

Taylor, M. B. 2006, in Astronomical Society of the Pacific Conference Series, Vol. 351, Astronomical Data Analysis Software and Systems XV, ed. C. Gabriel, C. Arviset, D. Ponz, & S. Enrique, 666

Terebey, S., Shu, F. H., & Cassen, P. 1984, ApJ, 286, 529

Testi, L., Birnstiel, T., Ricci, L., et al. 2014, Protostars and Planets VI, 339

Thalmann, C., Grady, C. A., Goto, M., et al. 2010, ApJ, 718, L87

Thi, W.-F., Mathews, G., Ménard, F., et al. 2010, A&A, 518, L125

Thi, W.-F., Pinte, C., Pantin, E., et al. 2014, A&A, 561, A50

Tobin, J. J., Hartmann, L., & Loinard, L. 2010, ApJ, 722, L12

Toomre, A. 1964, ApJ, 139, 1217

Torres, C. A. O., Quast, G. R., Melo, C. H. F., & Sterzik, M. F. 2008, Young Nearby Loose Associations, ed. B. Reipurth, 757

Torres, R. M., Loinard, L., Mioduszewski, A. J., & Rodríguez, L. F. 2007, ApJ, 671, 1813

Triaud, A. H. M. J., Collier Cameron, A., Queloz, D., et al. 2010, A&A, 524, A25

Trilling, D. E., Bryden, G., Beichman, C. A., et al. 2008, ApJ, 674, 1086

Trilling, D. E., Lunine, J. I., & Benz, W. 2002, A&A, 394, 241

Troland, T. H. & Crutcher, R. M. 2008, ApJ, 680, 457

Trotta, R. 2008, Contemporary Physics, 49, 71

Udry, S., Mayor, M., & Santos, N. C. 2003, A&A, 407, 369

van Boekel, R., Min, M., Waters, L. B. F. M., et al. 2005, A&A, 437, 189

van der Marel, N., van Dishoeck, E. F., Bruderer, S., et al. 2013, Science, 340, 1199

van Dishoeck, E. F. 2014, Faraday Discuss., 168, 9

Vandenbussche, B., Sibthorpe, B., Acke, B., et al. 2010, A&A, 518, L133

Varnière, P., Blackman, E. G., Frank, A., & Quillen, A. C. 2006, ApJ, 640, 1110

Vicente, S. M. & Alves, J. 2005, A&A, 441, 195

Villaver, E. & Livio, M. 2009, ApJ, 705, L81

Villaver, E., Livio, M., Mustill, A. J., & Siess, L. 2014, ApJ, 794, 3

Vogt, N., Schmidt, T. O. B., Neuhäuser, R., et al. 2012, A&A, 546, A63

Walker, M. F. 1956, ApJS, 2, 365

Walker, M. F. 1957, ApJ, 125, 636

Walker, M. F. 1959, ApJ, 130, 57

Weidenschilling, S. J. 1977, Ap&SS, 51, 153

Werner, M. W., Roellig, T. L., Low, F. J., et al. 2004, ApJS, 154, 1

Whittet, D. C. B., Prusti, T., Franco, G. A. P., et al. 1997, A&A, 327, 1194

Wilking, B. A., Gagné, M., & Allen, L. E. 2008, Star Formation in the ρ Ophiuchi Molecular Cloud, ed. B. Reipurth, 351

Wilking, B. A., Meyer, M. R., Robinson, J. G., & Greene, T. P. 2005, AJ, 130, 1733

Williams, J. P. & Cieza, L. A. 2011, ARA&A, 49, 67

Winston, E., Cox, N. L. J., Prusti, T., et al. 2012, A&A, 545, A145

Winston, E., Megeath, S. T., Wolk, S. J., et al. 2009, AJ, 137, 4777

Wood, K., Lada, C. J., Bjorkman, J. E., et al. 2002, ApJ, 567, 1183

Wright, E. L., Eisenhardt, P. R. M., Mainzer, A. K., et al. 2010, The Astronomical Journal, 140, 1868

Wright, J. T., Marcy, G. W., Howard, A. W., et al. 2012, ApJ, 753, 160

Wu, Y. & Murray, N. 2003, ApJ, 589, 605

Wyatt, M. C. 2008, ARA&A, 46, 339

Wyatt, M. C., Smith, R., Su, K. Y. L., et al. 2007, ApJ, 663, 365

Yasui, C., Kobayashi, N., Tokunaga, A. T., & Saito, M. 2014, Monthly Notices of the Royal Astronomical Society, 442, 2543

Young, K. E., Harvey, P. M., Brooke, T. Y., et al. 2005, ApJ, 628, 283

Zapatero Osorio, M. R., Béjar, V. J. S., Pavlenko, Y., et al. 2002, A&A, 384, 937

Zhu, Z., Nelson, R. P., Hartmann, L., Espaillat, C., & Calvet, N. 2011, ApJ, 729, 47

Zuckerman, B., Rhee, J. H., Song, I., & Bessell, M. S. 2011, ApJ, 732, 61